3725-00049

Geochemical Analysis and Geophysical Modeling For Hydrogeologic Assessment of the Steamboat Hills and Southern Truckee Meadows Area, Washoe County, Nevada

---

Washoe County Department of Water Resources

July 31, 2001

Department of Water Resources

Geochemical Analysis and Geophysical Modeling For Hydrogeologic Assessment of the Steamboat Hills and Southern Truckee Meadows Area, Washoe County, Nevada

By John D. Skalbeck

Washoe County Department of Water Resources

July 31, 2001

Copies of this report can be obtained from:

Washoe County
Department of Water Resources
Resource Planning & Management Division
Post Office Box 11130
Reno, NV 89520-0027

Department of

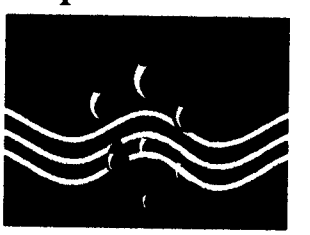

Water Resources

TABLE OF CONTENTS

LIST OF FIGURES

CHAPTER 2

LIST OF FIGURES (continued)

LIST OF FIGURES (continued)

LIST OF TABLES

ABSTRACT

Three studies constitute the hydrogeologic assessment of the Steamboat Hills area, Washoe County, Nevada. Geophysical modeling and geochemical analysis are used to assess the hydrogeologic connection between a fractured bedrock geothermal system used to produce electrical power and surrounding alluvial aquifer basins used for municipal drinking water supply. Understanding the hydrogeologic connection between these two water resources is important for long-term management of these resources.

Coupled 2.75-D forward modeling of multiple gravity and aeromagnetic profiles constrained by geological and physical properties (density, magnetic susceptibility, remanent magnetic) data yields a detailed 3-D geologic model of the geothermal system and the alluvial basins. A new method is presented for modeling the geothermal reservoir based on altered physical properties of host rock that yields a reservoir volume estimate that is double the previously assumed volume. The configuration of the modeled geothermal reservoir suggests that a previously unrecognized thermal water up-flow zone may exist along the west flank of the Steamboat Hills. Model results delineate the elevation and thickness of geologic units that can be used in numerical modeling of groundwater flow, planning exploration drilling, and evaluating fully 3-D forward modeling software.

The Steamboat Hills geothermal resource area offers an excellent opportunity to test an exploration strategy using magnetics. A zone of demagnetized rock within the geothermal resource area resulting from thermochemical alteration due to thermal water flow along faults and fractures is apparent as an aeromagnetic low anomaly. Anomalously low ground magnetic data delineate a fault that conducts thermal water from the geothermal system to an alluvial aquifer. Vertical magnetic susceptibility from core measurements yields an average value for altered granodiorite used in forward modeling. Permeable fractures and a major fault zone noted in the core hole log correspond to low magnetic susceptibility values suggesting thermal alteration or mineral replacement along fractures.

Temporal variations in B and Cl concentrations, water levels, and temperature are used to assess the mixing of thermal and non-thermal waters in alluvial aquifers north of the Steamboat Hills. Previously undocumented temporal variations indicate that the degree of mixing is dependent on proximity to north-trending faults connecting the geothermal reservoir and the alluvial aquifer. Mixing trends at selected wells suggest temperature dependent boron adsorption.

ACKNOWLEDGEMENTS

The author wishes to thank Dr. Robert Karlin for the use of the Mackay School of Mines (MSM) Paleomagnetic Laboratory, Dr. Robert Watters for the use of the MSM Geomechanics Laboratory, and Dr. Patrica Cashman and her research assistants for the refresher on paleomagnetic field and laboratory techniques. Dr. Robert Karlin, Dr. Lisa Shevenell, Dr. John Louie, Dr. Gary Oppliger, Dr. Jane Long, and Michael Widmer provided critical review that is gratefully acknowledged.

CHAPTER 1

INTRODUCTION

Scope of Work

This research includes three separate but related studies focusing on understanding the hydrogeology of the Steamboat Hills area, Nevada. Geochemical analysis is used to demonstrate that specific faults conduct thermal water from the geothermal system to the alluvial aquifer. Modeling of gravity and aeromagnetic data constitutes the bulk of the research and yields a three dimensional (3-D) model of the subsurface geology and structure to be used in planning for both drinking water and geothermal exploration and as the framework for a numerical groundwater flow model. Ground magnetic surveys were conducted across a fault known to transmit thermal water based on the geochemisty study and vertical magnetic susceptibility was measured in whole rock core to yield an average value to represent the geothermal reservoir host rock. Finally, a strategy is proposed for geothermal resource exploration using aeromagnetic and ground magnetic surveys and core/borehole logging of magnetic susceptibility and total magnetic intensity.

Research Objectives

The overall objective of this research is to expand the application of potential fields (gravity and aeromagnetic data) modeling and magnetic methods for use in hydrogeologic investigations. The Steamboat Hills area, Nevada is an excellent location to develop and test new methods because of the abundantly available geological, geochemical, and geophysical data and because the area contains developed geothermal and drinking water resources that are under increasing resource pressure.

A complex network of faults and fractures are the primary features controlling groundwater flow within the geothermal reservoir beneath Steamboat Hills. Previous investigations (e.g., White et al., 1964 and White, 1968) identified ubiquitous faults throughout the study area and concluded, in a general sense, that some of these faults and their associated fracture network likely control the connection between the geothermal system and alluvial aquifers used as a drinking water resource. While faults are known to conduct thermal water from the geothermal system to the surrounding alluvial aquifer, identification and delineation of specific permeable faults has been elusive. In general, many geophysical methods have been applied to mapping faults and fractures, but identification of the hydrologically significant faults and fractures remains a challenge (National Research Council, 1996).

The main focus of this research is to investigate methods for identifying faults and fractures that conduct thermal water using the integration of geochemical, geologic, and physical properties data, potential fields modeling, and ground magnetic surveys. The hypothesis is that rocks adjacent to faults and fractures that conduct thermal water exhibit a distinct magnetic low signature due to changes in magnetic mineralogy resulting from diffusion of thermal water into the matrix rock. Thermochemical reactions are known to alter the magnetic mineralogy in rocks resulting in decreased magnetic susceptibility and magnetic remenance (Nagata, 1961; O'Reilly, 1984). The resulting magnetic signature

for faults and fractures that conduct thermal water should be a magnetic low anomaly. Magnetic measurements should be capable of detecting bedrock faults buried by alluvial deposits even if no vertical offset has occurred. This geophysical method offers advantages over electromagnetic and seismic methods that often involve complications due to the alluvial materials, which prohibit identification of hydrogeologically significant faults found in this type of geologic setting.

Magnetic measurements of rock core or within a borehole are dependent on the percent of ferromagnetic magnetic minerals (primarily magnetite) contained in the rock. If a fracture creates a void in the rock the observed magnetic properties (magnetic susceptibility and remanent magnetization) adjacent to the fracture should be significantly lower than the host rock. Likewise, if thermal water migrates along a fracture, thermochemical alteration may reduce or completely destroy the original magnetic minerals and result in low magnetic properties. Additionally, fractures may be filled with calcite and/or quartz, which exhibit paramagnetic behavior that results in negative values of magnetic susceptibility and no remanent magnetization.

A number of questions are posed by this research:

- Can analysis of temporal variations in boron versus chloride concentrations provide information on the characteristics of non-thermal and thermal water mixing in the alluvial aquifer that relate to permeable faults?;
- Does the thermal and chemical alteration of rocks in contact with thermal water from the geothermal system produce a magnetic signature that can be used to identify conductive faults and delineate a geothermal reservoir?;
- Can potential fields modeling improve the conceptual model of the geothermal system and the surrounding alluvial basins?;
- What resolution of aeromagnetic and ground magnetic data is required for conductive fault identification?;
- Are vertical magnetic susceptibility data from whole rock core (or borehole logging useful for potential fields modeling and for identification of permeable fractures and faults?

Organization

The findings of this study are presented as separate manuscripts in Chapters 3, 4 and 5. Chapter 2 describes the analysis of temporal variations in boron (B) and chloride (Cl) concentrations, water levels, and temperature to evaluate the mixing of thermal and non-thermal waters. The analysis of temporal B vs Cl concentration variation to evaluate mixing had not been previously applied at Steamboat Hills. The geochemical time series data support the conceptual model of a single geothermal system (rather than two separate systems proposed by some researchers) and clearly demonstrate that north-trending faults provide a hydrogeologic connection between the geothermal system and the alluvial aquifer. Chapter 2 is formatted for the journal Geothermics and will be published in September (Skalbeck et al., 2001). The data compiled for this manuscript are presented in Appendix A.

In Chapter 3, potential fields (gravity and aeromagnetic profile) modeling is used to construct a 3-D geologic model of the Steamboat Hills geothermal system and the surrounding alluvial basins of the southern Truckee Meadows. This formatted for the journal Geophysics. This is the first use of multiple profiles for 2.75-D forward modeling of gravity and aeromagnetic data that are highly constrained by geologic and physical properties data to obtain a 3-D representation of subsurface geologic structure. This is also the first time a geothermal reservoir has been characterized as altered host rock to match observed aeromagnetic and gravity data. The 3-D model can serve as a planning tool for municipal well field development and as a framework for a numerical model to estimate groundwater flow. Physical properties data for each block in the 2.75-D forward models and the data from the 3-D model are presented in Appendix B.

Chapter 4 presents the results of using ground magnetic data to delineate a fault that conducts thermal water from the Steamboat Hills geothermal system into the Mount Rose Fan alluvial aquifer. The advantages and limitations of using aeromagnetic data for reconnaissance of potential geothermal systems are also tested. An exploration strategy is proposed using magnetic methods and potential fields modeling that could be important for future geothermal resource characterization and development. This manuscript will be submitted to the journal The Leading Edge. Ground magnetic data from this chapter is presented in Appendix C.

Chapter 5 presents the summary and conclusions of this dissertation. A summary of the research objectives, advancements and new findings, and results from each study are discussed. Conclusions are presented with recommendations for future research.

Water Resources Stakeholders

In the Reno-Sparks area, approximately 15% of the public drinking water comes from groundwater with the remaining 85% diverted from the Truckee River. Since June 1990, the Reno-Sparks area has been placed on water use restrictions because of below normal stream flow in the Truckee River and the increasing demand on the public-supply water (Clary et al., 1994). The population growth of Reno has increased rapidly in the past 10 years and is expected to continue into the next decade. Much of this growing population is concentrated in the south Truckee Meadows where the responsibility for ensuring adequate water resources for new residential and business developments falls on the Washoe County Department of Water Resources (Washoe County, 1996). The additional production capacity to meet this growing demand for potable water comes primarily from groundwater in alluvial basins surrounding the Steamboat Hills.

Two geothermal electric power generation facilities (Far West Capital, operated by SB Geo, Inc., and Caithness Power, Inc.) are currently operating in the Steamboat Hills. The initiation of geothermal production in the Steamboat Hills around 1985 was coincident with Washoe County's development of the Mount Rose Fan well field for drinking water needs. Hot-spring flow at Steamboat Springs, located northeast of the Steamboat Hills, began declining in 1986 and ceased completely in 1987. This prompted the U.S. Geological Survey to initiate a study of the factors affecting hot-spring activity in the area (Sorey and Colvard, 1992). They concluded that below-normal precipitation from 1986 through 1994, reduced irrigation in fields along the Steamboat Ditch, and

development of potable water and geothermal water resources each contributed to hot-spring decline.

Recognizing that successful long-term management of water resources in the Steamboat Hills area depends on a thorough understanding of the relationship between the alluvial aquifers and the geothermal system, Washoe County and SB Geo Inc. agreed in 1998 to share data for the research that constitutes this dissertation. Much of the data originated from unpublished quarterly groundwater monitoring reports, consultant reports, compiled databases, and internal memorandums and files from Washoe County, SB Geo Inc., and Caithness Power Inc.

Previous Work at Steamboat Hills

Geology and Hydrogeology

The geology of the area has been described by White et al. (1964), Thompson and White (1964), Tabor and Ellen (1975), Silberman et al. (1979), Bonham and Rogers (1983), Bonham and Bell (1993), and Stewart (1999). The basement bedrock consists of fractured Cretaceous granodiorite intruded into older metasedimentary and metavolcanic rocks. The basement rocks are overlain by Tertiary andesite, dacite, and basalt flows, flow breccias, intrusive bodies, and tuff-breccias. These rocks are disrupted by at least three prominent fault systems that trend north-south (range-front system), northeast-southwest, and northwest-southeast (White et al., 1964). Quaternary rhyolite domes that occur along the northeast-southwest fault trend are dated at 1.2 my based on K/Ar dating (Silberman et al., 1979). Geothermal production is primarily from the fractured granodiorite and metamorphic rocks, predominantly along the northeast-southwest trending fault system.

The Quaternary sediments of the Mount Rose Fan Complex are the dominant alluvial deposits west and north of the Steamboat Hills. Alluvial bajada deposits and the Alluvial Fan of Woody Hill consist of clayey sand and pebble gravels derived from older outwash and fan deposits. The Tahoe Outwash and the Donner Lake Outwash of the Mount Rose Fan Complex consist of generally sandy cobble to boulder gravels and sandy to muddy poorly sorted gravel, respectively. These alluvial deposits (referred collectively from here as Qal), as well as the underlying fractured volcanic rocks, are the primary sources of municipal and domestic water supply. Drilling logs indicate that the maximum thickness of these sediments is over 365 m (Washoe County, internal files) and gravity data suggest that the depth to bedrock may be as much as 400 m (Abbott and Louie, 2000). Drill logs indicate that silica sinter (opal and chalcedony) deposits occurring on the terraces along the northeast flank of Steamboat Hills are up to 80 m thick.

Cohen and Loeltz (1964) discuss the hydrogeology and geochemistry of Truckee Meadows. A quantitative evaluation of the hydrology and hydrogeology of the area is given by Cooley et al. (1971). Rush (1975) has mapped relative well yields and depth to water for the Reno area and Cooley et al. (1974) have mapped depth to water for the Washoe Lake area. Water-level contours indicate that the general groundwater gradient in the alluvial aquifer is from the range fronts (Carson and Virginia Ranges) toward Steamboat Creek. Groundwater flows generally toward the northeast across the Mount

Rose Fan. Katzer et al. (1984) calculated recharge from the Galena Creek basin at 2700 gallons per minute into the fractured bedrock. Streamflow measurements show that Steamboat Creek is a gaining stream throughout the southern Truckee Meadows and thus is a discharge region for both thermal and non-thermal waters (Lyles, 1985).

Geothermal Studies

White (1968) presents an extensive discussion of the hydrology, activity, and heat flow of Steamboat Springs. Bateman and Schiebach (1975) and Flynn and Ghusn (1984) have evaluated geothermal activity in the Truckee Meadows area. Garside and Schilling (1979) include a review of Steamboat Springs in their compilation of thermal waters in Nevada. Many studies were conducted by geothermal facility consultants to evaluate water chemistry and assess potential impacts from geothermal production (e.g. Yeamans, 1985; Yeamans, 1988; van de Kamp and Goranson, 1990; Goranson, 1991; Environmental Management Associates, 1993). Goranson (1991) and DeRocher (1996) summarize the geochemistry from geothermal well monitoring in the Steamboat Hills. A thorough review of studies related to geothermal and water resources development in the Steamboat Hills area is presented by Sorey and Colvard (1992).

Studies of major and trace element chemistry and stable isotope for thermal and non-thermal waters in Steamboat Hills area have been conducted by Nehring (1980), Ingram and Taylor (1991), and Mariner and Janik (1995). Isotope data have been used to suggest possible recharge areas in the Steamboat Hills area. Oxygen and hydrogen isotope data imply hot-spring waters from Steamboat Springs are enriched in ^{18}O due to high-temperature (140 to 230°C) rock-water interaction; however, deuterium values for the hot-springs water matches values for present day precipitation falling at elevations near 2,100 m in the Carson Range (Nehring, 1980).

Thermal waters are characterized by: temperatures greater than 20°C; total dissolved solids concentrations up to 2200 mg/L; elevated concentrations of As, B, and Cl; and a uniform Cl/B ratio of about 20 (Bateman and Scheibach, 1975; White, 1968). Concentrations of Cl in flashed thermal water range from 800 to 900 mg/L (DeRocher, 1996; Goranson, 1991), whereas concentrations in non-thermal water are generally less than 3 mg/L (Cohen and Loeltz, 1964).

DeRocher (1996) and van de Kamp and Goranson (1990) postulate two geothermal systems within the Steamboat Hills: a high temperature system (220°C) tapped by CPI wells and a moderate temperature system (170°C) tapped by SBG wells. Sorey and Colvard (1992) and Mariner and Janik (1995) postulate a single geothermal reservoir that supplies thermal water to both plants. Similarities in water chemistry characteristics and decreases in hydraulic head at monitoring wells suggest that the fractured bedrock geothermal reservoir and alluvial aquifer are hydrologically connected within a regional scale flow system (Sorey and Colvard, 1992).

Geophysical Studies

Regional gravity surveys and their structural interpretations have been published by Thompson and Sandberg (1958), Erwin and Berg (1977), Erwin (1982), and Plouff (1992). Peterson (1975) reported gravity data from Steamboat Hills and Wabaska areas. The data from these studies has been compiled by Hittelman et al. (1994). The Washoe

County Department of Water Resources (Washoe County) commissioned a gravity survey on the Mount Rose Fan in 1996 that included an east-west and two north-south transects (Carpenter, 1996). The 166 gravity stations from the Washoe County study were combined with data from Hittelman et al. (1994) for total coverage in the study area that included 503 stations.

White et al. (1964) measured vertical magnetic intensity along 25 ground magnetic traverses across the geothermal area in the northeastern portion of the Steamboat Hills. The contour map shows a magnetic low anomaly coincident with the Steamboat Springs Fault system that the authors conclude is due to hydrothermal alternation along an east dipping normal fault. The results of one Traverse 8 across the Mud Volcano Basin Fault (MVBF) are discussed in Chapter 4. The USGS (1981) published an aeromagnetic map of the Steamboat Hills area from a survey flown at a constant altitude of 120 m above ground with east west flight lines separated by 400 m. Regional aeromagnetic maps and discussions of their significance to the study area have been published by Nevada Bureau of Mines and Geology (1977) and Hendricks (1992). These surveys were flown at constant elevations of 5000 m above sea level and downward continued to 305 m for the final contour maps. In 1994, Washoe County conducted a draped airborne geophysical survey over the study area that included northwest-southeast flight lines (flown at altitudes of 30 m to 120 m above ground surface) with line spacing of 610 m. Total field aeromagnetic data and three frequencies (900, 7200, and 56000 Hz) of electromagnetic data were recorded every 3 m along each flight line (Dighem, 1994).

Ground measurements of resistivity on the same 25 traverses as the magnetic survey show a relationship with depth to saline water and thickness of low porosity sinter deposits (White et al, 1964). Resistivity data from a deep-looking constant altitude airborne electromagnetic survey indicate a correlation between a north-trending conductor with an unnamed fault in the vicinity of the MVBF (Christopherson et al., 1980; Hoover and Pierce, 1986). In 1975, the USGS published data and maps from a self-potential (SP) survey (Hoover, Batzle, and Rodrigues, 1975), an audio-magnetotelluric (AMT) survey (Long and Brigham, 1975), and two telluric traverses (Hoover, O'Donnell, and Batzle, 1975). Hoover et al. (1978) present results of AMT investigations at 40 geothermal areas including Steamboat Hills. Corwin and Hoover (1979) show linear SP anomalies associated with the MVBF and High Terrace Faults and suggest the faults conduct thermal water.

Potential Field Techniques

Theory

Gravity and magnetics are considered potential fields because they are force fields. A force field describes the forces that act at each point of space at a given time. Both are vector fields, which can be characterized by field lines (lines of force) that are tangent at each point to the vector field. The potential of a vector field is defined as the work function and any vector field that has a work function with continuous derivatives (gradients) is conservative. A conservative field **F** has a scalar potential ϕ given by:

$\mathbf{F} = \nabla\phi$ and **F** is considered a potential field.

Newtons Law of Gravitation is given by:

$F_g = -G\frac{m_1 m_2}{r^2}$ where m_1 and m_2 are mass objects, $\mathbf{F_g}$ is the force of attraction between two objects, r is the distance between the center of masses, and G is the Universal Gravitational Constant (6.67E-11 Nm^2/Kg^2). The gravitational attraction **g** produced by m_1 on m_2 is found by dividing $\mathbf{F_g}$ by m_2 as given by:

$g = -G\frac{m_1}{r^2}\hat{r}$ where $\hat{r}$ is the direction of attraction

Because **g** is force divided by mass, it has units of acceleration and is sometimes referred to as gravitational acceleration. Since **g** is a conservative field, it can describe as the gradient of a scalar potential:

$\mathbf{g} = \nabla U$ where $U = G\frac{m_1}{r}$ U is the gravitational potential and **g** is a potential field (Blakely, 1995).

Magnetic force $\mathbf{F_m}$ is given by:

$\mathbf{F_m} = \frac{1}{\mu}\frac{p_1 p_2}{r^2}$ where p_1 and p_2 are magnetic poles, r is the distance between the center of masses, and μ is magnetic permeability. For this equations the magnetic poles are assumed to be a sufficient distance apart to be isolated and not affect each other. The magnetic field intensity **H** produced by p_1 is found by dividing **H** by p_2 as given by:

$\mathbf{H} = \frac{1}{\mu}\frac{p_1}{r^2}\hat{r}$ where $\hat{r}$ is the direction of magnetic polarization. Since **H** is a conservative field it can described a the gradient of a scalar potential:

$H = -\nabla V$ where $V = \frac{1}{\mu}\frac{P}{r}$ and V is the magnetic potential and **H** is a potential field (Dobrin, 1960). Magnetization held in rocks is described by the vector quantity magnetization **M** of a volume V. **M** is the vector sum of dipole moments divided by the volume:

$\mathbf{M} = \frac{1}{V}\sum_i m_i$ where m_i is an individual dipole moment. Total magnetization **M** of a rock is the vector sum of remanent magnetization $\mathbf{M_r}$ and induced magnetization $\mathbf{M_i}$ as given by:

$\mathbf{M_i} = k\mathbf{H}$ where k is the magnetic susceptibility, thus

$\mathbf{M} = \mathbf{M_r} + k\mathbf{H}$

Magnetic permeability and magnetic susceptibility are related by:

$\mu = 1 + 4\pi k$

Similarities in the gravitational and magnetic potentials are best summarized by Poisson's Relation which states:

$$V = -\frac{\mathbf{Mg}}{G\rho} d\hat{r}$$ where ρ is density (Dobrin, 1960; Blakely, 1995).

The Poisson's Relation states that for a body with uniform magnetization and uniform density, the magnetic potential at any point is proportional to the gravitational attraction in the direction of magnetization. The relationship exists because **H** and **g** are both inversely proportional to the squared distance from their point sources.

The primary differences between the gravity and magnetic fields are as follows:

- The fundamental parameter controlling gravity is rock density which has small (1 to 3 gm/cm^3) spatial variability whereas the fundamental parameter controlling gravity is magnetic, magnetic susceptibility can vary by four to five orders of magnitude;
- Gravitational force is always attractive but magnetic force can be attractive or repulsive;
- Magnetic monopoles can not be found alone-they always occur in pairs (one + and one -) referred to as a dipole whereas a single density mass can exist;
- The gravitational field does not vary significantly over time but the magnetic field is highly time dependent;
- The gravitational field is always generated by subsurface variations in rock density. The magnetic field can originate from variations in induced magnetization or in remanent magnetization.

Corrections to Field Data

Gravity measurements ($\mathbf{g}_{obs}$) are influenced by the earth's shape (ellisoid), latitude, elevation, topography, earth-tides and density variations beneath the measured point. A number of standard corrections are applied to $\mathbf{g}_{obs}$ to account for variations in these effects. Field gravity measurements are first corrected for the reference ellipsoid, which is a theoretical calculation accounting for gravity variation with latitude due to ocean bulges form the gravitational pull of the moon and sun and also the earth's rotation. The reference ellipsoid ($\Delta\mathbf{g}_o$) calculated using the 1967 Geodetic Reference System formula:

$$\Delta\mathbf{g}_o = 978{,}031.846\ (1 + 0.005278895 \sin^2\phi + 0.0000023462 \sin^4\phi)\ \text{(mGal)}$$

where ϕ is latitude (Telford et al., 1990). For the Reno area, an International Gravity Reference Network base is established at the Scrugham Engineering Building on the University of Nevada, Reno campus with $\Delta\mathbf{g}_o$ value of 979,674.65 mGal. The correction has the effect of subtracting off from the field measurement the effect of the earth's theoretical gravity beneath sea level. Since gravity varies inversely with distance squared between two masses, the Free Air Correction ($\Delta\mathbf{g}_{fa}$) compensates for the decrease in gravity as the elevation increases above sea level by:

$$\Delta\mathbf{g}_{fa} = 0.308596 \times \text{station elevation (m)}$$

The Bouguer correction ($\Delta\mathbf{g}_{sb}$) accounts for the density of mass between the station and the reference spheroid elevation was ignored in the free air correction. The simple Bouguer correction assumes a slab of infinite horizontal extent and uniform density

(commonly 2.67 g/cm^3 for crustal rocks) with a thickness equal to the station elevation above sea level and is calculated by:

Δg_{sb} = 0.04192 x station elevation (m) x density

The terrain correction (Δg_t) accounts for the gravitational effects of the surrounding terrain such as a valley or mountain. This correction is computed by the use of "Hammer zones" which partition elevation differences by distance from the station. Terrain corrections are added to the gravity reading whether these corrections are for depressions or hills. Correcting the gravity reading for all of the above gravitational effects produces the Complete Bouguer Anomaly (g_{cb}) as:

$\Delta g_{cb} = g_{obs} - \Delta g_0 + (\Delta g_{fa} - \Delta g_{sb} + \Delta g_t)$.

The earth's magnetic field is conceptualized as lines of magnetic flux that intercept the earth at a direction that also varies with latitude. The magnetic direction is described by declination and inclination where declination is the angle between the magnetic meridian and the geographic meridian and inclination is the angle where the magnetic flux line dips below the horizontal. Magnetic intensity and inclination varies with latitude where it is approximately 25,000 nanoTeslas (nT) and horizontal at the equator and approximately 70,000 nT and vertical at the earth's poles. The earth's magnetization is subject to diurnal fluctuations of 25 to 50 nT due to the sun's solar wind that creates an external magnetic field in the earth's ionosphere. Consequently, these fluctuations are subtracted from magnetic survey data using data collected at a base station magnetometer within or nearby the survey area. The International Geomagnetic Reference Field (IGRF) is a global model of the earth's magnetic field that is recalculate every five years. The IGRF is often subtracted from the magnetic survey data to produce total magnetic field anomaly data. Over small are the IGRF may be a constant value; however, for large survey area it the IGRF magnetic field may vary significantly with latitude and longitude. Because the magnetic field inclination varies with latitude, magnetic anomalies are not necessarily symmetrical over a uniform magnetic body. A fast fourier transform process referred to as reduction-to-pole can be applied to a magnetic survey to eliminate this complexity. This transformation creates the anomaly that would be measured at the north magnetic pole (Blakely, 1995). There are many other magnetic processing techniques (e.g. upward and downward continuation, directional derivatives, phase transformations) that are presented in Blakely (1995).

Advantages and Limitations

Applying magnetic and gravity surveys in a hydrogeologic investigation is typically conducted to estimate the geometry of an alluvial basin. One advantage of a gravity investigation is the relatively low cost of obtaining the data. Another advantage is that density values within a given rock type do not vary significantly and typical density values for certain rock types are widely published. Therefore, a preliminary estimate of basin depth and geometry is relatively straightforward and can be obtained even in the absence of site-specific rock density measurement and control on depths to bedrock. One disadvantage using gravity alone is that generally only large-scale structures can be obtained unless the number of gravity stations is quite high. Another disadvantage is that without any subsurface control (i.e. borehole logs), distinguishing between different rock units (volcanic flow over a granitic basement) can be difficult.

Large-scale faults with no vertical displacement, faults that may have hydrogeologic significance, are likely undetectable using gravity. The number of measurement stations for a gravity survey are much less than for a magnetic survey.

One advantage of magnetic surveys is the rapid rate that measurements can be collected. Measurements for a ground-based survey are almost instantaneous so the rate is dependent on the travel rate of the operator. For airborne surveys, magnetic measurements can be collected as frequently as every 3 m and therefore a lot of data can be collected along a profile line. A large area can be covered using an airborne survey but the cost is significant. Faults with no vertical displacement may be detectable using a magnetic survey depending on the degree of discontinuity in the magnetic properties of the host rock. Magnetic surveys are more sensitive to near surface structures than gravity surveys because for many geometric bodies the magnetic field declines relative to the inverse distance cubed while the gravity squared. Another advantage for magnetic surveys is that magnetization can be altered by heat and chemical reactions which may lead to detection of significant hydrogeologic features such as alteration zones along faults. A major disadvantage for magnetic surveys is that cultural noise (power lines, fences, subsurface pipelines) may inhibit surveys in developed areas. Another disadvantage is that magnetic susceptibility in rocks can vary by as much as 4 to 5 orders of magnitude and the remanent magnetization can vary significantly in orientation and polarity relative to the present day magnetic field. These variations can create difficulties for modeling subsurface structure.

Aeromagnetic Data and Potential Field Modeling at other Geothermal Areas

Aeromagnetic data have been used at many geothermal resource areas throughout the world. This section presents some important studies where aeromagnetic data have been used for characterizing the geologic setting and estimating subsurface heat flow. The 1965 U.S. Geological Survey aeromagnetic survey of the Salton Sea geothermal field in southeastern California revealed a broad magnetic high attributed to igneous intrusions at depths of 2 km or greater (Griscom and Muffler, 1971). A northeast-trending elliptical magnetic high corresponds with the geothermal field and a number of local magnetic anomalies correspond to Quaternary rhyolite extrusions. Hildenbrand and Kucks (1983) developed a conceptual model of the geothermal system in southwestern South Dakota from aeromagnetic, gravity, geologic, geothermal gradient, and geothermometry data. Derivative maps of gravity and magnetic data enhance the lithologic and structural boundaries of the area and several gravity and magnetic lineaments may correspond to permeable faults. Rapolla et al. (1989) found poor correlation between gravity and aeromagnetic data from the Ishia-Phlegrean geothermal fields near Naples, Italy. The authors present one interpretation that anomalies are due to discontinuities in the intermediate-deep crust and a second interpretation that relate the gravity anomalies to deep partically melted basalts and the magnetic anomalies to a local shallow Curie temperature isotherm surface (See discussion in following paragraph). Analysis of aeromagnetic and gravity derivative maps reveals several lineaments corresponding to faults that are closely related to the conductive transport of thermal water. Bibby et al. (1992) utilized aeromagnetic data from constant elevation (1525 m above sea level) and draped (60 m above ground) surveys along with ground magnetic and resistivity data for

an investigation of the geothermal systems in the Rotorua area, New Zealand. The authors found a low magnetic anomaly in an area with low resistivity that they attributed to a thermal up-flow zone. Ross et al. (1996) collected high-resolution aeromagnetic data (380 m flightline spacing and altitude of 230 m above ground) over the central portion of the Ascension Island in the south Atlantic. The authors associate a low-magnetization with a shallow (1-3 km) geothermal system. A high-resolution aeromagnetic survey (400 m flightline spacing and altitude of 295 m above ground) for the Geysers geothermal area was designed to investigate shallow crustal magnetization (Blakely and McLaughlin, 1997). Using a wavelength-filtering method, the authors found that aeromagnetic anomalies show no evidence for a shallow (<7 km) magma chamber beneath the Geysers area.

Aeromagnetic data has been used to infer subsurface heat sources by estimating the basal depth of magnetic sources from a method known as Curie temperature isotherm analysis. For temperatures above 580°C (for magnetite at atmospheric pressure) rocks become non-magnetic. The Curie temperature isotherm analysis; therefore, yields a depth where the rock temperature exceeds 580°C. Connard et al. (1983) analyzed aeromagnetic data from a constant elevation (2743 m above sea level) survey over the central Oregon Cascade Range to estimate the Curie temperature isotherm depth. Calculations based on spectral analysis of magnetic anomalies yield Curie temperature isotherm depths ranging from 6 to 14 km that imply high heat flow and suggest this area may be an important geothermal resource area. Using a statewide compilation of aeromagnetic data from Nevada, Blakely (1988) examined spectral information obtained from a Fourier domain technique to estimate the depth to the Curie temperature isotherm. Depth estimates range from 10 to 30 km for the state and a shallow depth to the Curie temperature isotherm corresponds with the Battle Mountain heat flow anomaly. A Curie temperature depth map was generated from aeromagnetic data in a national project to assess the geothermal resources of Japan (Okubo and Ogawa, 1989). The estimated depths agree well with measured temperature-gradient data for high gradient regions of volcanic chains, intermediate gradient regions of the backarc basins, and low gradient regions of the forearc basins.

Modeling of gravity and aeromagnetic data has been applied at a number of geothermal resource areas. Serpa and Cook (1984) used joint 2.5-D inversion modeling of gravity and aeromagnetic data to determine the source of heat in the Meadow-Hatton geothermal study area in south-central Utah. Results provide no evidence for a buried igneous body as a heat source so the authors conclude that migration of thermal water along deep faults accounts for the elevated temperatures in this geothermal resource area. Alvarez (1984) used 3-D modeling of gravity and aeromagnetic data for structural interpretation of the Los Humerous Caldera geothermal field in Mexico. Results were used to guide exploratory drilling that yielded two vapor-producing wells. Youngs et al. (1985) analyzed gravity and aeromagnetic data to evaluate low-temperature geothermal resources in the Santa Rosa-Sonoma area in northern California. Results from a 2-D model of the gravity data along one profile indicate that the geothermal resources are associated with the Sonoma Volcanics and that faults act as conduits for up-flow of thermal water. Blakely and Stanley (1993); Stanley and Blakely (1993); Stanley and Blakely (1995) report on model results from a single profile of gravity and aeromagnetic

data using 2.5-D forward and inverse techniques to assess the possible presence of a partial melt magma chamber at Geysers geothermal area. These results, combined with results from a model of electromagnetic data and ideal body analysis of gravity data, suggest that a large magma chamber may be present at 15 to 20 km and that shallow melt zones may also exist. Ross et al. (1996) used 3-D modeling of aeromagnetic survey from the Asecension Island in the South Atlantic ocean to evaluate the geothermal potential of the island. These results suggest that most magnetic sources occur within a few 100 meters of the surface.

REFERENCES

Abbott, R.E., and Louie, J.N., 2000, Depth to bedrock using gravimetry in the Reno and Carson City, Nevada, area basins, Geophysics, 65(2), 340-350.

Alvarez, R., 1984, 3-D modeling of Aeromagnetic and gravimetric surveys over Los Humerous Caldera geothermal field, Mexico [abs.], Geophysics, 49(50), 617.

Bateman, R.L., Scheibach, R.B., 1975, Evaluation of geothermal activity in the Truckee Meadows, Washoe County, Nevada, Nevada Bureau of Mines and Geol., Rpt. 25, 38 p.

Bibby, H.M., Dawson, G.B., Rayner, H.H., Bennie, S.L. and Bromly, C.J., 1992, Electrical resistivity and magnetic investigation of the geothermal systems in the Rotorua area, New Zealand, Geothermics, 21(1-2), 43-64.

Blakely, R.J., and McLaughlin, R.J., 1997, The Geysers geothermal reservoir, California; constraints from high-resolution aeromagnetic anomalies, Geol. Soc. of America, Abs. with Programs, 29(5), 5.

Blakely, R.J., 1995, Potential theory in gravity & magnetic applications: Cambridge University Press, Cambridge, 441 p.

Blakely, R.J., and Stanley, W.D., 1993, The Geysers magma chamber: Constraints from gravity data, density measurements, and well information, Geothermal Res. Council Trans., 17, 227-233.

Blakely, R.J., 1988, Curie temperature isotherm analysis and tectonic implications of aeromagnetic data from Nevada, Jour. of Geophysical Res., 93(B10), 11,817-11,832.

Bonham, H.F., Jr., and Bell, J.W., 1993, Geologic map, Steamboat quadrangle, Nevada Bureau of Mines and Geol., Map 4Fg.

Bonham, H.F., Jr., and Rogers, D.K., 1983, Geologic map, Mt. Rose NE quadrangle: Nevada Bureau of Mines and Geol., Map 4Bg.

Carpenter, T., 1996, Gravity data acquisition and processing, Mount Rose Fan project, Washoe County, Nevada, unpublished report for Washoe County Utility Division, November 1996.

Christopherson, K., Long, C.L., and Hoover, D.B., 1980, Evaluation of airborne electromagnetic surveys for geothermal exploration [Abs.], Annual meeting of the Society of Exploration Geophysicists, Houston, Texas, 458.

Clary, S. L., McClary, D. R., Whitney, R., and Reeves, D. D, 1994, Water resources data, Nevada, Water Year 1994: U. S. Geol. Surv. Water-Data Report NV-94-1.

Cohen, P., Loeltz, O.J., 1964, Evaluation of hydrogeology and hydrogeochemistry of the Truckee Meadows area, Washoe County Nevada, U.S. Geol. Surv. Water Supply Paper 1779-S, 63 p.

Cooley, R.L., Spane, F.A., Jr., and Scheibach, R. B., 1974, Reno folio-hydrologic map, Nevada Bureau of Mines and Geol. Environmental Series, prepared in cooperation with U.S. Geol. Surv.

Cooley, R.L., Fordham, J.W., Westphal, J.A., 1971, Hydrology of Truckee Meadows, Nevada, Center for Water Research, Desert Research Institute, University of Nevada System, Project Rpt. 15, 49 p.

Connard, G., Couch, R., and Gemperle, M., 1983, Analysis of aeromagnetic measurements from the Cascade Range in Central Oregon, Geophysics, 48(3), 376-390.

Corwin, R.F., and Hoover, D.B., 1979, The self potential method in geothermal exploration, Geophysics, 44 (2), 226-245.

DeRocher, T., 1996, Historical summary of Caithness Power, Inc., Hydrologic monitoring of the Steamboat Hills region, 1987-Present, draft unpublished report for Yankee/Caithness, 46 p.

Dighem, 1994, Dighem^{V} survey for Utility Division, Washoe County Public Works, Washoe County, Nevada, unpublished report #612, December 28, 1994.

Dobrin, M.B., 1960, Introduction to geophysical prospecting: McGraw-Hill Book Company, New York, 630 p.

Erwin, J.W., 1982, Discussion of a set of regional gravity data for the Reno 1 By 2° sheet, Nevada, Nevada Bureau of Mines and Geol., Open-File Report 82-7, 5 p.

Erwin, J.W., and Berg, J.C., 1977, Bouguer gravity map of Nevada-Reno Sheet, Nevada Bureau of Mines and Geol., Map 58.

Environmental Management Associates, 1993, Yankee/Caithnes Joint Venture, L.P. Steamboat Hills geothermal project, plan of operation/plan of utilization amendment for geothermal fluid rate increase, preliminary environmental assessment, unpublished report for Yankee/Caithness.

Flynn, T., Ghusn, G. Jr., 1984, Geologic and hydrologic research on the Moana geothermal system, Washoe County, Nevada, Division of Earth Sciences, UNLV report, 148 p.

Garside, L.J. and Shilling, J.H., 1979, Thermal waters of Nevada, Nevada Bureau of Mines and Geol., Bull. 191, 163 p.

Goranson, C., 1991, Summary and interpretation of six years of groundwater monitoring data and four years of geothermal production and injection well operations at the SB GEO, Inc. geothermal binary power plant, Steamboat Springs, Nevada. Prepared for SB GEO, Inc., 44 p.

Griscom, A., and Muffler, L.J.P., 1971, Aeromagnetic survey of the Salton Sea geothermal field, southeastern, California, Geological Society of America, Abstracts with Programs, 3(2), 129.

Hendricks, J. D., 1992, Total-intensity magnetic-anomaly map of the Reno 1° by 2° quadrangle, Nevada and California, U.S. Geol. Surv. Misc. Field Studies Map MF-2154-C.

Hildenbrand, T.G., and Kucks, R.P., 1983, Model of the geothermal system in southwestern South Dakota from gravity and aeromagnetic studies [Abs.], Geophysics, 48(4), 454.

Hittelman, A. D., Dater, D., Buhmann, R. and Racey, S., 1994, Gravity CD-ROM and user's manual, National Oceanic and Atmospheric Administration, National Geophysical Data Center.

Hoover, D.B. and Pierce, H.A., 1986, Airborne electromagnetic mapping of geothermal systems in the Basin and Range and Cascade Provinces, USA, in Airborne Resistivity Mapping, ed. G.J. Palacky, Geological Survey of Canada, Paper 86-22, 139-143.

Hoover, D.B., Long, C.L., and Senerfit, R.M., 1978, Some results from audio-magnetotelluric investigations in geothermal area, Geophysics, 43, 1501-1514.

Hoover, D.B., Batzle, M., and Rodriquez, R., 1975, Self-potential map, Steamboat Hills, NV, U.S. Geol. Surv. Open-file Report 75-446.

Hoover, D.B., O'Donnell, J., and Batzle, M., 1975, Telluric profiles in Steamboat Hills, NV, U.S. Geol. Surv. Open-file Report 75-445.

Ingraham, N.L., Taylor, B.E., 1991, Light stable isotope systematics of large-scale hydrologic regimes in California and Nevada, WRR., 27(1), 77-90.

Katzer, T., Durbin, T.J., Maurer, D.K., 1984, Water-resources appraisal of the Galena Creek basin, Washoe County, Nevada, U.S. Geol. Surv. Open-File Rpt. 84-433, 59 p.

Long, C.L., and Brigham, R.H., 1975, Audio-magnetic data log for Steamboat Hills, Nevada, U.S. Geol. Surv. Open-file Report 75-447, 7 p.

Lyles, B.F., 1985. Time-variant hydrogeologic and geochemical study of selected thermal springs in Western Nevada, unpublished M.S. Thesis, University of Nevada, Reno, 203 p.

Mariner, R.H., Janik, C.J., 1995, Geochemical data and conceptual model for the Steamboat Hills geothermal system, Washoe County, Nevada, Geothermal Res. Council Trans., 19, 191-200.

Nagata, T., 1961, Rock Magnetism, Maruzen Company Ltd., Tokyo.

National Research Council, 1996, Rock fractures and fluid flow: Contemporary understanding and applications, National Academy Press, Washington D.C., 551 p.

Nehring, N.L., 1980, Geochemistry of Steamboat Springs, Nevada, U.S. Geol. Surv. Open-File Rpt. 80-887, 61 p.

Nevada Bureau of Mines and Geology, 1977, Aeromagnetic map of Nevada-Reno Sheet, Prepared in cooperation with U. S. Geological Survey, Map 54.

O'Reilly, W., 1984, Rock and Mineral Magnetism, Blackie and Sons Ltd., Glasgow and London., 220 p.

Okubo, Y., Tsu, H., and Ogawa, K., 1989, Estimation of Curie point temperature and geothermal structure of island arcs of Japan, Tectonophysics, 159(3-4), 279-290.

Peterson, D.L., 1975, Principle facts for gravity stations in Steamboat Hills and Wabaska, NV, U.S. Geol. Surv Open-file Report 75-443.

Plouff, D., 1992, Bouguer gravity anomaly and isostatic residual gravity maps of the Reno 1° by 2° quadrangle, Nevada and California, U.S. Geol. Surv. Map MF-2154-C.

Rapolla, A., Fedi, M., Fiume, M.G., 1989, Crustal structure of the Ishia-Phlegrean geothermal fields, near Naples, Italy, from gravity and aeromagnetic data, Goephysical Journal, 97, 409-419.

Ross, H.P., Nielson, D.L., and Green, D.J., 1996, Aeromagnetic survey and interpretation, Asecension Island, South Atlantic Ocean: Geothermics, 25(4/5), 471-488.

Rush, E.F., 1975, Washoe City Folio-Hydrologic Map, Nevada Bureau of Mines and Geol. Environmental Series.

Serpa, L.F., and Cook, K.L., 1984, Simultaneous inversion modeling of gravity and aeromagnetic data applied to a geothermal study area in Utah, Geophysics, 49(8), 1327-1337.

Shevenell, L., Garside, L.J., and Hess, R.H., 2000, Nevada geothermal resources, Nevada Bureau of Mines and Geol., Map 126.

Silberman, M.L., White, D.E., Keith, T.E.C., Dockter, R.D., 1979, Duration of hydrothermal activity at Steamboat Springs, Nevada, from ages of spatially associated volcanic rocks, U.S. Geol. Surv. Prof. Paper 458-D, 14 p.

Skalbeck, J.D., Shevenell, L., and Widmer, M.C., 2001, Mixing of thermal and non-thermal waters the Steamboat Hills area, Nevada, Geothermics, 30, *in press*.

Sorey, M.L., and E. M. Colvard, 1992, Factors affecting the decline in hot-spring activity in the Steamboat Springs area of critical environmental concern, Washoe County, Nevada, U.S. Geol. Surv., adm. report for U.S Bur. of Land Manag., 109 p.

Stanley, W.D., and Blakely, R.J., 1993, New geophysical models related to heat sources in the Geysers-Clear Lake region, California, Geothermal Res. Council Trans., 17, 267-272.

Stanley, W.D., and Blakely, R.J., 1995, The Geysers-Clear Lake geothermal area, California-An updated geophysical perspective of heat sources: Geothermics, 24, 187-221.

Stewart, J.H., 1999, Geologic map of the Carson City 30 x 60 minute quadrangle, Nevada, Nevada Bureau of Mines and Geol., Map 118.

Tabor, R.W., and Ellen, S., 1975, Geologic Map, Washoe City Folio, Nevada Bureau of Mines and Geol. Environmental Series.

Telford, W.M., Geldart, L.P. and Sherriff, R.E., 1990, Applied Geophysics, Cambridge University Press, Cambridge, 770 p.

Thompson, G.A., and Sandberg, C.H., 1958, Structural significance of gravity surveys in the Virginia City-Mt. Rose area, Nevada and California: Geol. Soc. Am. Bull., 69, 1269-1282.

Thompson, G.A., White, D.E., 1964. Regional geology of the Steamboat Springs area, Washoe County, Nevada, U.S. Geol. Surv. Prof. Paper 458-A, 52 p.

van de Kamp, P.C., Goranson, C.B., 1990. Summary of the hydrological characteristics of the Steamboat Hills area, Nevada, unpublished report for Caithness Power, Inc. and Yankee-Caithness Joint Venture, L.P.

Washoe County, 1996, The 1995-2015 Washoe County comprehensive regional water management plan, Regional Water Planning Commission, unpublished draft report, November 13.

White, D.E., Thompson, G.A., Sandberg, C., 1964. Rocks, structure and geologic history of the Steamboat Springs thermal area, Washoe County, Nevada, U.S. Geol. Surv. Prof. Paper 458-B, 63 p.

White, D.E., 1968, Hydrology, activity, and heat flow of the Steamboat Springs thermal system, Washoe County, Nevada, U.S. Geol. Surv. Prof. Paper 458-C, 109 p.

USGS, 1981, Total field aeromagnetic map of the Steamboat Hills Known Geothermal Resource Area, Nevada, U.S. Geological Survey Open-file Report 81-996.

Yeamans, F., 1985, Hydrology of Steamboat Springs geothermal system, 1984, unpublished report for Philips Petroleum Company, 151 p.

Yeamans, F., 1988, Hydrogeology and water chemistry in the vicinity of Brown School, Steamboat, Nevada, unpublished report for the Nevada Division of Environmental Protection and ORMAT Systems, Inc., 24 p.

Youngs, L.G., Chapman, R.H., and Chase, G.W., 1985, Geophysical investigations and geothermal resources; Santa Rosa-Sonoma area, Sonoma and Napa counties, California, California Geology, 38(11), 243-253.

CHAPTER 2

Mixing of Thermal and Non-thermal Waters in the Steamboat Hills Area, Nevada

John D. Skalbeck, Lisa Shevenell, Michael C. Widmer

ABSTRACT

Groundwater monitoring began in 1985 at two geothermal facilities in the Steamboat Hills area, Nevada. Wells representing non-thermal, thermal, and mixed waters are evaluated by assessing temporal variations in B and Cl concentrations, water levels, and temperature. The objective is to assess the hydrologic and geochemical connection between the fractured bedrock geothermal reservoir and the alluvial aquifer. Results suggest that fault-controlled groundwater flow between the geothermal system and the alluvial aquifer is the dominant hydrologic process. Temporal trends suggest that the thermal water component in the alluvial aquifer has increased in most areas but decreased in at least one area.

INTRODUCTION

Rapid growth in the southern Truckee Meadows (south of Reno, Nevada) during the past decade has placed a large demand on water resources near the Steamboat Hills area (Fig. 1). The demand has been for non-thermal water to satisfy municipal and domestic needs, and for thermal water to produce electric power at two power facilities. Development of these resources to serve the growing suburban community poses special problems related to the close proximity and interconnected nature of these two water resources. Many communities in the western United States face similar questions regarding management of water resources for competing uses.

The Washoe County Department of Water Resources, Utility Services Division (Washoe County) began producing municipal water supply from alluvial aquifers around the Steamboat Hills in 1985. The two geothermal production facilities, currently SB Geo, Inc. (SBG) and Caithness Power, Inc. (CPI), began operating in the Steamboat Hills in January 1987 and February 1988, respectively. Washoe County, SBG, and CPI are interested in long-term production of their resources but recognize that a thorough understanding of the hydrogeology of the collective groundwater system is essential for preservation of the water resources in the area. The key question regarding the hydrogeology of the system is the nature of the hydraulic connection between the fractured bedrock geothermal reservoir and the alluvial aquifer. By evaluating the interconnection between the geothermal reservoir and alluvial aquifers systems, resource management decisions can be made in attempts to minimize adverse impacts to both resources. This study employs geochemical data to evaluate mixing of non-thermal and thermal waters to provide insight into the hydrogeology of the area.

Hot-spring flow at Steamboat Springs, located northeast of the Steamboat Hills began declining in 1986 and ceased completely in 1987. Below-normal precipitation from 1986 through 1994, as well as reduced irrigation (resulting in reduced recharge to the alluvial aquifer) in fields along the Steamboat Ditch (Fig. 1), caused water-level declines in alluvial aquifer monitor wells. The initiation of non-thermal water and thermal water production were coincident with these events and prompted the U.S. Geological Survey to initiate a study to evaluate factors affecting hot-spring activity in the area (Sorey and Colvard, 1992). The focus of that study was to identify the pertinent causes for the change in hydraulic conditions in the area. Additional studies were conducted following initiation of resource production to evaluate water chemistry

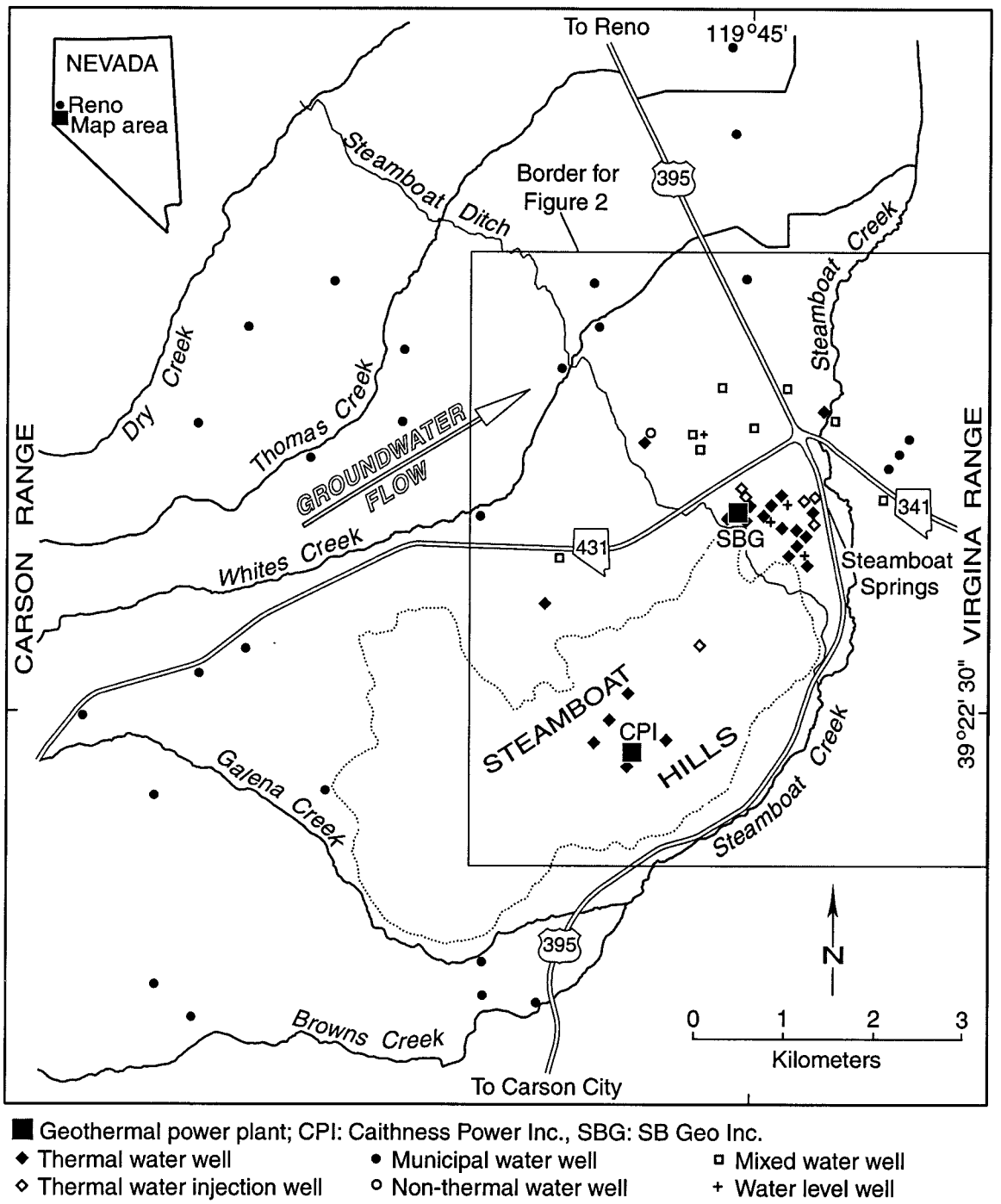

Figure 1. Location map of the Steamboat Hills area, Nevada.

relationships in the area and assess potential impacts from geothermal production (Yeamans, 1988; van de Kamp and Goranson, 1990; Goranson, 1991; Environmental Management Associates, 1993). Major and trace element chemistry and stable isotope data were also obtained from thermal and non-thermal waters in Steamboat Hills, Steamboat Springs, regional streams and creeks, and precipitation (Nehring, 1980; Ingram and Taylor, 1991; Mariner and Janik, 1995). These data suggest that the same thermal source fluid is intercepted at the two geothermal power facilities; however, the existing data did not provide clear evidence that the recharge origin for the geothermal system is similar to the alluvial aquifer.

The development of both thermal and non-thermal water resources have affected wells in the combined discharge area east of Steamboat Hills near Steamboat Creek (Fig. 1, near the junction of US 395 and Nevada 431 and 341). The purpose of this study is to identify causes of water quality degradation or improvement at public and domestic water supply wells in this discharge area, and to document changes in the contribution of thermal waters to this area, along with possible causes. The temporal relationship of production activities and water quality trends for both of these water resources is evaluated to determine the importance of faults to fluid flow.

BACKGROUND

Location and climatic setting

The Steamboat Hills consist of a northeast-southwest trending topographically prominent bedrock ridge located at the southern boundary of Truckee Meadows in central Washoe County, Nevada. The Truckee Meadows is a north–south trending basin bordered on the west by the Carson Range and on the east by the Virginia Range. The Steamboat Hills lie between US 395 and Nevada 431 (Fig. 1). The city of Reno is located approximately 15 km to the north but recent expansion has filled in most of the area between Reno and the Steamboat Hills.

Precipitation is influenced greatly by oroclinal effects from the Carson Range, which creates a strong rain-shadow effect. Annual precipitation, falling primarily as snow, averages 147 cm at higher elevations in the Carson Range (based on 19 year average at Marlette Lake), whereas the average annual precipitation in Reno, falling primarily as rain, is only about 18 cm (based on 54 year average at Reno/Tahoe International Airport; Desert Research Institute, 2000). Steamboat Creek is the principal drainage within the area and is a major tributary to the Truckee River, which originates at Lake Tahoe (located 20 km southwest of Steamboat Hills) and discharges into Pyramid Lake (located 60 km northeast of Steamboat Hills). The majority of runoff comes from snow that precipitates on the east flank of the Carson Range. The predominant tributaries in the area include: Dry Creek, Thomas Creek, Whites Creek, Galena Creek and Browns Creek. The Steamboat Springs geothermal area is located on the northeastern flank of the Steamboat Hills (Fig. 1).

Geology

The geology of the area has been described by White et al. (1964), Thompson and White (1964), Tabor and Ellen (1975), Bonham and Rogers (1983), and Bonham and Bell (1993). The basement bedrock consists of fractured Cretaceous granodiorite intruded into older metasedimentary and metavolcanic rocks. The basement rocks are overlain by faulted andesite, dacite, and basalt flows, flow breccias, intrusive bodies, and tuff-breccias of the Tertiary Kate Peak Formation. These rocks are disrupted by at least three prominent fault systems that trend north-south (range-front system), northeast-southwest, and northwest-southeast. Quaternary

rhyolite domes occur along the northeast-southwest fault trend. Geothermal production is primarily from the fractured granodiorite, predominantly along the northeast-southwest trending fault system.

The generally sandy cobble to boulder gravel-rich sediments of the Mount Rose Fan Complex are the dominant alluvial deposits located west and north of the Steamboat Hills. These alluvial deposits, as well as the fractured volcanic rocks, are the primary sources of municipal and domestic water supply. Drilling logs indicate that the maximum thickness of these sediments is over 365 m (Washoe County, internal files) and gravity data suggest that the depth to bedrock may be as much as 400 m (Abbott and Louie, 2000).

Hydrogeology and geochemistry

Cohen and Loeltz (1964) discuss the hydrogeology and geochemistry of Truckee Meadows. The hydrology, activity, and heat flow of Steamboat Springs is discussed by White (1968) and time-variant hydrogeology and geochemistry is presented by Lyles (1985). Cooly et al. (1971) developed numerical models of surface water and groundwater hydrology in the Truckee Meadows. Bateman and Schiebach (1975) and Flynn and Ghusn (1984) have evaluated geothermal activity in the Truckee Meadows area. Goranson (1991) and DeRocher (1996) summarize the geochemistry from geothermal well monitoring in the Steamboat Hills.

Water-level contours show that the general groundwater gradient in the alluvial aquifer is from the range fronts (Carson and Virginia Ranges) toward Steamboat Creek. In the study area, the groundwater flows generally toward the northeast (Fig. 1). Streamflow measurements show that Steamboat Creek is a gaining stream throughout the southern Truckee Meadows and thus is a discharge region for both thermal and non-thermal waters (Lyles, 1985). Similarities in water chemistry characteristics and decreases in hydraulic head at monitoring wells suggest that the fractured bedrock geothermal reservoir and alluvial aquifer are hydrologically connected within a regional scale flow system (Sorey and Colvard, 1992). Isotope data have been used to delineate possible recharge areas in the Steamboat Hills area. Oxygen and hydrogen isotope data show that hot-spring waters from Steamboat Springs are enriched in ^{18}O due to high-temperature (140 to 230°C) rock-water interaction; however, deuterium values for the hot-springs water matches values for present day precipitation falling at elevations near 2,100 m in the Carson Range (Nehring, 1980).

Production testing at both facilities indicates that flow of thermal water is fracture controlled. van de Kamp and Goranson (1990) postulate two geothermal systems within the Steamboat Hills: a high temperature system (220°C) tapped by CPI wells with a maximum depth of 760 m (elevation of 915 m above mean sea level [amsl]), and a moderate temperature system (170°C) tapped by SBG with depths between 122 m and 213 m (elevations between 1220 m and 1430 m amsl). Sorey and Colvard (1992) and Mariner and Janik (1995) postulate a single geothermal reservoir that supplies thermal water to both plants.

Thermal and non-thermal waters are chemically distinct in the Steamboat Hills area. Thermal waters are characterized by: temperatures greater than 20°C; total dissolved solids concentrations up to 2200 mg/L; elevated concentrations of arsenic (As), boron (B), and chloride (Cl); and a uniform Cl/B ratio of about 20 (Bateman and Scheibach, 1975 and White, 1968). Cl, which is assumed to act as a conservative tracer in groundwater, is characteristically found at higher concentrations in thermal water relative to non-thermal water. Concentrations of Cl in flashed thermal water range from 800 to 900 mg/L (DeRocher, 1996; Goranson, 1991), whereas concentrations in non-thermal water are generally less than 3 mg/L (Cohen and Loeltz, 1964).

METHODS

Data compiled by Washoe County from SBG and CPI reports and data from Nehring (1980), Ingraham and Taylor (1991), and Mariner and Janik (1995) were used for this study. Wells selected to represent non-thermal, thermal, and mixed waters (Fig. 2) were evaluated by assessing the temporal variations in B and Cl concentrations, water levels, temperature, and calculated the percent of thermal water in alluvial wells located in the discharge area of the geothermal system. Available well log data (Washoe County internal files) and mapped faults (Tabor and Ellen, 1975; Bonham and Rogers, 1983; Bonham, and Bell, 1993) were used to assess groundwater flow paths and the possible hydrologic connections between the fractured bedrock geothermal system and the alluvial aquifer.

RESULTS

Completion details for wells evaluated in this study are provided in Table 1. A summary of available water chemistry for the study wells is presented in Table 2. The summary includes minimum and maximum temperature and B and Cl concentrations, date of the maximum value of each, factor of increase from minimum to maximum, and the range of sampling dates.

The B versus Cl data from the current work, Nehring (1980), Ingraham and Taylor (1991), and Mariner and Janik (1995) are plotted on Figure 3. These data represent cold waters (springs, creeks, snowmelt, non-thermal wells: Nehring, 1980; Ingraham and Taylor, 1991; and Washoe County data reported here), non-thermal domestic and municipal wells, domestic wells with mixed non-thermal and thermal water and geothermal production wells (Mariner and Janik, 1995 and current work). The majority of data fall along the same linear trend suggesting simple mixing of thermal and non-thermal waters and indicate a common source fluid for the thermal waters produced at both power plants. These data suggest a single geothermal system for Steamboat Hills as postulated by Sorey and Colvard (1992) and Mariner and Janik (1995). Subsequent B versus Cl plots include this local mixing trend line. For the purpose of this study, the data from the CPI wells are assumed to represent the geothermal reservoir water.

Temporal plots of B versus Cl for wells screened in the alluvial aquifer show that the waters are either non-thermal (e.g. Peigh Domestic well, Fig. 4a,), thermal (e.g. Curti Barn Geothermal well, Figs. 4b), or mixed (e.g. Herz Geothermal well, Figs. 4c) water chemistry. These results show no temporal variation and thus can be used as type members for comparison with other wells. Based on these data, the Herz Geothermal well has mixed type water chemistry that has not varied appreciably over time.

The temporal variation of B versus Cl for the Curti Domestic well shows a steady trend from non-thermal to mixed type water in 1988, with the maximum occurring in 1993, and with large variability during 1990 and thereafter (Fig. 5a). The Flame well also shows a steady trend from predominantly non-thermal water in 1985 to mixed type water chemistry through the last sampling date in June 1990 (Fig. 5b). The Pine Tree Ranch #1 well shows a similar trend (Fig. 5c) to the Flame well (i.e., trend from non-thermal water in 1985 to mixed type water chemistry in June 1990); however, the maximum concentrations in the Pine Tree Ranch #1 well are approximately 20 percent of the maximum concentrations in the Flame well. The Steinhardt well exhibits the opposite B versus Cl variation, trending from mixed water in 1987 toward non-thermal type water chemistry through 1990 (Fig. 5d). The mixing trend at each of these wells follows the local mixing trend for the study area.

Table 1. Completion details for selected wells.

Well Name	Date Drilled	Well Elevation (m)	Total Depth (m)	Screen Interval (m)	Seal Depth (m)	Water Depth[a] (m)	Water Temp[a] (°C)
Brown School	NA	1384	116	NA	NA	NA	NA
CoxI-1	1980	1538	1058	538 - 1058[b]	538	116	182
Curti Barn Geothermal	1982	1379	79	55 - 74	15	6	102
Curti Domestic	1982	1379	29	24 - 29	24	5	54
Herz Domestic	1955	1399	34	12 - 34	NA	9	cold
Herz Geothermal	NA	1402	47	NA	16	NA	57
Flame	NA	1412	30	NA	NA	11	NA
Peigh Domestic	1959	1442	44	16 - 26	NA	18	cold
Peigh Pool Geothermal	1970	1442	70	OB	24	27	115
Pine Tree Ranch #1	1971	1415	34	18 - 32	14	17	43
Pine Tree Ranch #2	1959	1414	133	OB	38	16	Hot
SBG-PW1	1985	1438	192	181 - 192	181	9	165
SBG-TH1	1991	1420	272	169 - 272[b]	169	15	164
SBG-TH2	1991	1423	262	183 - 262[b]	183	19	163
SBG-TH3	1991	1414	277	201 - 277[b]	201	20	163
STMGID #4	1981	1570	253	213 -253	33	150	cold
Steinhardt	1979	1402	41	33 - 41	16	23	cold
TranSierra 4	1970	1391	57	55 - 57	15	20	cold

a: Following well completion
b: Open hole interval
NA: Not Available
OB: Open at bottom

Table 2. Summary of chemistry data from study wells.

	Brown School	Curti Barn Geothermal	Curti Domestic	Flame	Herz Domestic	Herz Geothermal	Peigh Domestic	Pine Tree Ranch #1	Steinhardt
Temperature (°C)									
Minimum	15	35	21	44	3	49	26	33	32
Maximum	42	54	37	59	31	55	42	48	34
Maximum Date	Sep-98	Sep-98	Sep-97	Dec-87	Sep-94	Aug-89	Dec-98	Jun-90[b]	Jun-92
Factor increase	2.8	1.5	1.8	1.3	10.3	1.1	1.6	1.5	1.1
Boron (mg/L)									
Minimum	0.1	32	1.6	6.9	0.1	1	0.1	0.1	5.6
Maximum	40.5	41.1	16.7	25.7	4.5	19	0.3	4.9	13
Maximum Date	Jun-94	Jun-97	Jun-97	Jun-90[b]	Jun-93	Oct-89	Sep-97[c]	Jul-89	May-87[a]
Factor increase	405.0	1.3	10.4	3.7	45.0	19.0	3.0	49.0	2.3
Chloride (mg/L)									
Minimum	3	660	43	112	1	184	1	2	130
Maximum	743	844	317	485	297	390	15	94	300
Maximum Date	Sep-96	Mar-96	Mar-93	Jun-90[b]	Dec-92	Jul-89	Sep-97	Jun-90[b]	May-87[a]
Factor increase	247.7	1.3	7.4	4.3	297.0	2.1	15.0	47.0	2.3
Range of Dates									
Beginning	Dec-84	May-87	May-87	Dec-84	Dec-84	Dec-84	Dec-84	Dec-84	May-87
Ending	Dec-98	Sep-98	Dec-98	Jun-90	Dec-94	Jun-93	Dec-98	Jun-90	Jun-92

a: First data point collected from the well.
b: Last data point collected from the well.
c: Data fluctuate; maximum attained on more than one date.

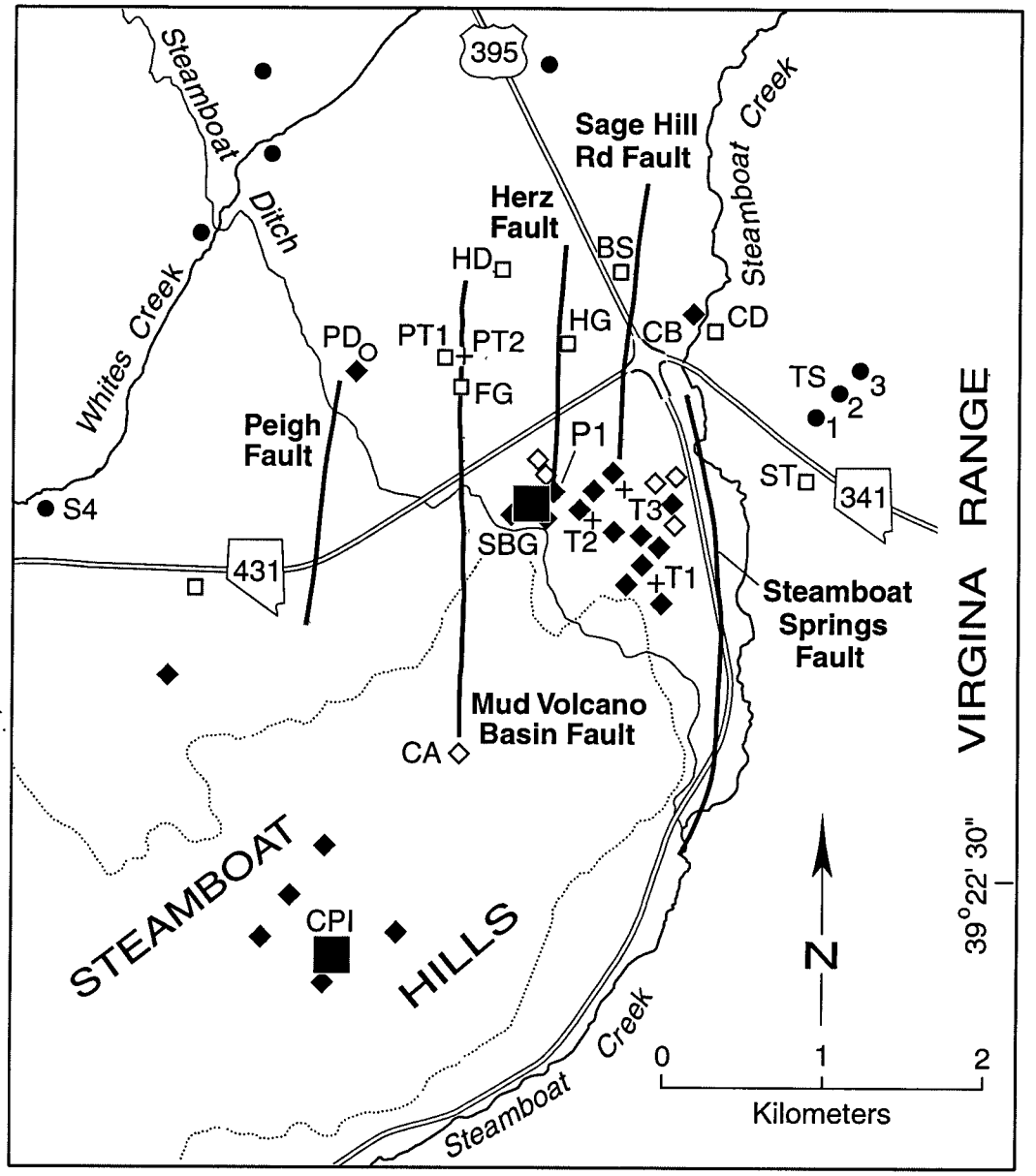

■ Geothermal power plant
CPI:Caithness Power Inc.
SB:SB Geo Inc.

◆ Thermal water well
P1:SB Geo; SBG-PW1
CB:Curti Barn Geothermal

◇ Thermal water injection well
CA:Caithness; CoxI-1

● Municipal water well
S4:STMGID #4
TS:TranSierra wells 1,2,3

o Non-thermal water well
PD:Peigh Domestic

▫ Mixed water well
BS:Brown School
ST:Steinhardt
CD:Curti Domestic
HD:Herz Domestic
HG:Herz Geothermal
FG:Flame Geothermal
PT1: Pine Tree Ranch #1

\+ Water level well
PT2:Pine Tree Ranch #2
T1:SB Geo; SBG-TH1
T2:SB Geo; SBG-TH2
T3:SB Geo; SBG-TH3

Figure 2. Study area location map. Thermal, non-thermal, mixed water, and water level wells and hydrologically significant faults referenced in this study are labeled.

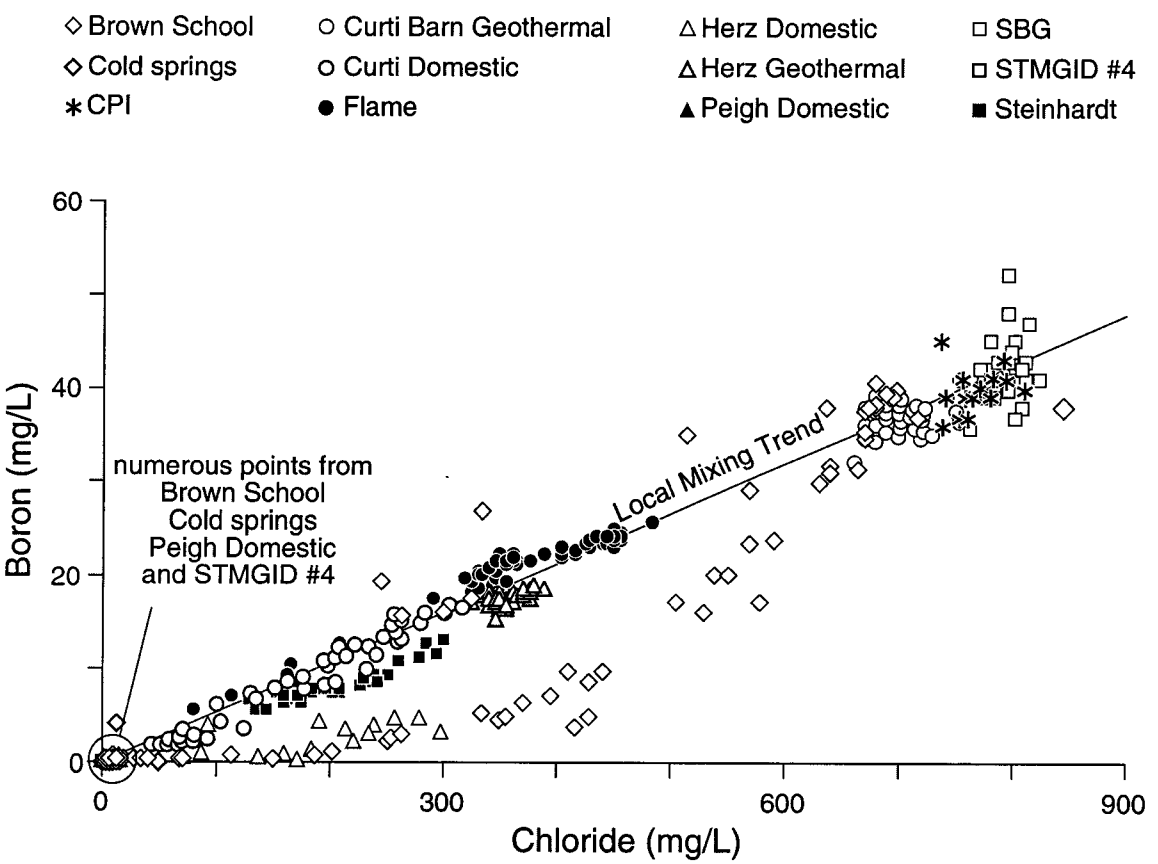

Figure 3. Boron versus Cl for various water types in the Steamboat Hills area, Nevada. Local mixing trend is from the origin to maximum B/Cl concentration represented by the CPI/SBG geothermal production data. This local mixing trend is included on subsequent B versus Cl plots. Data for Cold Springs, Peigh Domestic, and STMGID #4 plot near the origin but are hidden under other symbols.

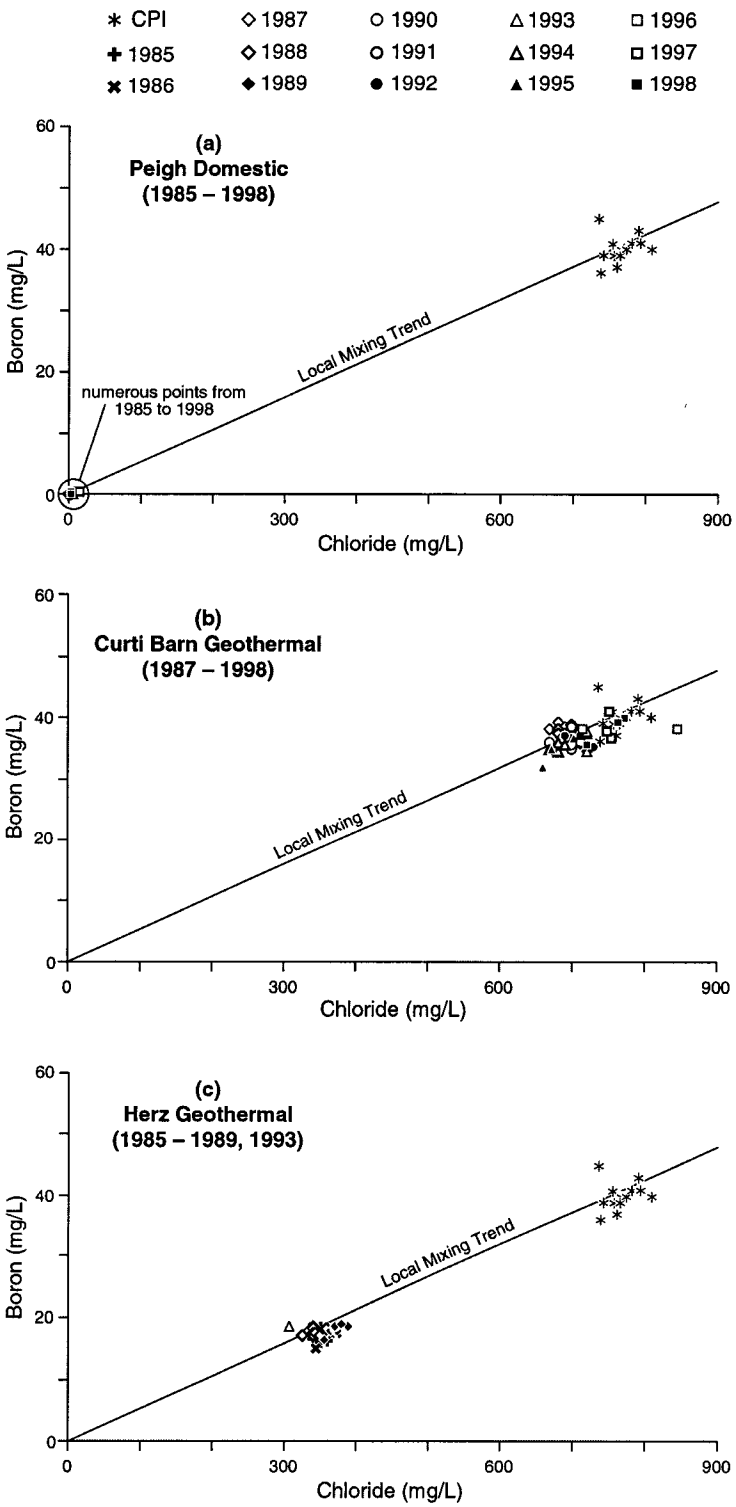

Figure 4. Boron versus Cl over time for each well with consistent water chemistry. (a) Peigh Domestic well shows non-thermal type water chemistry. (b) Curti Barn Geothermal well shows thermal type water chemistry. (c) Herz Geothermal well shows mixed type water chemistry.

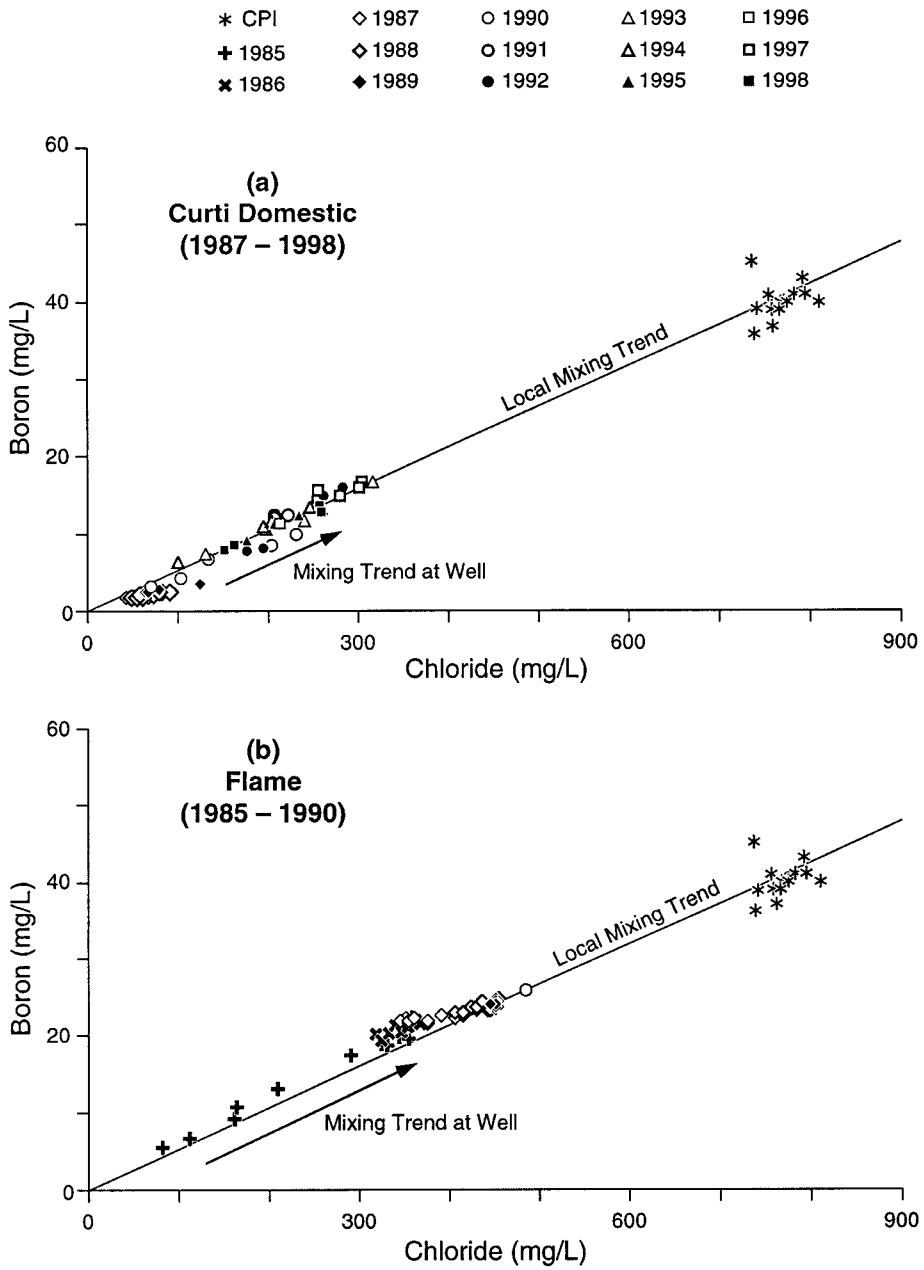

Figure 5. Boron versus Cl over time for each well shows mixing with time along the local mixing trend. (a) Curti Domestic well shows trend from non-thermal to mixed type water chemistry (increased thermal component). (b) Flame well shows trend from non-thermal to mixed type water chemistry. Figures 5 (c) and (d) on following page.

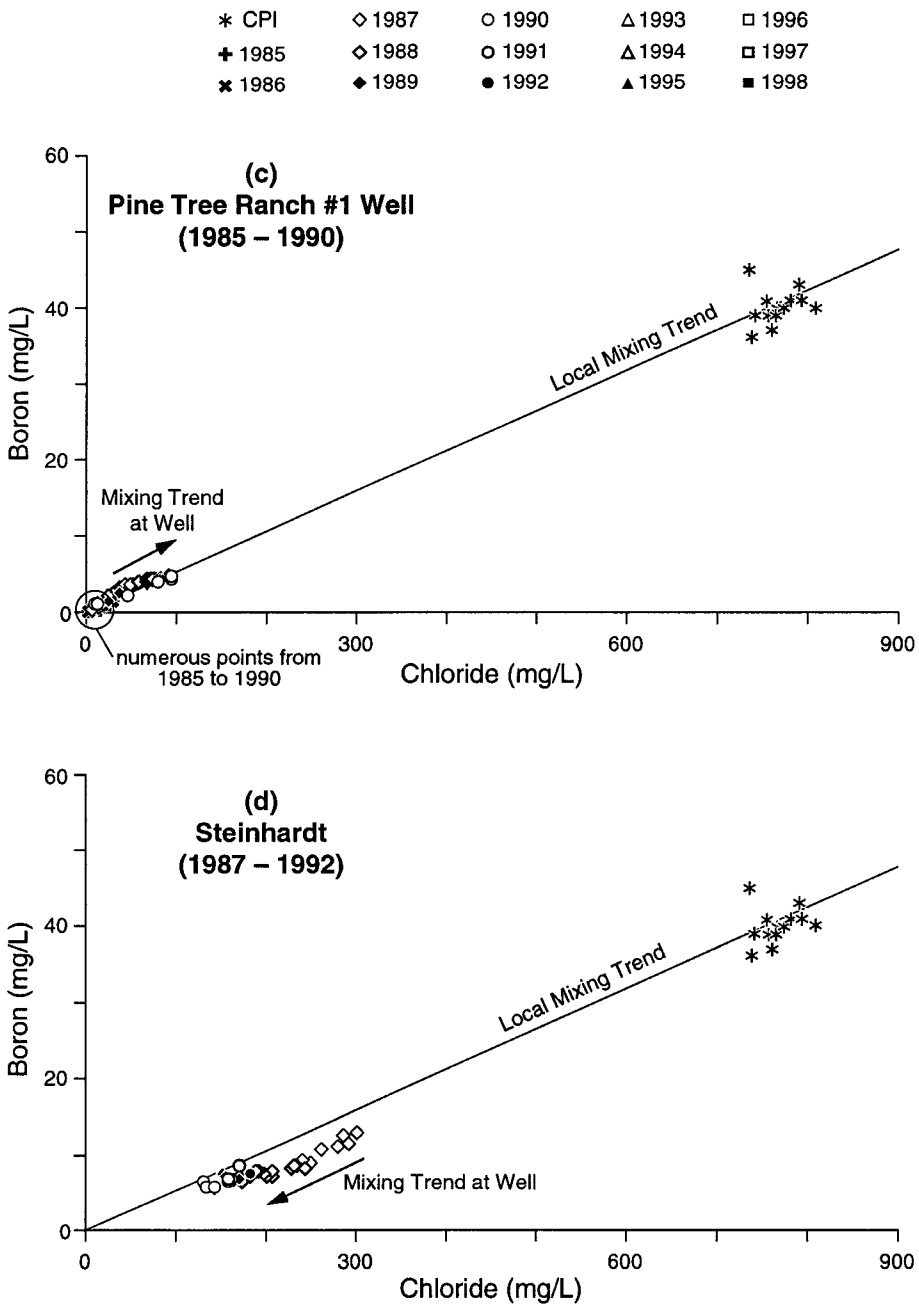

Figure 5 (cont). (c) Pine Tree Ranch #1 well shows increased mixing to lesser degree than the nearby Flame well. (d) Steinhardt well shows trend from mixed to non-thermal type water chemistry (decreased thermal component).

Cl vs B concentrations in the Herz Domestic well illustrate three distinct mixing trends (Fig. 6a). The Brown School well shows the same three trends but with greater definition due to higher concentrations and greater variability through time (Fig 6b). The first trend shows significant increases in Cl with only slight increase in B through 1991 for the Herz Domestic well and through 1989 for the Brown School well. The second trend shows B and Cl variations trending toward the thermal type water signature through 1992 (Herz Domestic well) and through 1996 (Brown School well). The 1996 Cl and B concentrations in the Brown School well are nearly identical to the thermal type water found in CPI wells. The third trend is defined by decreasing B and Cl concentrations through the last sampling date of 1994 (Herz Domestic well) and 1998 (Brown School well). The mixing trends observed for these two wells with respect to B adsorption and the proximity to faults are discussed below.

Water levels from 1985 to 1998 in domestic wells and geothermal reservoir monitoring wells are shown in Figure 7. The Herz Geothermal well shows relatively consistent water levels whereas other wells show declining water levels through 1995, with distinct water-level increases in all eight wells between 1995 and 1998. Seasonal fluctuations are evident in the Pine Tree Ranch #1 and Steinhardt wells. Water levels were measured from the Pine Tree Ranch #2 well rather than the Pine Tree Ranch #1 well beginning in September 1996. Water levels for these wells were similar following well completion (See Table 1) and appear consistent following September 1996.

Water temperatures over time for alluvial aquifer wells are shown in Figure 8. The higher temperature wells (Curti Barn Geothermal, Flame, Herz Geothermal) generally range from 40° to 60°C. Consistent temperatures between 49° and 53°C occur in the Herz Geothermal well. Low temperatures (3° to 30°C) occur in the Brown School, Curti Domestic, and Herz Domestic wells with strong seasonal fluctuations exhibited in the Brown School and Herz Domestic wells. After 1990, temperatures steadily increased in the Brown School well to 42°C in September 1998, and in the Curti Domestic well to 37°C in September 1997. Temperatures in the Pine Tree Ranch #1 well also show seasonal variation with a range from 33°C in January 1985 to 48°C in June 1990 (last measurement date). The Peigh Domestic and Steinhardt wells show relatively consistent temperatures of 30° to 40°C.

DISCUSSION

Regional groundwater flow in the alluvial and fractured volcanic rock aquifer is generally toward the northeast. The general flow direction in the geothermal reservoir system is also toward the northeast; however, the flow of thermal fluids is strongly controlled by faults and therefore local directions of flow can vary greatly. The degree of non-thermal and thermal water mixing at a particular well is highly dependent on the location of the well with respect to faults. In some areas vertical flow is important and evaluation of relative well depths and subsurface geology is discussed. The discussion is organized based on the following three groups of wells: 1) wells showing no temporal variability, 2) wells showing local mixing, and 3) wells showing mixing associated with B adsorption. The final section discusses mixing in the discharge area.

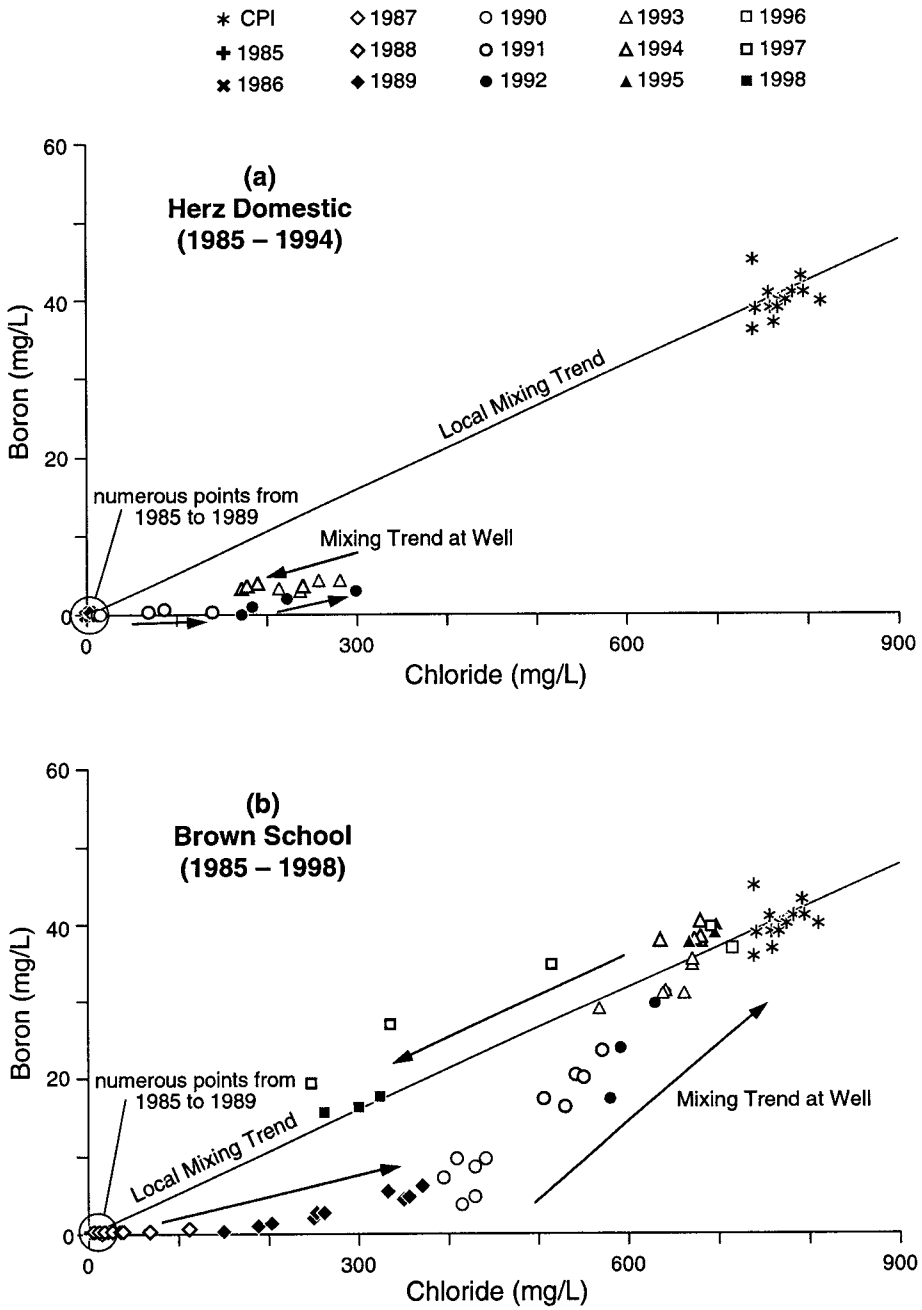

Figure 6. Boron versus Cl over time for each well where mixing may indicate boron adsorption onto clays in the alluvial aquifer. (a) Herz Domestic well shows increasing chloride concentrations with minimal change in boron concentrations. (b) Brown School well shows multiple mixing trends suggesting temperature dependent boron adsorption.

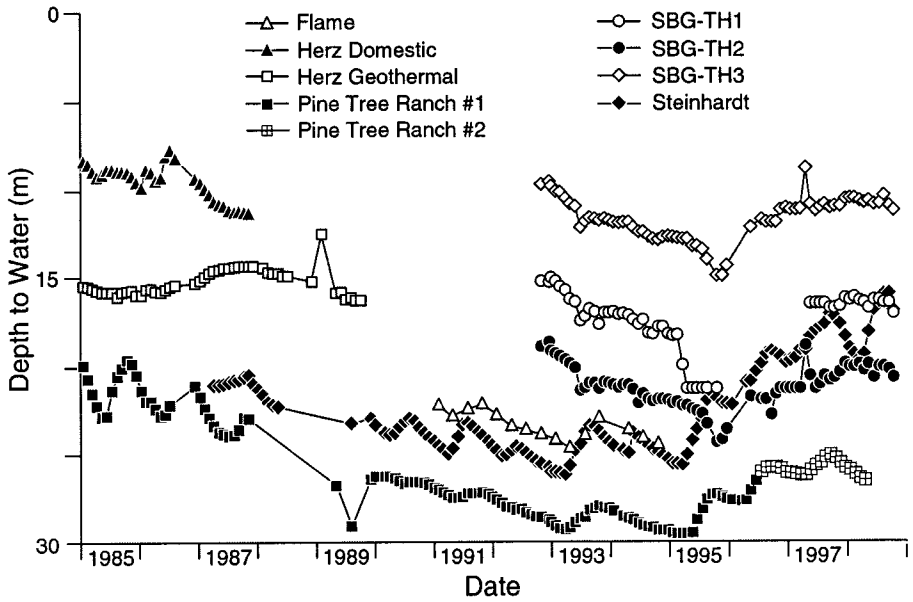

Figure 7. Water levels over time for alluvial aquifer wells and geothermal reservoir monitoring wells.

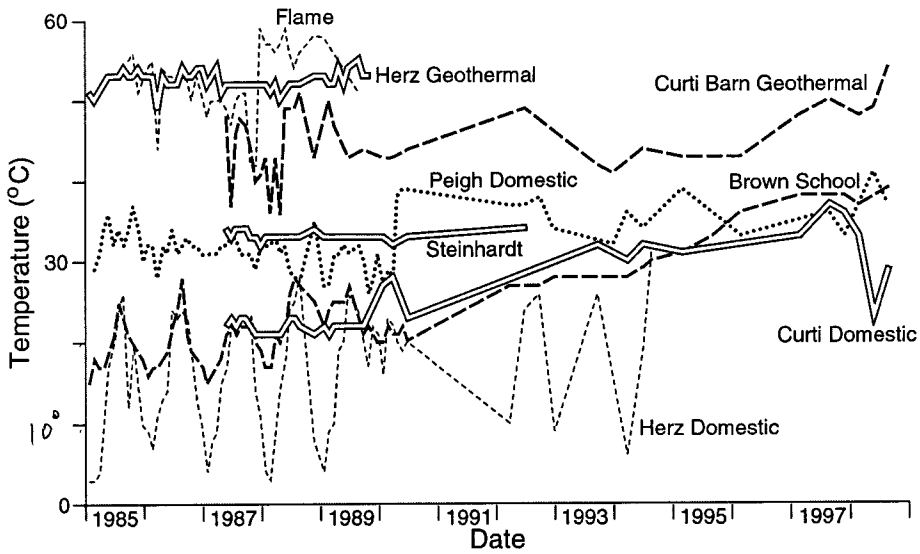

Figure 8. Temperature over time for alluvial aquifer wells.

Wells showing no temporal variability

The Peigh Domestic well is located adjacent to a north-trending unnamed fault (Peigh Fault for the purpose of this paper) mapped entirely within the alluvial fan (Bonham and Rogers, 1983). The fluid chemistry for this well indicates that it contains non-thermal water, yet the temperature of this water is warm (26-42°C) relative to other domestic wells. This suggests a nearby thermal source may heat non-thermal water conductively, without any accompanying mixing of thermal water. The Peigh Domestic well is screened from 16 to 26 m below ground surface (bgs) in alluvial gravel, which is underlain by approximately 8 m of clay and the fractured volcanic bedrock (Fig. 9a). The
nearby Peigh Pool Geothermal well, with temperatures between 110° and 115°C, is cased to a depth of 70 m bgs with an open bottom in fractured bedrock. The log for this well indicates that approximately 12 m of clay was encountered between the alluvial gravel and the fractured bedrock (Fig. 9a). The clay layer in this area appears to function as an aquitard limiting vertical fluid mixing in this area but may allow thermal conduction to produce the elevated temperatures observed in the Peigh Domestic well.

The Herz Geothermal well is located between the north-trending Herz Fault and Sage Hill Road Fault (Yeamans, 1988) as shown in Figure 1. The southern extent of these two faults is coincident with SBG injection wells IW-1 and IW-2. The Herz Geothermal well exhibits remarkably consistent B and Cl data of mixed type water chemistry as well as consistent temperature and water level data over time. These relationships suggest that the proportion of non-thermal to thermal water has not varied at this location.

The Curti Barn Geothermal well is located northeast of the SBG production field within the discharge area of the geothermal system. The Curti Barn Geothermal well, screened within the alluvial aquifer from 55 to 74 m bgs (Fig. 9b), exhibits nearly constant thermal type water chemistry and relatively consistent temperatures generally above 40°C. These data suggest that the lower portion of the alluvial aquifer is in direct connection with thermal water leaking from the geothermal reservoir. The characteristics of the upper portion of the alluvial aquifer are illustrated through the results of the Curti Domestic well as discussed in the following section.

Wells showing local mixing 78'-95'

The Curti Domestic well is screened from 24 to 29 m bgs and is located within 30 m of the Curti Barn Geothermal well (Fig 9b). Temperature data are consistent with B and Cl data indicating an increased component of thermal water beginning in 1990. The B and Cl data indicate mixing for this well is coincident with the local mixing trend suggesting a direct hydraulic connection with the geothermal system. The chemistry data suggest that an upward vertical hydraulic gradient within the alluvial aquifer may produce mixing in the Curti Domestic well; however, no water level data are available to confirm this hypothesis. The dynamics of mixing in this geothermal discharge area will be further discussed in a following section.

The Flame well is located along the northern portion of the north-trending Mud Volcano Basin Fault (Fig. 2). The B versus Cl temporal variation along the local mixing trend suggests a direct connection with the geothermal reservoir, with steadily increasing inputs of thermal water to this well from 1985 to 1990. No data are available from the Flame well after 1990. Well completion information is not available for the Flame well; however, Yeamans (1988) reported that the well is thought to be completed with the total depth similar to the nearby Pine Tree Ranch #1 well with a total depth of 30 m (Fig 9c). Thus, the Flame well is likely completed in

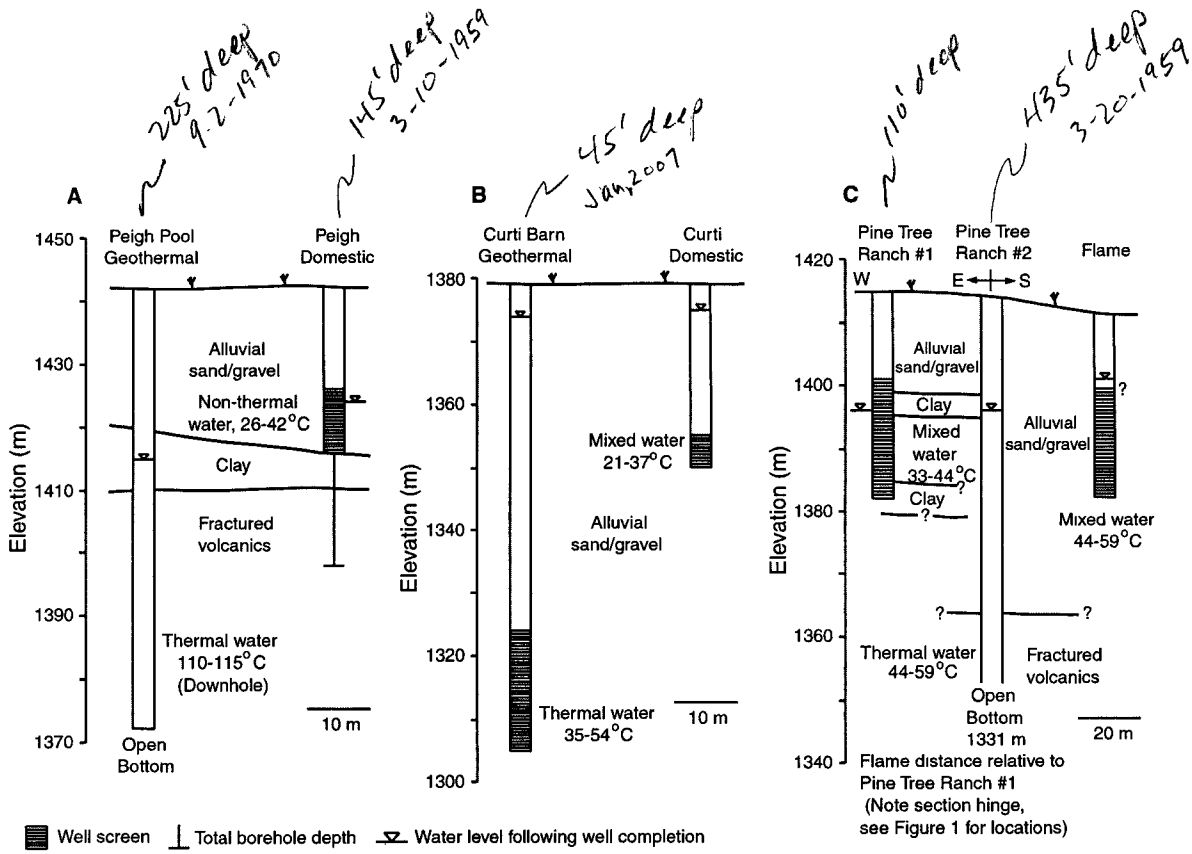

Figure 9. Cross-sections of local geology, well completion details, water chemistry type and water temeperatures. Temperature for Peigh Pool Geothermal well was measured downhole; temperatures for other wells measured from samples. (a) Peigh Domestic and Peigh Pool Geothermal wells. (b) Curti Domestic and Curti Barn Geothermal wells. (c) Pine Tree Ranch #1 and #2 and Flame wells. Note: horizontal distances between wells are from the well centers and well diameter is not to scale.

the alluvial aquifer. The Flame well illustrates that migration of thermal water occurs along a permeable fault. The CPI Cox I-1 geothermal injection well, situated near the southern extent of the Mud Volcano Basin Fault, was likely installed to utilize the permeable nature of this fault. The Cox I-1 injection well was completed in May 1981 and began accepting thermal fluid in May 1987.

The Pine Tree Ranch #1 well is located approximately 30 m west of the Pine Tree Ranch #2 well and approximately 60 m north of the Flame well (Figs. 2 and 9c). The Pine Tree Ranch #2 and the Flame wells both are located within the trace of Mud Volcano Basin Fault and therefore the Pine Tree Ranch #1 well is located approximately 30 m from this fault. The Pine Tree Ranch #1 well is screened from 18 to 32 m bgs within the alluvial aquifer while the Pine Tree Ranch #2 well has an open bottom at 133 m bgs within the fractured volcanics. Historical sampling has not been conducted for the Pine Tree Ranch #2 well but recent sampling indicates thermal water in this well. The B and Cl variation for the Pine Tree Ranch #1 well is along the local mixing trend indicating a direct connection with the geothermal reservoir; however, the B and Cl concentrations are less than those in the Flame well. This decrease of B and Cl concentrations with distance from a fault suggests that most of the geothermal fluid flows along the permeable fault rather than through the matrix of the geothermal reservoir. Mixing of thermal and non-thermal water is greatest in close proximity to a permeable fault and thermal water characteristics decrease with distance from the fault.

The Steinhardt well is located east of the SBG production field on the opposite side of the north-trending Steamboat Springs Fault system. This fault system is spatially coincident with historical hot springs and is likely a zone of upward vertical groundwater flow. The declining B versus Cl temporal trend in the Steinhardt well indicates a decrease in the thermal water component that is consistent with the decline in hot spring activity. Clearly, less thermal water migrates across this fault system after 1987. In addition, cessation of Washoe County production from nearby Trans Sierra 1, 2, and 3 wells in 1985 (Washoe County internal files) could have contributed to the observed decrease in B and Cl concentrations. Reduced production by Washoe County may have resulted in more non-thermal water and initiation of production at the power plants may have resulted in less thermal water available for mixing. Relatively constant temperatures for this well do not provide any corroborative evidence for changes in the amount of thermal and non-thermal water inputs to this area.

Wells showing mixing associated with boron adsorption

The Brown School well is located approximately 50 m west of the north-trending Sage Hill Road Fault, whereas the Herz Domestic well is situated between the north-trending Herz Fault and Mud Volcano Basin Fault approximately 250 m from each fault (Fig. 2). As discussed above, the greater changes in B and Cl concentrations at the Brown School well compared to those at the Herz Domestic well could be a result of its closer proximity to a north-trending fault. The mixing trends observed in these two wells may result from B adsorption on clays in the alluvial aquifer as fluids flow away from the faults into the porous media of the alluvial aquifer. The B and Cl concentrations observed in other wells plot along the local mixing trend line; however, the first mixing trend observed at the Herz Domestic and Brown School wells clearly shows that B is retarded relative to Cl. This trend suggests that clays in the alluvial aquifer may adsorb B.

The second mixing trend observed after 1989 (Brown School well) and after 1991 (Herz Domestic well) may represent desorption of B from clays as a result of increasing temperature, or decreased adsorption of B on clays in the alluvial aquifer. The period of dates over which this second mixing trend occurs is coincident with increasing temperature in the Brown School well. Goldberg et al. (1993) have demonstrated that B adsorption on clays in soil decreases with increasing temperature. However, data for the Herz Domestic well do not conclusively show an increase in temperature for this time period. An alternative interpretation could be decreased adsorption of B on clays in the alluvial aquifer. Vengosh and Keren (1996) found delayed arrival times of B relative to Cl migrating vertically through the unsaturated zone and suggested that cation-exchange reactions might control ion transport in groundwater. These authors conclude that once exchangeable and adsorbed sites are filled, B is no longer adsorbed and behaves conservatively like Cl.

The third mixing trend, illustrated best by the Brown School well, shows the B and Cl variation following the local mixing trend that suggests both ions are behaving conservatively. The decrease in concentrations is coincident with alluvial aquifer water level recovery in the study area and suggests that more non-thermal water is available for mixing.

Discharge area mixing

The close proximity of the Curti Domestic and Curti Barn Geothermal wells, located in the discharge area of the geothermal system, allows for evaluation of mixing relationships. The factor increase (Table 2) for each constituent (except for As) of the Curti Barn Geothermal well is nearly identical with the temperature factor increase suggesting a clear, uncomplicated mixing relation between thermal and non-thermal water. Because As concentrations are low, slight variability in As concentrations can lead to high variability in the factor increase. The Curti Domestic well shows an identical temperature factor increase to that of the Curti Barn Geothermal well but with greater and variable increases for each constituent suggesting non-thermal and thermal water mixing in this well. Since Cl acts conservatively in groundwater, the Cl concentration can be used to calculate the percentage of thermal water in the Curti Domestic well over time (Fig. 10). The percent of thermal water for each sample date was calculated assuming a constant non-thermal Cl concentration of 3 mg/L (average concentration in Peigh Domestic well) and the Cl concentration in the Curti Barn Geothermal well (660 to 844 mg/L). The percentage of thermal water in the Curti Domestic well ranges from 6 % to 44 % with a peak value in March 1993. A strong seasonal trend is evident with lower thermal input in the fall and greater percentages of thermal water in the spring. This trend shows an inverse relationship between groundwater recharge of non-thermal water and the percentage of thermal water in the Curti Domestic well. More non-thermal water is available for mixing in the fall due to groundwater recharge from irrigation in surrounding agricultural fields over the summer months. A similar relation between Cl and static water levels was attributed to groundwater recharge from irrigation (Yeamans, 1985). The overall trend shows an increase in the thermal water component over time suggesting that more thermal water is available due to shallow injection of spent fluid at geothermal power facilities.

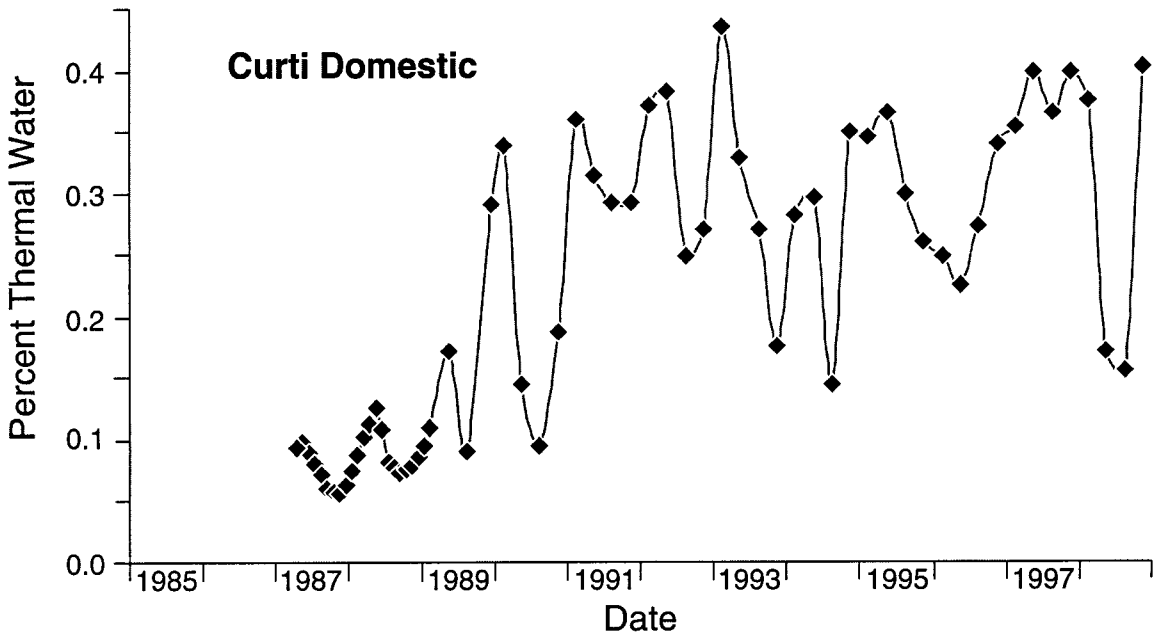

Figure 10. Percentage of thermal water over time in the Curti Domestic well.

CONCLUSIONS

B and Cl data for non-thermal, thermal, and mixed type waters fall along a common trend suggesting simple mixing of thermal and non-thermal waters and a common source of thermal water for both power plants. Three wells (Peigh, Curti Barn Geothermal, Herz Geothermal) show consistent B and Cl values over time. These wells represent type members of non-thermal, thermal, and mixed waters that are used for comparison with other wells. Temporal B versus Cl trends show strong mixing in the geothermal discharge area and along prominent north-trending faults (e.g. Herz Fault and Mud Volcano Basin Fault) that apparently connect the geothermal reservoir to the alluvial aquifer. Temperature and water level data provide supporting evidence for the timing of the mixing. Potential mechanisms for the initiation of changes in the proportions of thermal and non-thermal waters include: (1) increased groundwater extraction from alluvial aquifers for municipal water supply, thus reducing the available non-thermal component (eg. Herz Domestic and Pine Tree Ranch #1 wells); (2) water level declines because of decreased recharge due to reduced irrigation and below normal precipitation from 1986-94, also reducing the available non-thermal component (eg. Herz Domestic and Pine Tree Ranch #1 wells); and (3) injection of thermal waters in geothermal reservoir areas that may have greater connectivity to the alluvial aquifers than the extraction areas, increasing the thermal water component (e.g. Curti Domestic and Flame wells). Comparison of the Pine Tree Ranch #1 well with the Flame well illustrates that the amount of thermal water decreases with distance from a permeable fault. The Steinhardt well shows reduced thermal water component with time; cessation of municipal production of non-thermal water has likely increased the percentage of non-thermal water in the area. The calculated percent of thermal water in the Curti Domestic well in the geothermal discharge area shows a strong inverse relation with seasonal groundwater recharge (maximum recharge in the fall). The geothermal reservoir and the alluvial aquifer are hydraulically connected in at least some portions of the study area and fault-controlled flow apparently provides the connectivity.

Based on data discussed here, a number of faults that conduct thermal fluids from the geothermal system to the alluvial aquifer have been identified. Wells located near these faults respond to hydrologic changes to a greater degree than wells located between faults. Further delineation of these hydrologically significant faults, and identification of others, will allow for a better understanding of the connectivity of these two resources.

REFERENCES

Abbott, R.E., and Louie, J.N., 2000. Depth to bedrock using gravimetry in the Reno and Carson City, Nevada, area basins, Geophysics, 65(2), 340-350.

Bateman, R.L., Scheibach, R.B., 1975. Evaluation of geothermal activity in the Truckee Meadows, Washoe County, Nevada, Nevada Bureau of Mines and Geology, Rpt. 25, 38 p.

Bonham, H. F., Jr., and Rogers, D. K., 1983. Geologic map, Mt. Rose NE quadrangle: Nevada Bureau of Mines and Geol., Map 4Bg.

Bonham, H. F., Jr., and Bell, J. W., 1993, Geologic map, Steamboat quadrangle: Nevada Bureau of Mines and Geol., Map 4Fg.

Cohen, P., Loeltz, O.J., 1964. Evaluation of hydrogeology and hydrogeochemistry of the Truckee Meadows area, Washoe County Nevada, U.S. Geol. Surv. Water Supply Paper 1779-S, 63 p.

Cooley, R.L., Fordham, J.W., Westphal, J.A., 1971. Hydrology of Truckee Meadows, Nevada, Center for Water Research, Desert Research Institute, University of Nevada System, Project Rpt. 15, 49 p.

Desert Research Institute, 2000. Western Regional Climate Center, Western U.S. Climate Historical Summaries and SNOWTEL Data, World Wide Web Site, [On-line], Available at http://www.wrcc.dri.edu/.

DeRocher, T., 1996. Historical summary of Caithness Power, Inc., Hydrologic monitoring of the Steamboat Hills region, 1987-Present, draft unpublished report for Yankee/Caithness, 46 p.

Environmental Management Associates, 1993. Yankee/Caithnes Joint Venture, L.P. Steamboat Hills geothermal project, plan of operation/plan of utilization amendment for geothermal fluid rate increase, preliminary environmental assessment, unpublished report for Yankee/Caithness.

Flynn, T., Ghusn, G. Jr., 1984. Geologic and hydrologic research on the Moana geothermal system, Washoe County, Nevada, Division of Earth Sciences, UNLV report, 148 p.

Goldberg, S., Forester, H.S., Heick, E.L., 1993. Temperature effects on boron adsorption by reference minerals and soils. Soil Science, 156(5), 316-321.

Goranson, C., 1991. Summary and interpretation of six years of groundwater monitoring data and four years of geothermal production and injection well operations at the SB GEO, Inc. geothermal binary power plant, Steamboat Springs, Nevada. Prepared for SB GEO, Inc., 44 p.

Ingraham, N.L., Taylor, B.E., 1991. Light stable isotope systematics of large-scale hydrologic regimes in California and Nevada. Water Resources Research, 27(1), 77-90.

Lyles, B.F., 1985. Time-variant hydrogeologic and geochemical study of selected thermal springs in Western Nevada, unpublished M.S. Thesis, University of Nevada, Reno, 203 p.

Mariner, R.H., Janik, C.J., 1995. Geochemical data and conceptual model for the Steamboat Hills geothermal system, Washoe County, Nevada. Geothermal Resources Council Transactions, 19, 191-200.

Nehring, N.L., 1980. Geochemistry of Steamboat Springs, Nevada. U.S. Geol. Surv. Open-File Rpt. 80-887, 61 p.

Sorey, M.L., Colvard, E.M., 1992. Factors affecting the decline in hot-spring activity in the Steamboat Springs area of critical environmental concern, Washoe County, Nevada. U.S. Geol. Surv., Administrative Report for the Bureau of Land Management, 109 p.

Tabor, R. W., and Ellen, S., 1975, Geologic Map, Washoe City Folio: Nevada Bureau of Mines and Geol. Environmental Series.

Thompson, G.A., White, D.E., 1964. Regional geology of the Steamboat Springs area, Washoe County, Nevada: U.S. Geol. Surv. Prof. Paper 458-A, 52 p.

Vengosh, A., and Keren, R., 1996. Chemical modifications of groundwater contaminated by recharge of treated sewage effluent, Jour. of Cont. Hydrol., 23(4), 347-360.

van de Kamp, P.C., Goranson, C.B., 1990. Summary of the hydrological characteristics of the Steamboat Hills area, Nevada. Prepared for Caithness Power, Inc. and Yankee-Caithness Joint Venture, L.P.

White, D.E., Thompson, G.A., Sandberg, C., 1964. Rocks, structure and geologic history of the Steamboat Springs thermal area, Washoe County, Nevada: U.S. Geol. Surv. Prof. Paper 458-B, 63 p.

White, D.E., 1968. Hydrology, activity, and heat flow of the Steamboat Springs thermal system, Washoe Count, Nevada. U.S. Geol. Surv. Prof. Paper 458-C, 109 p.

Yeamans, F., 1985. Hydrology of Steamboat Springs geothermal system, 1984. Prepared for Philips Petroleum Company, 151 p.

Yeamans, F., 1988. Hydrogeology and water chemistry in the vicinity of Brown School, Steamboat, Nevada. Prepared for the Nevada Division of Environmental Protection and ORMAT Systems, Inc., 24 p.

CHAPTER 3

Gravity and Aeromagnetic Modeling of the Steamboat Hills Geothermal Area and Southern Truckee Meadows Alluvial Basins, Reno, Nevada

John D. Skalbeck, Robert E. Karlin, and Michael C. Widmer

ABSTRACT

Concurrent development and production of nearby geothermal and drinking water resources in the Steamboat Hills area, Nevada requires an understanding of the hydrogeologic connection between these two resources. The need to identify the structural controls for groundwater flow in this complex hydrogeologic setting prompted us to construct a detailed 3-D geologic model based on 2.75-D forward modeling of multiple gravity and aeromagnetic profiles constrained by geological and physical properties (density, magnetic susceptibility, remanent magnetic) data. Data along 11 profiles allow detailed modeling of alluvium, volcanic rocks, granodiorite, rhyolite intrusions, metamorphic rocks, and alteration zones. A 3-D representation of the geothermal reservoir, consisting of altered granodiorite and metamorphic rocks, suggests thermal water up-flows along a fault along the western flank of the Steamboat Hills. Northeast-trending faults distribute thermal water along the axis of the hills and connect the two producing geothermal fields. North-trending faults that conduct thermal water from the geothermal system to the alluvial aquifer appear to be zones of altered volcanics that produce subtle aeromagnetic anomalies. Our results can be used to develop a numerical model of groundwater flow for resource evaluation, plan exploration drilling for drinking water and geothermal wells, and evaluate fully 3-D forward gravity and magnetic modeling software.

INTRODUCTION

Most hydrogeologists rely on limited borehole logs (lithologic and geophysical) and surface geologic mapping for development of municipal well fields and/or construction of numerical models for flow and transport simulations. This requires correlating geologic units at large distances and assuming basement structure from sparse data. Some groundwater and water resources studies have used geophysical (gravity, magnetic, seismic) data to estimate basement structure (Blakely et al., 1998; Berger et al., 1996; Ayers, 1989; Haeni, 1986); however, limited data for model constraint may require simplification of the conceptual models. Blakely et al. (1998) used 3-D inversion of gravity data to delineate a topographically complex basement structure overlain by sedimentary and volcanic deposits in the Amaragosa Desert and Pahrump Valley, California and Nevada. The authors note that the limitations of gravity inversion are due to simplifying assumptions of the basin-basement model, data density variations, grid spacing, and the depth density function. Berger et al. (1996) used forward modeling of gravity and aeromagnetic data and seismic refraction surveys to estimate the thickness of basin fill in Spanish Springs Valley, Nevada. The non-unique forward modeling results for three profiles were constrained with well log data at only one or two locations. Seismic refraction and reflection (common-offset and common-depth-point) surveys used to map the bedrock surface beneath alluvial flood plain deposits of the Platte River in east-central Nebraska (Ayers, 1989). The author found that the reflection methods provided greater detail of the bedrock surface but requires more field time, data processing, and more complex interpretation. Haeni (1986) used seismic refraction methods to determine depth to the water table, saturated aquifer thickness, and depth to bedrock in glacial aquifers in New England. The author noted economical advantage for using this method to define hydrgeologic boundaries and outlined the limitations due to blind zones (thin intermediate seismic velocity refractors) and slow layers underlying high seismic

velocity layers. Assuming basement structure and simplifying the conceptual geologic model adds uncertainty to the simulation results and the accuracy of a groundwater model. We have incorporated potential fields (gravity and aeromagnetic data) modeling to obtain well-constrained results for estimating the structure of multiple geologic units within a complex hydrogeologic setting that includes both geothermal and potable water resources.

Rapid population growth across the western United States during the past decade has placed large demands on scarce water resources for municipal supply and, in some areas, geothermal water for electric power production and direct use thermal applications (e.g. space heating). In areas such as Steamboat Hills near Reno, the concurrent development of and competition between drinking water and geothermal water resources necessitates thorough understanding of the hydrologic communication between these two resources. The primary goal of this study is to develop a well-constrained model of the 3-D geologic structure in the Steamboat Hills area for evaluating the hydrologic connection between the fresh water and geothermal resources. This study presents a methodology for geologic modeling in a complex hydrogeologic setting by using potential fields data, surface and subsurface geology, and physical properties of rocks. The results of this study will serve as a framework for a numerical groundwater flow model and for planning exploration drilling. The results also suggest how to identify hydrologically significant faults that may facilitate communication between the two water resources.

Hydrogeologic Setting

The study area is located along the western margin of the extensional Basin and Range province in the western United States. The Steamboat Hills are a topographically prominent northeast-trending bedrock ridge that represents the southern extent of the fault-bounded Truckee Meadows basin, which contains the cities of Reno and Sparks approximately 15 km north of Steamboat Hills (Figure 1). The study area is bordered on the west by the Carson Range of the Sierra Nevada Mountains and on the east by the Virginia Range.

The geology of the area has been described by White et al. (1964), Thompson and White (1964), Tabor and Ellen (1975), Bonham and Rogers (1983), Bonham and Bell (1993), and Stewart (1999). A simplified geologic map is presented in Figure 2. The core of these ranges consists of Cretaceous granodiorite (*Kgd*) beneath older metasedimentary and metavolcanic rocks (*pKm*), that in turn are overlain by Tertiary volcanic flows, breccias, and tuffs (*Tv*). A veneer of Quaternary alluvial fan and basin deposits (*Qal*) range from clayey sand to boulder gravels. The *Qal* deposits and *Tv* rocks are the primary source of water supply for Washoe County and private residences in the southern Truckee Meadows. At least three prominent fault systems trending north-south, northeast-southwest, and northwest-southeast (White et al., 1964) are found in the study area. A series of five Pleistocene rhyolite domes (*Qsh*) that occur along the northeast-southwest fault trend are dated at 1.2 my (Silberman et al., 1979). The Steamboat Hills geothermal field occurs predominantly along this same northwest-southeast trending faults within the *Kgd* and *pKm* rocks. Thin surface deposits of silica sinter (*Sr*) are associated with the geothermal discharge area near the Steamboat Springs Fault System along the east flank of Steamboat Hills. White et al. (1964) and Silberman et al. (1979) associate the hydrothermal activity at Steamboat Springs with the magma that supplied the Pleistocene eruptions that created

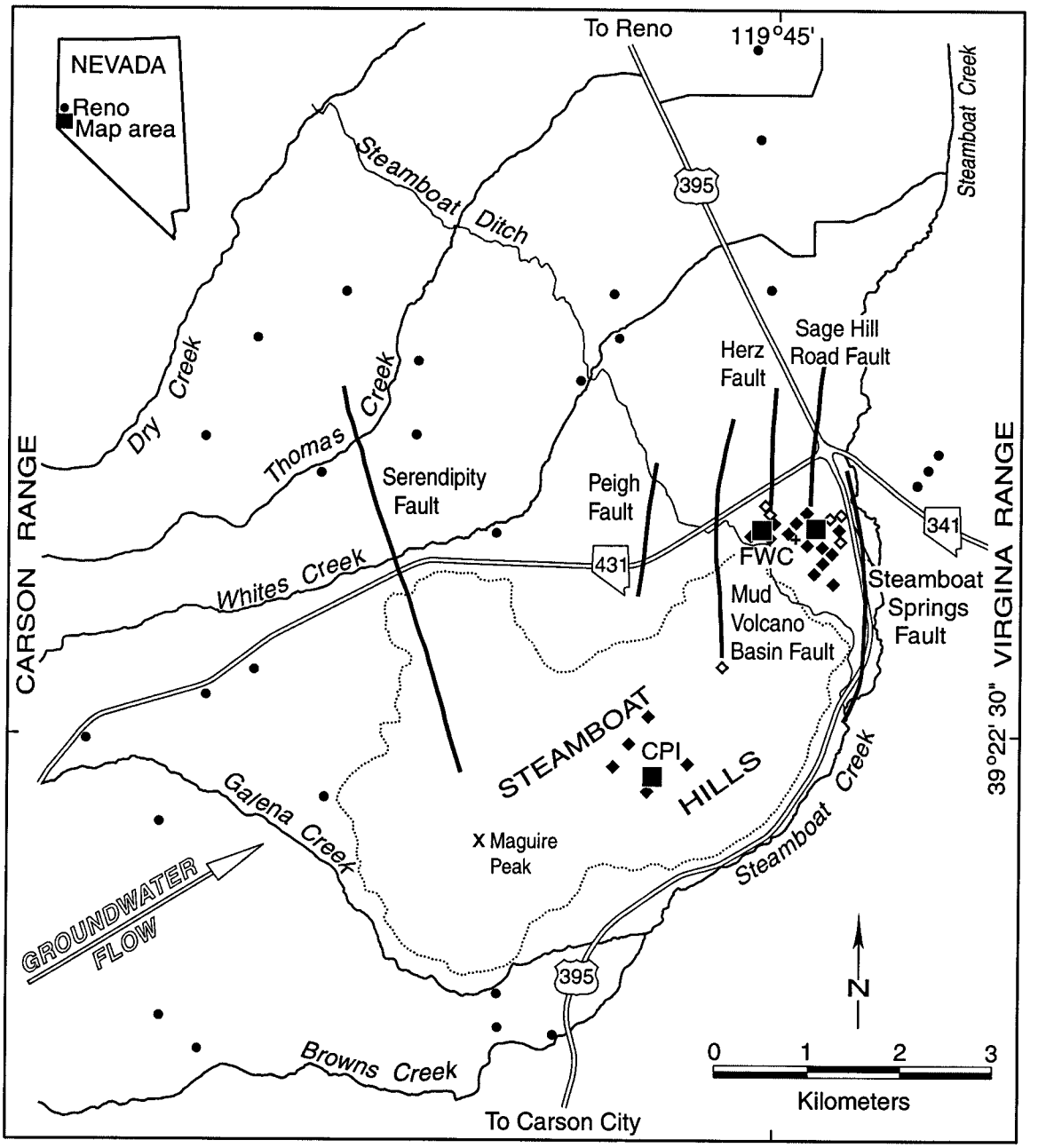

■ Geothermal power plant; CPI: Caithness Power Inc.; FWC: Far West Capital
◆ Geothermal Production well
◇ Geothermal Injection well
• Municipal water well

Figure 1. Location map of the southern Truckee Meadows and Steamboat Hills area, Washoe County, Nevada. Delineation of faults is an interpretation by the author, modified from Bonham and Rogers (1983).

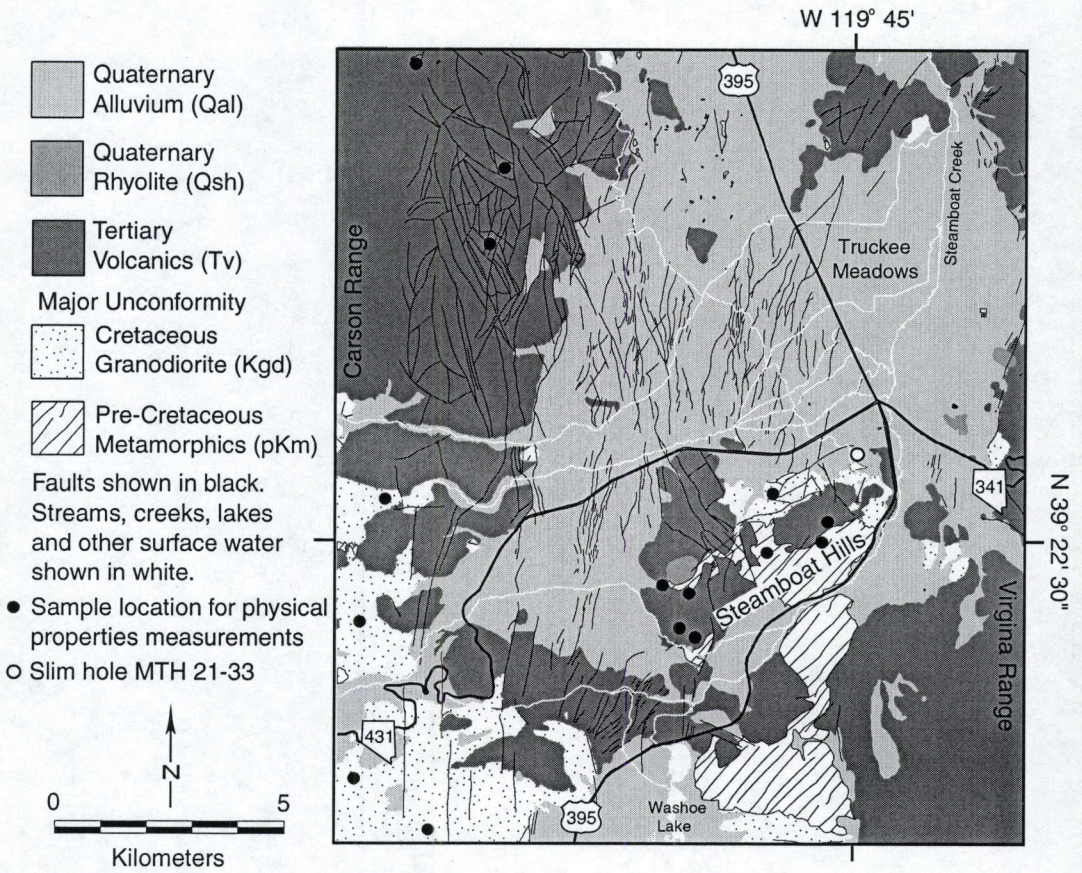

Figure 2. Generalized geologic map modified from Bonham and Rogers (1983), Bonham and Bell (1993) and Tabor and Ellen (1975). Map shows geologic contacts used for horizontal control of geologic blocks in 2.75-D forward models and sample locations for physical properties measurements (Table 2).

the rhyolite domes. Table 1 presents the abbreviations used for these geologic units throughout the paper.

Table 1. Abbreviations for geologic units at Steamboat Hills, Nevada.

Geologic Unit	Abbreviation
Quaternary silica sinter	*Sr*
Quaternary alluvium	*Qal*
Pleistocene rhyolite domes	*Qsh*
Tertiary volcanic rocks	*Tv*
Cretaceous granodiorite	*Kgd*
Pre-Cretaceous metamorphic rocks	*pKm*

Note: Altered geologic units preceded with *Alt.*

Groundwater originates primarily from snowmelt infiltration in the Carson Range and flows eastward toward Steamboat Creek (Cohen and Loeltz, 1964). Depths to groundwater range from around 80 m near the center of the alluvial fan to land surface at Steamboat Springs. Sorey and Colvard (1992) note that similarities in chemical characteristics and decreases in hydraulic head suggest that the geothermal reservoir and alluvial aquifer are hydrologically connected. Using mixing trends between thermal and non-thermal waters within the alluvial aquifer, Skalbeck et al. (2001) found hydraulic connection of the drinking and geothermal water resources along north-trending faults. These north-trending faults provide preferential flow for thermal water toward the north.

Previous Studies Using Potential Fields Modeling

A number of recent publications illustrate the application of potential fields modeling for a variety of geologic studies. Berger et al. (1996) used 2-D forward modeling of magnetic and gravity data along 3 profiles to obtain basin-fill thickness as part of a numerical groundwater model of Spanish Springs, Nevada. Mankinen et al. (1999) constructed 2.5-D forward and inverse models of gravity and aeromagnetic data for 13 profiles in the Pahute Mesa and Oasis Valley Region, Nevada to provide information for groundwater models of the Nevada Test Site. Blakely and Stanley (1993) modeled a profile of gravity and aeromagnetic data using 2-D forward and inverse techniques to assess the possible presence of a partial melt magma chamber at Geysers geothermal area. In assessing heat sources in the Geysers-Clear Lake geothermal area, Stanley and Blakely (1995) modeled a profile of gravity and aeromagnetic data using 2.5-D forward and inverse techniques. Langenheim and Hildenbrand (1997) constructed 2.5-D inverse models of two gravity and aeromagnetic profiles to evaluate the Commerce geophysical lineament, extending from central Arkansas to southern Illinois. Zeng et al. (2000) used 2-D forward modeling of gravity data to evaluate emplacement mechanisms of the Linglong granitic complex in the Shandong Province of east China. As part of a seismic hazard evaluation of basins in the Reno and Carson City, Nevada area, Abbott and Louie (2000) constructed a 2.5-D forward model of residual gravity from a profile located approximately 10 km north of the Steamboat Hills area and tied it into a basin-wide gravity analysis.

To our knowledge, this is the first use of multiple 2.75-D forward model profiles of gravity and aeromagnetic data to obtain a 3-D representation of pertinent geologic units within a geothermal system. These model profiles are highly constrained by geologic and physical

properties measured within the study area. We model asymmetric strike lengths about the profile (2.75-D) based on mapped geology rather infinite strike lengths (2-D) and we include remanent magnetization data from the study area in addition to induced magnetization to represent the total magnetic field.

METHODS

Potential fields modeling provides non-unique solutions since numerous different model geometries and assigned physical properties can produce fields that closely match the observed anomalies. For example, decreasing the model's density contrast between alluvium and bedrock, and increasing the depth to bedrock could both produce a computed field similar to the previous configuration. However, geologic insight and additional geological and geophysical data can more realistically constrain models. Forward modeling of gravity and aeromagnetic data with input of physical property data (density, magnetic susceptibility, and remanent magnetic measurements), surface geology, and subsurface geology from well logs greatly constrains possible interpretations of the subsurface structure in the Steamboat Hills area. The following section describes the origin of the gravity, aeromagnetic, and physical properties data and the forward modeling methodology.

Gravity Surveys

Gravity data at 166 stations from a study (Carpenter, 1996) contracted by Washoe County Department of Water Resources (Washoe County) was merged with existing gravity coverage (Hittelman et al., 1994) for total coverage that included 503 points. Nearest neighbor distance between stations ranged from 100 to 4000 m. Figure 3 shows the northern portion of the residual isostatic gravity contour map derived from minimum curvature gridding (Briggs, 1974). Values for each forward model profile were extracted at 300 m intervals from the gridded data along aeromagnetic flight lines.

Aeromagnetic Survey

Washoe County contracted a draped airborne geophysical survey consisting of 41 helicopter flight lines oriented at N45W with 609 m spacing and 3 tie lines oriented at N20E with about 5000 m spacing (DIGHEM, 1994). A cesium vapor magnetometer was towed 20 m below the helicopter and draped above ground surface at heights of 30 to 120 m. The total field data were International Geomagnetic Reference Field (IGRF) corrected using the IGRF95 model (IAGA Division V, Working Group 8, 1995), minimum curvature gridded (Briggs, 1974), and reduced-to-pole using a 2-D fast fourier transform algorithm (Figure 4). A 10 factor decimation of the aeromagnetic data resulted in 40 to 60 m data spacing for the 11 profiles that replicates the full data set.

Physical Properties

Physical property data used in modeling were obtained from published data and laboratory measurements in the study. Fifty-eight hand samples and 36 paleomagnetic core samples of altered and unaltered volcanic rocks, altered and unaltered granodiorite, and metamorphic rocks were collected from the Steamboat Hills and the adjacent Carson Range (Figure 2). Densities, magnetic susceptibilites, and remanent magnetic (direction and intensity)

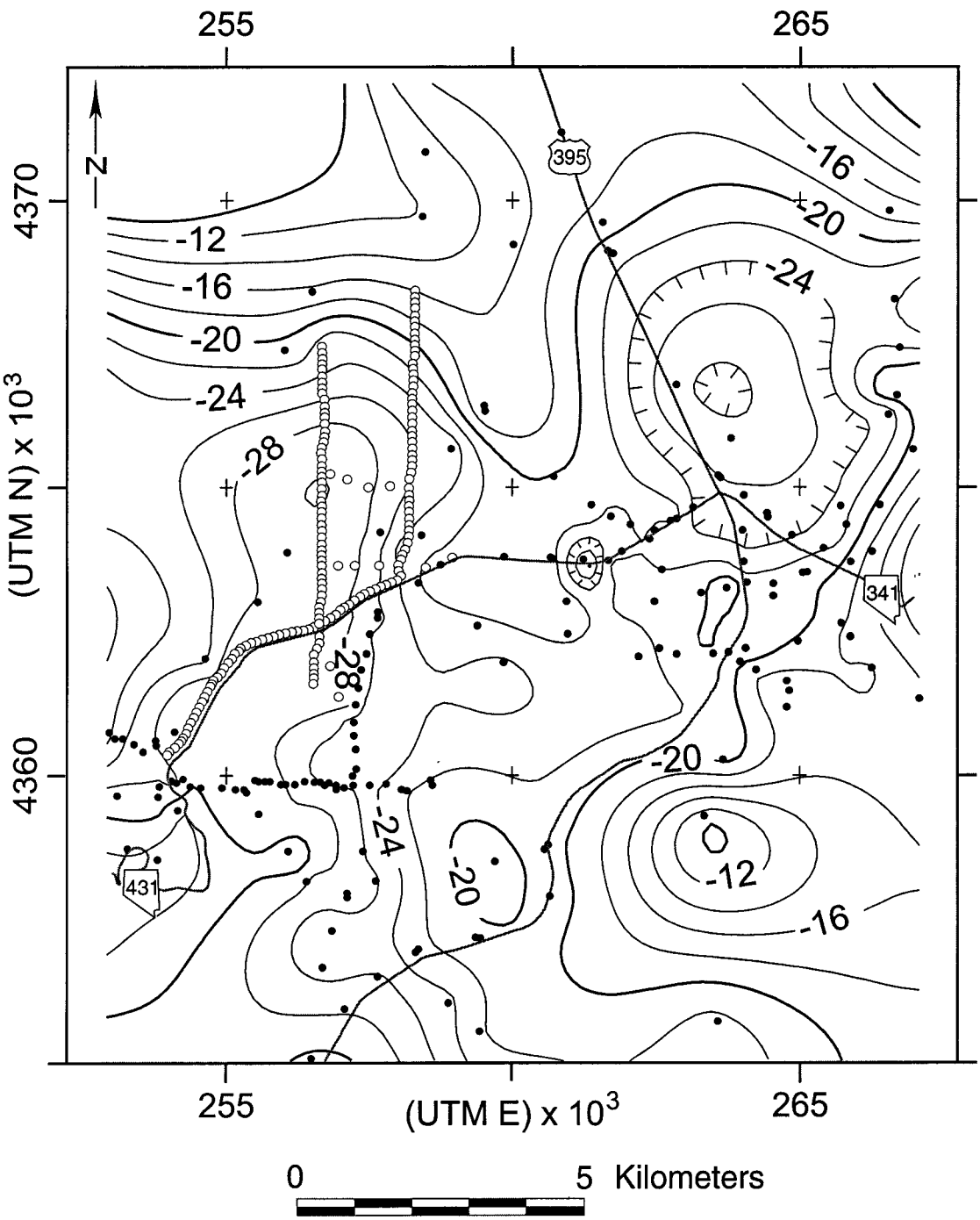

Figure 3. Residual isostatic gravity map of southern Truckee Meadows and Steamboat Hills. Open circles are stations from Carpenter (1996) and closed circles are from Hittelman et al. (1994). Contour interval is 2 mGal.

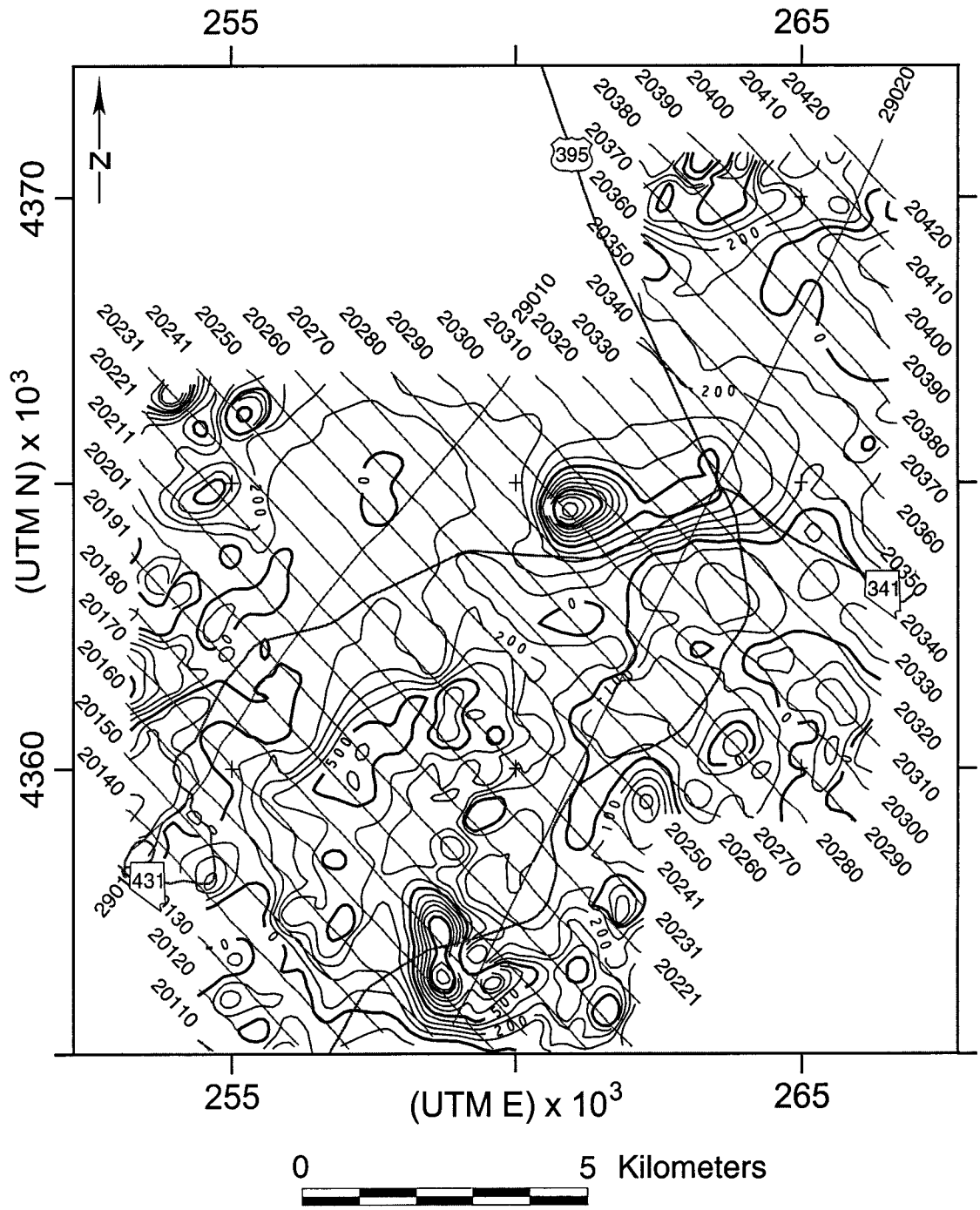

Figure 4. Residual reduced-to-pole aeromagnetic map of southern Truckee Meadows and Steamboat Hills shown with helicopter flight lines. Contour interval is 100 nT.

measurements were made using standard methods at UNR laboratories (Skalbeck, 1998). Whole core magnetic susceptibility for altered granodiorite was measured on 155 m (61 to 216 m depth) of rock from core hole MTH 21-33 drilled in the Far West Capital (FWC) area of the Steamboat Hills geothermal reservoir. Density and magnetic susceptibility results from this study compare closely with published density data (Thompson and Sandberg, 1958; Thompson and White, 1964; Krank and Watters, 1983) and magnetic susceptibility data (Hendricks, 1992) obtained regionally (Table 2). The results of remanent magnetic measurements provide confirmation of antipodal (south- and north-seeking) directions in volcanic rocks and provided constraint for assigning remanent magnetization intensity in the forward models.

2.75-D Coupled Gravity and Aeromagnetic Modeling

The 2.75-D coupled forward modeling of gravity and aeromagnetic data on ten N45W and one N20E oriented profiles (Figure 5) was done using the commercially-available modeling program (GM-Sys™ by Northwest Geophysical Associates) based on Talwani et al. (1959) and Talwani and Heirtzler (1964). A 2.75-D model better represents the off-profile geology with variable strike lengths than a 2-D model (infinite strike length) and a 2.5-D model (symmetric strike length about the profile). Model block strike lengths were extended perpendicular to the profile based on the mapped geology. The perpendicular strike orientation was chosen based on the local structural trend. Density and magnetic properties within a given model block were assumed constant.

The mapped surface geology provides horizontal control of geologic blocks and was strictly honored for all profiles. Well log data from domestic, Washoe County, and geothermal wells (Table 3 and Figure 5) provided vertical control of geologic blocks; however, strict adherence to this vertical data proved somewhat subjective because of the projected distance of wells to model profiles. Data from wells located near a profile were weighted more heavily than from wells located further from a profile.

A large number of iterative adjustments to geologic block configuration, density, and magnetic properties were made to minimize the root mean square error (RMSE) between observed and calculated gravity and aeromagnetic anomalies. Care was taken to maintain reasonable consistency of density and magnetic properties from profile to profile. Additionally, a N20E profile (29020) served as a "tie line" between the N45W profiles. By experimentation and experience from previous modeling of aeromagnetic data in the Galena Fan area (Karlin, 1996), models were judged acceptable when the percent RMSE (%RMSE; [RMSE/anomaly range]) was below 5% for gravity and 10% for aeromagnetic data. The tie line was an exception because its fit resulted in a 6.4 %RMSE. Less than perfect fits can be attributed to cultural noise, surface weathering of rocks, heterogeneity of physical properties, and off-axis (3-D) effects.

Constant density and magnetic properties for *Qal*, *Kgd*, and *Sr* are assumed in all models. Since the *Tv* and *pKm* units included a range of rock types, variations in density and magnetic properties were allowed for these units. North-seeking (reversed) remanent magnetization was assigned only when south-seeking (normal) remanent magnetization could not reproduce the observed aeromagnetic anomaly. Remanent magnetization measurements of *Tv* samples support using both normal and reverse directions for this unit. Altered granodiorite (*Alt Kgd*) and *pKm* were modeled to represent the geothermal reservoir, and the overlying altered Tertiary volcanics (*Alt Tv*) were assumed to represent the geothermal reservoir cap rock. Vertical fault zones in volcanic rocks known to conduct thermal water from the geothermal reservoir to the alluvial

Table 2. Summary of physical properties measurements, published data, and values used in 2 3/4-D forward models.

Mean Physical Properties Measurements Steamboat Hills and Carson Range				Density[1,2,3] and k[4] From Previous Studies Near the Study Area			Density and Magnetic Properties used in 2 3/4-D Forward Models		
Rock Type	Number of Samples	Density Range (g/cm^3)	Mean Density (g/cm^3)	Number of Samples	Density Range (g/cm^3)	Mean Density (g/cm^3)	Density Range (g/cm^3)		
Qal	NA	NA	NA	NA	NA	NA	(1.97)[5]		
Sr	1	NA	1.94	NA	1.32 - 2.56	2.02	1.97		
Tv	15	2.22 - 2.69	2.49	38	1.84 - 2.69	2.42	2.27 - 2.47		
Kgd	8	2.55 - 2.84	2.72	11	2.62 - 2.73	2.67	2.67		
pKm	3	2.61 - 2.78	2.71	6	2.69 - 2.75	2.69	2.57 - 2.77		
Alt Tv	NA	NA	NA	21	2.07 - 2.72	2.50	2.42		
Alt Kgd	1	NA	2.52	6	2.46 - 2.62	2.55	2.52		
Rock Type	Number of Samples	k Range (SI x 10^3)	Mean k (SI x 10^3)	Number of Samples	k Range (SI x 10^3)	Mean k (SI x 10^3)	k Range (SI x 10^3)	M_r Range (A/m x 10^3)	Q Range
Qal	NA	NA	NA	NA	NA	NA	0	0	NA
Sr	NA	NA	NA	NA	NA	NA	0	0	NA
Tv	14	8 - 25	20	13	NA	16	13 - 38	1000 - 9000	1.2 - 7.3
Kgd	8	6.3 - 32	22	3	NA	38	23	74	0.1
pKm	3	0.2 - 21	7.2	3	NA	0.6	1.3 - 13	10 - 1700	0.2 - 4.7
Alt Tv	5	0.02 - 0.03	0.025	NA	NA	NA	0.025	4	3.9
Alt Kgd	1	NA	0.1	3	NA	0.3	NA	NA	NA
Alt Kgd (c)	See Notes	-0.2 - 35	5.9	3	NA	0.3	5.9	20	0.1

Notes:
Qal: Alluvium, Sr: Sinter; Tv: Volcanics; Kgd: Granodiorite; pKm: Metamorphics; Alt: Altered
k: Magnetic susceptibility
NA: Not measured, not available, or not applicable
Alt Kgd (c) k values: From core of MTH 21-33, 1 cm intervals from depth of 61 to 216 m.
M_r: Remanent magnetization
Q : Koenigsberger ratio, Q = Remanent magnetization / Induced magnetization

1: Thompson and Sandberg (1958)
2: Thompson and White (1964)
3: Krank and Watters (1983)
4: Hendricks (1992)
5: Grant and West (1965, p. 200)

Table 3. Well data used in 2.75-D forward models and 3-D model depth to bedrock.

No. on Figures 5-11	Profile No.	Well Name	Surface Geology	Surface Elevation (m)	Depth to Tv (m)	Depth to Kgd (m)	Depth to pKm (m)	Total Well Depth (m)	3-D Model Depth to Bedrock (m)	Reference
1	20170	SJ-1	Qal	1737	90			110	60	PN 59330
2	20170	SJ-2	Qal	1747	52			183	40	PN 59631
3	20191	SJ-MW2	Qal	1662	70			195	65	PN 59303
4	20191	SJ-MW1	Qal	1662	79			240	70	PN 59632
5	20191	MR-5	Qal	1765	172			242	175	PN M/O-334
6	20191	MR-6	Qal	1770	192			231	180	PN 65364
7	20211	MR-3	Qal	1652	67			104	65	PN 35149
8	20211	ST-12	Tv	1626			390	539	0	NA
9	20211	Tessa 1	Qal	1763	73			242	75	PN 61267/61268
10	20231	Tessa 2	Qal	1715	79			224	80	PN 61269/61270
11	20231	ST-7	Qal	1429	65		414	506	55	21772
12	20250	AC-3	Qal	1732				335	320	PN 43607
13	20270	AC-2	Qal	1638				216	200	PN 35159
14	20270	STM-PW4	Qal	1579	43	98		253	45	LN 22665
15	20270	STM-TH10	Qal	1600	30	165		215	25	NA
16	20270	ST-5	Qal	1525		113		518	110	LN 21795
17	20270	ST-6	Qal	1513			18	515	15	LN 21768
18	20270	32-5	pKm	1650				897	0	NA
19	20270	28-32	Tv	1713		30		805	20	NA
20	20290	STM-MW1	Qal	1528	164			189	180	NA
21	20290	AC-1	Qal	1556	149			233	150	PN 57160
22	20290	COXI-1	Tv	1497		25		1058	0	LN 22782
23	20310	GS-5	Sr/Qal	1423	41	166		175	25	White et al., 1964
24	20310	IW-3	Sr/Qal	1433	69	152		158	15	NA
25	20310	Old IW-1	Qal	1432	53	213		499	45	NA
26	20310	PTR-2	Qal	1423	21	51		132	25	LN 4532
27	20310	STM-MW3	Qal	1439	122			134	135	PN 47066
28	20310	STM-PW3	Qal	1444				207	185	LN 2571
29	20310	STM-PW11	Qal	1469				156	200	PN 65080
30	20330	Herz Domestic	Qal	1386				34	170	4061
31	20330	Brown School	Qal	1387				116	165	NA
32	20330	Steinhardt	Qal	1387				41	170	NA
33	20350	ST-1	Qal	1371	70			599	115	LN 21792
34	20350	DD-1	Qal	1370				130	150	NA
35	29020	ST-13	Tv	1608			17	520	0	LN 23431
36	29020	21-5	Sr	1682	49	893	100	930	0	LN 21769
37	29020	GS-7	Sr	1622	77	100		122	0	White et al., 1964
38	29020	GS-6	Sr	1534		30		289	0	White et al., 1964
39	29020	PW-1	Sr	1453	28	54		64	0	NA
40	29020	IW-2	Sr	1432	88	149		427	15	NA
41	29020	ST-9	Tv	1549		29		289	0	NA

Qal: alluvium, Sr: sinter; Tv: volcanics; Kgd: granodiorite; pKm: metasediments and metavolcanics.
Reference: LN refers to DWR log number; PN refers to DWR permit number;
NA: No DWR log number or permit number indicated on log; DWR: State of Nevada, Division of Water Resources.

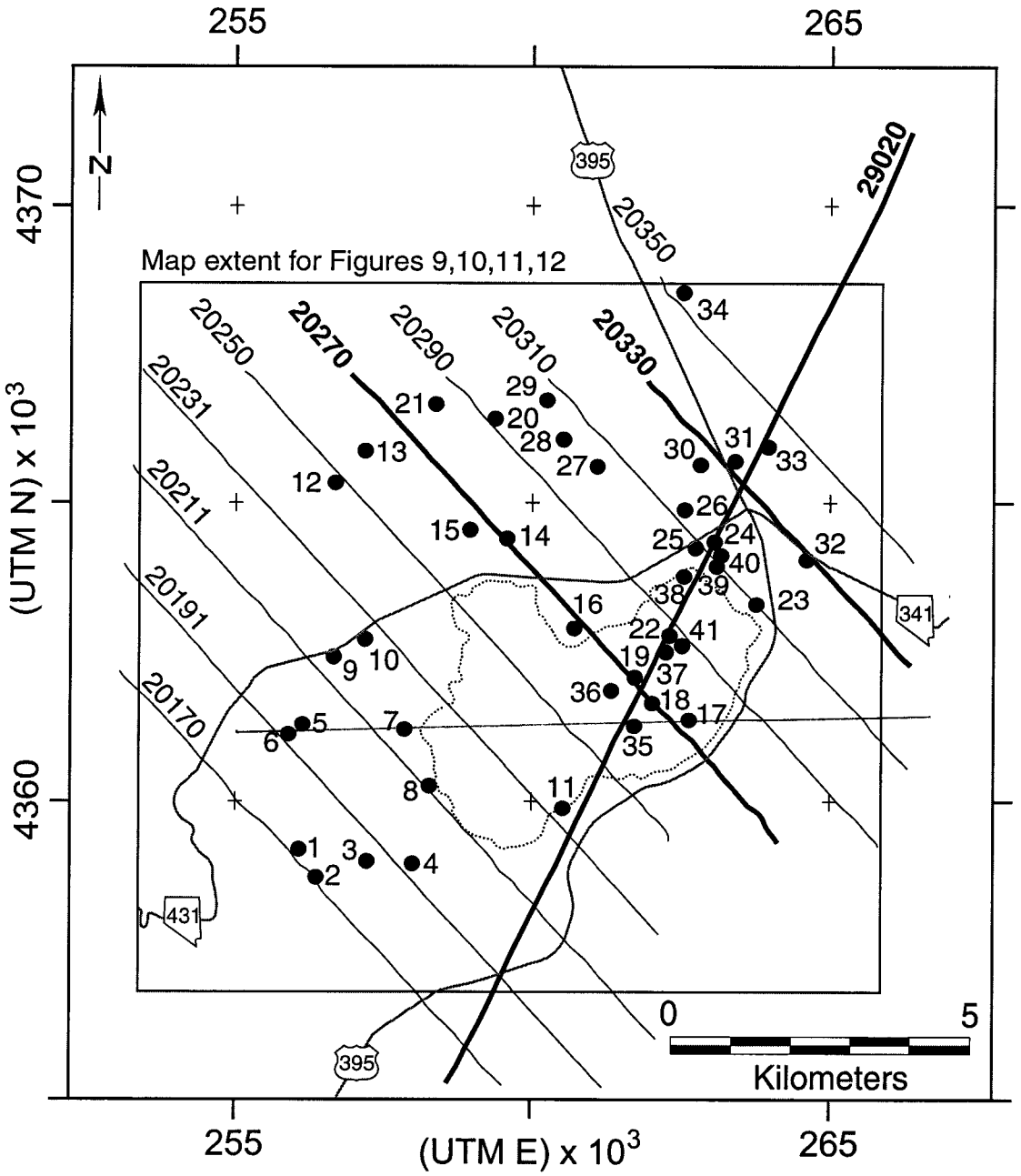

WELL IDENTIFICATION						
1 SJ-1	7 MR-3	13 AC-2	19 28-32	25 Old IW-1	31 Brown Sch	37 GS-7
2 SJ-2	8 ST-12	14 STM-PW4	20 STM-MW1	26 PTR-2	32 Steinhardt	38 GS-8
3 SJ-MW2	9 Tessa 1	15 STM-TH10	21 AC-1	27 STM-MW3	33 ST-1	39 PW-1
4 SJ-MW1	10 Tessa 2	16 ST-5	22 COXI-1	28 STM-PW3	34 DD-1	40 IW-2
5 MR-5	11 ST-7	17 ST-6	23 GS-5	29 STM-PW11	35 ST-13	41 ST-9
6 MR-6	12 AC-3	18 32-5	24 IW-3	30 Herz Dom	36 21-5	

Figure 5. Map showing locations of forward model profiles and of wells used for vertical control of geologic blocks in forward models. Table 3 provides data for wells. Bold profiles (20270, 20330, 29020) indicate profiles discussed in text (Figures 6, 7, 8). Other profiles are discussed in Chapter 2.

aquifer (Skalbeck et al., 2001) were modeled as zones of *Alt Tv* based on the hypothesis that the thermal water produced thermochemical alteration of magnetic minerals in the rock near the fault. Top and base elevations for each geologic unit were extracted at 300 m intervals along the 10 northwest-southeast model profiles for the 3D modeling. These data, combined with the surface elevation data, were computed by kriging (Cressie, 1990) to obtain bedrock surface elevation, *Qal* thickness, *Tv* thickness, *Alt Kgd* and *pKm* thickness, and *Kgd* depth.

Qualitative sensitivity analysis indicates that for model depths less than 300 m, a 5 m change in depth is needed to significantly influence the RMSE. The models were found to be sensitive to 10 m depth changes for depths between 300 and 1000 m and to 20 m depth changes for depths greater than 1000 m.

RESULTS

2.75-D Models of Selected Profiles

Of the 11 profiles modeled in this study, Profiles 20270, 20330, and 29020 are described here to highlight key features within the study area. The upper portion of each figure shows the aeromagnetic data while the center section shows the gravity data. The lower section illustrates the geologic model where the horizontal distances are relative to the northwest end of the profile and elevations are relative to mean sea level.

Profile 20270 (Figure 6) crosses the Washoe County drinking water production field in the Mount Rose Fan alluvial basin, the production area of the CPI geothermal field located at the crest of the Steamboat Hills, and the southern extent of Steamboat Valley. An acceptable fit for gravity (%RMSE of 4.8%) and a good fit for aeromagnetic data (%RMSE of 7.8%) were obtained for this model. Excellent vertical geologic control data are provided from 6 wells (Table 3). *Qal* and the underlying *Tv* show maximum thickness of 190 m and 370 m, respectively, near distance 2350 m. Shallow *Tv* creates two sub-basins in the alluvial fan near well STM-TH10 where *Qal* thickness is 30 m and *Tv* thickness is 135 m. An intrusive body with slightly higher density (2.75 g/cm^3) and magnetic susceptibility (0.038 SI) than *Kgd* is modeled at distance 3900 m to account for local gravity and aeromagnetic anomalies. In well ST-5, 113 m of *Qal* overlies *Kgd* suggesting faulting and erosion eliminated *Tv* in this area. *Alt Kgd* is projected to a depth of 2750 m in the CPI geothermal field near wells 28-32 and 32-5 on this profile although the model lacks resolution to confirm this depth. This zone lies between two apparent southeast dipping faults bracketing a mapped fault that may be a splay of the Steamboat Springs Fault system. The *pKm* shows reverse remanent magnetization and a maximum thickness of 2700 m near well ST-6. *Tv* underlies the entire valley with maximum model thickness of 350 m. The *pKm* at the southeast end of the profile contains two blocks of different density (2.62 and 2.77 g/cm^3) to accommodate the observed anomaly.

Profile 20330 (Figure 7) is located in the northeast portion of the study area. The model for this profile provides a good fit for gravity with a %RMSE of 4.0% and an excellent fit for aeromagnetic data with a %RMSE of 2.6%. The minimum thickness of *Qal* in the center of the model is constrained by the total depth data from three domestic wells that did not encounter volcanics (Table 3). The maximum *Qal* thickness of 280 m is between the Herz domestic well and the Herz Fault (Figure 1). The underlying *Tv* has a maximum model thickness of 1820 m including 250 m of *Alt Tv*; the model is not constrained at this depth. Local undulations of the Tv upper surface produce a good fit for the aeromagnetic low anomaly located over the Herz Fault. A smaller aeromagnetic low anomaly over the Sage Hill Road Fault (Figure 1) is also

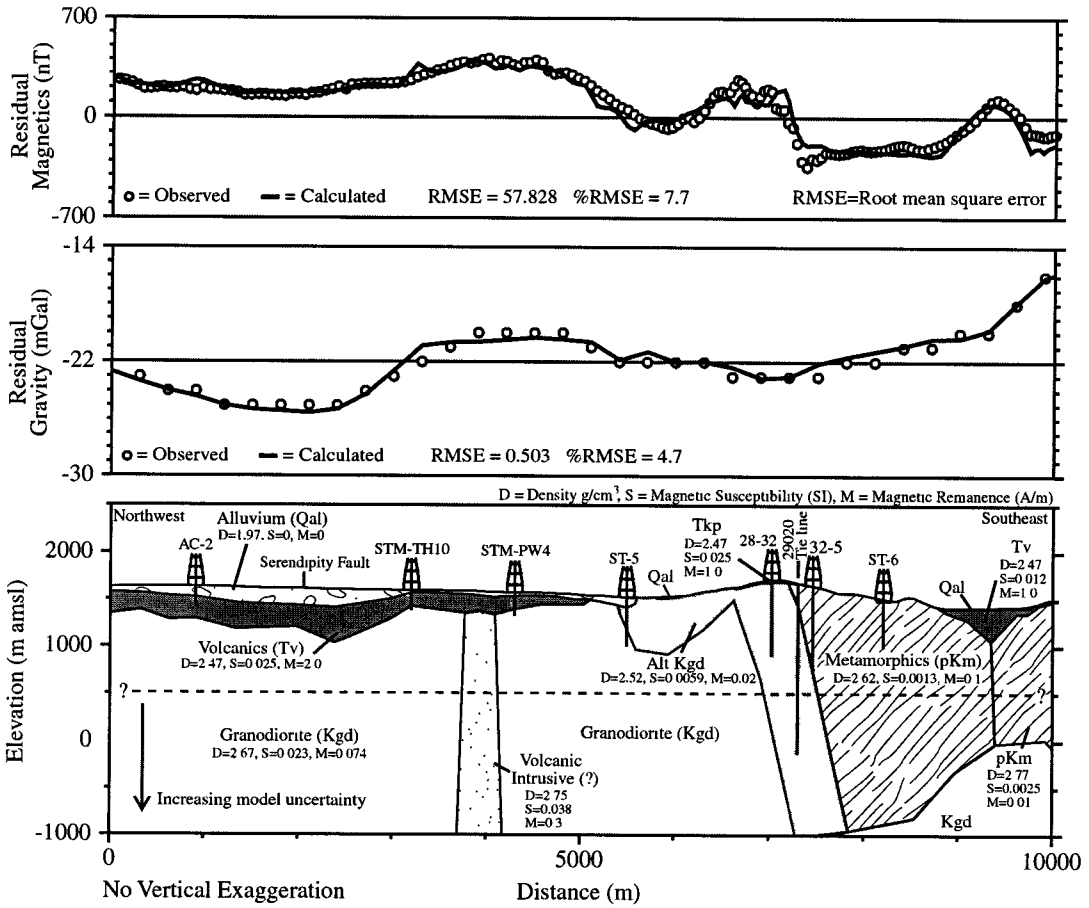

Figure 6. Profile 20270 cross-section as computed by 2.75-D forward modeling of gravity and aeromagnetic data.

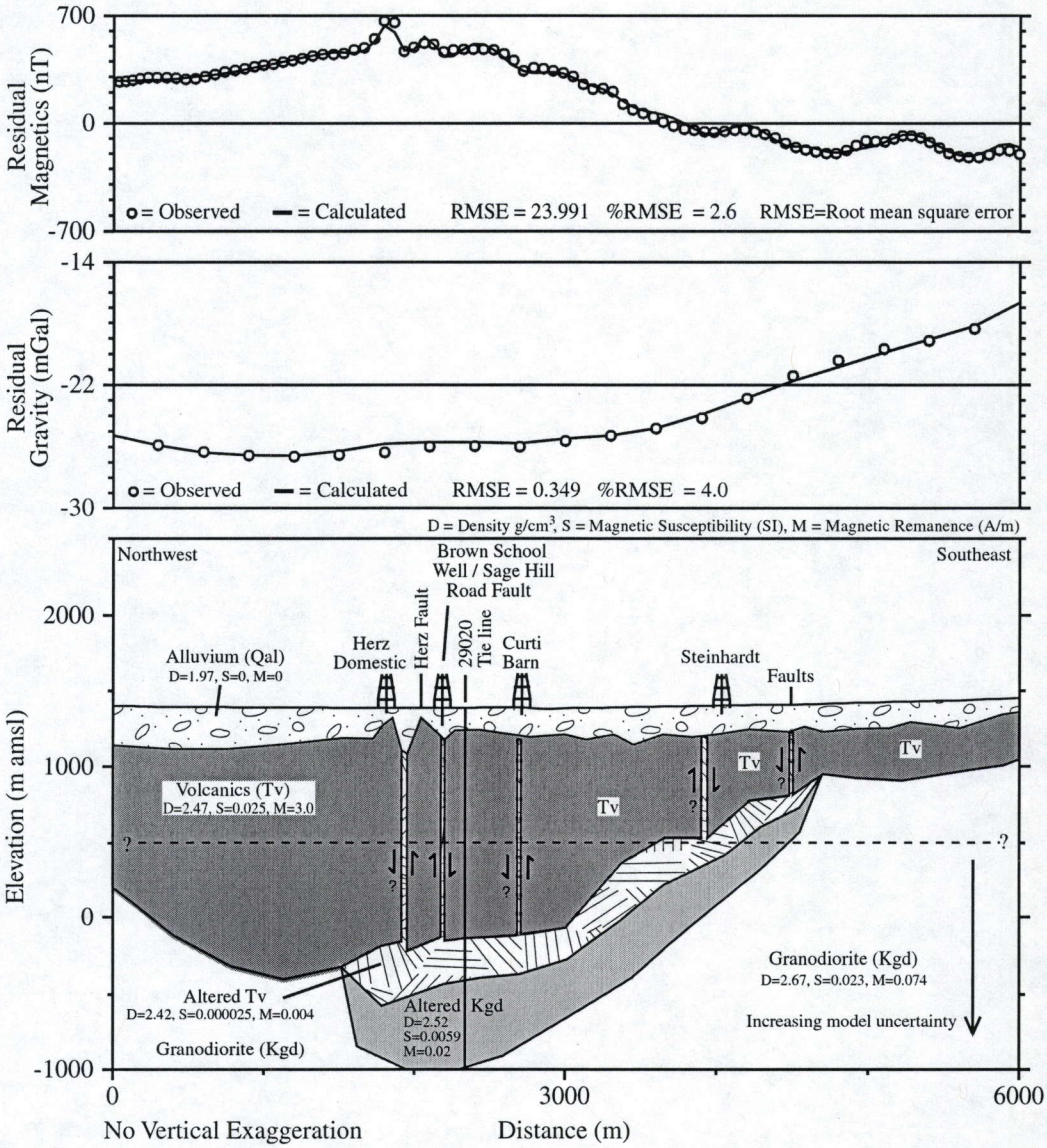

Figure 7. Profile 20330 cross-section as computed by 2.75-D forward modeling of gravity and aeromagnetic data.

reproduced by the model. Thermal water is known to migrate along the Herz and Sage Hill Road Faults and is also known to exist in the Curti Barn and Steinhardt domestic wells, which are both completed in the alluvial aquifer (Skalbeck et al., 2001). Subtle aeromagnetic low anomalies near these two wells are modeled as vertical zones of *Alt Tv* to represent faults that conduct thermal water. A group of mapped faults, located southeast of the Steinhardt domestic well, also correlates with a aeromagnetic low and is modeled as a vertical zone of *Alt Tv*.

Profile 29020 (Figure 8) is the "tie line" that trends SW/NE and intercepts each of the profiles in the study area. This profile begins in the southern Washoe Valley extends across Washoe Lake, eastern Steamboat Hills, and into southern Truckee Meadows. This model represents a good fit for aeromagnetic data with a %RMSE of 7.7% but the fit for gravity with a %RMSE of 7.5 is outside the target value of 5.0%. The majority of error in the gravity fit occurs from Washoe Hill (distance 12000 m) to the crest of Steamboat Hills (distance 17700 m) where very few gravity stations exist. Excellent vertical geologic control exists for this profile with data from 7 wells (Table 3). Five of these wells (21-5, GS-7, PW-1, IW-2, IW-9) provide data control on the depth to *Tv* and *Kgd*. Wells 21-5 and ST-13 include depth to *pKm* and well GS-6 includes depth to *Kgd*. In Washoe Valley, the gravity and magnetic low anomalies are nicely modeled by a deep basin of *Qal* (900 m) and thick unit of *Tv* (1300 m) with reverse remanent magnetization that occur within a depression of *Kgd*. Although not visible in the figure, Washoe Lake is modeled at the surface with assumed density of 1.0 g/cm3, magnetic susceptibility of zero, and average depth of 5 m. The prominent magnetic high and gravity high anomalies near Profile 20170 (distance 11000 m) are modeled by shallow depth to *Tv* with normal remanent magnetization underlain by *pKm*. The *Tv* outcrop at Washoe Hill and underlying *pKm* and *Alt Kgd* rest on a structural high of *Kgd*. The *Tv*, *pKm* and *Alt Kgd* reach maximum thickness for this area near the southern extent of Pleasant Valley. The magnetic anomaly is modeled well for this area but the gravity anomaly, as described above, is not well modeled. Sparse gravity data in this area of the Steamboat Hills likely contributes to the poor model fit. The thickest unit of the *Alt Kgd* (2000 m) is found beneath Steamboat Hills and this portion of the model provides a reasonable fit to the gravity data but a marginal fit to the aeromagnetic data. The thick unit of *Tv* (1950 m) beneath the southern Truckee Meadows modeled within a structural depression of *Kgd* nicely fits the gravity low and magnetic high anomalies.

3-D Geometry of Geology

The *Qal* thicknesses derived from the forward models (Figure 9), superimposed on a USGS 30-minute digital elevation model, indicate that the alluvial deposits surrounding Steamboat Hills originate predominately from the Carson Range. The Galena Fan appears as a southeast-trending basin west of the Steamboat Hills with maximum *Qal* thickness of 210 m near Nevada Hwy 431. The Mount Rose Fan consists of two sub-basins over 200 m thick within an east-trending trough that is generally parallel to slope of the alluvial fan and the groundwater flow direction. The maximum *Qal* thickness (315 m) is found in the western sub-basin, near the base of the Carson Range. The saddle of thinner *Qal* (165 m) that divides the Mount Rose Fan occurs along the Serendipity Fault. An eastern sub-basin reaches maximum *Qal* thickness of 270 m near US Hwy 395. A small circular sub-basin adjacent to Nevada Hwy 431 north of the Steamboat Hills reaches maximum *Qal* thickness of 270 m. A northwest-trending basin with maximum *Qal* thickness of 195 m occurs along Nevada Hwy 341 east of the Steamboat Hills. Steamboat and Pleasant Valleys have maximum *Qal* thickness of 90 m and 55 m, respectively.

From the 41 wells used for vertical geologic control in the 2.75-D forward models, data

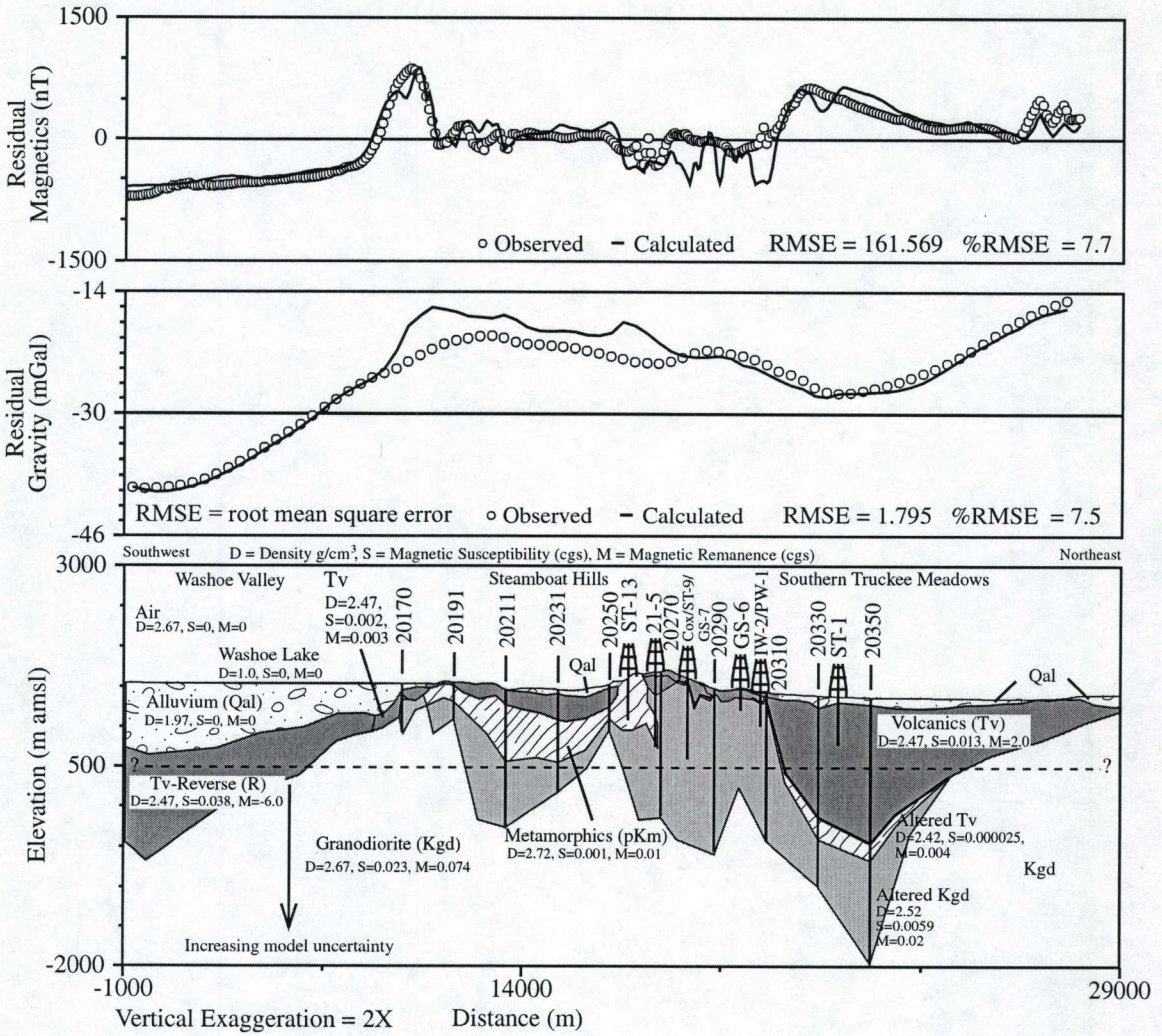

Figure 8. Profile 29020 (Tie Line) cross-section as computed by 2.75-D forward modeling of gravity and aeromagnetic data.

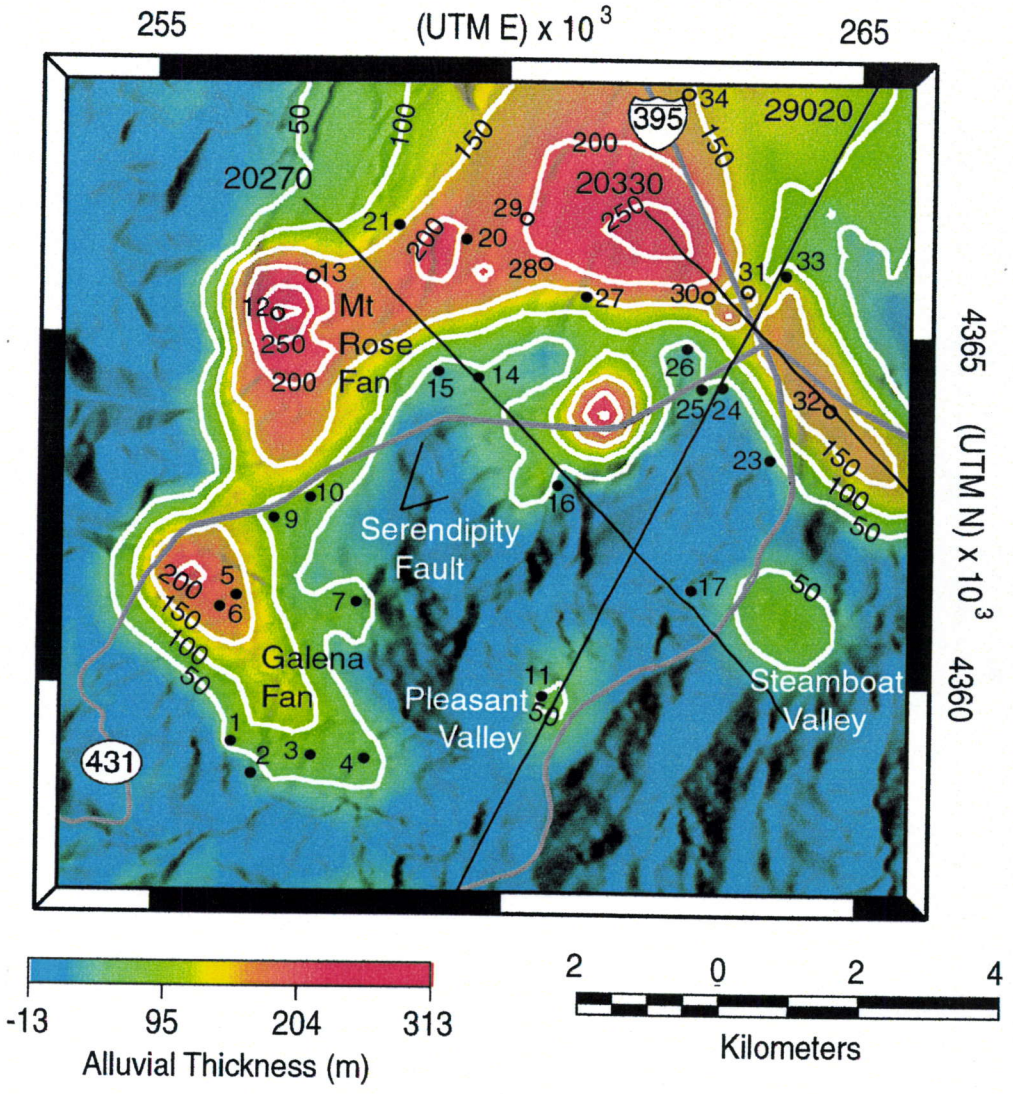

Figure 9. Alluvial thickness in basins surrounding the Steamboat Hills from 3-D model as derived from 2.75-D forward models of gravity and areomagnetic data. Contour interval is 50 m. Solid circles indicate wells that constrain alluvial thickness, open circles indicate wells that yield minimum thickness data because bedrock was not encountered. Well numbers correspond to Table 3.

from 25 wells were analyzed to assess the accuracy of the 3-D model in matching observed *Qal* thickness. Ten wells (No. 8, 23-24, 36-41, Table 3) were not included in this analysis because surface geology is *Tv, pKm,* or *Sr* rather than *Qal.* The model accurately predicts depth to bedrock at 0 m for each these wells except for well IW-2 (No. 40, Table 3). Six wells (No. 28-32 and 34, Table 3) were excluded since *Qal* thickness could not be calculated because bedrock was not encountered. Except for well STM-PW3 (No. 28, Table 3), the model accurately predicts depth to bedrock deeper than the total well depth. Using only depths from the model profiles, a good match (R^2 = 0.89) is found between 3-D modeled and observed *Qal* thickness. The accuracy improves (R^2 = 0.97) when well log data in the actual locations are included in the 3-D model. The RMSE for the 28 data pairs is 13 m giving a %RMSE of 4%.

The *Tv* thickness map (Figure 10) shows that Tertiary volcanics are thickest (2130 m) in the northeast (closest to the Kate Peak source area in the Virginia Range) and thinnest (10 m) beneath Steamboat Valley. *Tv* is absent only in a small area on either side of Steamboat Creek between Pleasant and Steamboat Valleys where *pKm* crops out and in small areas in the Steamboat Hills and northeast of Steamboat Valley where *Kgd* crops out. *Tv* thickness is 1140 m in the Carson Range near Thomas Creek. A broad southeast-trending zone of *Tv* gradually thins to 440 m near the fault swarm along Callahan Ranch Road and increases to 840 m at Maguire Peak. A narrow northwest-trending zone of thin *Tv* (50 m) lies beneath the Galena Fan basin. Along the western extent of the Mount Rose Fan basin, two narrow northwest-trending zones with minimum *Tv* thickness of 90 m are separated along the Serendipity Fault where *Tv* thickness is 180 m. At the southern end of this basin, another narrow northwest-trending zone has a minimum *Tv* thickness of 140 m near well STM-PW3. The northwest-trending area between these thin zones has a maximum *Tv* thickness of 940 m.

The combined thicknesses of *Alt Kgd* and *pKm* (Figure 11) are a representation of the geothermal reservoir beneath the Steamboat Hills. A new geothermal reservoir volume is estimated at 58 km^3 from this map. The overall northeast trend of this feature is aligned with the northeast-trending fault system and associated series of mapped Quaternary rhyolite domes (Figure 2). Superimposed on this main structural trend are smaller northwest- and north-trending features. The northwest-trend along the western flank of the Steamboat Hills reaches a maximum thickness of 1300 m west of Maguire Peak near a rhyolite dome. A minimum thickness of 330 m is found near the southern extent of the Serendipity Fault. The CPI production and injection areas have maximum thicknesses of 2540 m (3000 m depth) and 2000 m (2030 m depth), respectively. The FWC production and injection area has a maximum thickness of 1700 m. A north-trending zone from the CPI to FWC production areas is coincident with the Mud Volcano Basin Fault. A northwest-trending zone with maximum thickness of 1560 m occurs beneath the alluvial deposits northeast of the Steamboat Springs Fault System, which is the discharge area for the geothermal system.

The depth to *Kgd* map (Figure 12) is a representation of the unaltered granodiorite basement. A northwest-trending subsurface ridge of shallow *Kgd,* delineated by wells STM-TH10 and ST-5 coincides with a narrow linear zone of thin *Tv.* This subsurface ridge is aligned with *Kgd* outcrops in the Steamboat Hills and becomes deeper toward the northwest. A similar northwest-trending subsurface ridge of shallow *Kgd* is observed in the Galena Fan basin. *Kgd* depth is 15 m near Washoe Hill at the southeast end of the basin and 950 m near well Tessa 2 at the northwest end of the basin.

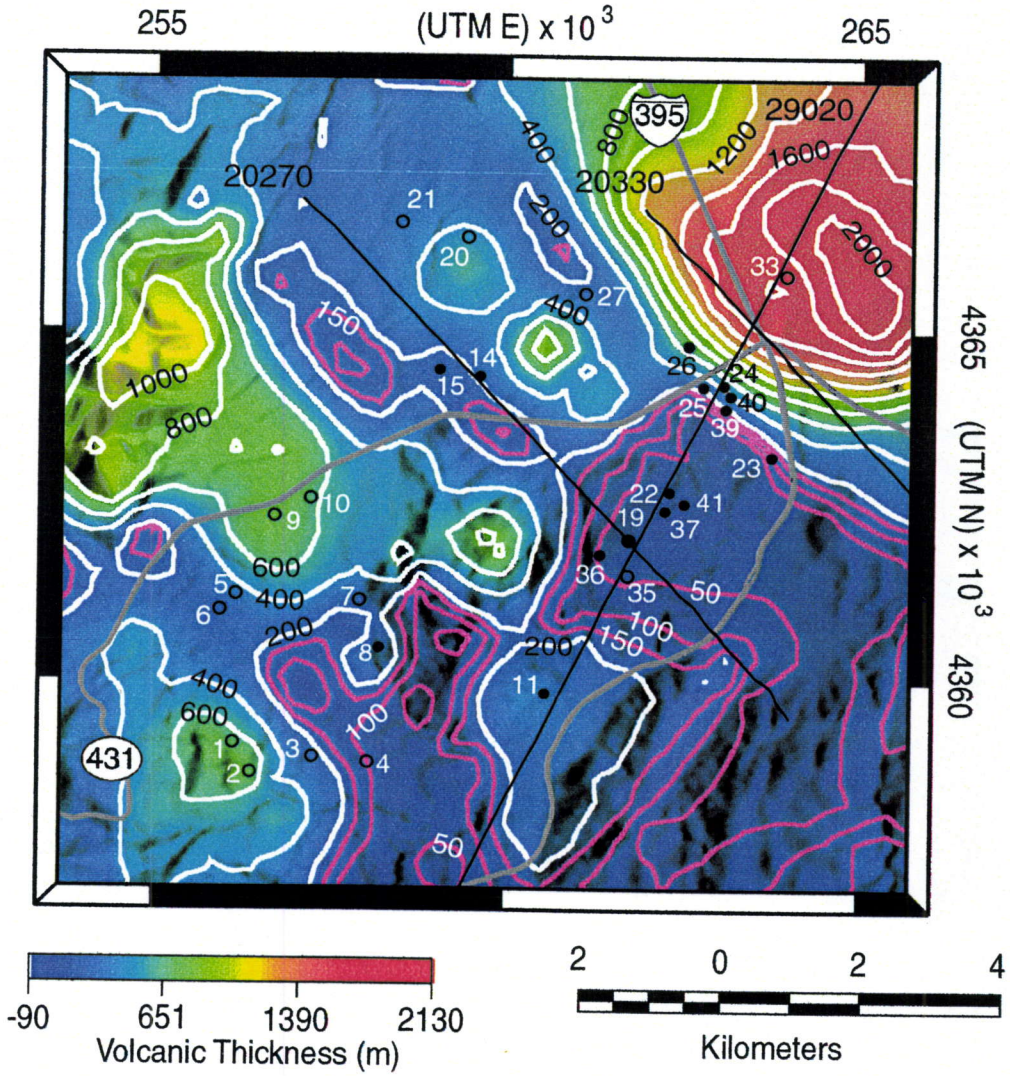

Figure 10. Thickness of Tertiary volcanic rocks from 3-D model as derived from 2.75-D forward models of gravity and aeromagnetic data. Contour interval is 50 m (pink) and 200 m (white). Solid circles indicate wells that constrain volcanic thickness, open circles indicate wells that constrain only the top of volcanic unit. Well numbers correspond to Table 3.

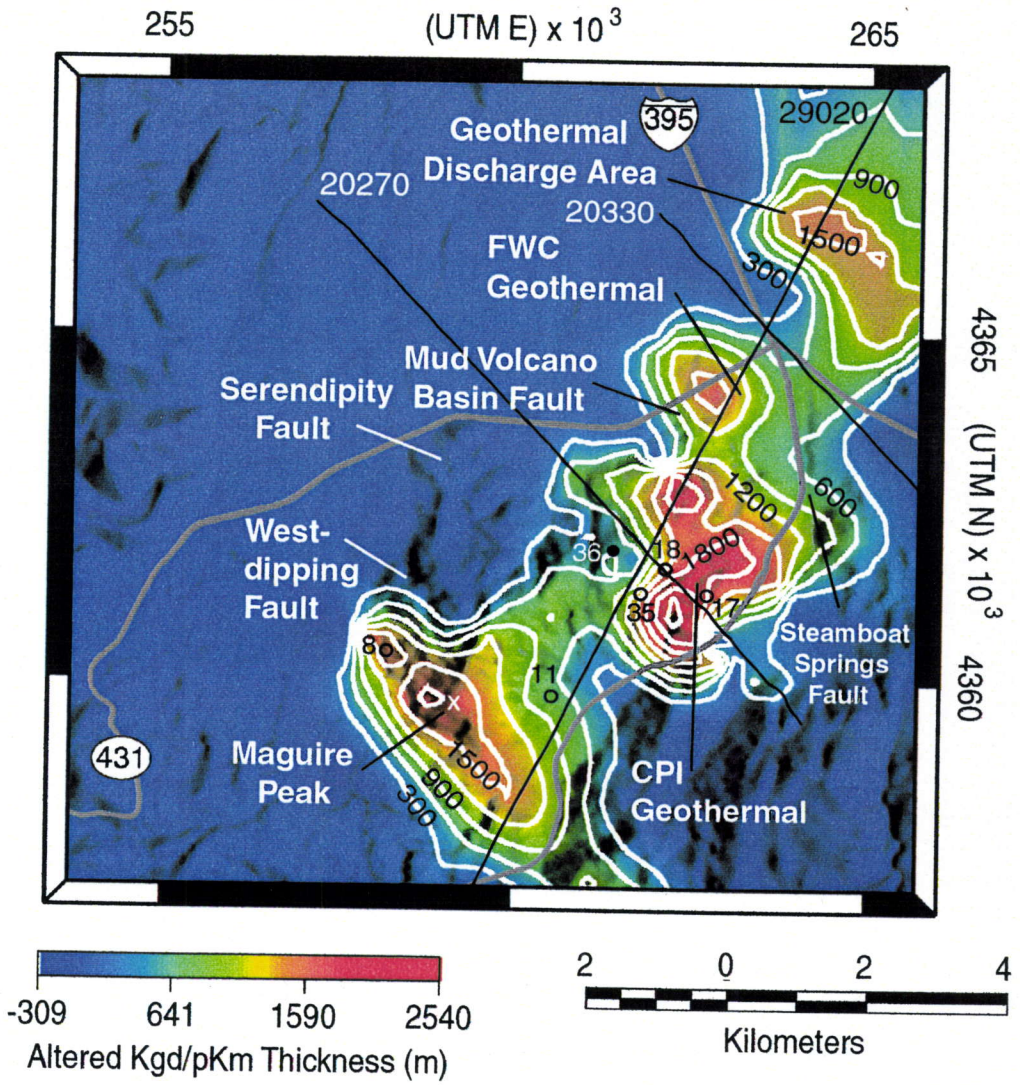

Figure 11. Combined thickness of altered granodiorite and metamorphic rocks from 3-D model as derived from 2.75-D forward models of gravity and aeromagnetic data. This combined thickness represents an interpretation of the geothermal reservoir. Contour interval is 300 m. Solid circles indicate wells that constrain unit thickness, open circles indicate wells that constrain only the top of metamorphic unit. Well numbers correspond to Table 3.

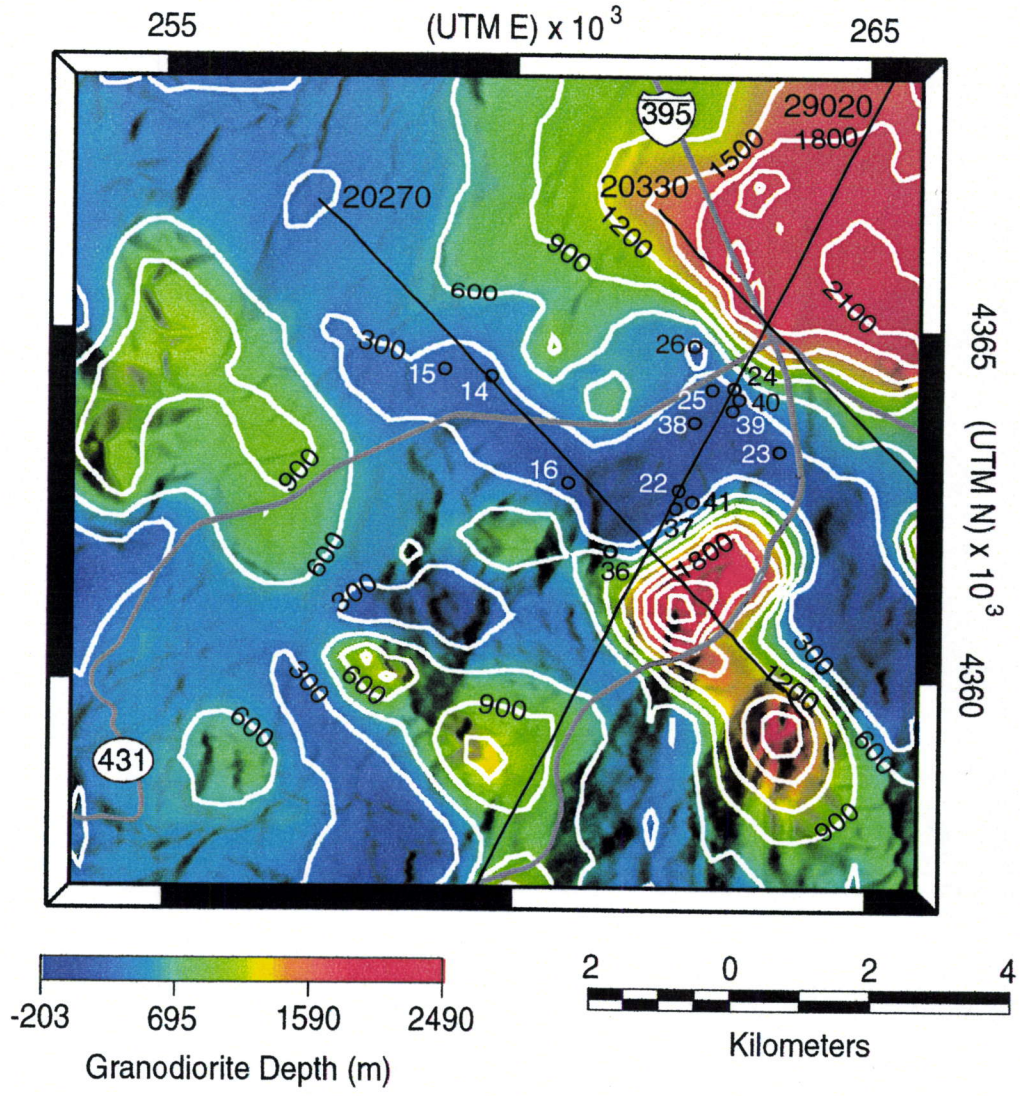

Figure 12. Depth to unaltered granodiorite from 3-D model as derived from 2.75-D forward models of gravity and aeromagnetic data. Contour interval is 300 m. Open circles indicate wells that constrain the depth to granodiorite. Well numbers correspond to Table 3.

Conceptual Model of Geothermal System

In general, most researchers agree with the basics of the conceptual model for the Steamboat Hills geothermal area proposed by White (1968). This model includes deep circulation (>3000 m) of meteoric water recharging primarily in the Carson Range with some recharge from the Virginia Range with circulation occurring in fractured and faulted Mesozoic granitic and metamorphic rocks. The driving forces include head differences between the recharge area and the Steamboat Springs and density and temperature differences between cold down-flowing and hot up-flowing water. The water becomes heated presumably by a magma chamber and rises by convection through a complex network of fractures and faults before being discharged to Steamboat Creek, the alluvial aquifer north of the Steamboat Hills, and hot springs at Steamboat Springs. The age of the Steamboat Hills geothermal system is between 100,000 and 1 million years (White et al. 1964). Disagreement does occur over the details of the conceptual model. A conceptual model for the Steamboat Hills postulated van de Kamp and Goranson (1990) includes two separate geothermal systems: a deep (1000 m above sea level) high temperature system (220°C) and a shallow (1400 m above sea level) moderate temperature system (170°C). Their model includes a high temperature upflow zone beneath the CPI production wells, a low temperature upflow zone between the CPI production wells and the CoxI-1 injection well. Mariner and Janick (1992) propose a single high-temperature geothermal system for Steamboat Hills with differences in thermal water due to boiling. Their conceptual model includes a high temperature (243°C) upflow zone directly beneath the Caithness production wells and an upflow zone related to boiling west of the CoxI-1 injection well. DeRocher (1996) indicates that the Mud Volcano Basin Fault may form a barrier between the high temperature and lower temperature resources; however, he does not specifically state that these are two separate systems. DeRocher (1996) also postulates that the heat source and the upflow zones for the geothermal system is the Steamboat Hills rhyolite located southwest of the existing producing fields. Finger et al. (1994) suggest that an undetected shallow rhyolite intrustion is the heat source. Some investigators believe the rhyolite is too old (1.2 my) to be the heat source (Chris Henry and Patrick Muffler, personal communication, 2001). White and Brannock (1950) presume a cooling magmatic body at depth is the heat source for the geothermal system and White (1968) suggests that a batholith volume of 100-1000 km^3 is required to supply heat for this geothermal system over the life of this system.

The potential fields modeling results from this study suggest a single geothermal system for Steamboat Hills in agreement with basic concepts postulated by White (1968) and proposed by Mariner and Janik (1992). The results from geochemical analysis (Skalbeck et al., 2001) support this single system conceptual model. Figure 8 provides a good cross-sectional representation and Figure 11 provides reasonable 3-D representation for discussion of the conceptual model of the Steamboat Hills geothermal area. A schematic of the conceptual model of the geothermal system is shown in Figure 13. The geothermal system is modeled as altered granodiorite/metamorphic rocks based on the concept that the host rock contains a complex network of factures that permit migration of thermal water. Thermochemical alteration of original magnetic minerals reduces the magnetic properties (magnetic susceptibility and remanent magnetization) of the rock adjacent to the fractures. Although, nearly complete demagnetization of the rock occurs near the factures, the rock matrix further from the fracture in not likely altered. Thus, magnetic properties assigned in the model for altered granodiorite/metamorphic units represent an average for the host rock. This concept is consistent

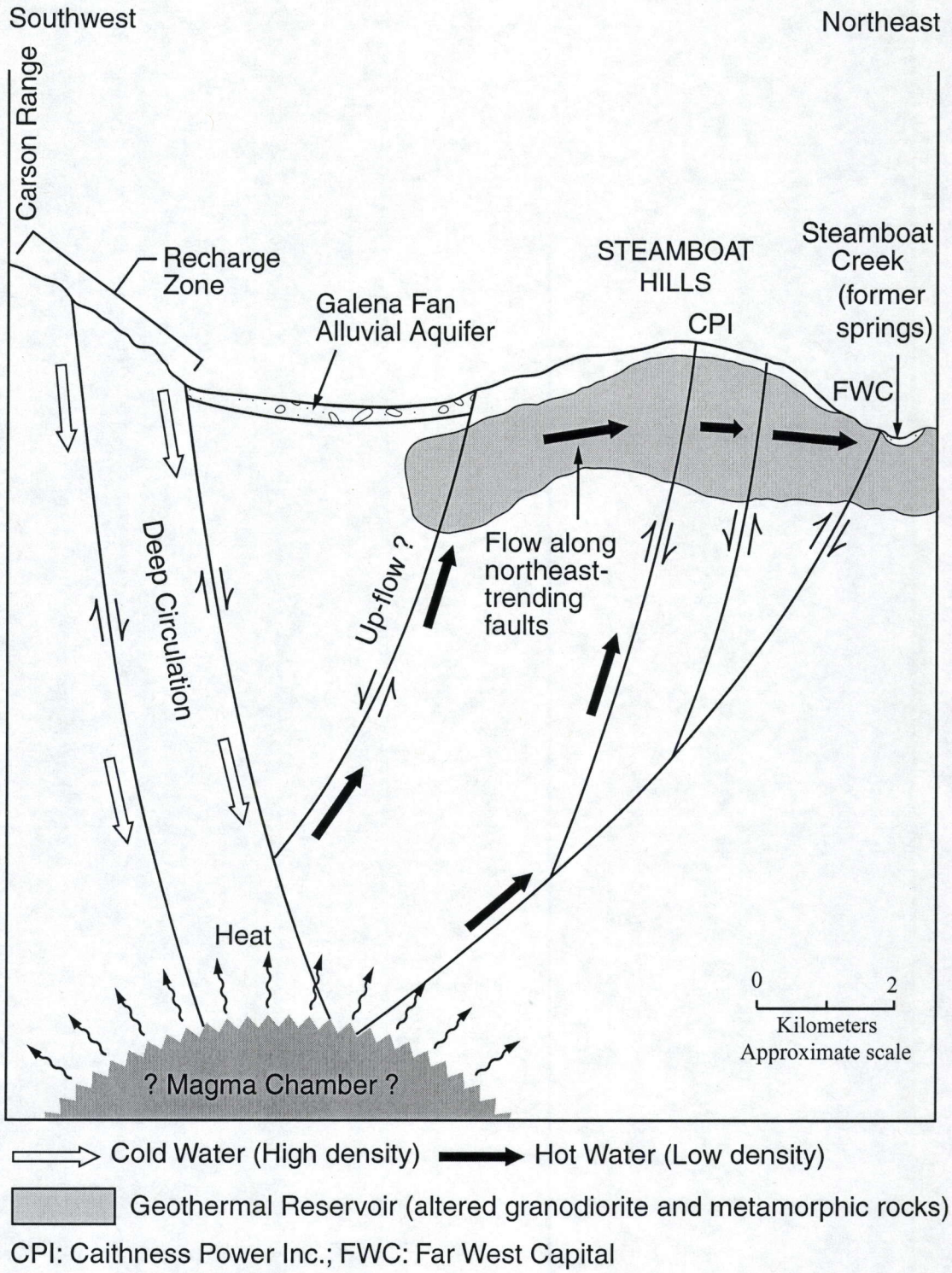

Figure 13. Conceptual model of the Steamboat Hills geothermal system. Modified from White (1968), Mariner and Janik (1995), and DeRocher (1996) based on results of potential fields modeling (this study).

with Muffler (1979), which considers the geothermal reservoir to be the volume of rock and water regardless of porosity and permeability.

The overall southwest-northeast trend of the geothermal system coincides with northeast-trending faults and a series of Pleistocene rhyolite domes. A northwest-trend and a north-trend in the modeled reservoir thickness (Figure 11) along the western flank and the eastern portion of the Steamboat Hills, respectively appear to correlate with major faults. The thick zone of altered granodiorite/metamorphic rocks (Figure 8 near Profile 20221 and Figure 11 near Maguire Peak) is coincident with a north-northwest trending fault that may represent an upflow zone for the geothermal system. This fault may be part of a west-dipping fault modeled by Abbott and Louie (2000) that extends northward into Reno (Chris Henry, personal communication, 2001). This major west-dipping fault may intersect at depth with the east-dipping Range Front fault system providing a conduit for upflow of thermal water along the west flank of the Steamboat Hills. The heat source may be deep circulation (>3000 m) beneath the Galena Fan. For this model, cold water from precipitation in the Carson Range is circulated deep along east-dipping, normal (down to the east) Range Front faults, and perhaps faults associated with Galena and Browns Creeks. Water is heated at depth, perhaps by a large magma chamber, and hot water up-flows along the west-dipping normal fault along the western flank of the Steamboat Hills. The prominent northeast-trending fault system along the axis of the Steamboat Hills likely conducts the thermal water toward the CPI and SBG production areas and eventually discharges to the alluvial deposits northeast of Steamboat Hills.

The north-trending zone of thick *Alt Kgd* and *pKm* (Figure 11) extending from the CPI to the FWC production zones that coincides with the Mud Volcano Basin Fault suggests that the two production zones are in hydraulic communication. This interpretation agrees with a conceptual model based on geochemical data (Mariner and Janik, 1995; Skalbeck et al., 2001). Some thermal water is conducted into the alluvial aquifer north of Steamboat Hills along north-trending faults (Skalbeck et al., 2001). These faults may also provide conduits for thermal water discharge to Steamboat Creek.

DISCUSSION AND CONCLUSIONS

The subsurface geology along 11 profiles derived from 2.75-D forward modeling of gravity and aeromagnetic data is constrained by geologic, physical property, and well data. The large amount of surface and vertical geologic data utilized for this study allows for a detailed delineation of the geologic units found in the Steamboat Hills area. The physical property values assigned to yield the best-fit forward models are consistent with data measured from samples collected in the area and published regional data. Reasonable consistency in the geologic structure and assigned physical property data between each profile model was built into this study by modeling the "tie line" profile (Figure 8). The high degree of constraint and the good to excellent fit between the observed and calculated gravity and aeromagnetic data for the 2.75-D forward models yields reliable depth data for the 3-D model, which in turn allows for a confident interpretation of the geologic structure of the Steamboat Hills and surrounding alluvial basins.

The good match between observed and 3-D model *Qal* thickness (derived only from profiles) illustrates that the well data was used appropriately in the model profiles even though adherence was subjective at times due to the projected distance between the well and profile locations. The match also indicates that 3-D model accurately represents between profile variations. Combining well log data with model profiles data obviously improves the match but,

more importantly, increases the constraints on the 3-D model. Our *Qal* thickness results in the Mount Rose Fan area agree quite well with the gravity results from Abbott and Louie (2000), which use fewer data (no magnetic data and fewer well log and gravity data). The maximum *Qal* thickness (depth to bedrock) from our model is within 25% of the maximum depth to bedrock from their study. We consider these two study results to closely agree since Abbott and Louie (2000) report a potential depth error of 50% because of highly speculative density values. We note that our *Qal* thickness results were obtained from multiple profiles of 2.75-D coupled forward modeling of gravity and aeromagnetic data while Abbott and Louie (2000) calculated depth to bedrock using an infinite slab approximation. It is also noteworthy that the density contrast range (-0.30 to -0.65 g/cm^3) between basin fill and bedrock used by Abbott and Louie (2000) is similar to the density contrast (-0.30 to -0.50 g/cm^3) between *Qal* and *Tv* used in our models. The close agreement of these independent results provides validation for both studies. Because of higher resolution due to greater data density and the use of aeromagnetic data however, our results; provide better definition of the alluvial basins adjacent to Steamboat Hills. Since we have vertical geologic control from numerous well logs, we can confidently model 50 m contours for the *Qal* thickness that yields definition of the Galena Fan, Steamboat Valley and Pleasant Valley basins. The results also delineate sub-basins within the Mount Rose Fan resulting from the Serendipity Fault and a small deep sub-basin at the northern flank of the Steamboat Hills.

To assess our increased understanding of the alluvial basins surrounding the Steamboat Hills based on this study, we compare *Qal* thickness derived from the 2.75-D forward modeling of gravity and aeromagnetic data and well log data (Table 3) with *Qal* thickness obtained from only well log data (Figure 14). Although the general configuration of the alluvial basins is similar, the additional data derived from the potential fields data increases the definition of these basins. The three sub-basins located north and northeast of the Steamboat Hills are not defined with only well log data. Also the maximum depths in both the Mount Rose and Galena Fans are greater for the map derived from the potential fields and well log data. The volume of the basins defined by only the well log data is 7 km^3 compared with a volume of 11.5 km^3 defined by potential fields modeling and well log data, which represents a 64% increase. The more detailed alluvial basin configuration and increased basin volume estimate based on the *Qal* thickness results obtained from this study indicates that potential fields modeling adds valuable information for water resource investigations in the Steamboat Hills and southern Truckee Meadows area.

While well log data gives minimum *Tv* thickness at 14 locations, actual *Tv* thickness is known at 15 well locations (Figure 10 and Table 3). Prior to this study, *Tv* thickness was known to range from 25 to 390 m. Based on the 3-D model derived from potential fields modeling, Tv thickness is estimated to be as thick as 1000 m in the Carson Range and 2000 m in the geothermal discharge area near Nevada 341 and 431 and US 395. Tertiary volcanic rocks are thin beneath the deepest portions of the alluvial basins within the Galena and Mount Rose Fans. A broad ridge of thicker *Tv* extending from the Carson Range to the Steamboat Hills appears to act as a subsurface divide for these two alluvial basins. Within the Mount Rose Fan basin, the Serendipity Fault is coincident with a band of thicker *Tv* along that divides two northwest-trending zones of thinner *Tv*. The thickness of Tertiary volcanic rocks is important to Washoe County hydrogeologists because these rocks are an important source of supply water for the southern Truckee Meadows residential and commercial developments.

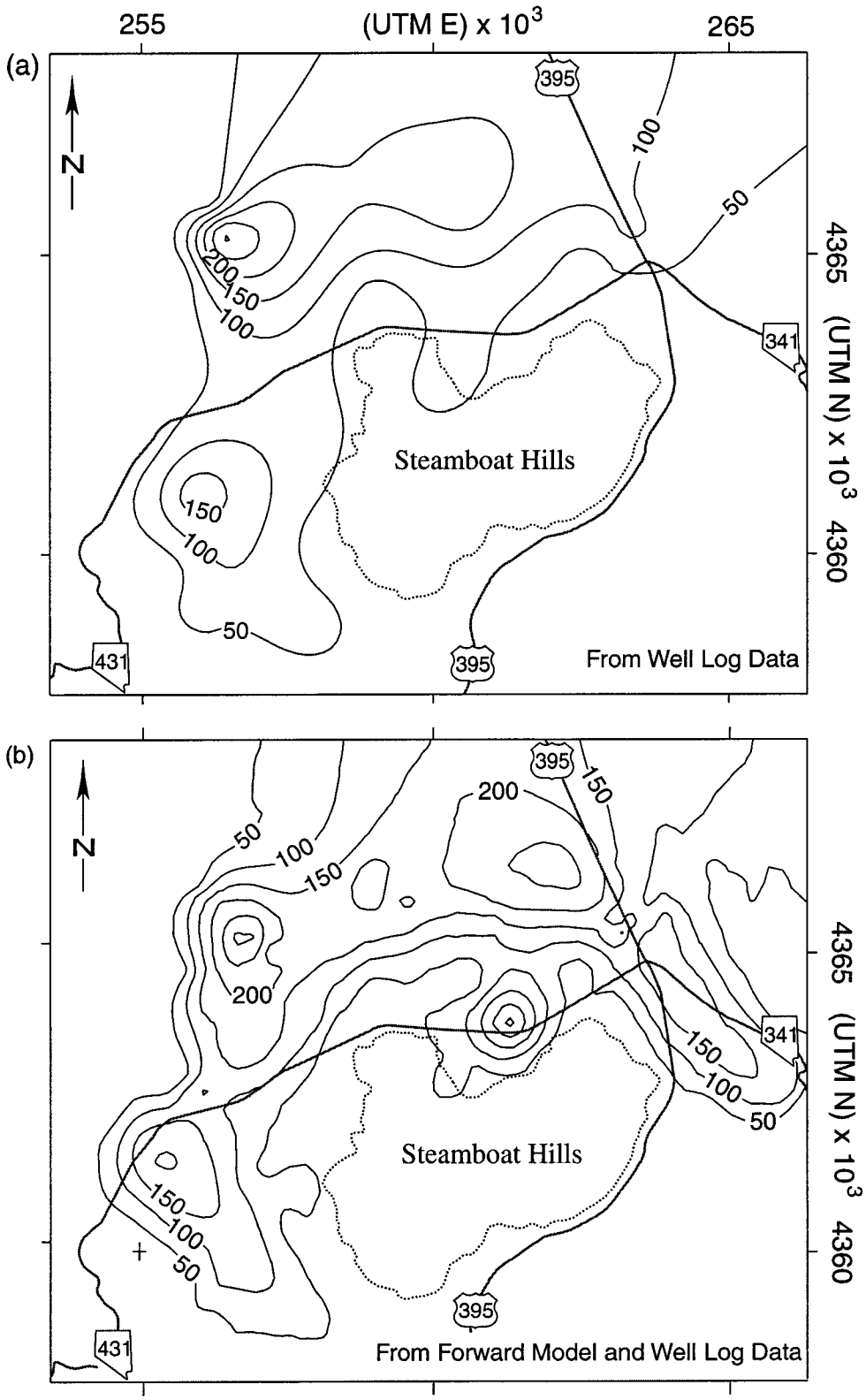

Figure 14. Alluvial thickness in basins surrounding the Steamboat Hills. (a) Derived from well log data alone (Table 3). (b) derived from 2.75-D forward models of gravity and areomagnetic data and well log data (Figure 9). Contour interval is 50 m.

By modeling *Alt Kgd* and *pKm* to represent the geothermal reservoir based on recognition that the reservoir rock has lower magnetic susceptibility due to thermal alteration along fractures, we present a new method to estimate geothermal reservoir volume from potential fields modeling. According to Muffler (1975) the largest uncertainty in estimating the thermal energy of a geothermal resource is estimating the reservoir area and depth (volume), which lead to uncertainty in calculating the geothermal recovery factor (Rg) for hot-water geothermal resource determination where Rg is the ratio of geothermal energy recovered at the wellhead (q_{wh}) to geothermal energy originally stored in the reservoir (q_r). Our method of modeling geothermal reservoir volume offers the opportunity to revise previous volume estimates and therefore recalculate Rg. Muffler (1979) estimated the mean reservoir volume for Steamboat Hills at 29 $\pm$ 12 km^3 whereas our new volume estimate is 58 km^3. Using our revised volume estimate, the Rg for Steamboat Hills is 12.5% versus the assumed 25% Rg value used by Muffler (1975). During the Joint UNR/USGS Geothermal Science Workshop on May 1, 2001, Muffler stated that the 25% Rg value is known to be high and that an Rg value of 9% has been calculated for the Geysers. The new Rg value for Steamboat Hills compares closely with the Geysers value.

SUMMARY

The following summarizes the new research, findings and results of this study:

- We use 2.75-D forward modeling of gravity and aeromagnetic data along multiple profiles that are highly constrained by geologic and physical properties to obtain a 3-D representation of pertinent geologic units for a geothermal system and alluvial aquifers;

- We present a new method to estimate geothermal reservoir volume by modeling altered granodiorite and metamorphic rocks to represent the geothermal reservoir based on recognition that the reservoir rock has lower magnetic susceptibility and density due to thermochemical alteration along fractures;

- An average magnetic susceptibility value obtained from whole rock core was a critical parameter used to represent altered granodiorite for the model geothermal reservoir host rock in order to match observed aeromagnetic data;

- A thick zone of altered granodiorite and metamorphic rocks suggests a thermal water up-flow zone may exist along a fault near the western flank of the Steamboat Hills, which was previously unrecognized;

- The 3-D alluvial basin configuration determined using potential fields model data with existing well log data indicates the basin volume surrounding the Steamboat Hills is 64% greater than the volume derived from well data alone;

- The 3-D model suggests that volcanic rocks, an increasingly important source of municipal water supply, underling alluvial deposits may be over 2000 m thick rather than the 390 m thickness indicated previously by well log data; and,
- North-trending faults that conduct thermal water from the geothermal system to the alluvial aquifer are modeled as zones of altered volcanics that correspond to subtle aeromagnetic anomalies.

The results from this study provide a reliable definition of the 3-D geometry of alluvium, volcanic rocks, granodiorite, and metamorphic rocks in the Steamboat Hills area that can be used by Washoe County and geothermal company hydrogeologists. Beyond the results presented here, data from this model can be presented as depth, thickness, and elevation for each geologic unit as needed. To develop an adequate numerical model for groundwater flow within the study area, reasonable representation of the elevation of the geologic units is required. When planning exploration drilling for drinking water and geothermal wells, hydrogeologists often prefer representation of the subsurface geology as depth to and/or the thickness of a particular unit. This 3-D model can accommodate the data requirements for both of these uses. Additionally, this study could provide an opportunity for evaluating results between the 2.75-D and true 3-D forward modeling methods. Although this study was focused on water resource evaluation, the methodology presented here can be used for other geologic assessments (e.g. mineral resources, basin delineation for seismic hazards, petroleum resources).

REFERENCES

Abbott, R.E., and Louie, J.N., 2000, Depth to bedrock using gravimetry in the Reno and Carson City, Nevada, area basins: Geophysics, **65**, 340-350.

Ayers, J.F., 1989, Application and comparison of shallow seismic methods in the study of an alluvial aquifer: Ground Water, **27**, 550-563.

Berger, D.L., Ross, W.C., Thodal, C.E., Robledo, A.R., 1996, Hydrology and simulated effects of urban development on water resources of Spanish Springs Valley, Washoe County, west-central Nevada: U.S. Geol. Surv. Water Res. Inv. Report 96-4297, 80 p.

Blakely, R.J., Morin, R.L., McKee, E.H., Schmidt, K.M., Langenheim, V.E., Dixon, G.L., 1998, Three-dimensional model of Paleozoic basement beneath Amargosa Desert and Pahrump Valley, California and Nevada: Implications for tectonic evolution and water resources: U.S. Geol. Surv. Open File Report 98-496, 29 p.

Bonham, H.F., Jr., and Rogers, D.K., 1983, Geologic map, Mt. Rose NE quadrangle: Nevada Bureau of Mines and Geol., Map 4Bg.

Bonham, H.F., Jr., and Bell, J. W., 1993, Geologic map, Steamboat quadrangle: Nevada Bureau of Mines and Geol., Map 4Fg.

Briggs, I.C., 1974, Machine contouring using minimum curvature, Geophysics, 39, 39-48.

Carpenter, T., 1996, Gravity data acquisition and processing, Mount Rose Fan project, Washoe County, Nevada: unpublished report for Washoe County Utility Division, November 1996, 6 p.

Cohen, P., and Loeltz, O.J., 1964, Evaluation of Hydrogeology and Hydrochemistry of Truckee Meadows Area, Washoe County, Nevada: U.S. Geol. Surv. Water Supply Paper 1779-S, 63 p.

Cressie, N.A., 1990, The origins of Kriging: Math. Geol., 22, 239-252.

DIGHEM, 1994, Dighem^{V} survey for Utility Division, Washoe County Public Works, Washoe County, Nevada: unpublished report #612, December 28, 1994, 36 p.

Hendricks, J.D., 1992, Total-intensity magnetic-anomaly map of the Reno 1° by 2° quadrangle, Nevada and California, U.S. Geol. Surv. Misc. Field Studies Map MF-2154-C.

Finger, J.T., Jacobson, R.D., Hickox, C.E., and Eaton, R.R., 1994, Steamboat Hills exploratory slimhole: Drilling and testing: Sandia Nat. Lab. Report SAND94-0551, October 1994, 59 p.

Grant, F.S., and West, G.F., 1965, Interpretation theory in applied geophysics: McGraw-Hill, Inc., 583 p.

Haeni, F.P. 1986, Application of seismic refraction methods in groundwater modeling studies in New England: Geophysics, 51, 236-249.

Hittelman, A. D., Dater, D., Buhmann, R. and Racey, S., 1994, Gravity CD-ROM and user's manual, National Oceanic and Atmospheric Administration, National Geophysical Data Center.

IAGA Division V, Working Group 8, 1995, International Geomagnetic Reference Field, 1995, adopted by the Internat. Assoc. of Geomagnetism and Aeronomy (IAGA) during the XXI General Assembly of the Internat. Union of Geod. Geoph., Boulder, USA in July 1995, [On-line] , Available at http://www.ngdc.noaa.gov/seg/potfld/igrf95.html

Karlin, R., 1996, Magnetic modeling of the Mount Rose Fan, unpublished report for the Washoe County Utilites Division, February, 12 p.

Krank, K.D., and Watters, R.J., 1983, Geotechnical properties of weathered Sierra Nevada granodiorite: Assoc. Eng. Geol. Bull., XX , 173-184.

Langenheim, V.E., and Hildenbrand, T.G., 1997, Commerce geophysical lineament-Its source, geometry, and relation to the Reelfoot rift and New Madrid seismic zone: Geol. Soc. Am. Bull., 109, 580-595.

Mankinen, E.A., Hildenbrand, T.G., Dixon, G.L., McKee, E.H., Fridrich, C.J., and Laczniak, R.J., 1999, Gravity and Magnetic Study of the Pahute Mesa and Oasis Valley Region, Nye County, Nevada: U.S. Geol. Open File Report, 99-303.

Mariner, R.H., and Janik, C.J., 1995, Geochemical data and conceptual model for the Steamboat Hills geothermal system, Washoe County, Nevada: Geoth. Res. Counc. Trans., 19, 191-200.

Muffler, P., 1979, Assessment of geothermal resources of the United States-1978, U.S. Geol. Surv. Circ. 790, 163 p.

Silberman, M.L., White, D.E., Keith, T.E.C., Dockter, R.D., 1979, Duration of hydrothermal activity at Steamboat Springs, Nevada, from ages of spatially associated volcanic rocks, U.S. Geol. Surv. Prof. Paper 458-D, 14 p.

Skalbeck, J.D., Shevenell, L., and Widmer, M.C., 2001, Mixing of Thermal and Non-Thermal Waters the Steamboat Hills Area, Nevada: Geothermics, 30, *in press*.

Skalbeck, J.D., 1998, Measurement of physical and paleomagnetic properties from rocks in Steamboat Hills and Carson Range: unpublished report for Washoe County Utility Division, February 1998, 47 p.

Sorey, M.L., and E.M. Colvard, 1992, Factors affecting the decline in hot-spring activity in the Steamboat Springs area of critical environmental concern, Washoe County, Nevada: U.S. Geol. Surv., administrative report for U.S Bur. of Land Manag., 109 p.

Stanley, W.D., and Blakely, R.J., 1995, The Geysers-Clear Lake geothermal area, California-An updated geophysical perspective of heat sources: Geothermics, 24, 187-221.

Stewart, J.H, 1999. Geologic map of the Carson City 30 x 60 minute quadrangle, Nevada, Nevada Bureau of Mines and Geol., Map 118.

Tabor, R.W., and Ellen, S., 1975, Geologic Map, Washoe City Folio: Nevada Bur. of Mines and Geol. Environmental Series.

Talwani, M. and Heirtzler, J.R., 1964, Computations of magnetic anomalies casued by two-dimensional bodies of arbitary shape, *in* Parks, G. A., Ed., Computers in the mineral industry, Part I, Stanford Univ. Publ., Geological Sciences, 9, 464-480.

Talwani, M., Worzel, J.L., and Landisman, M., 1959, Rapid gravity computations for two-dimensional bodies with application to the Mendocino Submarine fracture zone, J. Geophys. Res., 64, 49-59.

Thompson, G.A., and Sandberg, C.H., 1958, Structural significance of gravity surveys in the Virginia City-Mt. Rose area, Nevada and California: Geol. Soc. Am. Bull., 69, 1269-1282.

Thompson, G.A., and White, D.E., 1964, Regional geology of the Steamboat Springs area, Washoe County, Nevada: U.S. Geol. Surv. Prof. Paper 458-A, 52 p.

White, D.E, Thompson, G.A., and Sandberg, C.H., 1964, Rocks, structure, and geologic history of the Steamboat Springs thermal area, Washoe County, Nevada: U.S. Geol. Surv. Prof. Paper 458-B, 63 p.

Zeng, H., Wan, T., Teyssier, C., Yao, C. and Tikoff, B., 2000, The 3-D geometry of the Linglong granitic complex from 2-D gravity forward modeling, Shandong Province, east China: Geophysics, 65, 421-425.

CHAPTER 4

Delineation of a Hydrogeologically Significant Fault using Magnetic Methods in the Steamboat Hills Geothermal Area, Reno, Nevada

John D. Skalbeck, Robert E. Karlin, and Michael C. Widmer

ABSTRACT

Geothermal resources are currently a small but important renewable energy source for electric power production and direct-use applications. The need for exploration of potential geothermal sites increases with the increasing demand for global energy supplies. Magnetic data can be useful for fault and fracture zone identification during geothermal resource site exploration and characterization. We present an exploration strategy that includes initial reconnaissance using a draped aeromagnetic survey, delineation of hydrologically significant faults using ground magnetic surveys, and characterization of vertical magnetic susceptibility from borehole logging or core measurements. This strategy is based on evaluating the usefulness of these methods at the Steamboat Hills geothermal area. Results suggest that alteration of magnetic minerals in rocks within the geothermal reservoir produce a magnetic low anomaly observed in aeromagnetic data collected from 30 to 120 m above ground surface. Ground magnetic data show a pronounced low over the Mud Volcano Basin Fault that is known to conduct thermal water into an alluvial aquifer. Vertical magnetic susceptibility measurements of whole rock core provide an average value for altered granodiorite that is used in forward modeling of this fault. Permeable fractures and a major fault zone noted in the core hole log align with low values of magnetic susceptibility suggesting alteration and mineral replacement along fractures.

INTRODUCTION

Recent energy supply issues in the western United States have focused attention on the need to investigate alternative energy resources (e.g. geothermal, solar, wind,). The potential geothermal resources in Nevada are well documented (e.g. Garside and Schilling, 1979; Shevenell et al., 2000), but few sites have been fully characterized. In 1998, geothermal accounted for only 1.5% of Nevada's electrical generation capacity (DOE, 2001; Geothermal Education Office, 2001). Geothermal exploration and site characterization is likely to expand in the near future as the costs for natural gas and coal fired electric production becomes equivalent or surpasses the costs for electric power production from geothermal resources. Proven cost effective methods for fault and fracture zone identification will be important components of any geothermal resource site characterization particularly in Nevada where resources are predominately fault controlled. We present a strategy for site characterization of a potential geothermal resources area with magnetic survey and borehole logging methods using the Steamboat Hills as a test site. Aeromagnetic maps can provide an initial reconnaissance level indication of possible geothermal areas due to demagnetization of rocks by thermochemical alteration. Ground-based magnetic surveys across targeted faults (identified from geologic maps, digital elevation models, aerial photography) can estimate whether a given fault conducts a significant quantities of thermal water and thus provides a favorable location for an exploration drill site. Vertical magnetic susceptibility data from drill core can be used in potential fields modeling of the subsurface structure. Additionally, borehole logging for magnetic susceptibility and total field magnetic intensity can be used to identify fault zones and potentially productive fractures.

The hydrogeologic setting at the Steamboat Hills geothermal area is an excellent field site for testing methods based on principles of rock magnetism to identify hydrologically significant faults and fractures. Groundwater flow through the geothermal reservoir is known to be fault and fracture controlled (White, 1968). Geophysical data (Corwin and Hoover, 1979) and geochemical evidence (Skalbeck et al., 2001) suggest that the north-trending Mud Volcano Basin Fault (MVBF) conducts thermal water from the Steamboat Hills geothermal system northward into the alluvial aquifer. Thermal and chemical alteration of magnetic properties in rocks results in distinct magnetic low anomalies for rocks adjacent to faults and fractures that conduct thermal water. These magnetic low anomalies are used to: (1) outline the geothermal resource area; (2) identify faults that conducts thermal water from the geothermal system to the alluvial aquifer; and (3) delineate productive fractures in core rock from a slim hole drilled within the geothermal reservoir. Aeromagnetic data from a low altitude or draped survey can identify a geothermal area on a scale of 100s of meters to kilometers whereas ground magnetic data can delineate a fault at the ~~meter~~ 10 tens of meters scale. Vertical magnetic susceptibility is sensitive to fractures on the centimeter scale.

Hydrogeologic Setting

The study area is located along the western margin of the extensional Basin and Range province in the western United States. The Steamboat Hills are a topographically prominent northeast-trending bedrock ridge that represents the southern extent of the fault-bounded Truckee Meadows basin, which contains the cities of Reno and Sparks approximately 15 km north of Steamboat Hills (Figure 1). The study area is bordered on the west by the Carson Range of the Sierra Nevada Mountains and on the east by the Virginia Range. The core of these ranges consists of Cretaceous granodiorite beneath older metasedimentary and metavolcanic rocks that in turn are overlain by Tertiary volcanic flows, breccias, and tuffs. A veneer of Quaternary alluvial fan and basin fill deposits range from clayey sand to boulder gravels. Alluvial deposits and volcanic rocks are the primary source of water supply for Washoe County and private residences in the southern Truckee Meadows. At least three prominent fault systems trending north, northeast, and northwest are found in the study area (Figure 2) with the north-trending faults being the most numerous and youngest (White et al., 1964). The Steamboat Hills geothermal field occurs predominantly along northwest-southeast trending faults within the granodiorite and metamorphic rocks. Surface deposits of sinter up to 90 m thick are associated with the geothermal discharge area near Steamboat Springs along the east flank of Steamboat Hills (Thompson and White, 1964; White et al., 1964).

Groundwater originates primarily from snowmelt infiltration in the Carson Range and flows eastward toward Steamboat Creek (Cohen and Loetz, 1964). Depths to groundwater range from approximately 80 m near the center of the alluvial fan to land surface at Steamboat Springs. Sorey and Colvard (1992) note that similarities in chemical characteristics and decreases in hydraulic head suggest that the geothermal reservoir and alluvial aquifer are hydrologically connected. Skalbeck et al. (2001) found correlation between the amount of thermal water in alluvial aquifer wells and their proximity to north-trending faults that conduct thermal water from the geothermal reservoir. This suggests that north-trending faults provide preferential flow for thermal water into the alluvial aquifer.

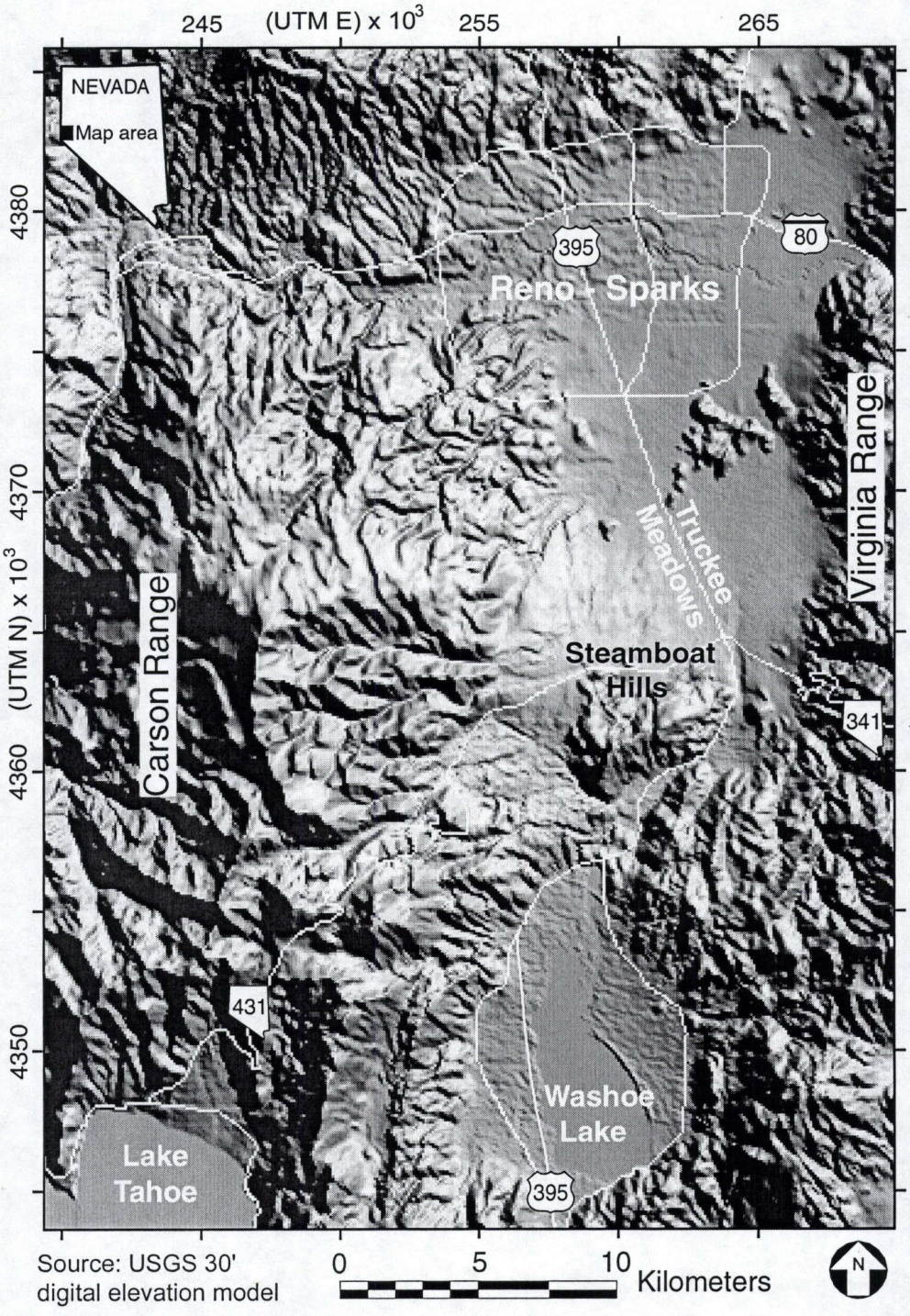

Figure 1. Location map of Steamboat Hills geothermal area, Washoe County, Nevada.

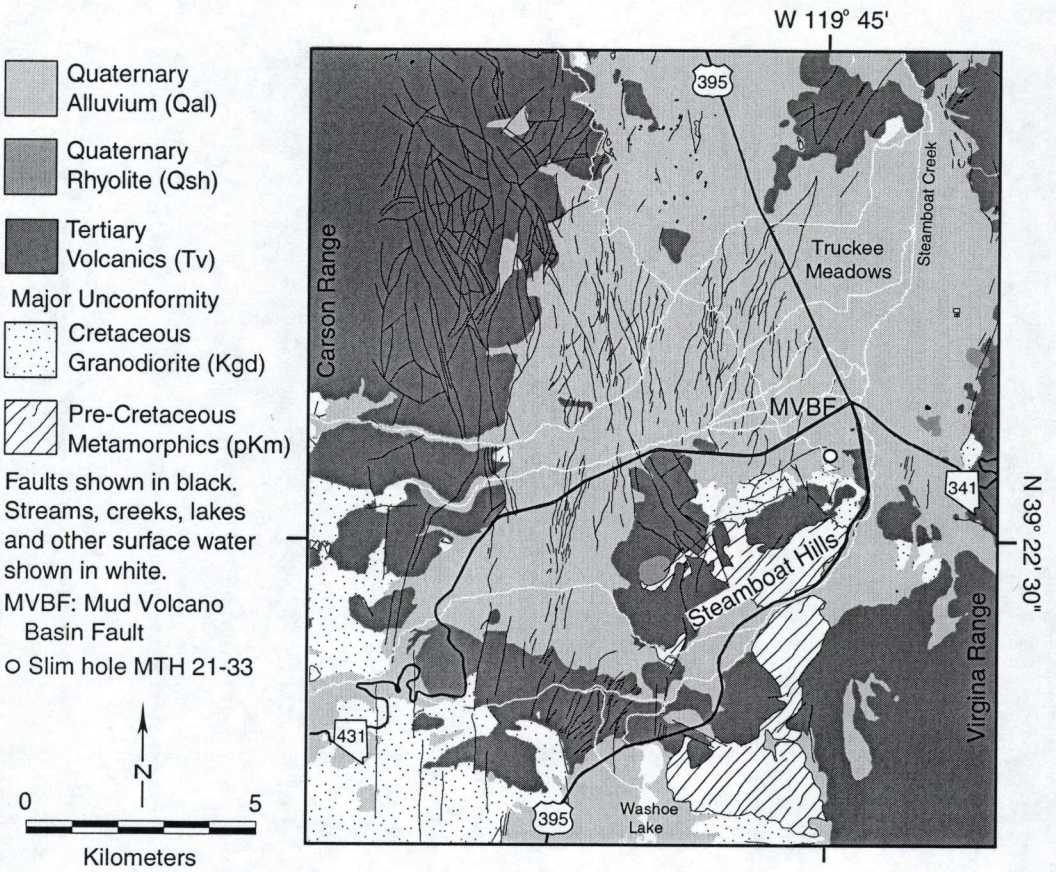

Figure 2. Generalized geologic map after Bonham and Rogers (1983), Bonham and Bell (1993) and Tabor and Ellen (1975).

Thermochemical alteration and demagnetization

Geomagnetists and paleomagnetists have long recognized the effects of temperature and chemical alteration on rock magnetization (Nagata, 1961; McElhinny, 1973, O'Reilly, 1984; McElhinny and McFadden, 2000). Heat will induce chemical changes in magnetic minerals resulting in the creation and destruction of magnetic minerals at certain temperatures and these thermochemical changes often result in demagnetization (reduced magnetic susceptibility and remanent magnetic intensity) of the rocks. The maximum water temperatures (230° to 243°C; Mariner and Janik, 1995) observed in the Steamboat Hills geothermal area are within the range of temperatures that causes alteration of magnetic minerals. Although elevated temperature in rocks can reduced magnetic susceptibility and remanent magnetic intensity without alteration of magnetic minerals, measurements in the Steamboat Hills area (Skalbeck et al., Chapter 3) were performed on cold rocks indicating that reduced magnetic properties results from alteration.

Skalbeck et al. (Chapter 3) found reduced remanent magnetic intensity and magnetic susceptibility in altered volcanic rocks and altered granodiorite. White et al. (1964) attributed a magnetic low anomaly associated with the Steamboat Springs Fault System to destruction of original magnetic mineralogy. They documented a magnetic low at the location of the MVBF in one traverse (Traverse 8), which they attribute to alteration of original magnetite to maghemite. Hoover and Pierce (1986) correlated a north-trending strong conductor from airborne electromagnetic data with an unnamed fault in the vicinity of the MVBF and suggested it formed the east side of a small graben. Corwin and Hoover (1979) correlated self-potential (SP) anomalies at the MVBF and High Terrace Faults and suggest the faults conduct thermal water; however, the SP anomalies did not extend northward into the alluvial basin.

Because the MVBF represents a significant hydrogeologic connection between the geothermal system and the alluvial aquifer (Skalbeck et al., 2001), we decided to characterize the magnetic signature surrounding this fault. Our objective was to identify the trace of the fault hidden beneath the alluvial deposits north of the geothermal area. Delineation by magnetic methods of faults that conduct thermal water could be important for geothermal exploration, site characterization, and well field development.

METHODS

The map of residual reduced-to-pole aeromagnetic data (Figure 3) is derived from a draped helicopter survey contracted by the Washoe County Department of Water Resources. Data were collected along 41 flight lines oriented at N45E with 609 m spacing and 3 tie lines oriented at N20E with 5000 m spacing. Total intensity magnetic data were collected by a cesium vapor magnetometer towed 20 m below the helicopter at heights of 30 to 120 m above ground surface. Details of data processing are described in Skalbeck et al. (Chapter 3).

Total field magnetic intensity ground data were collected at 424 stations (8 m intervals; 3 m for Transect 2) using a proton procession magnetometer along 5 east-west transects across the MVBF (Figure 4). Transects ranged in length from 100 to 1200 m (3100 m total). Base station measurements and reoccupation of local benchmark stations indicated no significant diurnal or instrument drift.

The draped aeromagnetic data for Transect 4 was extracted from a 300 m grid of the original draped aeromagnetic data. The gridded data was sampled at 8 m intervals to be consistent with the measurement spacing of the ground magnetic survey. Since the original draped aeromagnetic data is from N45W oriented flight lines with 609 m separation and Transect

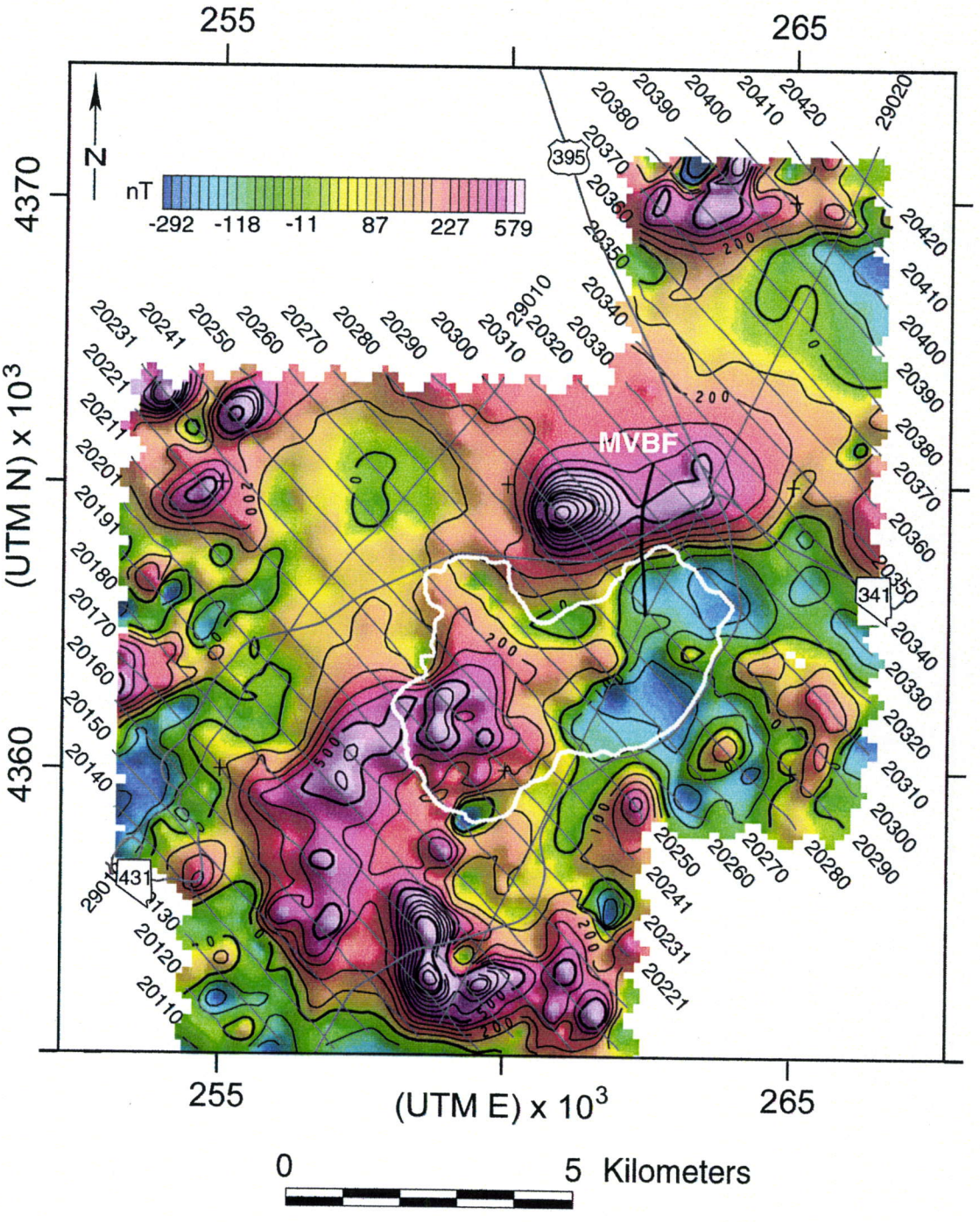

Figure 3. Residual reduced to pole aeromagnetic map from draped survey of the southerm Truckee Meadows and Steamboat Hills. Map shows magnetic low anomaly over the Steamboat Hills geothermal area. Outline of Steamboat Hills shown by dotted white line. MVBF indicates Mud Volcano Basin Fault shown in as solid black line.

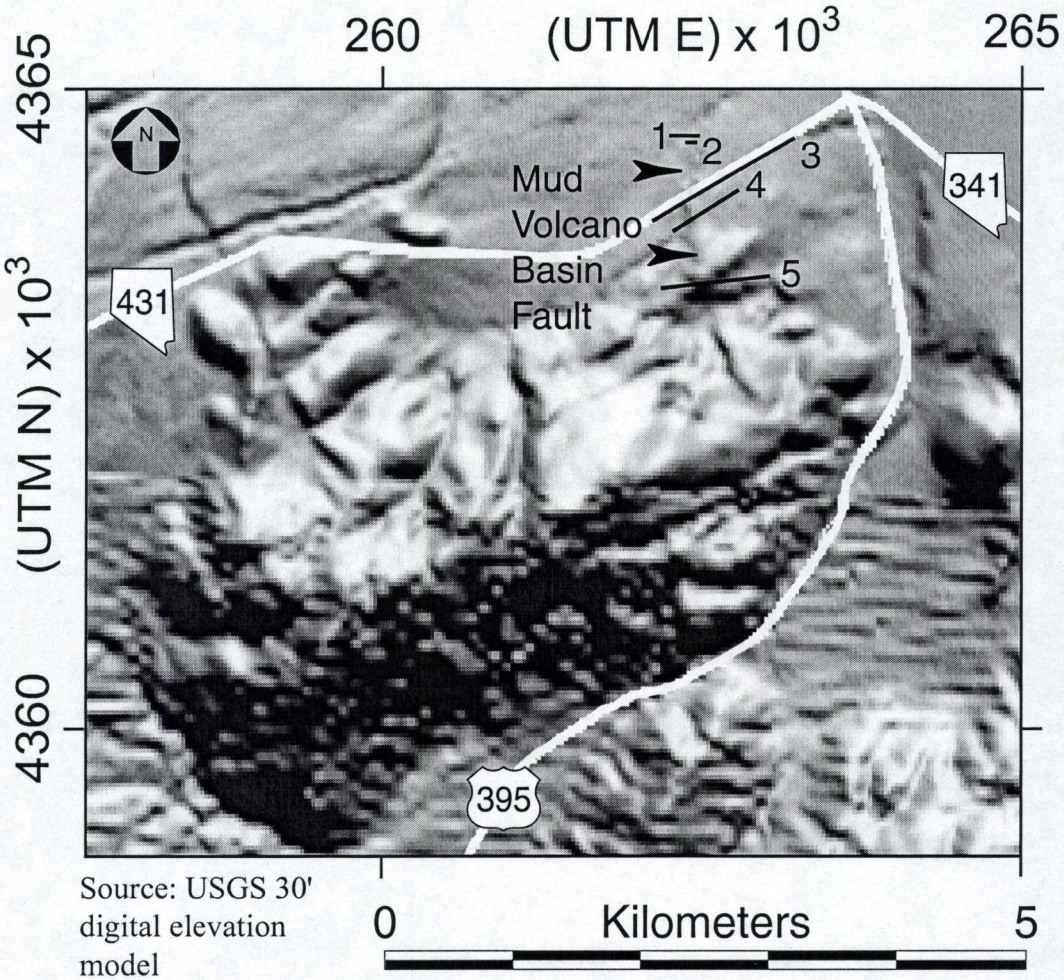

Figure 4. Ground magnetic transect locations across the Mud Volcano Basin Fault. Arrowheads point to the surface trace of the fault.

4 is oriented N60E, some loss in resolution of the anomaly is expected for the data sampled from the gridded data. We assume that a draped aeromagnetic flight line coincident with Transect 4 would yield better resolution of the MVBF anomaly. To simulate this assumed flight line, we upward continue the ground magnetic data a vertical distance of 50 m which is the average height above ground surface of the magnetic sensor during the draped aeromagnetic survey. The ground magnetic data was also upward continued 1250 m to simulate the constant elevation (2744 m) survey of Hendircks (1992).

Forward modeling of ground magnetic data from Transect 4 was done to estimate the width of the MVBF. The 2.75-D model configuration was constructed using the commercially-available modeling program (GM-Sys^{TM} by Northwest Geophysical Associates) based on Talwani et al (1959) and Talwani and Heirtzler (1964). Depths and magnetic properties (magnetic susceptibility, remanent magnetic direction and intensity) for the geologic units were obtained from Skalbeck et al. (Chapter 3). The MVBF was modeled as a zone of altered volcanic and granodiorite rock. Fault widths of 5, 10, and 15 m for ground magnetic data and fault widths of 3, 5, and 10 m for upward continued (50 m) data were evaluated for goodness of fit using the percent root mean square error (%RMSE; [RMSE/anomaly range]). Whole core magnetic susceptibility was measured at 1 cm intervals using a Barington M.S.2 susceptibility meter on 155 m (61 to 216 m depth) of rock from core hole MTH 21-33 drilled in the Far West Capital (FWC) area of the Steamboat Hills geothermal reservoir.

RESULTS

The 3-point moving average data of total field magnetic intensity along the five transects of the ground magnetic survey are shown in Figure 5. The distance along each transect was normalized with respect to the magnetic low anomaly assumed to represent the MVBF, which was set at the distance zero m. Figure 6 shows ground magnetic data along Transect 4 with data from the draped aeromagnetic survey. The 2.75-D forward models of ground magnetic data from Transect 4 (Figure 7) shows the geologic section for the 10 m fault width model of the MVBF with the calculated magnetic anomalies for the 5 m, 10 m, and 15 m fault width models and the associated %RMSE. Figure 8 shows the 2.75-D forward model results for 3 m, 5 m, and 10 m fault width models for the upward continued (50 m) data from Transect 4. The 3-point moving average of magnetic susceptibility versus depth (Figure 9) is shown with core hole log information (Goranson, 1994) and zones of inferred magnetic mineral alteration. Figure 10 shows the massive calcite in the core at depths from 193 to 196 m where negative magnetic susceptibility values are measured and thin fractures filled with calcite where moderate susceptibility values (up to 0.015 SI) are measured.

Aeromagnetic Survey

The aeromagnetic results show a magnetic low anomaly over the Steamboat Hills geothermal resource area. The metamorphic rocks in the southeastern portion of the Steamboat Hills have weak magnetic properties that contribute to the magnetic low anomaly; however, the volcanic and granodiorite rocks that comprise the majority of this area likely had strong original magnetic properties based on results from similar unaltered rocks in the Carson Range (Skalbeck et al., Chapter 3). This suggests that the volcanic and granodiorite rocks in the northeast portion of Steamboat Hills have been demagnetized by thermochemical alteration from the thermal water within the geothermal system.

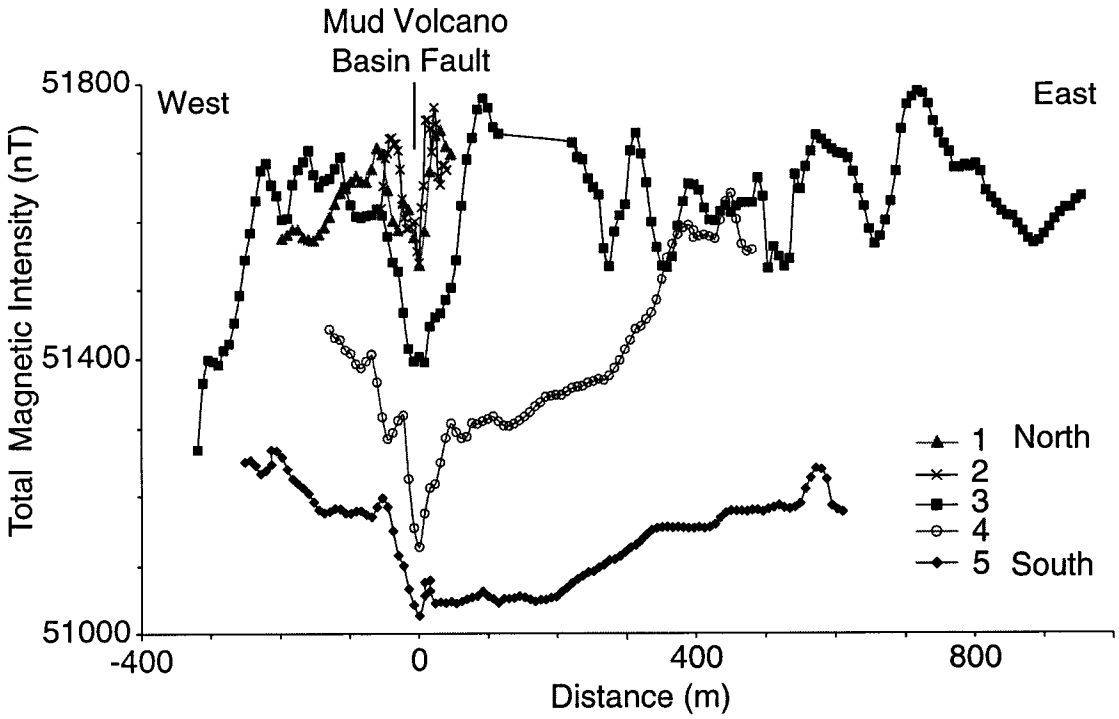

Figure 5. Total magnetic intensity along transects across Mud Volcano Basin Fault (MVBF). Transect locations are shown on Figure 4. The distance to the magnetic low associated with the MVBF was set at zero in each transect to illustrate the consistent anomaly.

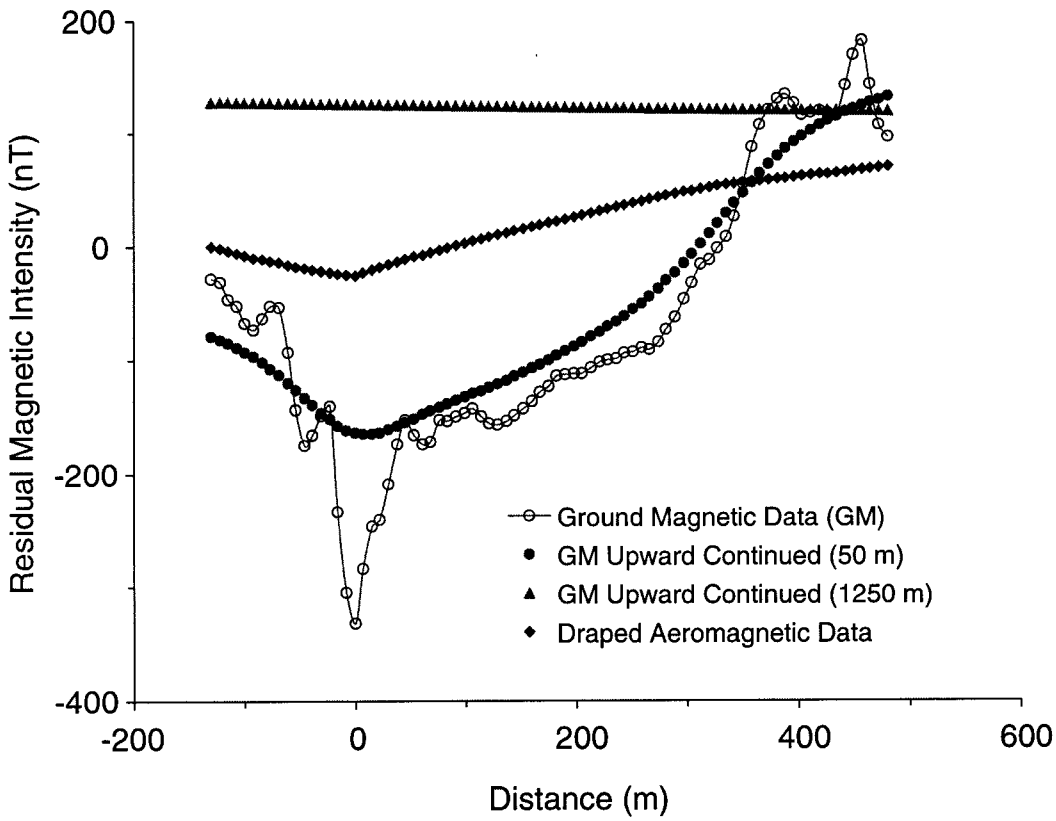

Figure 6. Residual magnetic intensity along transects across Mud Volcano Basin Fault Ground magnetic data is from Transect 4 (Figure 5).

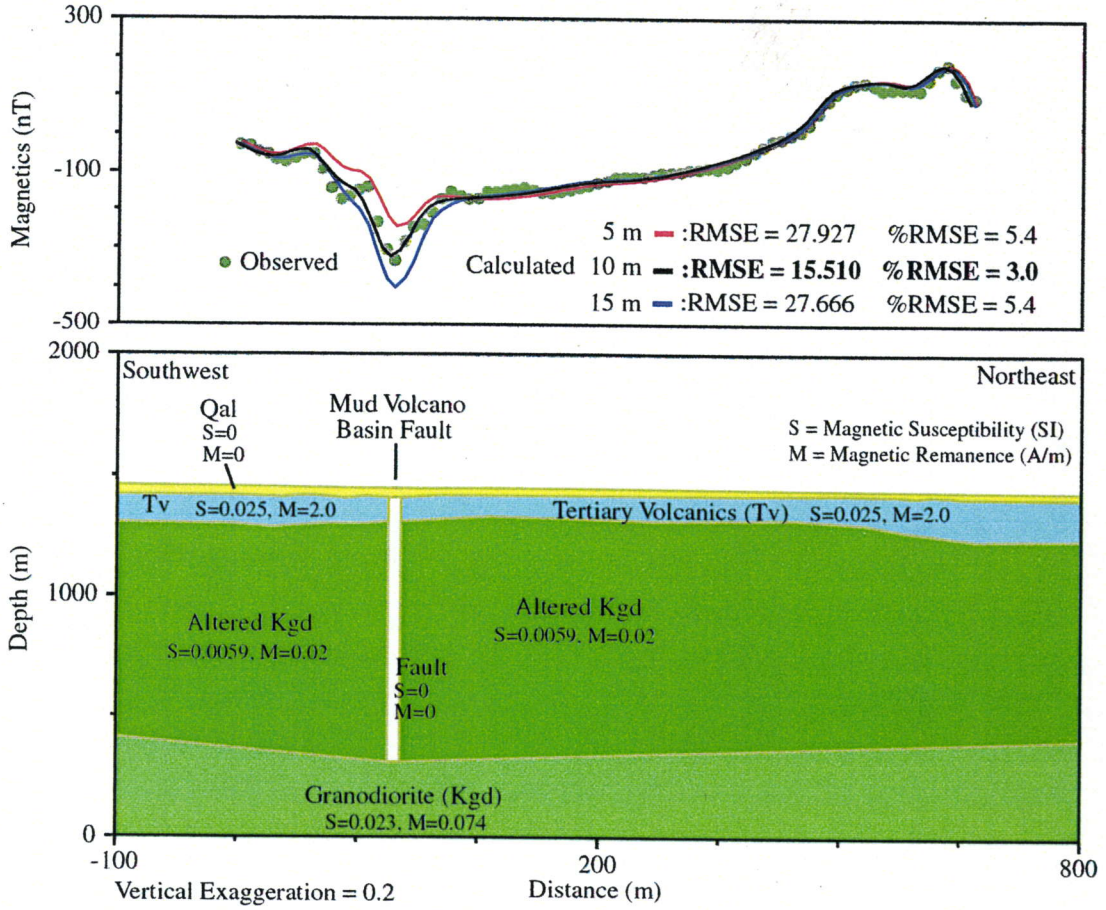

Figure 7. Cross-section of Transect 4 as computed by 2.75-D forward modeling of ground magnetic data showing calculated magnetic anomaly for 5 m, 10 m, and 15 m wide Mud Volcano Basin Fault. Geologic section and magnetic properties from Chapter 3. Bold RMSE and % RMSE values indicate best-fit model.

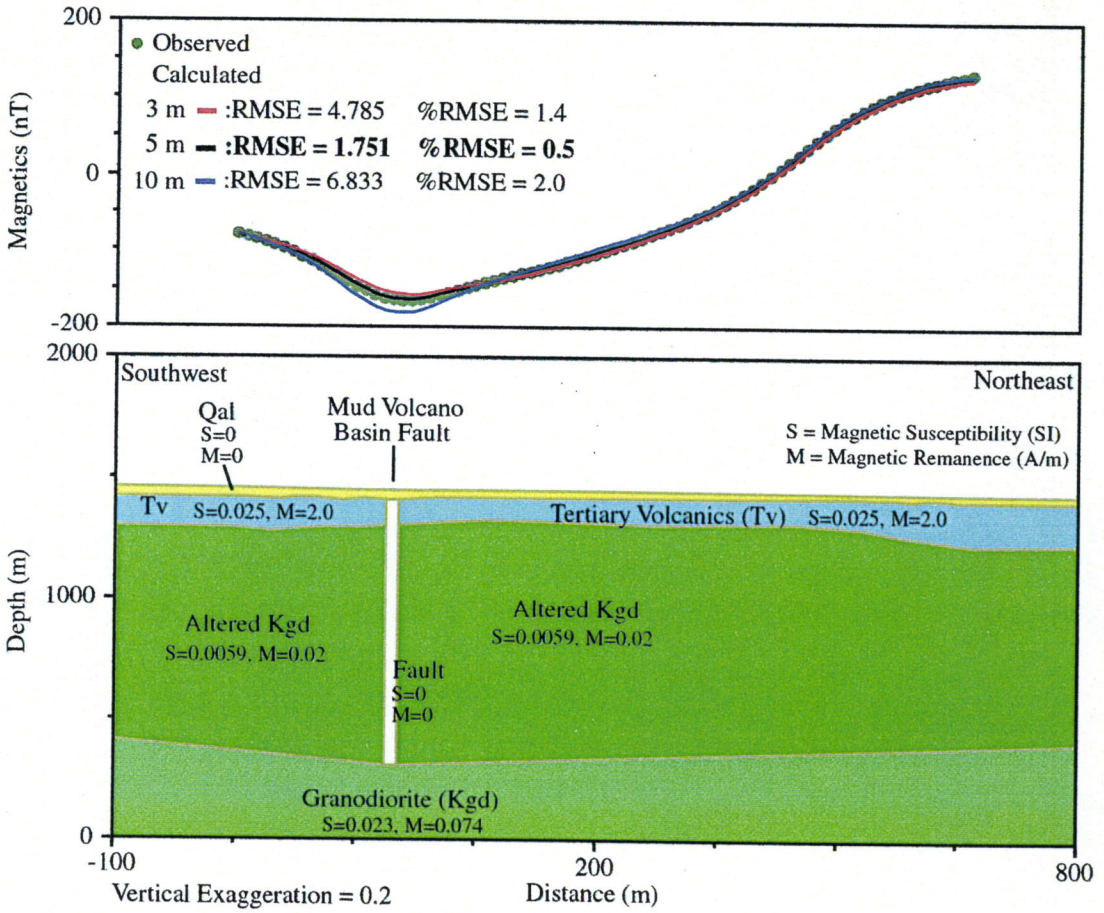

Figure 8. Cross-section of Transect 4 as computed by 2.75-D forward modeling of upward continued (50 m) ground magnetic data showing calculated magnetic anomaly for 3 m, 5 m, and 10 m wide Mud Volcano Basin Fault. Geologic section and magnetic properties from Chapter 3. Bold RMSE and % RMSE values indicate best-fit model.

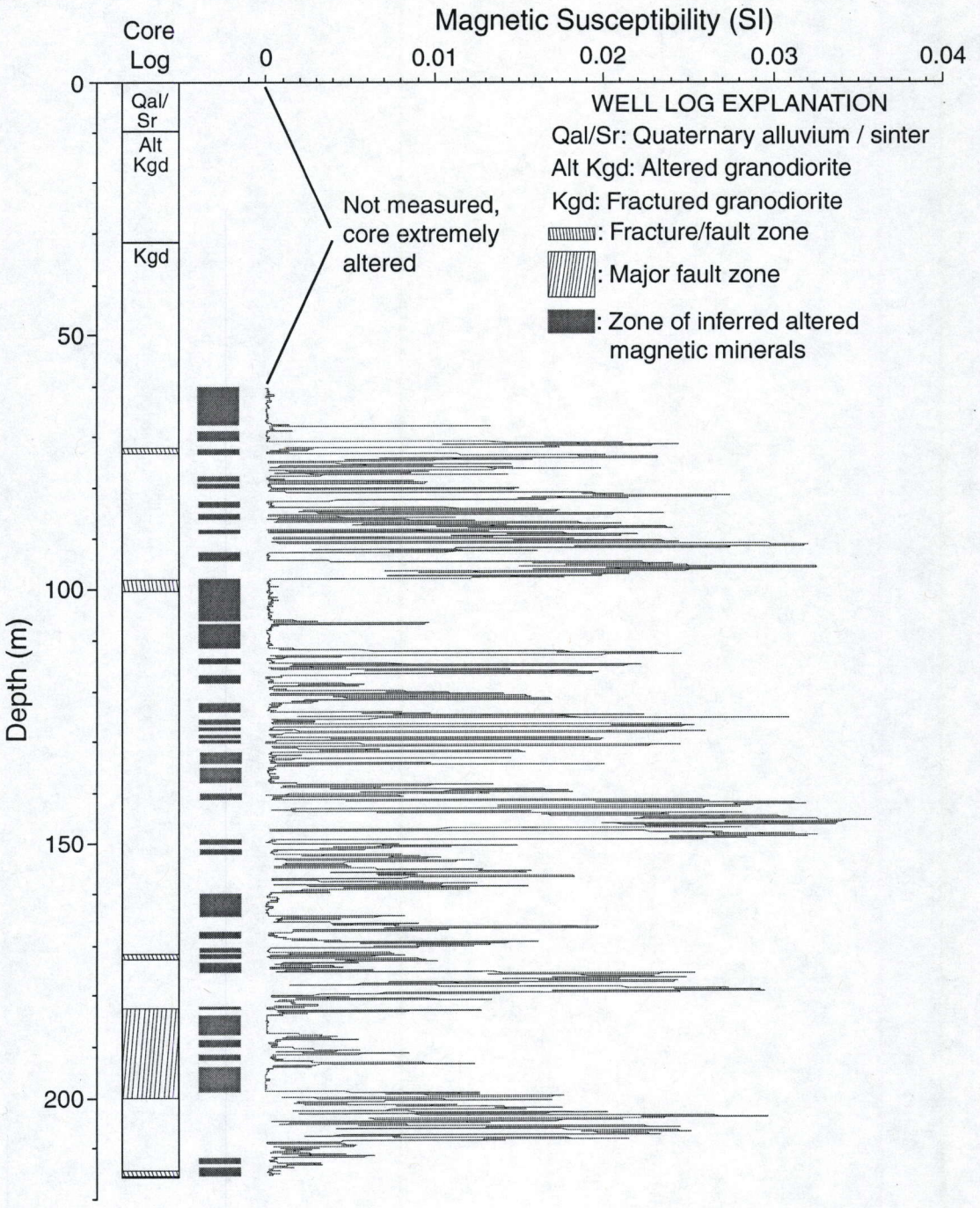

Figure 9. Vertical magnetic susceptibility profile for rock from core hole MTH 21-33. Also included are the core lithology, permeable fractures, and major fault zone as noted on core log (Goranson, 1994).

(a)

Depth from 193 to 196 m

10 cm

(b)

Depth from 118 to 121 m

10 cm

Figure 10. Photographs of rock from core hole MTH 21-33. (a) granodiorite showing massive calcite from major fault zone. (b) granodiorite showing thin fractures filled with calcite.

The magnetic high located north of the Mount Rose Highway (Nevada 431) shows a slightly lower saddle just east of the MVBF; however, this result does not definitively reveal a magnetic low coincident with this fault and may be due to some other structural feature. Even though a draped helicopter survey provides higher resolution than a constant elevation airplane survey, the resolution is not adequate for delineating a hydrologically significant fault in this geologic setting.

Ground Magnetic Survey

The higher total field magnetic intensities measured in Transects 1, 2, and 3 relative to Transects 4 and 5 are consistent with aeromagnetic data that reflect near surface Tertiary volcanics beneath alluvial fan deposits (Figure 3). The lower magnetic intensities found in Transects 4 and 5 reflect the alteration of magnetic minerals in granodiorite within the geothermal system. Highly variable data in Transect 3 result from abundant cultural noise (fences, light poles, sewer manholes) found along the Mount Rose Highway. Although the magnetic low anomaly at distance 1250 m in Transect 3 generally aligns with the north-trending Herz Fault that is thought to conduct thermal water (Skalbeck et al., 2001), a conclusive correlation is uncertain because of the degree of noise in this transect.

All five transects show a pronounced magnetic low anomaly (200 to 400 nT) corresponding to the MVBF (Figure 5). The magnetic low is interpreted as representing highly altered magnetic minerals in rocks adjacent to the MVBF resulting from thermal water conducted along the fault. The surface trace of the MVBF is verified along Transect 4 by steam vents located within 3 m of the minimum total field magnetic intensity measurement. A measurement was not obtained directly over the steam vent due to an obvious safety issue, so a lower minimum total field magnetic intensity may actually correspond to the fault. The degree of resolution for locating the surface trace of the MVBF suggested by the magnetic low anomaly for Transect 4 represents much greater resolution than topographic or digital elevation model maps, aeromagnetic maps, or geomorphic indicators (e.g., topographic depressions). The MVBF trace in the other four transects is inferred from the magnetic low. Transects 1 (northern most) through 4 show the magnetic low anomaly over very narrow distances. The width of the anomalies decreases with increasing distance from the geothermal area suggesting that the thermal alteration along the MVBF is focused more narrowing beneath the alluvial deposits to the north. Unlike the other four transects, Transect 5 (closest to the geothermal production area) shows a gradual increase in total magnetic intensity east of the low associated with the MVBF and appears to be associated with pervasive alteration observed at ground surface in the Mud Volcano Basin.

Ground magnetic, upward continued ground magnetic, and draped aeromagnetic data were evaluated to assess the resolution of detecting the magnetic low anomaly associated with the MVBF. The ground magnetic data upward continued 1250 m shows no magnetic anomaly. Each of the other data sets shows a magnetic low anomaly over the MVBF. As expected the ground magnetic data shows the most pronounced anomaly and the draped aeromagnetic data show the smallest anomaly. The decreased amplitude of the anomaly in the draped aeromagnetic and upward continued data illustrates that the magnetic field falls off at the rate of $1/r^3$ where r is distance from a magnetic source or sink. The draped aeromagnetic and upward continued (50 m) data produce smooth curves due to the attenuation of magnetic signal from surface or shallow subsurface sources.

Magnetic Susceptibility

Magnetic susceptibility from core hole MTH 21-33 ranged from -0.00013 to 0.036 dimensionless SI units with a mean of 0.0059 SI. Based on correlation with visibly altered section of the rock core, magnetic susceptibility values below 0.001 SI are assumed to represent zones of highly altered magnetic minerals or fractures filled with non-magnetic minerals (i.e. calcite). The number of magnetic susceptibility values below 0.001 SI is 47% of the total measurements for core hole MTH 21-33. For comparison, one surface sample of altered granodiorite from the Steamboat Hills had a magnetic susceptibility value of 0.0014 SI and eight samples of unaltered granodiorite collected in the Steamboat Hills and Carson Range had magnetic susceptibility ranging from 0.0063 to 0.032 SI with a mean of 0.023 SI (Skalbeck et al., Chapter 3).

The magnetic susceptibility results from core hole MTH 21-33 suggest that thermochemical alteration of magnetic minerals occurs along fractures but not within the rock matrix. The lower magnetic susceptibility value for the altered granodiorite is assumed to result from destruction of magnetic minerals primarily by flow of thermal water in fractures and filling of fractures with secondary non-magnetic minerals. Permeable fracture zones and a major fault zone (183 to 201 m depth) noted on the well log correspond to lower magnetic susceptibility values (Figure 9). For the purpose of modeling the ground magnetic data, the mean magnetic susceptibility (0.0059 SI) for the entire measured rock from core hole MTH 21-33 is assumed to represent a composite value for altered granodiorite within the geothermal system. This composite value reflects alteration of magnetic minerals along fractures but not in the rock matrix.

2.75-D Forward Modeling

Forward modeling of ground magnetic data across the MVBF (Figures 7 and 8) suggests that a fault width of 5 m and 10 m best represents the magnetic low anomaly associated with the MVBF along Transect 4 based on the upward continued (50 m) and ground magnetic data, respectively. The lower %RMSE values representing excellent fits for the upward continued (50 m) data reflect the attenuation of near surface magnetic noise from the original ground magnetic data. We suggest that the vertical zone of altered volcanic and granodiorite rocks along the MVBF is due to northward migration of thermal water from the geothermal system. Temporal variations of B and Cl in alluvial aquifer monitoring wells (Skalbeck et al., 2001) confirm thermal water is conducted along the fault. B and Cl concentrations in the Pine Tree Ranch #1 well located approximately 30 m from the MVBF are much lower than in the Flame well located on the trace of the fault. The water chemistry results imply that thermal water is conducted along a focused preferential flow path with less lateral flow away from the fault in to the surrounding rocks, and support magnetic forward modeling of the MVBF as a narrow alteration zone

These modeling results suggest that draped aeromagnetic data collected from heights of 50 m above ground surface can detect a hydrogeologically significant fault in this type of geothermal setting; however, we had a priori knowledge of the MVBF location. The slight inflection of the magnetic high along flight line 20310 (Figure 3) near the MVBF may give an unbiased observer an indication of the existence of a fault; however, the trace of the fault cannot be delineated from this data. Graugh (2001) describes high-resolution aeomagnetic surveys used to map intrabasinal faults in the Albuquerque basin, New Mexico as having nominal line spacing (no distance given) and sensor heights of 100-150 m above ground surface. The faults delineated in that study are typically 5-50 km in length. Since the MVBF is less than 3 km in length, any

draped aeromagnetic survey would need close flight line spacing. Based on the ground magnetic survey flight line spacing for a draped survey may need to be as close as 300 m to delineate the MVBF.

Gravity and Airborne Resistivity Evaluation for Delineating the MVBF

To assess whether other geophysical data could delineate the MVBF, we evaluated gravity and airborne resistivity data. Gravity data at 166 stations from a study (Carpenter, 1996) contracted by Washoe County Department of Water Resources (Washoe County) was merged with existing gravity coverage (Hittelman et al., 1994) for total coverage that included 503 points. Nearest neighbor distance between stations ranged from 100 to 4000 m. Figure 11 shows the northern portion of the residual isostatic gravity contour map derived from minimum curvature gridding (Briggs, 1974). Although there are a number of gravity stations along Nevada Hwy 431 and near the southern portion of the MVBF, the gravity data do not delineate the fault.

Electromagnetic (EM) data were collected with the magnetic data during the draped airborne survey (Dighem, 1994). Maps of apparent resistivity (Figure 12a, 12b, 12c) were produced from the 900, 7200, and 56000 Hz coplanar EM data using minimum curvature gridding. Low resistivity values (5-40 ohm-m) in the vicinity of the MVBF are part of a broad zone of low values coincident with the FWC geothermal production area, the discharge area of the geothermal system, and the distal portion of the Mount Rose Fan. The low resistivity values are due to higher clay content in the alluvial deposits and elevated total dissolved (TDS) solids in the groundwater. Since depth to groundwater is 15-20 m in this area (Skalbeck et al., 2001), calculating the depth of investigation for each frequency of resistivity would provide a qualitative assessment of the contribution of clay and TDS to low resistivity values. The depth of investigation is assumed to be one skin depth (δ) calculated by $\delta = 503\ (\rho/f)^{1/2}$ where ρ is resistivity and f is frequency (Telford et al., 1990). Table 1 summaries the depth of investigation calculated for each frequency. The calculated depth of investigation (13 m) for 56000 Hz suggests that clays in the alluvial deposits produce the low resistivity values at this frequency. Low resistivity values from 900 and 7200 Hz are due to clay and perhaps elevated TDS. The calculated depth of investigation (53 m) for 900 Hz suggests that this frequency reaches the top of fractured volcanics at approximately 40 m and therefore should sense the MVBF; however, none of the frequencies produce resistivity data that delineates the fault.

Table 1. Depth of investigation from apparent resistivity data near the Mud Volcano Basin Fault.

Frequency (f) (Hz)	Average Resistivity (ρ) (ohm-m)	One Skin Depth (δ) (m)
900	10	53
7200	15	23
56000	40	13

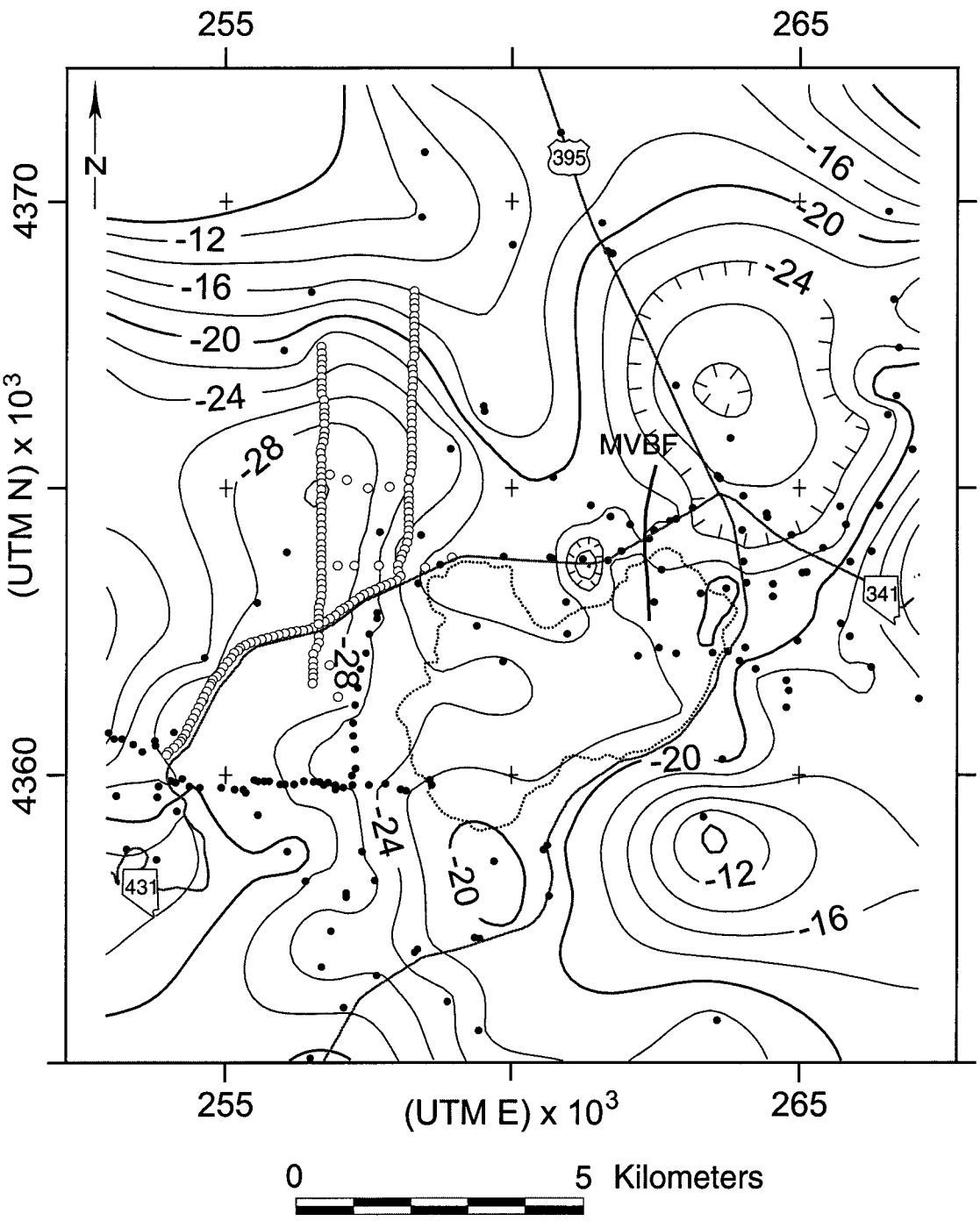

Figure 11. Residual isostatic gravity map of southern Truckee Meadows and Steamboat Hills. Open circles are stations from Carpenter (1996) and closed circles are from Hittelman et al. (1994). Contour interval is 2 mGal. Outline of Steamboat Hills shown by dotted black line. MVBF indicates Mud Volcano Basin Fault shown in as solid black.

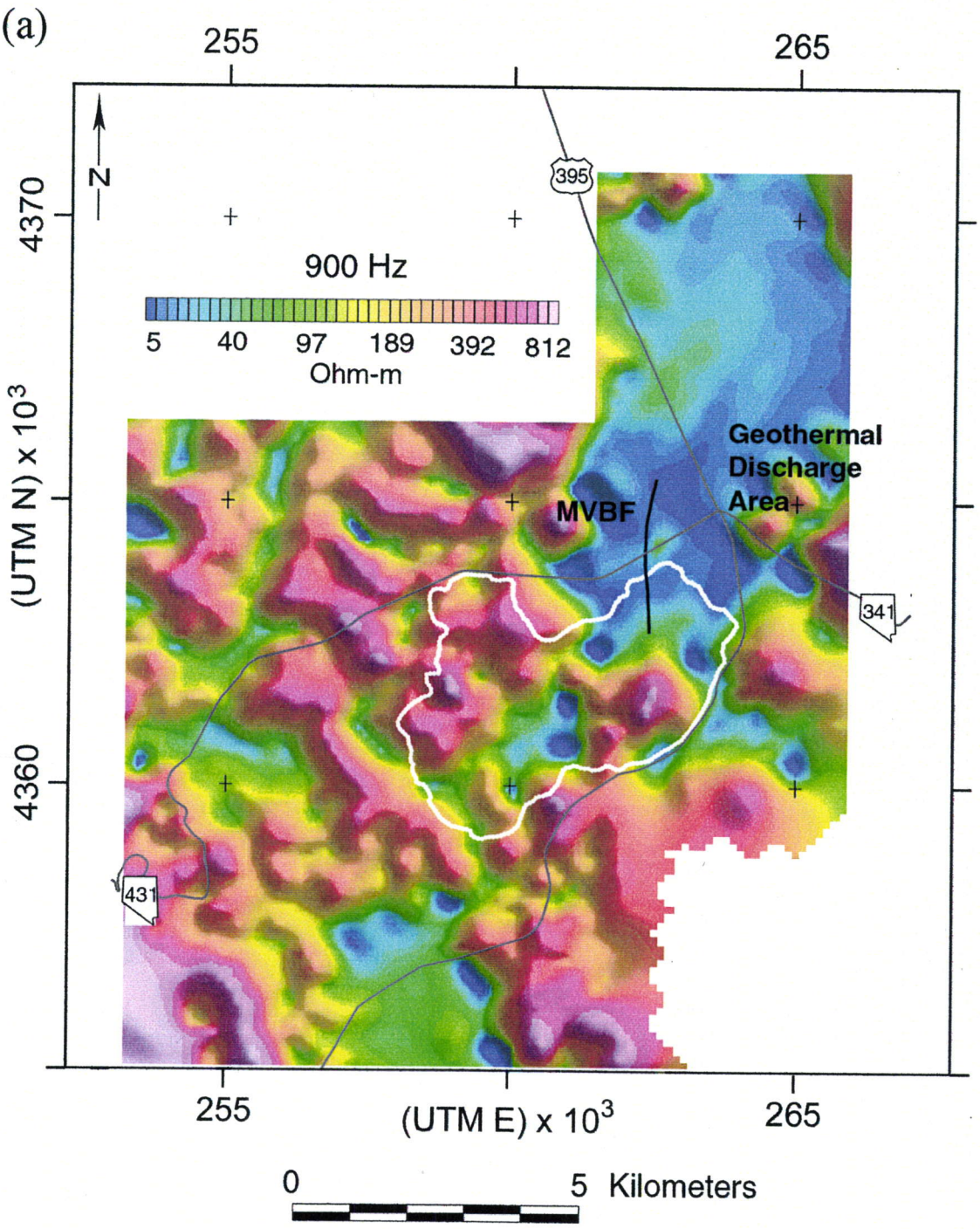

Figure 12a. Resitivity from draped survey of the southern Truckee Meadows and the Steamboat Hills area for 900 Hz frequency. Map shows low resitivity in geothermal discharge area Outline of Steamboat Hills shown by white line. MVBF indicates Mud Volcano Basin Fault shown as black line. Figures 12b and 12 c shown on following pages.

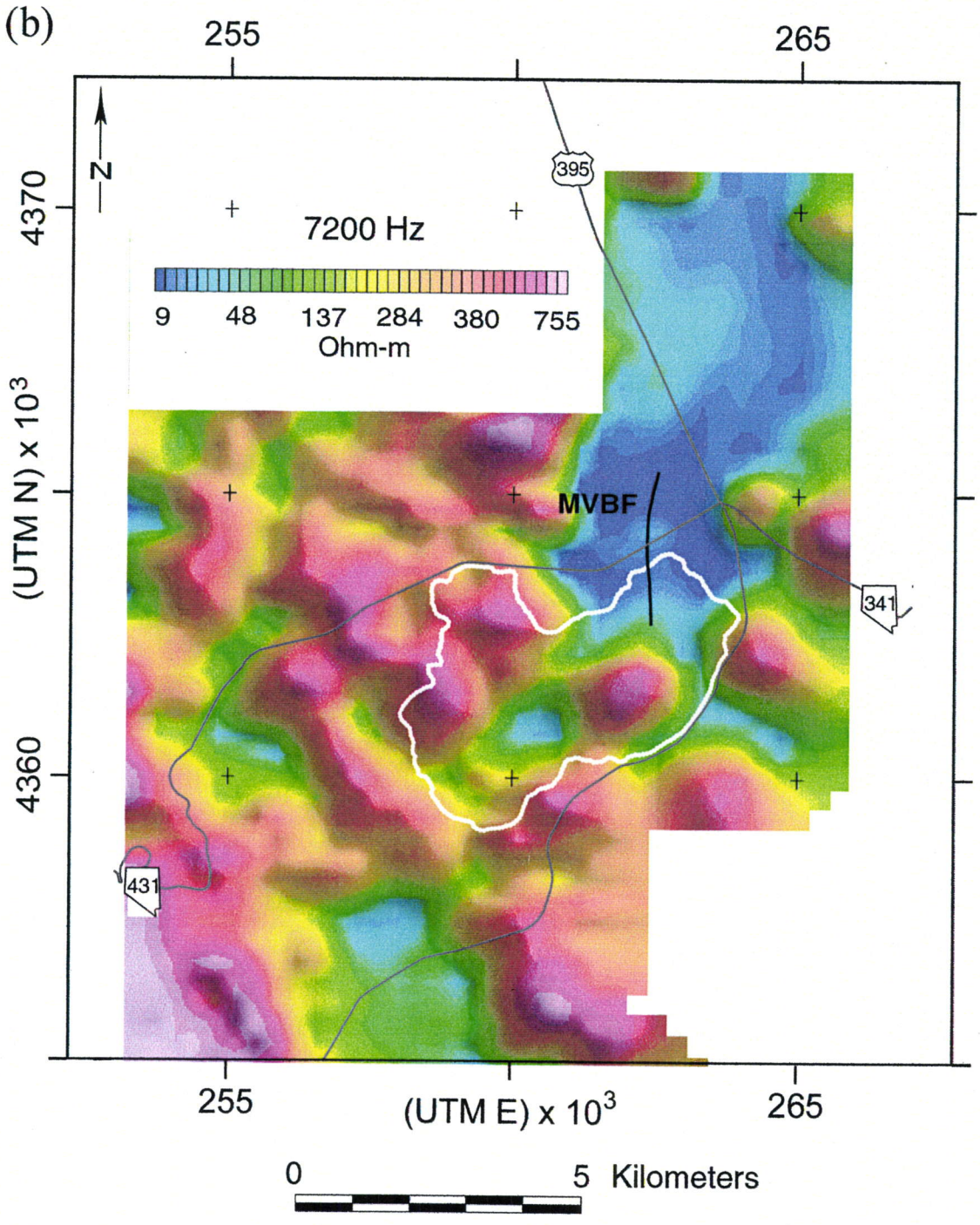

Figure 12b. Resitivity from draped survey of the southern Truckee Meadows and the Steamboat Hills area for 7200 Hz frequency. Map shows low resitivity in geothernal discharge area Outline of Steamboat Hills shown by white line. MVBF indicates Mud Volcano Basin Fault shown as black line. Figure12 c shown on following page.

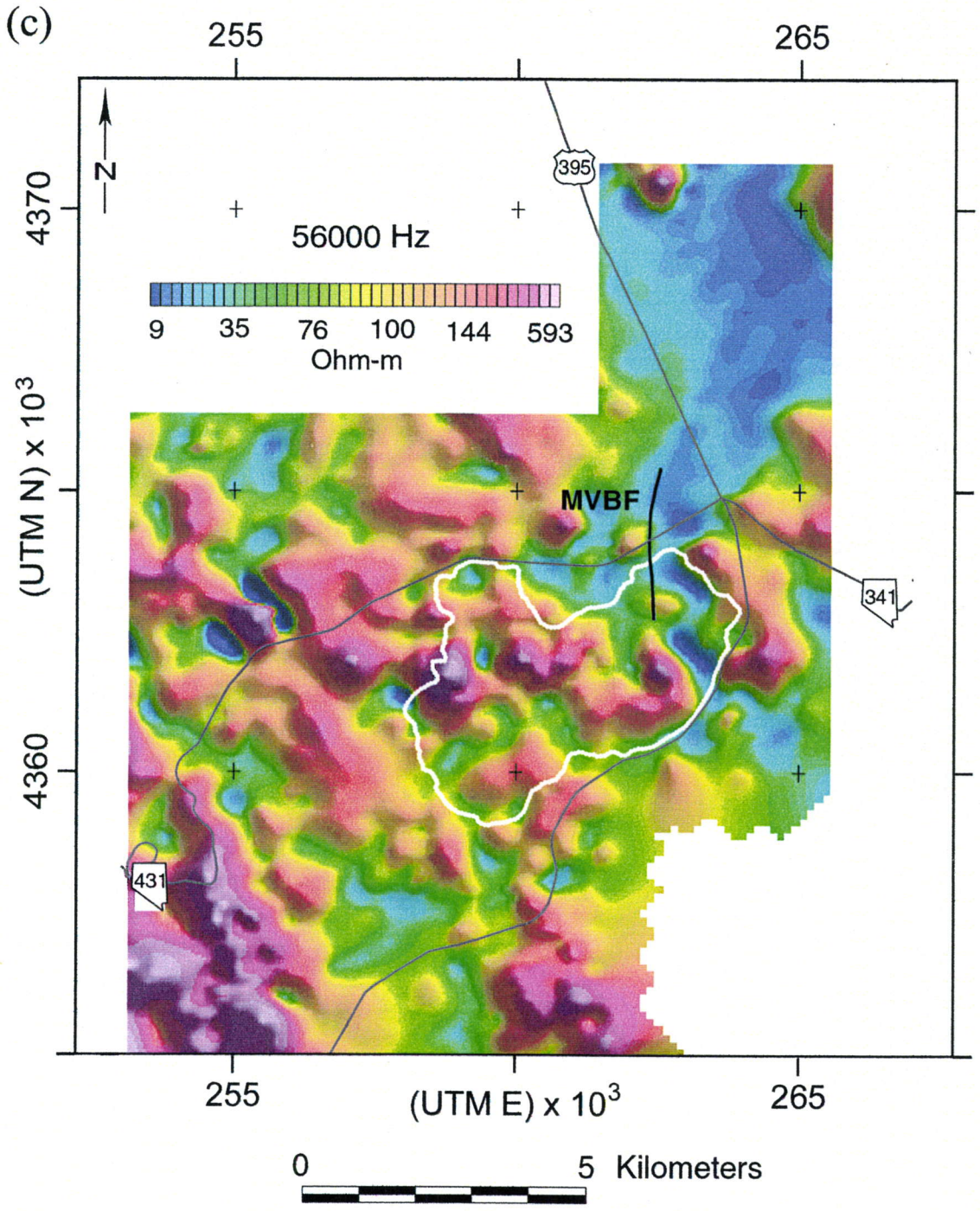

Figure 12c. Resitivity from draped survey of the southern Truckee Meadows and the Steamboat Hills area for 56000 Hz frequency. Map shows low resitivity in geothernal discharge area Outline of Steamboat Hills shown by white line. MVBF indicates Mud Volcano Basin Fault shown as black line.

DISCUSSION

The application of magnetic methods at the Steamboat Hills geothermal area yields results that formulate an exploration and site characterization strategy, which can be utilized at other geothermal resource sites. Once a prospective geothermal area is identified, the exploration and site characterization strategy begins with an initial reconnaissance of the geothermal area using a draped aeromagnetic survey. Ground magnetic surveys are then used to delineate of hydrologically significant faults that control the preferential flow of thermal water. Finally, vertical magnetic susceptibility measurements obtained during borehole logging or from whole rock core following drilling are used as magnetic property input for forward modeling of aeromagnetic data and as a possible indicator of permeable fractures.

The aeromagnetic low anomaly observed for the Steamboat Hills geothermal resource area from a draped helicopter survey (Figure 3) results from thermochemical alteration of the magnetic minerals in the reservoir and cap rocks. Ross et al. (1996) found a similar low-magnetization area in the central portion of the Ascension Island from a low altitude (200 m) survey that they associate with a shallow (1-3 km) geothermal system. This type of magnetic signature can be an indicator of geothermal resource potential at other uncharacterized or blind sites. This magnetic anomaly pattern at Steamboat Hills is not apparent in aeromagnetic data from a constant elevation (2743 m) airplane survey with flight line spacing of 3200 m and downward continuation to 305 m (Hendricks, 1992). These results demonstrate that the higher resolution draped helicopter aeromagnetic survey is best suited for adequate reconnaissance of potential geothermal resources sites.

Ground magnetic transect data show magnetic low anomalies (200 to 400 nT), which delineate the Mud Volcano Basin Fault (MVBF) with excellent resolution (Figure 5). Steam vents along Transect 4 verify the trace of the fault. Traverse 8 from White et al. (1964), located between Transects 4 and 5 from this study shows a 500 nT negative anomaly at the MVBF. White et al. (1964) mapped bleached volcanic breccia rocks, indicating hydrothermal alteration, along the MVBF. This alteration supports the hypothesis that the rocks adjacent to the fault are demagnetized resulting in the magnetic low anomaly. The magnetic anomalies delineate the trace of the MVBF beneath the alluvial fan deposits and thus map a preferential flow path for thermal water into the alluvial aquifer. The resistivity results (Figure 12) do not delineate the MVBF. Based on the depth of investigation calculations (Table 1), the resistivity lows in this area likely result from clays in the alluvial deposits that obscure any possible signal from thermal water along the MVBF.

Permeable fractures and a major fault zone noted on the core hole log match low magnetic susceptibility values; however, the magnetic susceptibility profile also shows low values where no permeable fractures are noted on the core hole log. We suggest that the low magnetic susceptibility values indicate open fractures, alteration along fractures that conduct thermal water, or fractures filled with calcite. The magnetic susceptibility results suggest a higher fracture frequency than the core log; however, more analysis is required to verify this hypothesis. Negative magnetic susceptibility values are indicative of materials that exhibit diamagnetic behavior where the induced magnetization is in the opposite direction of the applied field. Negative magnetic susceptibility measurements from this core are interpreted as calcite filled fractures. The most continuous section of negative magnetic susceptibility values (-6 to -130 x 10^{-6} SI) is found at depths from 196 to 198 m, which is the lower portion of the major fault zone (Figure 9). These values agree with typical values of magnetic susceptibility for calcite that

range from -13 to -40 x 10^{-6} SI (Schon, 1996) and with well log information indicating massive calcite at depths from 194 to 200 m (Goranson, 1994). Figure 8 shows the massive calcite in the core at depths from 193 to 196 m. An injection flow test conducted at depths from 180 to 216 m confirms that these fractures are productive (Goranson, 1994). Future research is needed to evaluate the correlations between magnetic susceptibility data and fracture frequency and fracture permeability.

An exploration and site characterization strategy for new geothermal resource sites would begin with an initial review of available information from state maps and databases (e.g, for Nevada; Garside and Shevenell, 2000). The review of existing geologic maps, aeromagnetic and gravity data, and available well data (lithologic, temperature, chemistry) is needed to design a high resolution draped aeromagnetic and additional gravity surveys. Analysis of this compiled data is used to identify potential permeable faults that may be favorable targets for exploratory drilling. A ground magnetic survey is designed to verify and delineate target permeable faults. Based on these results, exploratory drilling using slim hole techniques is conducted and followed by geophysical logging for temperature, pressure, spinner, and magnetic susceptibility. The magnetic susceptibility results can be used in potential fields modeling of the aeromagnetic and gravity data along multiple profiles to construct a 3-D representation of the subsurface structure.

The geologic setting needed for application of the proposed strategy must include rocks that have density and magnetic properties contrasts. The granitic, volcanic, and metamorphic rocks and alluvial deposists found at Steamboat Hills exhibit good property contrasts. A geologic setting with predominantly one rock type or with rocks that have similar density and magnetic properties would not be appropriate for this exploration strategy. Developed locations such as Dixie Valley and the Beowawe Geyesrs could provide confirmation of the proposed strategy since copious data has been generated at these sights. Similar to the Steamboat Hills area, the Beowawe Geyesrs geothermal area contains Paleozoic metasediment and metavolcanic rocks overlain by Tertiary basalt and andesite and Quaternary siliceous sinter and alluvium with northeast- and northwest-trending faults Garside and Schilling (1979). The geology of the Dixie Valley geothermal system consists of Jurassic gabbroic rocks of the Humboldt igneous complex overlain carbonates, silicic ashflow tuffs, basalt flows, and lake sediments (Plank et.al., 1999). Both geothermal areas contain rocks with sufficient density and magnetic properties contrasts for potential field modeling. A couple of undeveloped locations in Nevada (e.g. Rye Patch, Nixon) could be good test sites for this exploration and site characterization strategy.

CONCLUSIONS

A comprehensive characterization program for exploration of geothermal resources should include all available geologic, hydrogeologic, geochemical, and geophysical techniques. We have presented a strategy for using magnetic methods to assist in geothermal resource characterization. Widely available constant elevation aeromagnetic surveys that are typically >1000 m above ground surface likely will not be useful in site specific initial reconnaissance. However, the draped aeromagnetic survey flown from 30 to 120 m ground surface at Steamboat Hills and the low altitude constant survey of the Ascension Island both identify geothermal reservoir areas at the scale of kilometers.

Fault-controlled groundwater flow is common to most geothermal systems. Therefore, detailed fault delineation is critical for siting production and injection wells as well as evaluating the hydraulic connection with other geologic units (e.g. alluvial aquifers). For hydrogeologic

settings where a bedrock fault conducts thermal water along a focused flow path into an overlying alluvial aquifer, ground magnetic surveys are effective for high-resolution (meter scale) delineation of faults that conduct thermal water. Selection of exploratory drilling sites can then be based on identification of hydrologically significant faults.

Although a vertical magnetic susceptibility profile was generated from rock core for this study, a comparable profile can easily be produced using a borehole-logging tool. As demonstrated by Thibal et al. (1999), borehole logging of magnetic susceptibility can yield a less noisy signal than the core logging. For ideal characterization of the vertical magnetic properties of a drill site, we recommend borehole logging of magnetic susceptibility and total field magnetics along with the customary pressure, temperature, and spinner logs. Alternatively, the vertical magnetic properties can be obtained from the recovered core but noise is introduced from breaks in the core. The resulting magnetic profile can be useful in identifying lithologic variations and provides important property information for forward modeling of aeromagnetic data. The vertical magnetic data can also be important for fracture identification.

REFERENCES

Bonham, H.F., Jr., and Rogers, D.K., 1983, Geologic map, Mt. Rose NE quadrangle: Nevada Bureau of Mines and Geol., Map 4Bg.

Bonham, H.F., Jr., and Bell, J.W., 1993, Geologic map, Steamboat quadrangle: Nevada Bureau of Mines and Geol., Map 4Fg.

Briggs, I.C., 1974, Machine contouring using minimum curvature, Geophysics, 39, 39-48.

Carpenter, T., 1996, Gravity data acquisition and processing, Mount Rose Fan project, Washoe County, Nevada: unpublished report for Washoe County Utility Division, November 1996, 6 p.

Cohen, P., and Loeltz, O.J., 1964, Evaluation of Hydrogeology and Hydrochemistry of Truckee Meadows Area, Washoe County, Nevada: U.S. Geol. Surv. Water Supply Paper 1779-S, 63 p.

Corwin, R.F., and Hoover, D.B., 1979, The self potential method in geothermal exploration, Geophysics, 44, 226-245.

DIGHEM, 1994, Dighem^{V} survey for Utility Division, Washoe County Public Works, Washoe County, Nevada: unpublished report #612, December 28, 1994, 36 p.

Department of Energy (DOE), 2001, DOE State Energy Alternatives, [On-line], Available at http://www.eia.gov/emeu/state/main_nv.html.

Garside, L.J., and Schilling, J. H., 1979, Thermal waters of Nevada: Nevada Bureau of Mines and Geol., Bull. 91, 163 p.

Geothermal Education Office, 2001, [On-line], Available at http://www.geothermal.marin.org/map/usa.html.

Goranson, C., 1994, Summary of drilling and testing operations on core hole MTH 21-33 at the Far West Capital Meyberg Lease Area, Steamboat Springs, Nevada: unpublished report prepared for Far West Capital, Inc., May, 5 p.

Grauch, V.J.S., 2001, High-resolution aeromagnetic data, a new tool for mapping intrabasinal faults: Example from the Albuquerque basin, New Mexico: Geology, 29, 367-370.

Hendricks, J.D., 1992, Total-intensity magnetic-anomaly map of the Reno 1° by 2° quadrangle, Nevada and California, Map MF-2154-E.

Hittelman, A.D., Dater, D., Buhmann, R. and Racey, S., 1994, Gravity CD-ROM and user's manual: National Oceanic and Atmospheric Administration, National Geophysical Data Center.

Hoover, D.B., and Pierce, H.A., 1986, Airborne electromagnetic mapping of geothermal systems in the basin and range and cascade provinces, U. S. A.: *in* Airborne Resistivity Mapping, Ed. Palacky, G.J., Geol. Surv. Canada, Paper 86-22, 139-143

Mariner, R.H., and Janik, C.J., 1995, Geochemical data and conceptual model for the Steamboat Hills geothermal system, Washoe County, Nevada: Geothermal Resources Council Transactions, 19, 191-200.

McElhinny, M.W., 1973, Paleomagnetism and plate tectonics: Cambridge University Press, Great Britain, 357 p.

McElhinny, M.W., and McFadden, P.L., 2000, Paleomagnetism, Continents and oceans: Academic Press, San Diego, 386 p.

Nagata, T., 1961, Rock magnetism: Maruzen Company Ltd., Tokyo, 350 p.

O'Reilly, W., 1984, Rock and mineral magnetism: Blackie and Sons Ltd., Glasgow and London, 220 p.

Plank, G.L., Schweickert, R.A., Simmons, A., and Benoit, R., 1999, The influence of down-dip fault geometry on the location of the Dixie Valley Geothermal Area, Dixie Valley, Nevada [abs.]: 24th Stanford Geothermal Workshop, January 25-27.

Ross, H.P., Nielson, D.L., and Green, D.J., 1996, Aeromagnetic survey and interpretation, Asecension Island, South Atlantic Ocean: Geothermics, 25, 471-488.

Shevenell, L., Garside, L.J., and Hess, R.H., 2000, Nevada geothermal resources: Nevada Bureau of Mines and Geol., Map 126.

Schon, J.H., 1996, Physical Properties of rocks, Fundamental and principles of petrophysics: Elsevier Science Ltd., Oxford, 583 p.

Skalbeck, J.D., Shevenell, L., and Widmer, M.C., 2001, Mixing of Thermal and Non-Thermal Waters the Steamboat Hills Area, Nevada: Geothermics, 30, *in press*.

Sorey, M.L. and E.M. Colvard, 1992, Factors affecting the decline in hot-spring activity in the Steamboat Springs area of critical environmental concern, Washoe County, Nevada: U.S. Geol. Surv., administrative report for U.S Bur. of Land Manag., 109 p.

Tabor, R.W., and Ellen, S., 1975, Geologic Map, Washoe City Folio: Nevada Bureau of Mines and Geol. Environmental Series.

Talwani, M. and Heirtzler, J.R., 1964, Computations of magnetic anomalies casued by two-dimensional bodies of arbitary shape, *in* Parks, G.A., Ed., Computers in the mineral industry, Part I, Stanford Univ. Publ., Geological Sciences, 9, 464-480.

Talwani, M., Worzel, J.L., and Landisman, M., 1959, Rapid gravity computations for two-dimensional bodies with application to the Mendocino Submarine fracture zone, J. Geophys. Res., 64, 49-59.

Thibal, J., Etchecopar, A., Pozzi, J. -P., Barthes, V., and Pocachard, J., 1999, Comparison of magnetic and gamma ray logging for correlations in chronology and lithology: example from the Aquitanian Basin: Geophy. J. Internat., 137, 839-846.

Telford, W.M., Geldart, L.P., and Sheriff, R.E., 1990, Applied geophysics: Cambridge University Press, Cambridge UK, 770 p.

Thompson, G.A., and White, D.E., 1964, Regional geology of the Steamboat Springs area, Washoe County, Nevada: U. S. Geol. Surv. Prof. Paper 458-A., 52 p.

White, D.E., Thompson, G.A., and Sandberg, C.H., 1964, Rocks, structure, and geologic history of Steamboat Springs thermal system, Washoe County, Nevada: U. S. Geol. Surv. Prof. Paper 458-B., 62 p.

White, D.E., 1968, Hydrology, activity, and heat flow of the Steamboat Springs thermal system, Washoe County, Nevada: U. S. Geol. Surv. Prof. Paper 458-C., 109 p.

CHAPTER 5

SUMMARY AND CONCLUSIONS

Summary

Geochemistry (Chapter 2)

Temporal variations in B and Cl concentrations, water levels, and temperature in alluvial aquifer wells are used to evaluate the mixing of thermal and non-thermal waters. Data were compiled from a groundwater monitoring program begun in 1985 at two geothermal facilities in the Steamboat Hills area, Nevada and from three studies related to the geothermal system. Important findings are as follows:

- Results suggest a common origin for thermal and non-thermal waters.

B and Cl concentrations from all types of water (creeks, cold springs, non-thermal groundwater, mixed, and thermal waters) plot along a linear local trend. This trend suggests a common origin of the geothermal waters and simple mixing of non-thermal groundwater and thermal waters.

- Characteristic water chemistry is identified in three wells.

Consistent B and Cl concentrations found in the Peigh Domestic, Herz Geothermal, and Curti Barn Geothermal wells indicate characteristic non-thermal, mixed, and thermal type waters, respectively. These characteristic water types are important for evaluating the mixing at other wells.

- Results indicate thermal water flows along north-trending faults.

The characteristics of thermal and non-thermal water mixing indicate that a number of north-trending faults conduct thermal water into the alluvial aquifer. The results show increasing thermal water along the local trend line in the Flame and Pine Tree Ranch #1 wells that is dependent on proximity to the north-trending Mud Volcano Basin Fault (MVBF). The Flame well, located on the MVBF, shows maximum B and Cl concentrations similar to the characteristic mixed type waters observed in the Herz Geothermal well. The Pine Tree Ranch #1 well, located 40 m west of the MVBF, shows maximum B and Cl concentrations that are roughly 20% of the Flame well concentrations.

- Temperature dependant boron adsorption is suggested by mixing trends.

Three distinct mixing trends observed in the Brown School and Herz domestic wells suggest boron adsorption on clays in the alluvial deposits maybe temperature dependant. The higher B and Cl concentrations observed in the Brown School well reflect its proximity to the north-trending Sage Hill Road Fault. Decreasing thermal water in the Brown School well corresponds to water level recovery beginning in 1995.

- Temporal changes document initiation of thermal and non-thermal water mixing

Potential mechanisms for the initiation of changes in the proportions of thermal and non-thermal waters include: reduced non-thermal water component due to increased groundwater extraction from alluvial aquifers for municipal water supply; reduced non-thermal water component due to decreased recharge due to reduced irrigation and below normal precipitation; and increased thermal water component due to injection of thermal

waters in geothermal reservoir areas with greater connectivity to the alluvial aquifers than the extraction areas.

- Seasonal variations are evident in the temperature and chemistry data.

Seasonal variations in water recharge to the alluvial aquifer are observed from temperature data in the Brown School, Herz Domestic, and Peigh Domestic wells. B and Cl concentration differences between the Peigh Domestic and Peigh Pool Geothermal wells indicate that thermal water conducted along a fault does not mix with non-thermal water in the alluvial aquifer in this location. The percentage of thermal water in the Curti Domestic well calculated from Cl data also shows seasonal variations in alluvial aquifer recharge and illustrates an overall increase of thermal water in the alluvial aquifer.

Forward Modeling (Chapter 3 and Appendix B)

Coupled 2.75-D forward modeling of gravity and aeromagnetic data along 11 profiles is constrained by mapped geology, well log data, and measured physical properties (density, magnetic susceptibility, and remanent magnetization). These model results are used to construct a 3-D geologic model of the Steamboat Hills geothermal system and the surrounding alluvial basins of the southern Truckee Meadows. The 3-D model yields detailed depths, elevations, and thicknesses of Quaternary (*Qal*) alluvial deposits, Tertiary volcanics (*Tv*), pre-Cretaceous metamorphics (*pKm*), and Cretaceous granodiorite (*Kgd*). Altered granodiorite (*Alt Kgd*) and metamorphic rocks are modeled to represent the geothermal reservoir with altered volcanic rock (*Alt Tv*) as the cap rock. Important findings are as follows:

- A better definition of alluvial basin configuration is observed in the 3-D model.

The *Qal* thickness map derived from potential fields model and well log data shows a volume that is 64% greater than determined from well data only. This new estimate will be useful for assessing current well field utilization and planning future well field development of Washoe County drinking water supply. The *Qal* elevations along with elevations for *Tv* and *Kgd* will be useful for constructing a groundwater flow model for the basins in the southern Truckee Meadows.

- A revised estimate for the thickness of Tertiary volcanic rocks is obtained.

The 3-D model suggests that *Tv* thickness may be up to 600 m beneath the western portions of the Mount Rose Fan and Galena Fan rather than the 390 m thickness indicated previously by well log data. These rocks represent an increasingly important source of municipal water supply for Washoe County.

- A new estimate for geothermal reservoir volume based on magnetic susceptibility is presented.

Vertical magnetic susceptibility measurements of whole rock core from core hole MTH 21-33 are critical for recognizing and assigning properties for *Alt Kgd* to represent the geothermal reservoir. Results of modeling the geothermal reservoir as *Alt Kgd* and *pKm* yield a new estimate of the geothermal reservoir volume (58 km^3) that is double the previous volume estimate. This revised volume estimate yields a geothermal recovery factor (12.5%) that is more reasonable than previously assumed value (25%) when compared with a calculated value (9 %) for the Geysers.

- The 3-D model suggests a possible thermal water up-flow zone.

A thick linear zone of altered *Alt Kgd* and *pKm* is located along a fault near the western flank of the Steamboat Hills (west of the geothermal production fields). This result suggests the fault may act a conduit for thermal water up-flow within the geothermal system that was previously unrecognized. The results may help guide future exploration drilling in the Steamboat Hills and this method of geothermal reservoir modeling may be an important tool for geothermal exploration and characterization at other sites.

- Faults conducting thermal water can be modeled from potential fields data.

Alt Tv representing geothermal cap rock is modeled in the geothermal discharge area in the northeastern portion of the Steamboat Hills. Subtle aeromagnetic anomalies located over north-trending faults that conduct thermal water from the geothermal system to the alluvial aquifer are nicely matched when modeled as vertical zones of *Alt Tv*. Aeromagnetic anomalies over areas with thermal water but no mapped fault suggest that concealed faults may be present and detectable.

Magnetic Methods (Chapter 4)-Geothermal Exploration Strategy

The results from this chapter are summarized as a strategy for geothermal exploration. The exploration strategy proposed in Chapter 4 is based on the recognition that magnetic data can be useful for fault and fracture zone identification during geothermal resource site exploration and characterization, using the Steamboat Hills geothermal area as a test site. The strategy includes initial reconnaissance using a draped aeromagnetic survey, delineation of hydrogeologically significant faults using ground magnetic surveys, and characterization of vertical magnetic susceptibility from borehole logging or core measurements. The aeromagnetic low anomaly observed for the Steamboat Hills geothermal resource area from a draped helicopter survey results from thermochemical alteration of the magnetic minerals in the reservoir and cap rocks. This type of magnetic signature can be an indicator of geothermal resource potential at other uncharacterized or blind sites. Ground-based magnetic measurements across the Mud Volcano Basin Fault (MVBF) show a strong magnetic low anomaly (amplitude of 200 to 400 nT) associated with demagnetization from thermal alteration of the bedrock adjacent to the fault. The magnetic anomalies delineate the trace of the MVBF beneath the alluvial fan deposits north of the geothermal area. The best-fit 2.75-D forward model of one Transect 4 shows the fault as a narrow (5 to 10 m) zone of altered volcanic rock. This suggests that thermal water is conducted along a focused preferential flow path into the alluvial aquifer. Magnetic susceptibility data from rock core yields a mean value for altered granodiorite used in forward models. Low magnetic susceptibility values are used to infer zones of altered magnetic mineralogy indicating fractures that conduct or have conducted thermal water. Permeable fractures noted on the core log match the inferred alteration zones; however, the magnetic susceptibility values suggest a higher fracture frequency. Negative magnetic susceptibility values are attributed to calcite- and/or quartz-filled fractures.

Conclusions

The 3-D geometry of the Steamboat Hills and southern Truckee Meadows area derived from 2.75-D forward modeling of gravity and aeromagnetic data is important for developing a numerical model for groundwater flow and planning exploration drilling for drinking water and geothermal wells. The basin configuration and maximum *Qal* thickness in the Mount Rose Fan from our study agree quite well with the depth to bedrock results from Abbott and Louie (2000) derived from gravity; however, since we have vertical geologic control from numerous well logs we can confidently model 50 m *Qal* thickness contours that yields definition of the Galena Fan, Steamboat Valley, and Pleasant Valley basins. The vertical magnetic susceptibility data obtained from core hole MTH 21-33 yields a critical mean value for modeling the geothermal reservoir as *Alt Kgd*. The combined thickness of *Alt Kgd* and *pKm* results show a northwest-trending elongated zone coincide with a north-trending fault that may represent a thermal water up-flow zone for the geothermal system. A north-trending zone of thick *Alt Kgd* and *pKm* extending from the Caithness Power, Inc. to the Far West Capital production zones that coincides with the Mud Volcano Basin Fault suggests that the two production zones are in hydraulic communication. Recognition of subtle aeromagnetic low anomalies over faults (e.g., Herz and Sage Hill Road Faults) known to transmit thermal water, based on B vs Cl and temperature data, allows us to model these faults as vertical zones of *Alt Tv*. The 3-D model results support the proposed hydraulic connection between the geothermal reservoir and the Mount Rose Fan along north-trending faults (e.g., Mud Volcano Basin Fault, Herz Fault, Sage Hill Road Fault). The results of this study can also be used to evaluate fully 3-D forward modeling methods.

The use of magnetic methods is important for geothermal resource exploration and characterization. We show that a high-resolution draped aeromagnetic survey at Steamboat Hills is capable of identifying a geothermal reservoir that is not evident from constant elevation aeromagnetic surveys. Ground magnetic data is effective for high-resolution delineation of faults that conduct thermal water and are concealed by alluvial deposits. The fault cannot be delineated from resistivity data due to high clay content in the alluvial deposits or from gravity data due to low resolution. Identification of these hydrologically significant faults is critical for exploratory drilling site selection and for siting production and injection wells. A vertical magnetic susceptibility profile generated from rock core measurements yields important property information for forward modeling of aeromagnetic data and shows promise for delineating permeable fractures.

Temporal variation in B and Cl concentrations in the Flame well indicates increased thermal water in the alluvial aquifer during the monitoring period from 1985 to 1990 that may be related to injection. The B and Cl variation along the local mixing trend and the location of the Flame well along the trace of the Mud Volcano Basin Fault (MVBF) suggest that this fault is one connection between the geothermal system and the alluvial aquifer. The Pine Tree Ranch #1 well, located 30 m west of the Flame well, also displays an increasing component of thermal water along the local mixing trend but with concentrations of only 20% relative to the Flame well. The lower B and Cl concentrations suggest that thermal water is conducted along the MVBF in a narrow preferential flow path. Ground magnetic transects show pronounced magnetic low anomalies associated with the MVBF. Steam vents confirming the location of the fault

were observed at the location of the magnetic low. The magnetic low anomalies allow delineation of the fault trace where obscured beneath alluvial deposits. Forward modeling results of the ground magnetic data for Transect 4 indicates that the best fit is obtained using a 5 to 10 m wide alteration zone to represent the MVBF. The model results support water chemistry data that suggest the MVBF is a narrow permeable zone for preferential flow.

Future Investigations

The Qal thickness map derived from potential fields modeling and well log data indicates the western portion of the Mount Rose Fan and the northwest portion of the Galena Fan contain the thickest alluvial fill. Additionally, the modeled thicknesses of volcanic rocks are significant in these portions of the basins. These results suggest that future water supply development by Washoe County should focus on these areas.

For the potential field models, altered granodiorite and metamorphic rocks were modeled to represent the geothermal reservoir. A thick zone of these altered rocks that coincides with a north-trending fault along the west flank of the Steamboat Hills suggests an up-flow zone of thermal water may be responsible for this feature. Drilling exploration slim holes in this area should be conducted to test this hypothesized up-flow zone. Better understanding the geothermal system and perhaps additional geothermal production could be realized if an up-flow zone were found in this area.

The results of boron versus chloride time series data indicate preferential flow of thermal water along north-trending faults (e.g. Mud Volcano Basin, Herz, Sage Hill Road). These results suggest that important information could be gained by conducting tracer tests. Tracer studies would be useful for confirming the flow path of thermal water from the geothermal system to the alluvial aquifer and for estimating hydraulic conductivity of and flow velocities along these faults. A tracer test at the Caithness (CPI) Cox-I1 injection well with monitoring at the Pine Tree Ranch #1 and #2 wells would allow characterization of the Mud Volcano Basin Fault. Characterization of the Herz Fault could be accomplished with a tracer test at the FWC IW-2 or IW-3 injection wells with monitoring at Herz Geothermal, Herz Domestic, and NDOT (replacement for Brown School well). The tracer compounds 1,5-napthalene disulfonate, fluorescein, and rhodamine WT have been found to act conservatively and remain stable in the Far West Capital (FWC) production area at Steamboat Hills (Rose et al., 1999; Rose and Adams, 1994). Using a batch of these compounds would allow for evaluation of their effectiveness as conservative tracers in the higher temperature CPI field and in the alluvial aquifers. Additionally, a tracer test performed at the CPI CoxI-1 with monitoring wells in the FWC production field may help resolve the whether a single geothermal system or two separate systems exist at Steamboat Hills.

Analysis of interference tests by Petty (1992) indicates that the CPI production zone receives pressure support from injection at the Cox I-1well; however, Sorey and Colvard (1992) suggest that data from these tests are difficult to interpret and provide no conclusive evidence of pressure support. The conceptual model developed from this study indicates the Cox I-1 injection well is located at the southern end of the Mud Volcano Basin Fault and geochemistry data indicate that this fault conducts thermal fluid

toward the north into the alluvial aquifer. Although the 3-D model of subsurface geologic structure developed here does not directly resolve the pressure support debate, it does provide a more detailed geologic framework for future analysis and system modeling. This new geologic model will be useful for reanalysis of production and injection well locations.

Future research is needed to evaluate the correlation between magnetic susceptibility data and fracture frequency and fracture permeability. The vertical magnetic susceptibility results from core hole MTH21-33 suggest that low magnetic susceptibility values (0 to 0.001 SI) may correlate with fracture frequency; however, to establish a correlation the core rock should be systematically classified using a description method such the rock quality designation (RQD) as present by Deere (1963). Magnetic susceptibility values less than zero are due to calcite or quartz filled fracture that appear to correlate with productive zones. Detailed temperature, pressure, and spinner logging of core hole MT21-33 would be needed to establish a correlation.

References

Deere, D.U., 1963, Technical description of rock cores for engineering purposes, Rock Mech. Eng. Geol., 1, 16-22.

Petty, S., 1992, Discussion of USGS report on Steamboat Hot Springs, unpublished report for Caithness Power, Inc., 18 p.

Rose, P.E., Gorenson, C., Salls, D. and Kilbourne, P., 1999, Tracer testing at Steamboat Hills, Nevada, Using fluorescein and 1,5-naphthalene disulfonate, Proceedings, Twenty-Fourth Workshop on Geothermal Reservoir Engineering, Stanford University, Stanford, California, January 25-27, 1999, SGP-TR-162.

Rose, P.E., and Adams, M.C., 1994., The application of rhodamine WT as a geothermal tracer, Geothermal Res. Council Trans., 18, 237-240.

Skalbeck, J.D., Shevenell, L., and Widmer, M.C., 2001, Mixing of thermal and non-thermal waters the Steamboat Hills area, Nevada, Geothermics, 30, *in press*.

Sorey, M.L., and E. M. Colvard, 1992, Factors affecting the decline in hot-spring activity in the Steamboat Springs area of critical environmental concern, Washoe County, Nevada, U.S. Geol. Surv., adm. report for U.S Bur. of Land Manag., 109 p.

APPENDIX A

GEOCHEMISTRY DATA

Table A-1. Boron and chloride concentrations for Figure 3 of Chapter 2.

Boron (B) and chloride (Cl) concentrations in mg/L.

		Date	Cl	B	Reference
Cold Waters					
Dry Creek		6/8/1977	2	0	Nehring, 1980
Stock Spring		6/8/1977	3	0	Nehring, 1980
Thomas Creek Spring		6/8/1977	2	0	Nehring, 1980
Slide Mount Spring		6/11/1977	12	4.0	Nehring, 1980
Davies Ceek Well		6/11/1977	0	0	Nehring, 1980
Pleasant Valley School		6/12/1977	2	0	Nehring, 1980
Jumbo Grade Spring		6/9/1977	8	0	Nehring, 1980
Scorpion Springs		6/9/1977	3	0	Nehring, 1980
Alum Spring		6/9/1977	9	0	Nehring, 1980
Galena Creek Park		8/7/1993	0.5	0.1	Mariner and Janik, 1995
Tick Spring		8/7/1993	48	0	Mariner and Janik, 1995
Jumbo Grade Spring		8/7/1993	7	0.1	Mariner and Janik, 1995
Guton Ranch Well		6/12/1977	471	14	Nehring, 1980
Hidden Valley Well		6/12/1977	9	3	Nehring, 1980
STMGID # 4		11/8/1991	20	1	Mariner and Janik, 1995
Thermal					
PW-1	SBG	11/7/1991	781	45	Mariner and Janik, 1995
PW-1	SBG	1/29/1993	811	43	Mariner and Janik, 1995
PW-1	SBG	8/5/1993	808	38	Mariner and Janik, 1995
PW-1	SBG	7/27/1994	802	42	Mariner and Janik, 1995
PW-2	SBG	11/7/1991	800	43	Mariner and Janik, 1995
PW-2	SBG	1/29/1993	823	41	Mariner and Janik, 1995
PW-2	SBG	8/5/1993	795	43	Mariner and Janik, 1995
PW-2	SBG	7/24/1994	811	41	Mariner and Janik, 1995
PW-3	SBG	11/7/1991	809	42	Mariner and Janik, 1995
PW-3	SBG	8/5/1993	814	47	Mariner and Janik, 1995
PW2-1	SBG	1/28/1993	772	40	Mariner and Janik, 1995
PW2-1	SBG	8/4/1993	801	45	Mariner and Janik, 1995
PW2-2	SBG	1/28/1993	770	42	Mariner and Janik, 1995
PW2-2	SBG	8/4/1993	799	44	Mariner and Janik, 1995
PW2-2	SBG	7/26/1994	797	40	Mariner and Janik, 1995
PW2-3	SBG	1/29/1993	801	37	Mariner and Janik, 1995
PW2-3	SBG	8/4/1993	797	41	Mariner and Janik, 1995
PW2-4	SBG	1/28/1993	782	41	Mariner and Janik, 1995
PW2-4	SBG	8/5/1993	787	43	Mariner and Janik, 1995
PW2-4	SBG	7/26/1994	783	41	Mariner and Janik, 1995
PW2-5	SBG	1/29/1993	795	41	Mariner and Janik, 1995
PW2-5	SBG	8/4/1993	796	48	Mariner and Janik, 1995
PW2-5	SBG	7/26/1994	805	42	Mariner and Janik, 1995
PW3-1	SBG	1/28/1993	789	41	Mariner and Janik, 1995
PW3-1	SBG	8/4/1993	788	40	Mariner and Janik, 1995
PW3-1	SBG	7/26/1994	783	40	Mariner and Janik, 1995
PW3-2	SBG	1/28/1993	775	41	Mariner and Janik, 1995
PW3-2	SBG	8/4/1993	799	43	Mariner and Janik, 1995
PW3-3	SBG	1/28/1993	801	42	Mariner and Janik, 1995
PW3-3	SBG	8/5/1993	779	39	Mariner and Janik, 1995
PW3-3	SBG	7/26/1994	797	42	Mariner and Janik, 1995
PW3-4	SBG	1/28/1993	779	42	Mariner and Janik, 1995
PW3-4	SBG	8/4/1993	795	52	Mariner and Janik, 1995
PW3-4	SBG	7/26/1994	783	39	Mariner and Janik, 1995
PW2-1	SBG	1/28/1993	772	40	Mariner and Janik, 1995
PW2-1	SBG	8/4/1993	801	45	Mariner and Janik, 1995

Table A-1. Boron and chloride concentrations for Figure 3 of Chapter 2.

Boron (B) and chloride (Cl) concentrations in mg/L.

		Date	Cl	B	Reference
PW2-2	SBG	1/28/1993	770	42	Mariner and Janik, 1995
PW2-2	SBG	8/4/1993	799	44	Mariner and Janik, 1995
PW2-2	SBG	7/26/1994	797	40	Mariner and Janik, 1995
PW2-3	SBG	1/29/1993	801	37	Mariner and Janik, 1995
PW2-3	SBG	8/4/1993	797	41	Mariner and Janik, 1995
PW2-4	SBG	1/28/1993	782	41	Mariner and Janik, 1995
PW2-4	SBG	8/5/1993	787	43	Mariner and Janik, 1995
PW2-4	SBG	7/26/1994	783	41	Mariner and Janik, 1995
21-5	CPI	11/5/1991	760	37	Mariner and Janik, 1995
21-5	CPI	1/27/1993	742	39	Mariner and Janik, 1995
21-5	CPI	8/3/1993	755	41	Mariner and Janik, 1995
21-5	CPI	7/25/1994	766	40	Mariner and Janik, 1995
13-5	CPI	8/7/1993	765	39	Mariner and Janik, 1995
23-5	CPI	11/5/1991	792	43	Mariner and Janik, 1995
23-5	CPI	1/27/1993	774	40	Mariner and Janik, 1995
23-5	CPI	8/2/1993	783	41	Mariner and Janik, 1995
23-5	CPI	7/25/1994	810	40	Mariner and Janik, 1995
23-5	CPI	9/13/1994	793	41	Mariner and Janik, 1995
83A-6	CPI	11/6/1991	739	36	Mariner and Janik, 1995
83A-6	CPI	8/2/1993	737	45	Mariner and Janik, 1995
83A-6	CPI	7/25/1994	758	39	Mariner and Janik, 1995
GS-8 5/7	CPI	7/11/1977	878	41	Nehring, 1980
IW-3	CPI	11/7/1991	809	40	Mariner and Janik, 1995
IW-3	CPI	8/5/1993	813	39	Mariner and Janik, 1995
IW-5	CPI	8/5/1993	794	43	Mariner and Janik, 1995
13-5	CPI	8/7/1993	904	46	Mariner and Janik, 1995
13-5	CPI	8/7/1993	765	39	Mariner and Janik, 1995
COXI-1	CPI	11/6/1991	873	44	Mariner and Janik, 1995
COXI-1	CPI	8/3/1993	890	52	Mariner and Janik, 1995
COXI-1	CPI	7/27/1994	902	49	Mariner and Janik, 1995
GS-5	CPI	11/4/1991	925	47	Mariner and Janik, 1995
GS-5	CPI	1/29/1993	887	48	Mariner and Janik, 1995
GS-5	CPI	8/3/1993	949	56	Mariner and Janik, 1995

Notes:
SBG: SB Geo, Inc.
CPI: Caithness Power, Inc.

Table A-2. Data from alluvial aquifer and geothermal monitoring wells for Figures 3 through 8 of Chapter 2. Boron (B) and chloride (Cl) concentrations in mg/L

	Brown School			Curti Geothermal			Curti Domestic			Herz Geothermal				Herz Domestic			
			Temp			Temp			Temp			Temp	Water Depth			Temp	Water Depth
YEAR	Cl	B	(°C)	Cl	B	(°C)	Cl	B	(°C)	Cl	B	(°C)	(m)	Cl	B	(°C)	(m)
Jan-85	3	0	15							350	16.3	51	15.3	3	0	3	
FEB	7	0	18							340	16.6	50	15.5	4	0	3	7.7
MAR	7	0.2	17							340	17.4	51	15.6	3	0.2	4	8.4
APR	5	0.3	17							350	17.2	52	15.7	3	0.3	11	8.6
MAY	4	0.3	19							340	17.5	53	15.8	4	0.2	17	9.0
JUN	7	0.2	21							350	17.5	53	15.8	4	0.3	20	9.3
JUL	5	0.2	25							350	17.5	53	15.8	5	0.2	24	9.1
AUG	8	0.2	23							355	18.2	54	15.8	3	0.2	26	8.9
SEP	9	0.2	21							345	18.3	53	16.1	3	0.2	12	8.8
OCT	9	0.2	20							345	17.0	53	15.9	4	0.2	20	8.9
NOV	10	0.1	19							340	18.1	54	15.8	5	0.1	14	8.9
DEC	10	0.2	18							350	16.9	53	15.8	4	0.1	10	9.0
Jan-86	8	0.6	16							345	15.2	53	16.0	3	0.5	9	9.2
FEB	7	0.2	17							345	17.1	53	16.0	3	0.1	7	9.6
MAR	17	0.2	17							345	17.6	49	15.7	4	0.1	11	9.9
APR	17	0.2	18							345	17.6	53	15.7	3	0.1	13	8.9
MAY	10	0.2	19							345	17.3	52	15.8	2	0.1	14	8.9
JUN	11	0.2	22							355	17.4	52	15.9	4	0.1	24	9.5
JUL	10	0.2	24							375	17.7	52	15.7	3	0.2	23	9.3
AUG	11	0.2	28							350	17.4	54	15.5	2	0.2	24	8.1
SEP	14	0.2	21							350	18.1	53	15.5	3	0.1	23	7.8
OCT	13	0.1	19							345	17.7	53		1	0.1	18	8.2
NOV	13	0.1	18							345	17.6	54		3	0.1	13	
DEC	11	0.2	17							340	18.5	54		5	0	10	
Jan-87	6	0.2	15							340	18.2	52	15.4	3	0.1	4	
FEB	8	0.2	16							340	18.6	53	15.2	3	0.1	8	9.4
MAR	7	0.2	17							340	18.0	54	15.0	0	0.1	9	9.6
APR	6	0.3	18							340	18.0	51	14.8	4	0.1	15	10.0
MAY	5	0.2	21	680	38.2	48	67		22	340	18.1	52	14.7	3	0.1	17	10.3
JUN	15	0.1	22	680	39.2	37	70		23	340	18.2	52	14.6	3	0	22	10.7
JUL	7	0.2	21	700	38.6	46	66		22	340	18.2	52	14.5	6	0.2	21	10.8
AUG	5	0.2	22	690	38.3	48	59		23	335	18.0	52	14.5	2	0.1	23	10.9
SEP	5	0.3	22	670	38.1	47	51		23	340	18.2	52	14.4	5	0.2	23	11.2
OCT	8	0.3	23	700	37.2	44	46	1.7	22	345	17.4	52	14.4	3	0.1	21	11.3
NOV	5	0.3	20	710	36.5	40	44	1.6	21	340	17.4	52	14.4	3	0.1	14	11.2
DEC	6	0.3	19	700	35.9	41	43	1.7	21	340	17.5	52	14.4	3	0	11	11.3
Jan-88	7	0.3	17	700	36.8	43	48	1.8	21	340	17.5	52	14.4	2	0.1	4	11.4
FEB	14	0.3	17	680	37.6	36	54	1.9	21	340	17.6	51		2	0.1	3	11.5
MAR	13	0.3	21	680	38.1	43	63	2.1	21	325	17.2	52	14.5	2	0.1	8	11.7
APR	18	0.3	20	690	37.4	36	74	2.2	21	355	17.1	50	14.7	2	0.1	14	11.8
MAY	27	0.3	22	700	36.8	49	82	2.4	22	360	17.2	51	14.8	2	0.1	18	12.2
JUN	35	0.3	26	690	38.2	49	91	2.6	23	340	17.4	52	14.8	2	0.1	24	12.5
JUL	39	0.3	28	700	37.4	49	79	2.4	23	350	17.5	52	14.9	3	0.1	25	12.2
AUG	68	0.4	27	700	38.7	51	61	1.9	22	345	17.6	52	14.9	3	0.1	28	12.2
SEP	69	0.4		680	37.5	50	56	1.8		350	17.4			3	0.2		12.3
OCT				700	36.7	44	55	1.8									
NOV	112	0.7	25	710	36.1	43	57	2.2	21	360	18.3	53		5		8	

Table A-2. Data from alluvial aquifer and geothermal monitoring wells for Figures 3 through 8 of Chapter 2. Boron (B) and chloride (Cl) concentrations in mg/L

	Brown School			Curti Geothermal			Curti Domestic			Herz Geothermal				Herz Domestic			
YEAR	Cl	B	Temp (°C)	Cl	B	Temp (°C)	Cl	B	Temp (°C)	Cl	B	Temp (°C)	Water Depth (m)	Cl	B	Temp (°C)	Water Depth (m)
DEC				710	37.9	42	59	2.3									
Jan-89	150	0.5	22	700	36.9	48	63	2.5	22	355	16.6	53	15.2	5	0.1	4	
FEB	188	0.9	24	700	36.4	50	70	2.7	21	365	17.8	52		4	0.2	9	
MAR	203	1.3	25	700	38.5	47	80	2.9	22	370	17.9	52	12.6	2	0	10	
APR	250	2.1	25							370	18.2	54		6	0.1	19	
MAY	253	2.7	25							375	18.2	52	15.9	8	0.2	20	
JUN	263	2.8	27	700	36.8	43	124	3.4	22	375	18.1	54	15.8	9	0.1	26	
JUL	350	4.4								390	18.7		16.2	12	0.1		
AUG	355	4.9	23							375	18.6	55	16.2	15	0.1	24	
SEP				700	36.6	44	67	2.5	22	370	18.7	53	16.3	12	0.2	20	
OCT	333	5.4	21							380	19.0	53	16.3	11	0.1	17	
NOV	370	6.4	22											13	0	22	
DEC	370	6.3	21											12	0.1	21	
Jan-90	395	7.2	20	688	36.5	43	203	8.5	27					12	0	16	
FEB	415	3.8	20											12	0	23	
MAR	430	8.7	22	670	36.0	43	230	9.8	28					12	0	22	
APR	430	5.0	21											13	0	20	
MAY	440	9.7	21											16	0	19	
JUN	410	9.7	22	700	35.0	44	104	4.4	23					16	0	20	
JUL	420	9.2	20														
AUG																	
SEP	450	12.0		710	36.3	44	71	3.1									
OCT																	
NOV																	
DEC	480	13.2		700	35.6	46	135	6.7						33	0.5		
Jan-91	495	13.2															
FEB	505	15.4												40	0.2		
MAR	530	16.2		700	38.3		255	14.4						41	0.5		
APR	510	17.7												46			
MAY	490	16.3												59			
JUN	505	17.2		730	35.5		223	12.4						69			
JUL	510	17.8												67	0		
AUG	530	19.7												80	0.5		
SEP				710	38.9	47	208	12.5									
OCT	540	20.8												102	0.6		
NOV	550	21.5												140	0.9		
DEC	580	23.6		710	38.9		208	12.1						144	0.9		
Jan-92	570	23.6												160	0.9		
FEB	590	24.4												172	0.9		
MAR	590	23.7	27	690	36.1		263	14.8						184	1.0	10	
APR	570	22.2												156	0.9		
MAY	580	24.5												184	1.1		
JUN	580	17.3	27	700	37.8	49	283	15.8						172	0.1	24	
JUL	600	28.9												200	1.4		
AUG	630	30.5												156	1.4		
SEP	640	31.1	27	710	37.0		195	8.0						220	2.0	26	
OCT	630													210			
NOV	620													273			
DEC	630	29.8	28	690	36.9		175	7.8						297	3.1	9	
Jan-93																	

Table A-2. Data from alluvial aquifer and geothermal monitoring wells for Figures 3 through 8 of Chapter 2. Boron (B) and chloride (Cl) concentrations in mg/L

	Brown School			Curti Geothermal			Curti Domestic			Herz Geothermal				Herz Domestic			
YEAR	Cl	B	Temp (°C)	Cl	B	Temp (°C)	Cl	B	Temp (°C)	Cl	B	Temp (°C)	Water Depth (m)	Cl	B	Temp (°C)	Water Depth (m)
FEB																	
MAR	663	31.2		720	37.2		317	16.7						237	2.9		
APR																	
MAY																	
JUN	640	31.5		720	37.6		240	11.8						280	4.5		
JUL																	
AUG																	
SEP	670	34.7	28	720	35.3	42	198	10.6	32					257	4.4	26	
OCT																	
NOV																	
DEC	670	35.4	28	720	34.6	41	130	7.4						213	3.3		
Jan-94																	
FEB																	
MAR	680	38.1	28	680	34.4		195	10.9	30					238	3.8	6	
APR																	
MAY																	
JUN	680	40.5	29	680	36.0	44	205	11.8	32					190	4.0	19	
JUL																	
AUG																	
SEP	680	38.3	30	670	34.8		100	6.3						170	3.5	31	
OCT																	
NOV																	
DEC	670	37.8		690	35.5		245	13.6						177	3.6		
Jan-95																	
FEB																	
MAR	672	38.0	31	671	35.0	43	235	12.6	31								
APR																	
MAY																	
JUN	698	40.0		701	36.7		260	13.2									
JUL																	
AUG																	
SEP	693	39.2	33				207	11.3									
OCT																	
NOV																	
DEC	695	39.0		660	32.0		175	9.2									
Jan-96																	
FEB																	
MAR	715	37.0	36	844	38.0	43	213	11.2									
APR																	
MAY																	
JUN	719	38.0		714	33.0		164	8.5									
JUL																	
AUG																	
SEP	743	39.8		723	35.1		201	11.3									
OCT																	
NOV																	
DEC	691	38.0					247	13.6									
Jan-97																	
FEB																	
MAR	690	39.5	38	713	35.9	48	256	15.6	33								

Table A-2. Data from alluvial aquifer and geothermal monitoring wells for Figures 3 through 8 of Chapter 2. Boron (B) and chloride (Cl) concentrations in mg/L

	Brown School			Curti Geothermal			Curti Domestic			Herz Geothermal				Herz Domestic			
YEAR	Cl	B	Temp (°C)	Cl	B	Temp (°C)	Cl	B	Temp (°C)	Cl	B	Temp (°C)	Water Depth (m)	Cl	B	Temp (°C)	Water Depth (m)
APR																	
MAY																	
JUN	515	34.9		752	41.1		303	16.7									
JUL																	
AUG																	
SEP	335	26.8	38	753	36.5	50	279	15.0	37								
OCT																	
NOV																	
DEC	246	19.2	38	749	37.6	49	302	16.0	36								
Jan-98																	
FEB																	
MAR	263	15.6	37	771	40.0	48	293	15.6	33								
APR																	
MAY																	
JUN	324	17.6	38	764	39.2	49	134	7.2	23								
JUL																	
AUG																	
SEP	299	16.1	39	722	35.4	54	294	14.1	29								
OCT																	
NOV																	
DEC																	

Table A-2. Data from alluvial aquifer and geothermal monitoring wells for Figures 3 through 8 of Chapter 2. Boron and chloride concentrations in mg/L

	Peigh Domestic			Pine Tree Ranch			Water	Flame			Water	Steinhardt			Water
			Temp			Temp	Depth			Temp	Depth			Temp	Depth
YEAR	Cl	B	(°C)	Cl	B	(°C)	(m)	Cl	B	(°C)	(m)	Cl	B	(°C)	(m)
Jan-85	3	0	29	3	0	33	21.5	112	6.9	17					
FEB	4	0	29	4	0	34	22.9	165	10.6	9					
MAR	3	0.1	31	3	0.1	34	23.7	290	17.6						
APR	3	0.2	34	4	0.3	36	24.7	325	18.4	11					
MAY	3	0.2	36	12	0.4	38	25.5	330	18.5	17					
JUN	2	0.1	32	23	1.1	39	26.2	345	19.8	21					
JUL	2	0.1	34	28	1.6	40	26.1	350	21.0	27					
AUG	4	0.1	32	15	0.4	38	24.5	355	19.4	29					
SEP	2	0.1	34	4	0.2	37	23.6	355	22.3	55					
OCT	2	0.1	37	3	0.1	37	23.0	365	21.7	56					
NOV	3	0.1	34	3	0.1	36	22.5	162	9.3	51					
DEC	3	0.1	30	3	0.1	36	22.8	208	12.8	36					
Jan-86	3	0.2	32	2	0.1	36	23.5	345	20.5	54					
FEB	3	0.1	32	4	0.1	37	24.5	330	20.4	55					
MAR	3	0.1	28	8	0.3	38	25.2	325	19.7	44					
APR	3	0.1	32	13	0.5	38	25.1	330	20.2	54					
MAY	4	0.1	31	20	1.0	39	25.7	325	19.4	53					
JUN	3	0.1	34	26	1.5	40	26.1	330	19.9	53					
JUL	3	0.1	31	28	1.9	40	26.0	330	20.0	52					
AUG	3	0.2	32	30	2.2	40	25.4	333	20.1	53					
SEP	3	0.1	33	28	1.6			340	21.0	53					
OCT	2	0.1	32	9	0.2			355	21.2	50					
NOV	2	0.1	32	4	0.1			365	21.4	53					
DEC	4	0	31	3	0.1			360	21.8	51					
Jan-87	2	0	31	5	0.2	38	24.2	350	21.5	48					
FEB	3	0	31	19	1.0	39	24.9	350	22.2	50					
MAR	2	0.1	31	27	2.2	41	25.6	345	21.8	50					
APR	3	0	32	32	2.8	42	26.2	355	21.3	50					
MAY	4	0	32	36	3.1	42	26.7	355	21.7	49		300	13	34	21.1
JUN	3	0	33	39	3.2			360	22.0	47		286	12.5	33	21.1
JUL	2	0.1	33	42	3.2	42	27.3	375	21.6	50		293	11.6	34	21.1
AUG	1	0	31	44	3.5	43	27.3	375	21.8	51		280	11.2	34	21.0
SEP	2	0.1	31	48	3.3	43	27.3	390	22.4	51		260	10.7	34	20.9
OCT	2	0	31	51	3.7	43	27.0	405	22.1	42		250	9.2	33	20.8
NOV	3	0	29	52	3.6	42	26.4	405	22.3	42		240	9.4	33	20.7
DEC	3	0	32	49	3.5	42	27.1	425	23.1	59		233	8.7	32	20.6
Jan-88	2	0	32	57	3.9	43	26.5	415	22.4	57		243	8.4	33	21.1
FEB	3	0	32	57	4.0	43	26.8	442	23.3	57		227	8.2	33	21.4
MAR	2	0	33	59	4.1	43	27.2	405	23.0	56		207	7.3	33	21.7
APR	2	0	31	67	4.1	43	28.0	415	22.9	57		230	8.8	33	22.1
MAY	2	0	32	68	4.2	40	28.3	425	23.5	59		201	7.4	33	22.3
JUN	1	0	29	71	4.3	44	28.6	430	23.7	56		207	8.0	33	22.3
JUL	3	0	28	75	4.4	44	28.3	450	23.8	54		197	7.7	33	23.5
AUG	2	0	28	74	4.3	44	29.2	435	24.2	56		193	7.8	33	23.2
SEP	4	0						445	23.3			188	8.0	33	23.0
OCT												183	7.3	33	23.2
NOV	5		35	25	2.0	42		455	24.6	58		173	6.4	34	23.5

Table A-2. Data from alluvial aquifer and geothermal monitoring wells for Figures 3 through 8 of Chapter 2. Boron and chloride concentrations in mg/L

	Peigh Domestic			Pine Tree Ranch				Flame				Steinhardt			
YEAR	Cl	B	Temp (°C)	Cl	B	Temp (°C)	Water Depth (m)	Cl	B	Temp (°C)	Water Depth (m)	Cl	B	Temp (°C)	Water Depth (m)
DEC												170	7.1	33	23.8
Jan-89	6	0.1	27	37	2.7	43	27.1	450	23.2	58		163	6.6	33	22.6
FEB	7	0	27	84	4.4			450	24.8	28		170	6.9	33	22.8
MAR	6	0	31	83	4.7	44	29.2	455	23.7	10		143	5.6	33	24.5
APR	5	0	31	91	4.6			455	24.4	31					
MAY	6	0	32	82	4.5			450	24.2	27					
JUN	3	0	31	89	4.8	45	29.9	450	24	26					
JUL	4	0		90	4.9	45	30.7	450	23.7			152	7.6	33	24.7
AUG	4	0	32				30.1	450	24.1	51					
SEP	3	0.1	30				29.9	445	24.1	20		155	7.3	33	23.3
OCT	3	0	26												
NOV	3	0	28	24	1.6	46									
DEC	3	0	31	12	1.5	44									
Jan-90	3	0	27	10	1.1	43	30.1					130	6.6	33	24.0
FEB	4	0	29	11	1.0	44	30.0								
MAR	3	0	28	45	2.0	45	28.9					135	5.7	32	24.8
APR	5	0	38	79	3.8	46	30.0								
MAY	3	0	39	94	4.4	48	30.0								
JUN	2	0	39	94	4.7	47	30.1	485	25.7			143	5.7	33	24.8
JUL	3	0					30.3	490	24.5						
AUG	2	0					30.4								
SEP	3	0					30.3					158	6.5		24.9
OCT							30.3								
NOV							30.3								
DEC	5	0.2					30.4					160	6.9		25.5
Jan-91											22.0				
FEB	3	0					30.9				22.2	158	7.0		
MAR	4	0.1									22.4				
APR	5	0.1									22.6				
MAY	3	0.1					31.4				22.8	183	7.7		24.8
JUN	4	0.1									22.8				
JUL	3	0									22.6				
AUG	2	0.1					31.1				22.4	180	9.1		23.8
SEP											22.1				
OCT	4	0									22.1	183	9		23.7
NOV	3	0.1					31.0				22.3				
DEC	5	0									22.5				
Jan-92	3	0.1									22.7	195	8.5		24.5
FEB	3	0.1					31.5				23.0				
MAR	5	0		37							23.2				
APR	4	0									23.4	197	8.5	34	24.9
MAY	9	0.1									22.9				
JUN	4	0.1		37			32.0				23.5				
JUL	3	0									23.6	195	9		24.3
AUG	3	0.4									23.6				
SEP	3	0.1		38			32.3				23.7				
OCT	4										23.8	205	8.9		24.9
NOV	4										24.0				
DEC	5	0.1		34			32.6								
Jan-93															

Table A-2. Data from alluvial aquifer and geothermal monitoring wells for Figures 3 through 8 of Chapter 2. Boron and chloride concentrations in mg/L

	Peigh Domestic			Pine Tree Ranch			Water	Flame			Water	Steinhardt			Water
YEAR	Cl	B	Temp (°C)	Cl	B	Temp (°C)	Depth (m)	Cl	B	Temp (°C)	Depth (m)	Cl	B	Temp (°C)	Depth (m)
FEB											24.1				
MAR	5	0.2									24.2	252	10.2		25.5
APR											24.3				
MAY											24.5				
JUN	3	0.1					33.4				24.6	228	9.4		25.0
JUL											24.5				
AUG											24.3				
SEP	5	0					32.6				23.9	250	11.8		23.1
OCT											23.4				
NOV											23.1				
DEC	4	0.1	32				31.9				22.9	260	12.8		21.9
Jan-94											22.9				
FEB											23.0				
MAR	5	0.3	36				32.2				23.6				22.2
APR															
MAY															
JUN	4	0.1	34				32.7				24.0	223	12.0		20.9
JUL															
AUG															
SEP	4	0.1					33.2				24.4	200	10.2		19.4
OCT															
NOV															
DEC	4	0.1					33.5								
Jan-95															
FEB															
MAR	4	0.3	39				33.7					224	11.5		
APR															
MAY															
JUN	4	0.2					33.7					229	10.3		
JUL															
AUG															
SEP	5	0.1					32.1								
OCT															
NOV															
DEC							31.1								
Jan-96															
FEB															
MAR	5	0	33				31.5								
APR															
MAY															
JUN	4	0.1		Pine Tree Ranch #2			31.5								
JUL															
AUG															
SEP							29.7								
OCT															
NOV															
DEC	3	0.1					25.1								
Jan-97							25.4								
FEB							25.7								
MAR							25.9								

Table A-2. Data from alluvial aquifer and geothermal monitoring wells for Figures 3 through 8 of Chapter 2. Boron and chloride concentrations in mg/L

	Peigh Domestic			Pine Tree Ranch			Water	Flame			Water	Steinhardt			Water
			Temp			Temp	Depth			Temp	Depth			Temp	Depth
YEAR	Cl	B	(°C)	Cl	B	(°C)	(m)	Cl	B	(°C)	(m)	Cl	B	(°C)	(m)
APR							26.1								
MAY							26.4								
JUN	4	0.1					26.5								
JUL							26.5								
AUG							26.3								
SEP	15	0.3	36				26.0					225	12.0		
OCT							25.7								
NOV							25.7								
DEC	4	0.1	33									213	9.5		
Jan-98															
FEB															
MAR															
APR															
MAY															
JUN	3	0.1	41												
JUL															
AUG												171	7.9		
SEP	3	0.2	37												
OCT															
NOV															
DEC															

Table A-2. Data from alluvial aquifer and geothermal monitoring wells for Figures 3 through 8 of Chapter 2. Boron and chloride concentrations in mg/L

YEAR	TH-1 Water Depth (m)	TH-2 Water Depth (m)	TH-3 Water Depth (m)
Jan-85			
FEB			
MAR			
APR			
MAY			
JUN			
JUL			
AUG			
SEP			
OCT			
NOV			
DEC			
Jan-86			
FEB			
MAR			
APR			
MAY			
JUN			
JUL			
AUG			
SEP			
OCT			
NOV			
DEC			
Jan-87			
FEB			
MAR			
APR			
MAY			
JUN			
JUL			
AUG			
SEP			
OCT			
NOV			
DEC			
Jan-88			
FEB			
MAR			
APR			
MAY			
JUN			
JUL			
AUG			
SEP			
OCT			
NOV			

Table A-2. Data from alluvial aquifer and geothermal monitoring wells for Figures 3 through 8 of Chapter 2. Boron and chloride concentrations in mg/L

YEAR	TH-1 Water Depth (m)	TH-2 Water Depth (m)	TH-3 Water Depth (m)
DEC			
Jan-89			
FEB			
MAR			
APR			
MAY			
JUN			
JUL			
AUG			
SEP			
OCT			
NOV			
DEC			
Jan-90			
FEB			
MAR			
APR			
MAY			
JUN			
JUL			
AUG			
SEP			
OCT			
NOV			
DEC			
Jan-91			
FEB			
MAR			
APR			
MAY			
JUN			
JUL			
AUG			
SEP			
OCT			
NOV			
DEC			
Jan-92			
FEB			
MAR			
APR			
MAY			
JUN			
JUL			
AUG			
SEP			
OCT			
NOV			
DEC	15.2	18.9	9.8
Jan-93	15.3	18.7	9.6

Table A-2. Data from alluvial aquifer and geothermal monitoring wells for Figures 3 through 8 of Chapter 2. Boron and chloride concentrations in mg/L

YEAR	TH-1 Water Depth (m)	TH-2 Water Depth (m)	TH-3 Water Depth (m)
FEB	15.1	19.2	9.9
MAR	15.2	19.4	10.2
APR	15.5	19.5	10.2
MAY	15.8	19.7	10.5
JUN	16.2	19.9	10.8
JUL	16.4	20.2	11.0
AUG	17.5	21.4	12.2
SEP	17.2	21.3	11.9
OCT	16.8	21.0	11.7
NOV	17.0	21.0	11.7
DEC	17.7	21.3	11.8
Jan-94	17.0	21.0	11.7
FEB	17.0	21.0	11.8
MAR	17.0	21.1	11.9
APR	17.1	21.3	11.9
MAY	17.1	21.1	11.9
JUN	17.2	21.1	11.9
JUL	17.4	21.4	12.2
AUG	17.7	22.1	12.5
SEP	17.4	21.6	12.5
OCT	18.2	21.9	12.7
NOV	18.2	22.0	12.9
DEC	17.8	21.9	12.9
Jan-95	17.8	21.9	12.8
FEB	18.2	22.0	12.7
MAR	18.4	22.1	12.8
APR	18.3	22.1	12.8
MAY	20.0	22.3	12.9
JUN	21.3	22.3	12.9
JUL	21.3	22.5	13.3
AUG	21.3	22.6	13.3
SEP	21.3	22.8	13.5
OCT	21.3	23.3	14.0
NOV			
DEC	21.3	24.3	15.0
Jan-96		24.2	15.0
FEB		23.6	14.4
MAR			
APR			
MAY			
JUN			
JUL		21.8	12.2
AUG			
SEP		21.9	11.7
OCT		21.9	11.9
NOV		22.8	11.9
DEC		21.7	11.9
Jan-97		21.3	11.2
FEB		21.3	11.1
MAR		21.3	11.2

Table A-2. Data from alluvial aquifer and geothermal monitoring wells for Figures 3 through 8 of Chapter 2. Boron and chloride concentrations in mg/L

YEAR	TH-1 Water Depth (m)	TH-2 Water Depth (m)	TH-3 Water Depth (m)
APR		21.3	11.2
MAY		21.3	11.2
JUN		18.9	8.8
JUL	16.5	20.6	10.9
AUG	16.5	21.3	11.3
SEP	16.5	21.1	11.0
OCT	16.5	20.6	10.9
NOV	16.8	20.9	11.1
DEC	16.8	20.7	11.0
Jan-98	16.7	20.4	11.0
FEB	16.1	20.4	10.7
MAR	16.2	20.1	10.7
APR	16.2	20.1	10.7
MAY	16.4	20.0	10.7
JUN	14.9	20.3	10.7
JUL	15.9	20.5	10.8
AUG			
SEP			
OCT			
NOV			
DEC			

APPENDIX B

GEOPHYSICAL MODELING DATA

APPENDIX B

2.75-D FORWARD MODELING OF GRAVITY AND AEROMAGNETIC PROFILES

This appendix presents a description and figure for each of the 11 profiles from 2.75-D modeling of gravity and aeromagnetic data in the Steamboat Hills and southern Truckee Meadows area. A comparison of the geologic section from each model of the study is discussed and shown in Figure B-12. Physical properties (density, magnetic susceptibility, remanent magnetic intensity) data for each block in the 2.75-D forward models are presented in Table B-1 at the end of the appendix. The best fit model statistics based on the percent root mean square error (%RMSE; [RMSE/anomaly range] between observed and calculated gravity and aeromagnetic anomalies are summarized in Table B-2. The profile and well locations (Figure 5), and well depth information (Table 3) are presented in Chapter 3.

The mapped surface geology is strictly honored for each model with exception of one area for Line 20250. Available lithologic data from well logs are used to constrain vertical geologic contracts. The degree of adherence of each model to this data is somewhat subjective based on the projected distance of a well to the model profile. Data from wells located near a profile are honored more strictly than data from wells located further from a profile. Profiles with good vertical control were modeled first so that the density and magnetic properties of each geologic unit could be assigned. To provide consistency throughout the study, depths and properties of the geologic blocks from each profile that intersect the tie line profile (Line 29020) were adjusted until each model yielded an acceptable fit.

Alluvium (*Qal*), sinter (*Sr*), and granodiorite (*Kgd*) are modeled with constant density and magnetic properties for each model (note one exception for *Kgd* in Line 20350). Since the Tertiary volcanic rocks (*Tv*) and metamorphic rocks (*pKm*) units include a wide range of rock types, variations in density and magnetic properties are assumed for these units. Modeled values of density and magnetic properties are assigned within a tight range and with as much consistency along a profile and between adjacent profiles as possible. Reversed remanent magnetization is assigned for *Tv* and *pKm* units only when normal remanent magnetization could not reproduce the observed magnetic anomaly. To accommodate the observed gravity anomaly in the area of the Carson Range Front Fault (*RF*) system, a fault zone is modeled with an assumed density (2.27 g/cm^3) lower than the Kgd but with the same magnetic properties. The assumed dip is 60^o and the modeled thickness is 100 m for this fault system.

Thermal water is thought to alter both the magnetic and density properties of rocks due to the temperature and chemical reactions between the fluid and the rocks. Therefore, altered granodiorite (*Alt Kgd*), metamorphic rock, and altered Tertiary volcanics rocks (*Alt Tv*) are modeled to represent the geothermal reservoir and cap rock.

Each profile model is described below. The upper portion of each figure provides the magnetic data while the center section shows the gravity data. The lower section illustrates the geologic model. Horizontal distances are relative to the northwest (NW) end of the profile (southwest [SW] end for Line 29020), which is the left side of each figure. Descriptions begin at the NW end (SW for Line 29020) and progress toward the southeast (SE) end of each profile (northeast

[NE] end for Line 29020). Vertical descriptions of geologic unit are in terms of depths from ground surface and thickness. Significant variations of density and magnetic properties for a given unit are noted with the corresponding justification.

DESCRIPTION OF MODEL PROFILES

Profile 20170

The model for Profile 20170, located at the southwestern extent of the study area, is shown in Figure B-1. This profile crosses the southern extent of the Galena Fan and the northern portion of Washoe Valley. The model shows a reasonable fit for gravity (%RMSE of 4.1%, Table B-2) and a good fit for aeromagnetic (%RMSE of 5.5%, Table B-2) data. Data from Washoe County production wells SJ-1 and SJ-2 provide good control on the thickness of *Qal* and *Tv* (Table 3, Chapter 3) near the center of the model. The Shepley domestic well provides data on the depth to *Kgd* (*Qal* thickness) at the SE end of the profile.

At the NW end of the profile, a thin layer of *Tv* (40 m) is modeled at the surface overlying *Kgd*. A surface exposure of *Kgd*, adjacent to the *RF*, is modeled with a density of 2.47 g/cm^3 rather than the usual 2.67 g/cm^3 for this unit to account for the gravity low. Across the Galena Fan, *Qal* is modeled with a maximum thickness of 34 m. Thicker *Qal* is modeled near wells SJ-2 (52 m) and SJ-1 (90 m) reflecting the proximity of these wells to drainage basins of Browns Creek and a tributary to Galena creek. The underlying *Tv* is modeled with maximum thickness of 812 m in this area where the upper portion is modeled with reversed remanent magnetization. An apparent fault in the *Tv* is coincident with a mapped fault near well SJ-2. To the SE, an outcrop of *Tv* separates the Galena Fan basin from the Washoe Valley basin. The *Tv* thins to 51 m at distance 6900 m and thickens to 260 m near distance 7850 m to account for the large magnetic high anomaly. The thickest *Qal* in this basin (81 m) is modeled at distance 8400 m (near Profile 29020). Near distance 9800 m, *Tv* is modeled with reversed remanent magnetization at a depth of only 10 m and a thickness of 300 m to accommodate both the gravity high and the large magnetic low anomalies. Underlying the *Tv*, a zone of *pKm* is modeled with maximum thickness of 670 m. An apparent fault cutting the *Tv* and *pKm* at distance 11400 m corresponds to a mapped fault.

Profile 20191

Figure B-2 shows the geologic model for Profile 20191. The profile crosses the central portion of the Galena Fan and bisects Washoe Hill, which separates Pleasant Valley and Washoe Valley. This model yields good fits for both gravity and aeromagnetic data with %RMSE values of 3.7% and 6.9%, respectively (Table B-2). Excellent vertical geologic control is provided with data from 4 well logs (Table 3, Chapter 3). Washoe County production wells MR-5 and MR-6 provide depths to *Tv* (172 m and 192 m) in the NW portion of the profile. In the center of the profile, depths to *Tv* of 79 m and 70 m are obtained from Washoe County monitoring wells SJ-MW1 and SJ-MW2. Total depths for each of these wells provides for minimum thickness of *Tv* (minimum depth to *Kgd*).

A sequence of *Tv* with maximum thickness of 980 m is modeled in the Carson Range with the lower portion consisting of reverse remanent magnetization. The maximum *Qal* thickness of 215 m is modeled near distance 3300 m. A thin layer of *Tv* (30 m to 100 m) with reverse remanent magnetization underlies much of the basin. The *Qal* gradually thins to the SE as does the underlying *Tv*, which is modeled with normal remanent magnetization beginning near

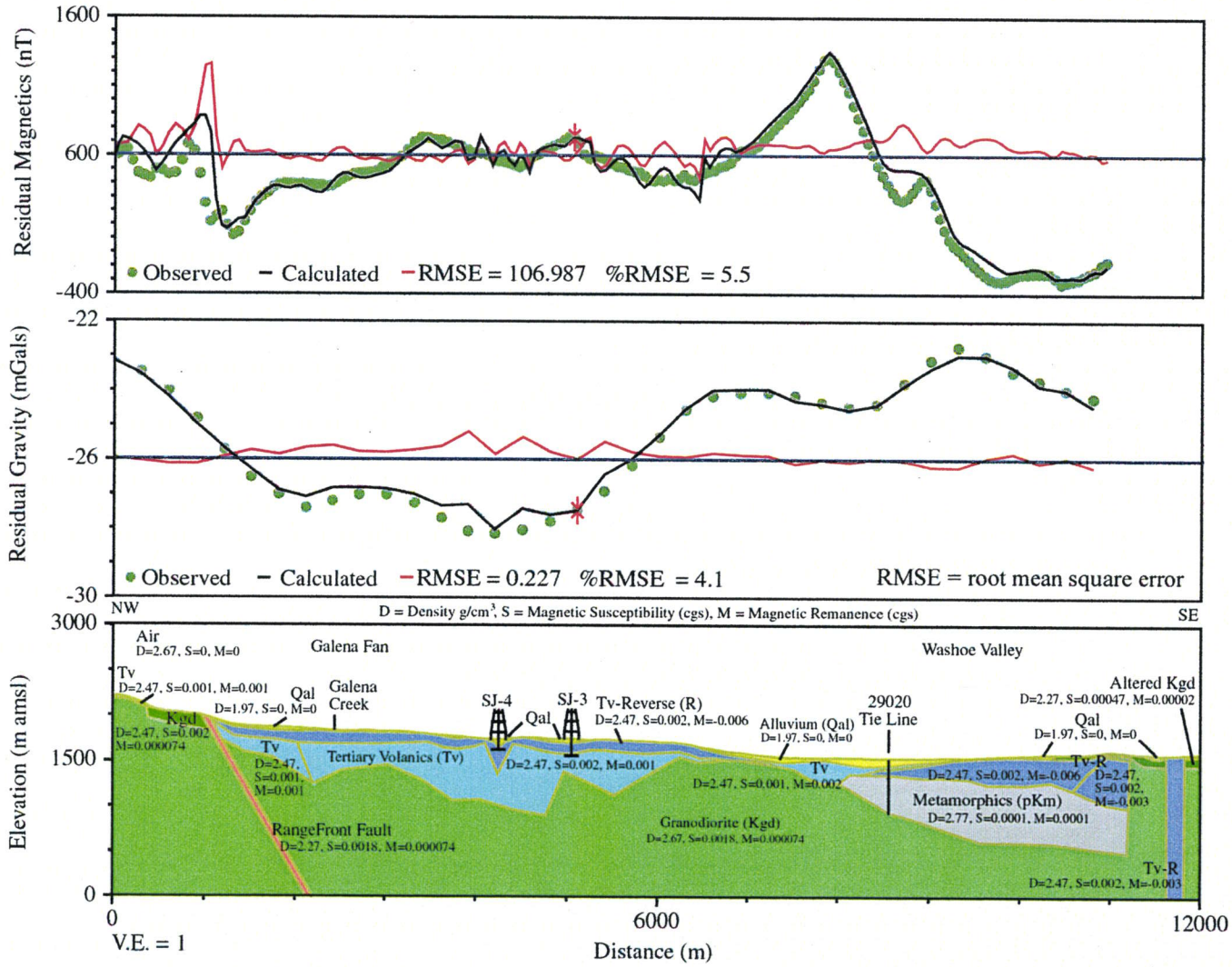

Figure B-1. Profile 20170 cross-section as computed by 2.75-D forward modeling of gravity and aeromagnetic data.

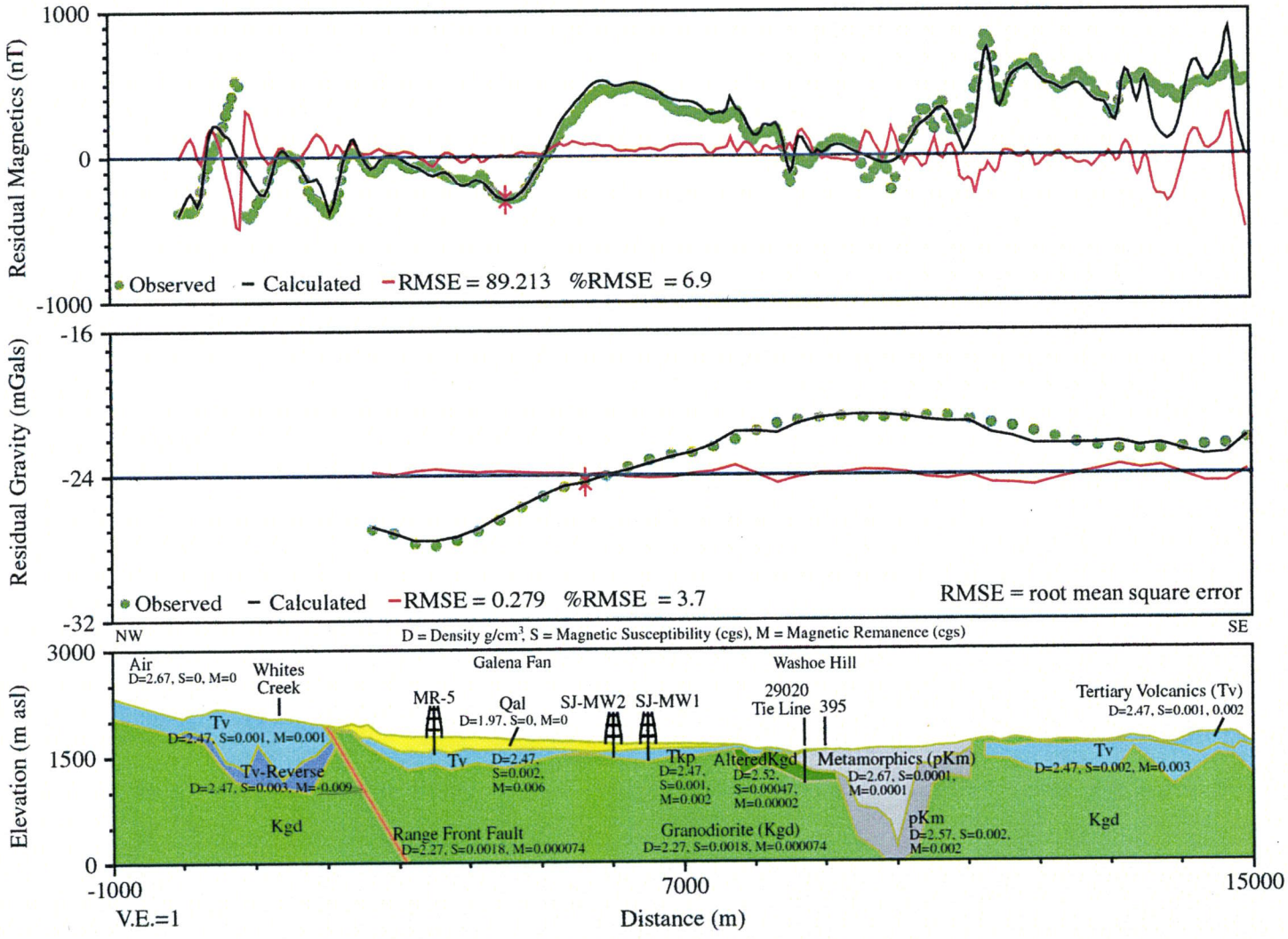

Figure B-2. Profile 20191 cross-section as computed by 2.75-D forward modeling of gravity and aeromagnetic data.

distance 5400 m. The thin zone of *Alt Kgd* between distances 7700 m and 9100 m represents the southern extent of the modeled geothermal reservoir. Two units are used to model the thick zone of *pKm* with the lower unit assigned magnetic properties an order of magnitude higher than the upper unit to accommodate the observed anomaly. The vertical dikes of *Tv* at the SE end of the profile nicely model the high frequency magnetic anomalies and represent a reasonable interpretation of the geology mapped adjacent to the profile.

Profile 20211

The model for Profile 20211, located in the southwestern portion of the study area, is shown in Figure B-3. The profile crosses the northern portion of the Galena Fan and the southern extent of both the Steamboat Hills and Pleasant Valley. This model represents a good fit for gravity data with a %RMSE of 3.7% and an acceptable fit for aeromagnetic data with a %RMSE of 9.7% (Table B-2). The thickness of *Qal* in the Galena Fan is constrained by depths to *Tv* of 67 m and 73 m at Washoe County production wells MR-3 and Tessa 1, respectively. Geothermal monitoring well ST-12 provides depth to *pKm* in the Steamboat Hills (Table 3, Chapter 3).

In the Carson Range, four layers of *Tv* with normal and reverse remanent magnetization form a sequence (1250 m maximum thickness) over *Kgd*. These layers are assigned density values of 2.27 g/cm^3 to account for the low gravity anomaly. SE of the RF, one layer of *Tv* with reverse remanent magnetization is modeled with a thickness of 780 m near Tessa 1, which thins to 150 m near well MR-3. The alluvial basin appears to have formed on an undulating surface of *Tv* with maximum *Qal* thickness of 180 m at distance 4100 m. *Tv* is modeled at a depth of 10 m near the eastern extent of the fault swarm (distance 5650 m) located west of Callahan Ranch Road. The shallow *Tv* creates a sub-basin in the alluvial fan with maximum thickness of 100 m. An apparent fault defining the NW boundary of *pKm* and *Alt Kgd* does not correlate with any mapped surface fault; however, mapped faults to the north and south along a similar tend suggest a fault hidden in the *Qal* is possible. In the Steamboat Hills (distance 6500 to 9500 m), layers of *Tv* with normal and reverse remanent magnetization and highly variable thickness (10 to 390 m) nicely model the high frequency magnetic anomalies. These layers overlie *pKm* with thickness ranging from 300 m to 1270 m, which overlies *Alt Kgd* with thickness ranging from 310 m to 725 m. The extent of the *Alt Kgd* is modeled to nearly the SE end of profile to accommodate the observed gravity. Thermal water found in shallow domestic wells around New Washoe City, located south of this profile, supports this interpretation.

Profile 20231

Figure B-4 shows the geologic model for Profile 20231. This profile begins in the Carson Range and crosses the Mount Rose Fan, Galena Fan, Steamboat Hills, and Pleasant Valley. This model produces a good fit for gravity (%RMSE of 3.6%, Table B-2) and an acceptable fit for aeromagnetic (%RMSE of 8.8%, Table B-2) data. Lithologic data from two wells (Tessa 2 and ST-7) are used to constrain vertical geologic contacts for this model (Table 3, Chapter 3). For the center of the model, data from well Tessa 2 includes a depth to *Tv* of 73 m and a total depth of 224 m that constrains the minimum depth to *Kgd*. Located in the SE portion of the model, well ST-7 provides depth to *pKm* of 414 m and a total depth of 506 m that constrains the minimum depth to *Kgd*. The well log for ST-7 indicates rhyolite from 65 m to 414 m that the author has interpreted as *Tv*.

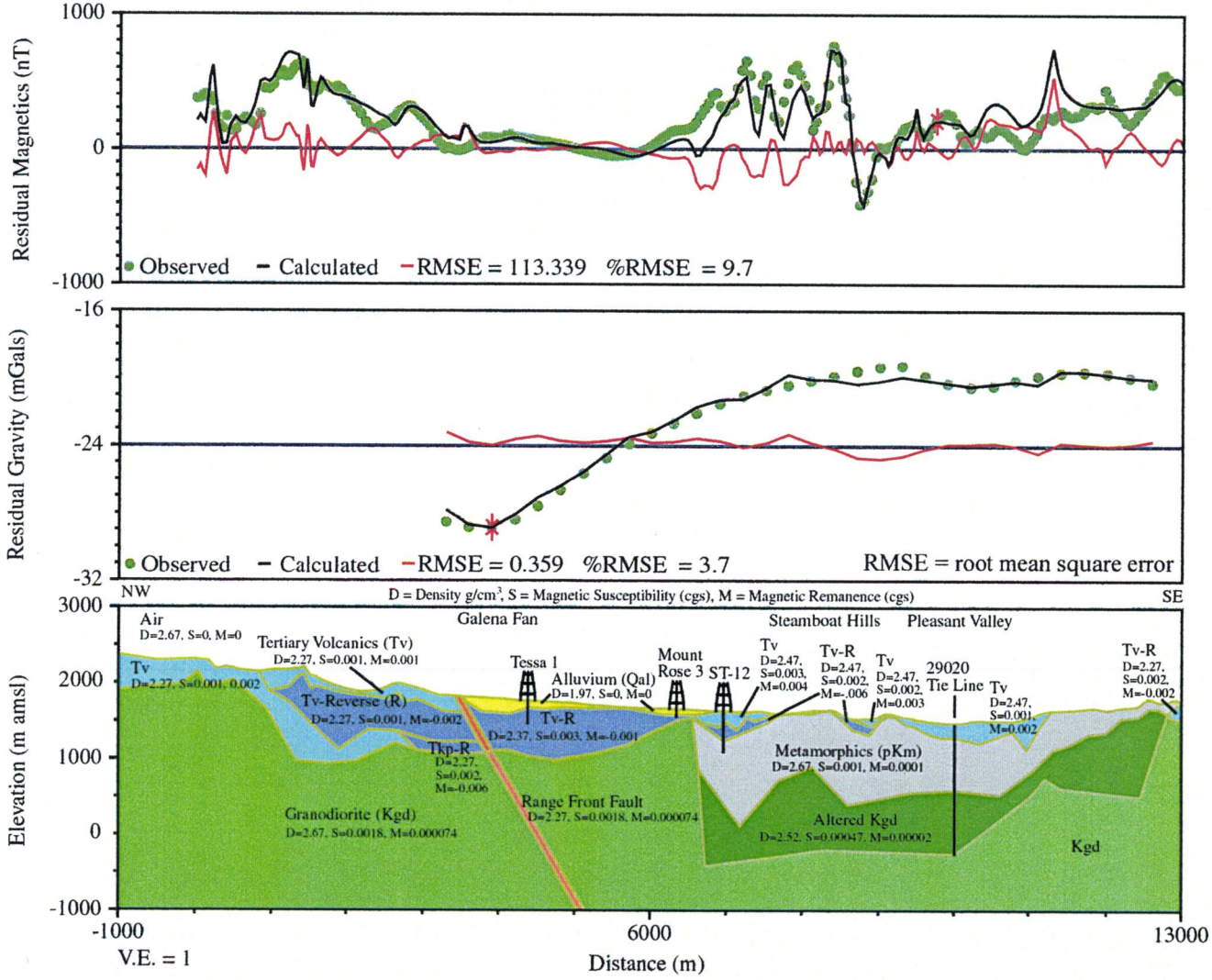

Figure B-3. Profile 20211 cross-section as computed by 2.75-D forward modeling of gravity and aeromagnetic data.

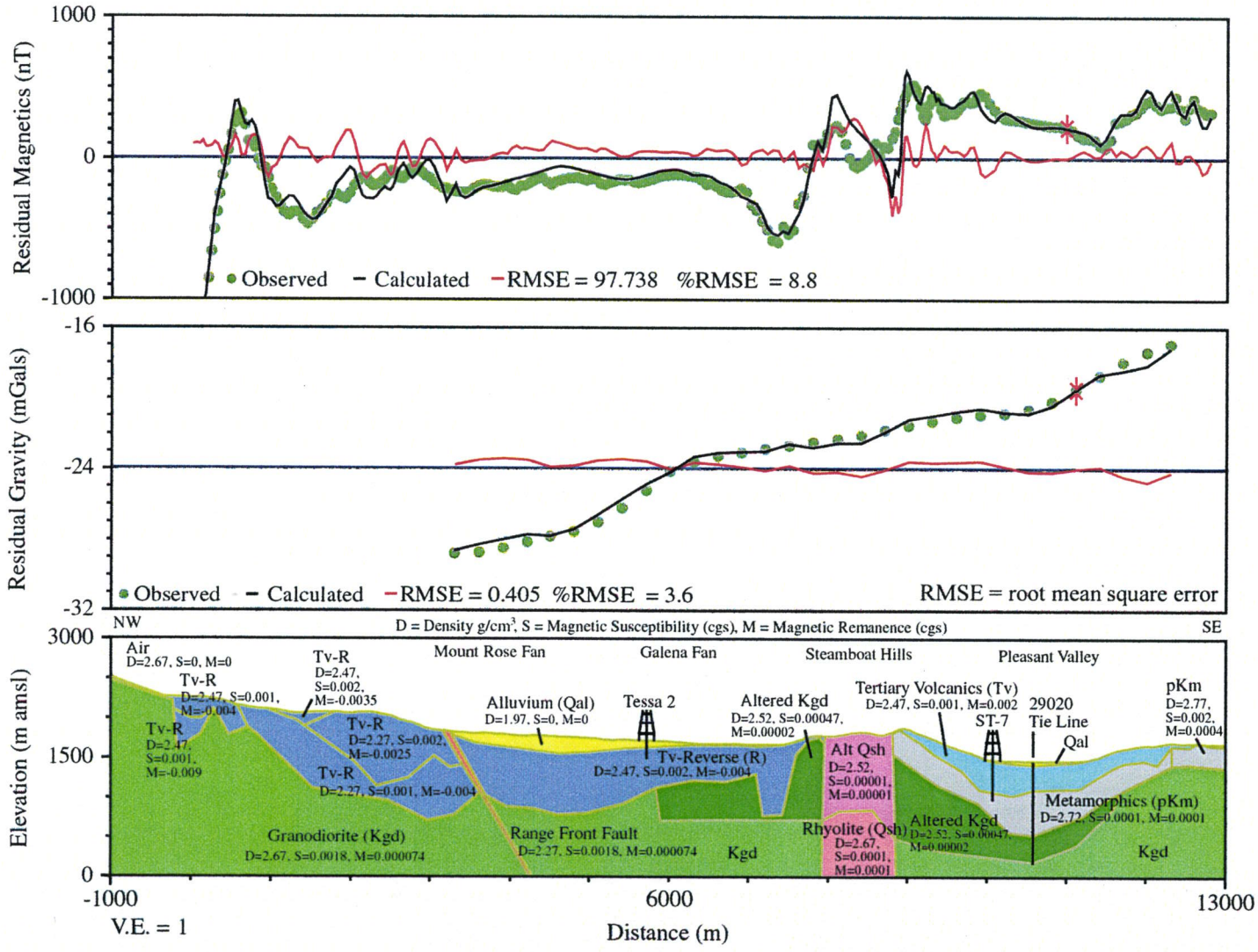

Figure B-4. Profile 20231 cross-section as computed by 2.75-D forward modeling of gravity and aeromagnetic data.

Five layers of *Tv* with reverse remanent magnetization are used to model the magnetic anomaly in the Carson Range. These layers are assigned density values of 2.27 g/cm^3 to account for the low gravity anomaly and the combined thickness of this sequence, which ranges from 125 m to 1100 m. The *Qal* of the Galena Fan is thickest (190 m) near the center of the basin at the 4900 m distance. Underlying the entire alluvial basin, one layer of *Tv* with reverse remanent magnetization is modeled with a maximum thickness of 850 m. A mapped dome of the Steamboat Hills Rhyolite (Qsh, Tabor and Ellen, 1975) is modeled around the 8400 m distance and is thought to be a possible heat source for the geothermal reservoir (Finger et al., 1994). *Alt Tv* and *Alt Kgd* are modeled to the NW of the dome; only *Alt Kgd* is modeled to the SE of the dome. The upper portion of the dome is assigned a density value of 2.52 gm/cm^3, consistent with *Alt Kgd*. The thickness of the modeled geothermal reservoir along this profile ranges from 260 to 1350 m. In Pleasant Valley, *Qal* is modeled with maximum thickness of 55 m. Units with relatively uniform thickness of *Tv* (315 m), *pKm* (550 m), *Alt Kgd* (365 m), and the *Kgd* basement underlie the entire alluvial basin.

Profile 20250

Figure B-5 shows the model for Profile 20250. The NW end of this profile is located in the Carson Range. The profile crosses the western extent of the Washoe County drinking water production field in the Mount Rose Fan, Steamboat Hills, and northern Pleasant Valley. This model yields acceptable fits for both gravity and aeromagnetic data with %RMSE values of 3.7% and 10.0%, respectively (Table B-2). Washoe County production well AC-3 provides the only vertical geologic control for this model where *Qal* is encountered over the total depth of 335 m (Table 3, Chapter 3).

A thick section of *Tv* (maximum 700 m) is modeled NW of the *RF* fault and a volcanic dike is modeled at distance 2900 m to account for a subtle magnetic low anomaly. The dike is modeled as originating from the *RF* fault at a depth of 3000 m. Concentric surface fault patterns and time-domain electromagnetic sounding data in this location support the interpretation of this dike. In the center of the profile (distance 7000 m), *Tv* thickens to 850 m and a lower layer with reverse remanent magnetization is modeled to account for the observed magnetic anomalies. The irregular contact between the two sub-units of *Tv* is required to model the high frequency magnetic anomalies observed between distances 5000 m and 7500 m. Alternatively, a more realistic model with smooth contacts but highly variable magnetic properties could produce a similar fit. The surface geology between distances 7500 m and 8500 m (mapped as a narrow band of *pKm* parallel to the profile) was modified to reflect the occurrence of *Tv* located within 50 to 100 m of the profile. This modification allows for modeling the observed magnetic anomaly and better represents the geology in this area. *Alt Kgd* is modeled between distances 7400 m and 9600 m with maximum thickness of 700 m near distance 8000 m. The surface projection of an apparent fault between *Tv* and *Alt Kgd* corresponds with a mapped fault at distance 7500 m. Modeled thickness of *Qal* in Pleasant Valley ranges from 40 m at the NW edge to 10 m in the center of the basin. *Tv*, *pKm*, and *Kgd* underlie the basin. An outcrop of *pKm* located at the base of the Virgina Range is modeled with maximum thickness of 1000 m.

Profile 20270

Figure B-6 shows the geologic model for Profile 20270. This profile crosses the Washoe County drinking water production field in the Mount Rose Fan alluvial basin, the production area

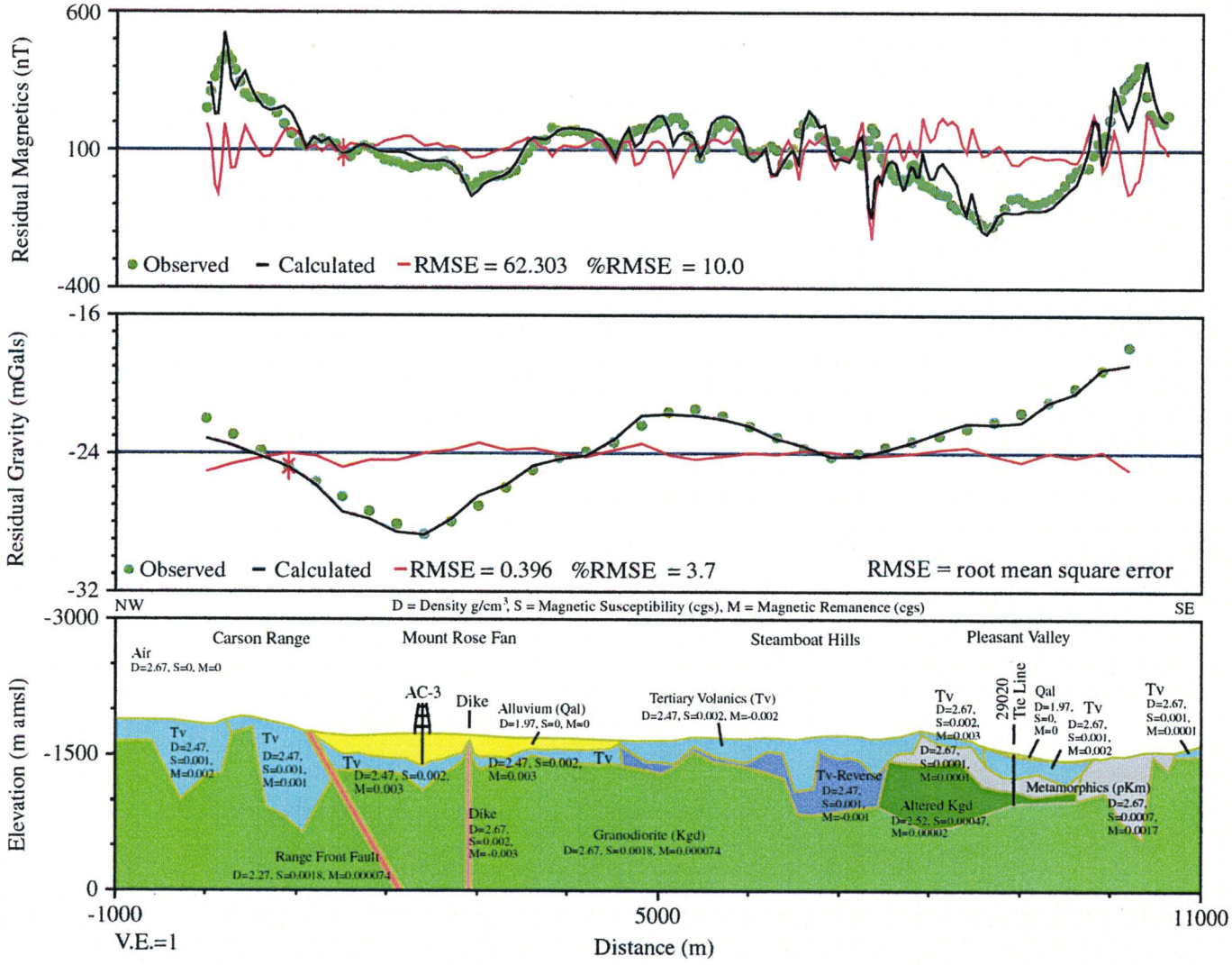

Figure B-5. Profile 20250 cross-section as computed by 2.75-D forward modeling of gravity and aeromagnetic data.

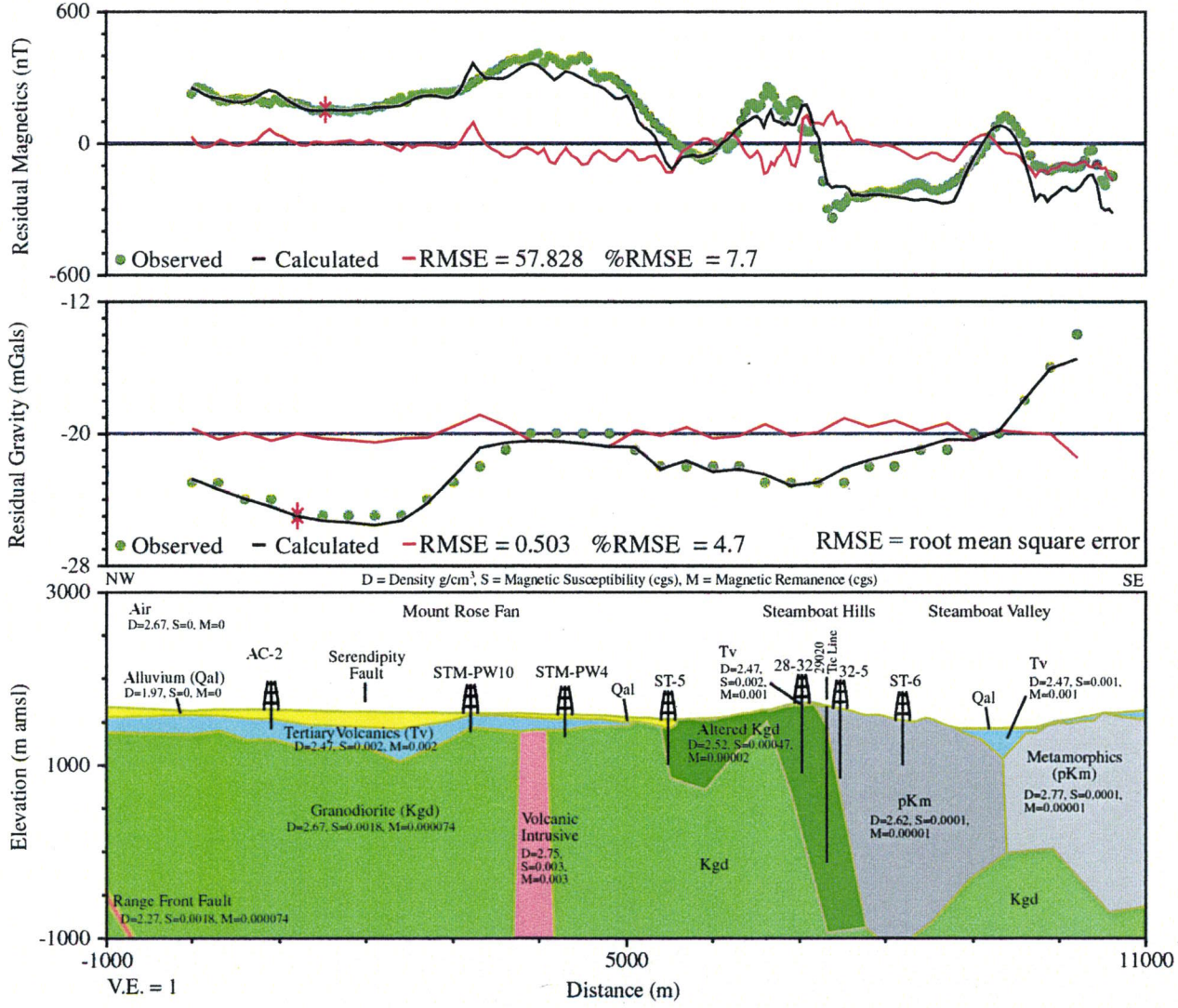

Figure B-6. Profile 20270 cross-section as computed by 2.75-D forward modeling of gravity and aeromagnetic data.

of the CPI geothermal field located at the crest of the Steamboat Hills, and the southern extent of Steamboat Valley. An acceptable fit for gravity (%RMSE of 4.7%, Table 2) and a good fit for aeromagnetic (%RMSE of 7.7%, Table B-2) data were obtained for this model. Excellent vertical geologic control data are provided from 7 wells (Table 3, Chapter 3). *Qal* and the underlying *Tv* show maximum thickness of 190 m and 370 m, respectively, near distance 2350 m. Shallow *Tv* creates two sub-basins in the alluvial fan near well STM-TH10 where *Qal* thickness is 30 m and *Tv* thickness is 135 m. An intrusive body with slightly higher density (2.75 g/cm^3) and magnetic susceptibility (0.003 cgs) than *Kgd* is modeled at distance 3900 m to account for local gravity and aeromagnetic anomalies. In well ST-5, 113 m of *Qal* overlies *Kgd* suggesting faulting and erosion eliminated *Tv* in this area. *Alt Kgd* is projected to a depth of 2750 m in the CPI geothermal field near wells 28-32 and 32-5 on this profile although the model lacks resolution to confirm this depth. This zone lies between two apparent southeast dipping faults bracketing a mapped fault that may be a splay of the Steamboat Springs Fault system. The *pKm* shows reverse remanent magnetization and a maximum thickness of 2700 m near well ST-6. *Tv* underlies Steamboat Valley with maximum model thickness of 350 m. The *pKm* at the southeast end of the profile contains two blocks of different density (2.62 and 2.77 g/cm^3) to accommodate the observed anomaly.

Profile 20290

Figure B-7 shows the geologic model for Profile 20290. This profile crosses the center of the Washoe County drinking water production field, the injection area for Caithness Power Inc. (CPI), and the center of Steamboat Valley. The model shows a reasonable fit for gravity (%RMSE of 4.6%, Table 2) and a good fit for aeromagnetic data (%RMSE of 6.5%, Table 2). Vertical geologic control for this model includes data from Washoe County production well AC-1 and monitoring well STM-MW1 located in the NW portion of the profile. Depth to *Tv* at these wells is 149 m and 164 m, respectively (Table 3, Chapter 3). Additionally, CPI CoxI-1 geothermal injection well provides the depth to *Kgd* (25 m) in the center of the model.

The most prominent features of this model are the gravity and magnetic high anomalies located around the 3000 m distance. These features are nicely modeled with shallow depth to *Tv* (minimum of 6 m), which creates two sub-basins within the alluvial fan with maximum depths of 260 m and 265 m. The *Tv* thickness ranges from around 100 m to nearly 1000 m in this area. Two apparent faults in *Tv* at distances of 2450 m and 3450 m correlate with projected traces of mapped faults. The NW boundary of *Alt Kgd* corresponds with the Peigh Fault, which is thought to transmit thermal water from the geothermal system toward the north. The *Alt Kgd* zone reaches a maximum thickness of 910 m in this model. A thick unit of *pKm* (1930 m) occurs adjacent to the *Alt Kgd*. The SE boundary of the *pKm* may correspond with the projection of a mapped fault. The trace of this projected fault could represent a fault splay of the Steamboat Springs Fault System. The *Qal* in Steamboat Valley is modeled with a maximum thickness of 90 m. A thin layer of *Tv* (45 m) is modeled underlying the *Qal*. This layer continues to the SE and crops out at the foothills of the Virgina Range where *Kgd* underlies these volcanics.

Line 20310

Figure B-8 shows the model for Profile 20310. The central portion of this profile bisects the Far West Capital (FWC) geothermal field. This model produces good fits for both gravity and aeromagnetic data with %RMSE values of 3.2% and 5.8% (Table B-2), respectively and contains the best vertical geologic control within the study area, utilizing data from 7 wells

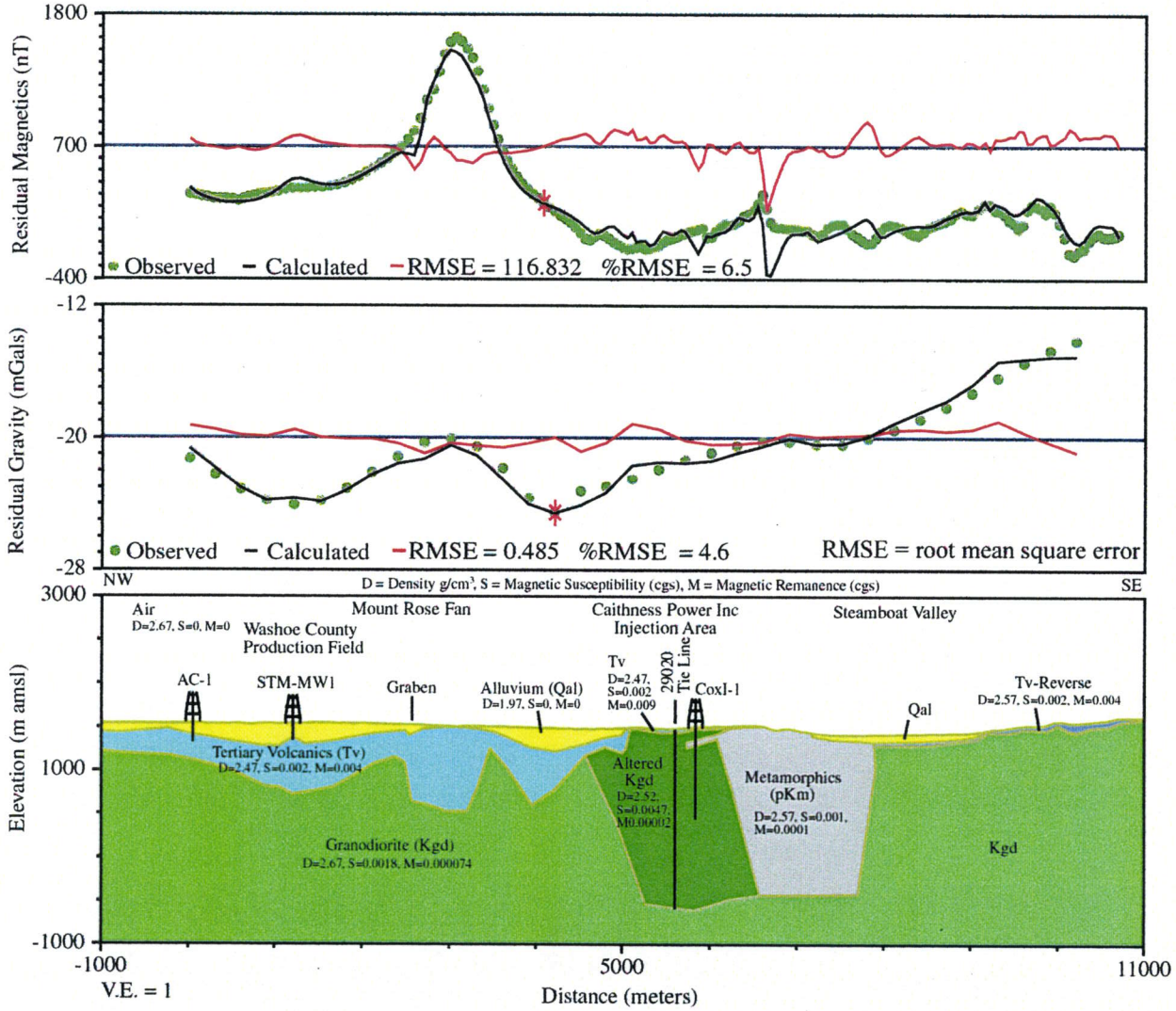

Figure B-7. Profile 20290 cross-section as computed by 2.75-D forward modeling of gravity and aeromagnetic data.

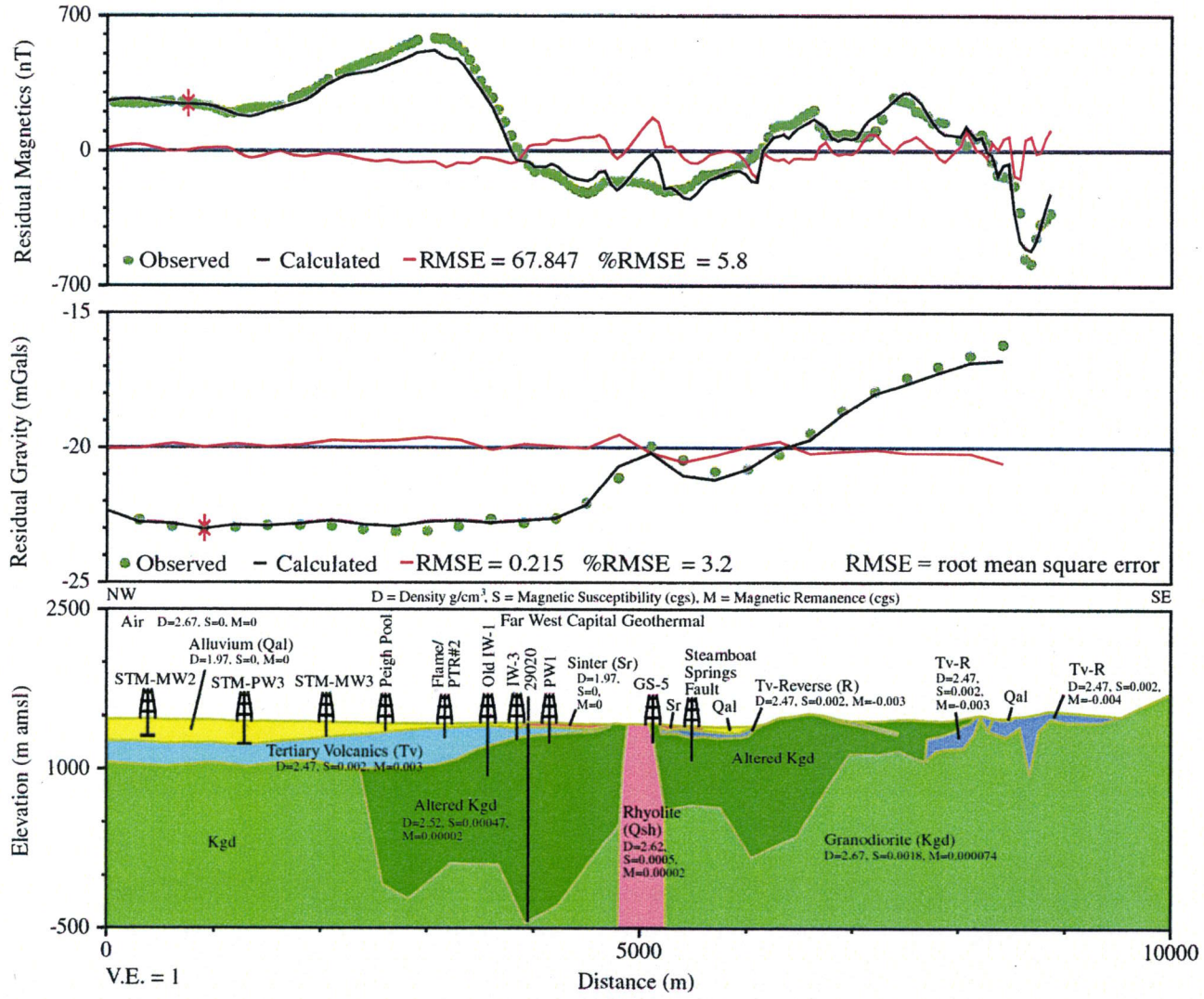

Figure B-8. Profile 20310 cross-section as computed by 2.75-D forward modeling of gravity and aeromagnetic data.

(Table 3, Chapter 3). Four of these wells (GS-5, IW-3, Old IW-1, PTR-2) provide data control on the depth to *Tv* and *Kgd* and well STM-MW3 provides control on depth to *Tv*. Again, modeled *Qal* is thickest (190 m) at the NW end and gradually thins to 35 m near the center of the profile (distance 3800 m). The underlying *Tv* ranges from 150 m near well STM-MW-2 to 460 m near well PTR-2. A thin (80 m) layer of *Alt Tv* overlies a thick zone (1310 m) of *Alt Kgd* in the center of this model representing the FWC geothermal field. The Mud Volcano Basin Fault (White et al., 1964) is modeled as *Alt Tv* extending under well PTR-2. A mapped dome of Qsh is modeled near the SE end of the geothermal field in the center of the profile. The narrow portion at the northern extent of Steamboat Valley (5600 to 6000 m distance) is modeled with maximum *Qal* thickness of 56 m. A 30 to 35 m thick layer of *Tv* underlies the entire basin. *Alt Kgd* is also present in this area but is considerably thinner (800 m) than in the center of the model. The *Tv* that crops out SE of Steamboat Valley is modeled as very thin (10 m). Near the end of the profile, a thicker unit of *Tv* (165 m to 585 m) is modeled with maximum thickness at the base of the Virgina Range. The configuration of *Tv* in this area may result from range front faulting.

Profile 20330

Figure B-9 shows the geologic model for Profile 20270. This profile is located in the northeast portion of the study area. The model for this profile provides a good fit for gravity data with a %RMSE of 4.0% and an excellent fit for aeromagnetic data with a %RMSE of 2.6% (Table B-2). The minimum thickness of Qal in the center of the model is constrained by the total depth data from three domestic wells that did not encounter *Tv* (Table 3, Chapter 3). The maximum Qal thickness of 280 m is between the Herz domestic well and the Herz Fault. The underlying Tv has a maximum model thickness of 1820 m including 250 m of *Alt Tv*; the model is not constrained at this depth. Local undulations of the Tv upper surface produce a good fit for the aeromagnetic low anomaly located over the Herz Fault. A smaller aeromagnetic low anomaly over the Sage Hill Road Fault (Figure 1) is also reproduced by the model. Thermal water is known to migrate along the Herz and Sage Hill Road Faults and is also known to exist in the Curti Barn and Steinhardt domestic wells, which are both completed in the alluvial aquifer (Skalbeck et al., 2001). Subtle aeromagnetic low anomalies near these two wells are modeled as vertical zones of *Alt Tv* to represent faults that conduct thermal water. A group of mapped faults, located southeast of the Steinhardt domestic well, also correlates with a aeromagnetic low and is modeled as a vertical zone of *Alt Tv*.

Line 20350

Figure B-10 shows the model for Profile 20350 located at the northeastern extent of the study area. This model represents the best model fit in the study area with a %RMSE for gravity data of 2.1% and a %RMSE for aeromagnetic data of 2.2% (Table B-2). Lithologic data from two wells (DD-1 and ST-1) are used to constrain vertical geologic contacts for this model (Table 3, Chapter 3). The total depth for Washoe County production well DD-1 is 130 m and constrains the minimum thickness of *Qal* at the NE end of the profile. For geothermal monitoring well ST-1, located near the center of the model, the *Tv* depth of 70 m constrains *Qal* thickness and the total depth of 599 m constrains the minimum depth to *Kgd*.

Qal is modeled with maximum thickness of 160 m at the NW end of the profile and gradually thins to 25 m at distance 5400 m. *Tv* is modeled as a thick unit that appears to have been deposited in a structural depression of the underlying *Kgd*. *Alt Tv* and *Alt Kgd*, representing the geothermal reservoir, are modeled at distance 4500 m with maximum thickness of 300 m and

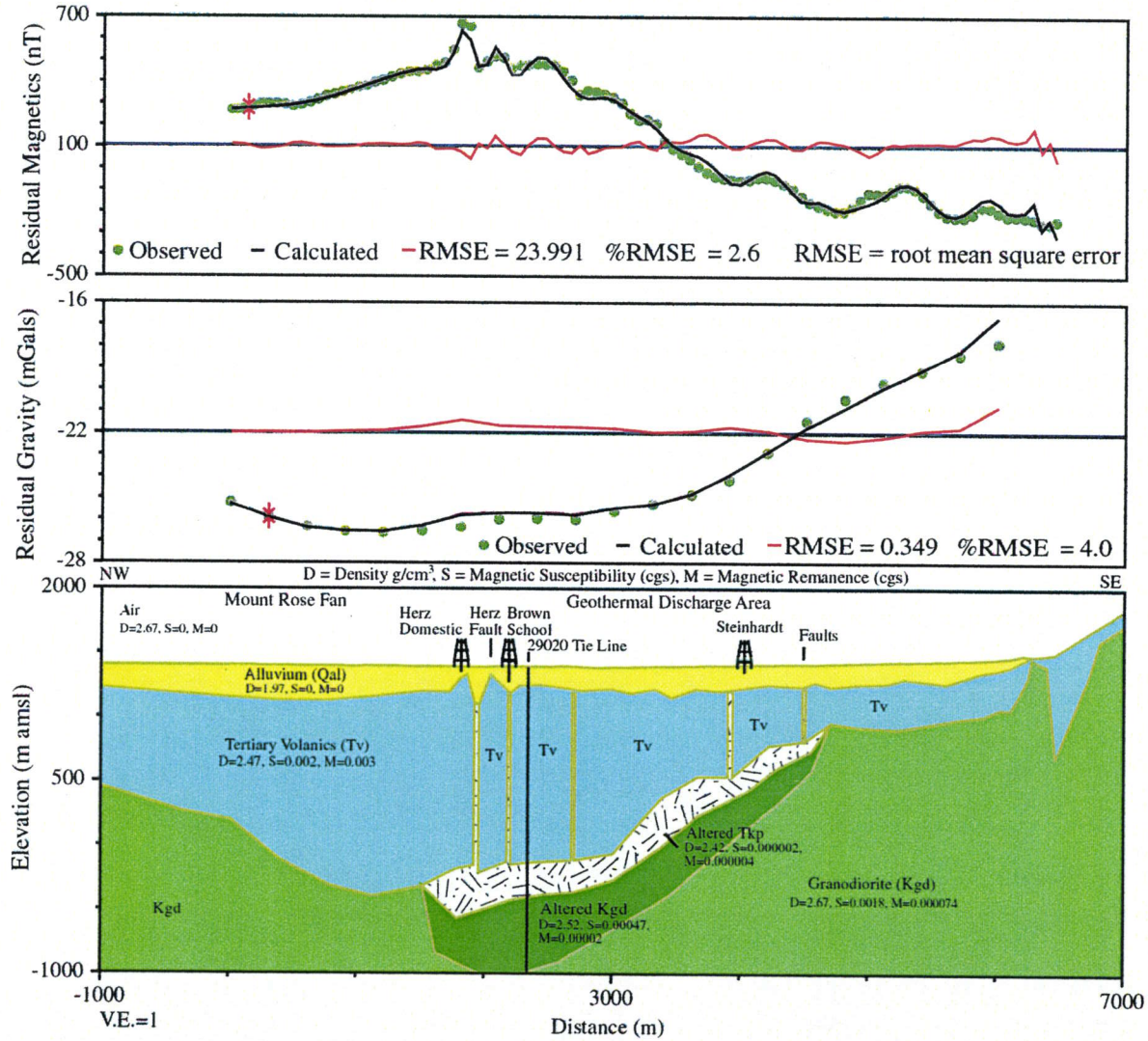

Figure B-9. Profile 20330 cross-section as computed by 2.75-D forward modeling of gravity and aeromagnetic data.

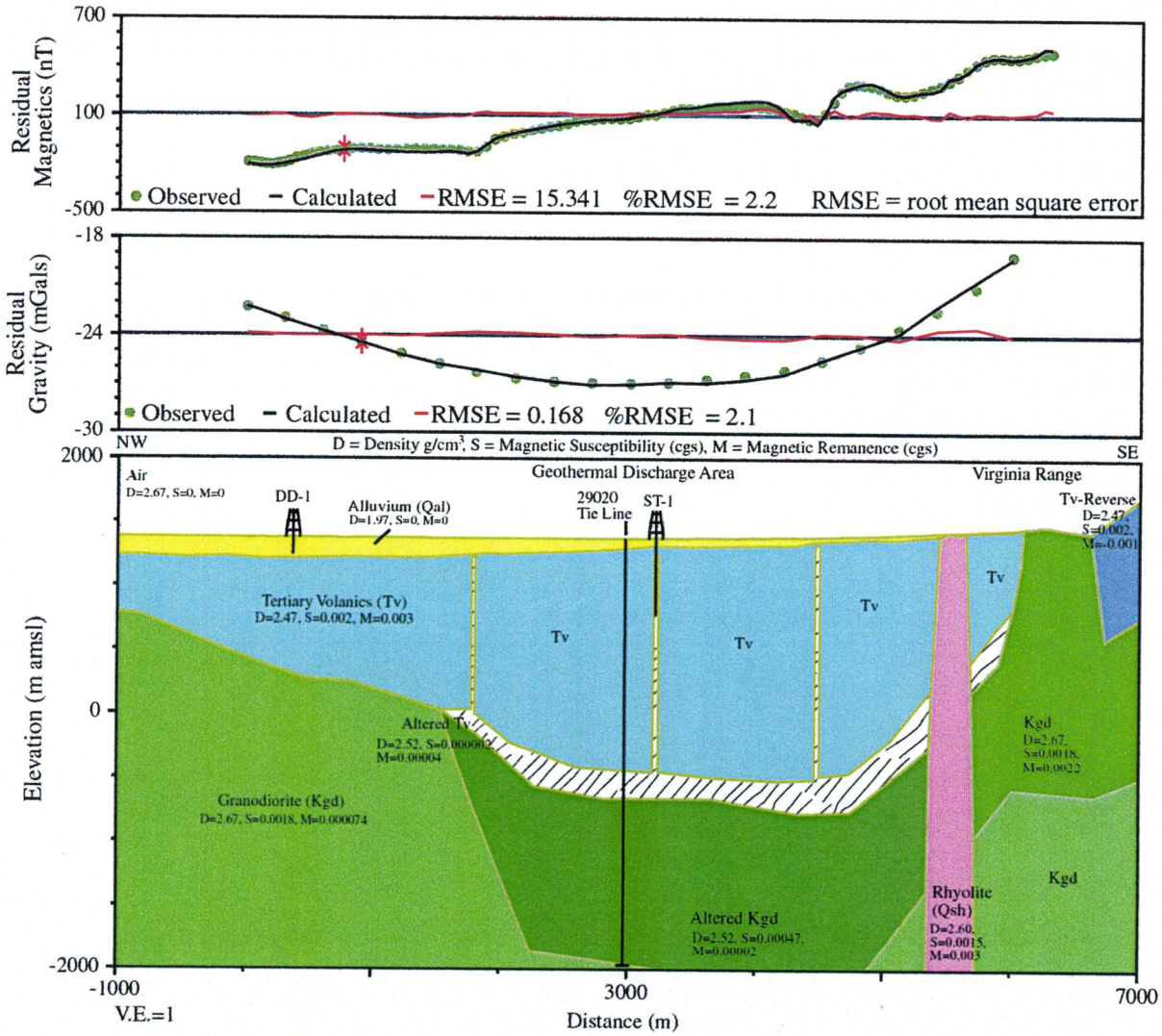

Figure B-10. Profile 20350 cross-section as computed by 2.75-D forward modeling of gravity and aeromagnetic data

1800 m, respectively. Thermal water is found in ST-1 and therefore a vertical fault is modeled as *Alt Tv* in this area. Magnetic low anomalies located at distances of 1740 m and 4470 m are also modeled as vertical faults. A mapped dome of the Steamboat Hills Rhyolite (*Qsh*, Bonham and Bell, 1983) is modeled near the SE end of the profile. To accommodate the magnetic anomaly in this area, a higher value of remanent magnetization is assigned for the *Kgd* that crops out SE of this dome.

Profile 29020

The model for Profile 29020 is shown in Figure B-11. This "tie line" profile trends SW/NE and intercepts each of the profiles in the study area. The location and depths of each profile model are annotated on this model. This profile begins in the southern Washoe Valley and extends across Washoe Lake, eastern Steamboat Hills, and into southern Truckee Meadows. Although this profile extends outside the study area to the SW into southern Washoe Valley and to the NE into southern Truckee Meadows, a geologic model was developed for the entire profile to ensure consistency with local geology.

This model represents a good fit for aeromagnetic data with a %RMSE of 7.7% but the fit for gravity data with a %RMSE of 7.5% is outside the target value of 5.0% (Table B-2). The majority of error in the gravity fit occurs from Washoe Hill (12000 m) to the crest of Steamboat Hills (distance 17700 m) where very few gravity stations exist. Therefore, the gravity data interpolated along this portion of the profile may not be accurate. Excellent vertical geologic control exists for this profile with data from 7 wells (Table 3, Chapter 3). Five of these wells (21-5, GS-7, PW-1, IW-2, ST-9) provide data control on the depth to *Tv* and *Kgd*. Wells 21-5 and ST-13 include depth to *pKm* and well GS-6 includes depth to *Kgd*. In Washoe Valley, the gravity and magnetic low anomalies are nicely modeled by a deep basin of *Qal* (900 m) and thick unit of *Tv* (1300 m) with reverse remanent magnetization that occur within a depression of *Kgd*. Although not visible in the figure, Washoe Lake is modeled at the surface with assumed density of 1.0 g/cm^3, magnetic susceptibility of zero, and average depth of 5 m. The prominent magnetic high and gravity high anomalies near Profile 20170 (distance 11000 m) are modeled by shallow depth to *Tv* with normal remanent magnetization underlain by *pKm*. The *Tv* outcrops at Washoe Hill, and underlying *pKm* and *Alt Kgd* rest on a structural high of *Kgd*. The *Tv*, *pKm* and *Alt Kgd* reach maximum thickness for this area near the southern extent of Pleasant Valley. The magnetic anomaly is modeled well for this area but the gravity anomaly, as described above, is not well modeled. The thickest unit of the *Alt Kgd* (2000 m) is found beneath Steamboat Hills and this portion of the model provides a reasonable fit to the gravity data but a marginal fit to the aeromagnetic data. The thick unit of *Tv* (1950 m) beneath the southern Truckee Meadows modeled within a structural depression of *Kgd* nicely fits the gravity low and magnetic high anomalies.

COMPARISON OF MODEL GEOLOGIC SECTIONS

Figure B-12 shows the model geologic cross sections for the 10 N45W oriented profiles. The tie line Profile 29020 (oriented at N20E) location was used to align each section. Wells used for vertical control are show with geothermal wells annotated by solid circles above the well symbol.

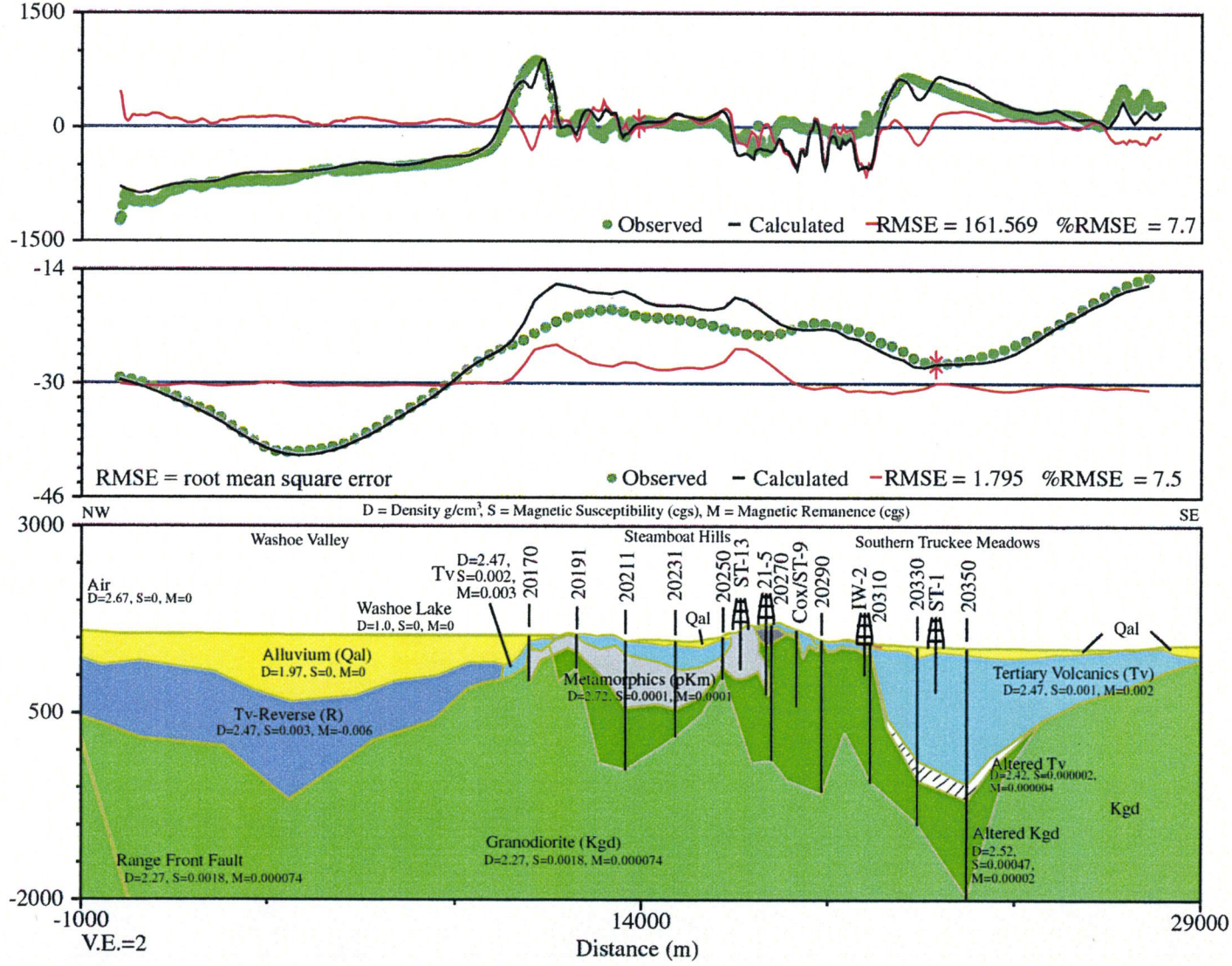

Figure B-11. Profile 29020 cross-section as computed by 2.75-D forward modeling of gravity and aeromagnetic data

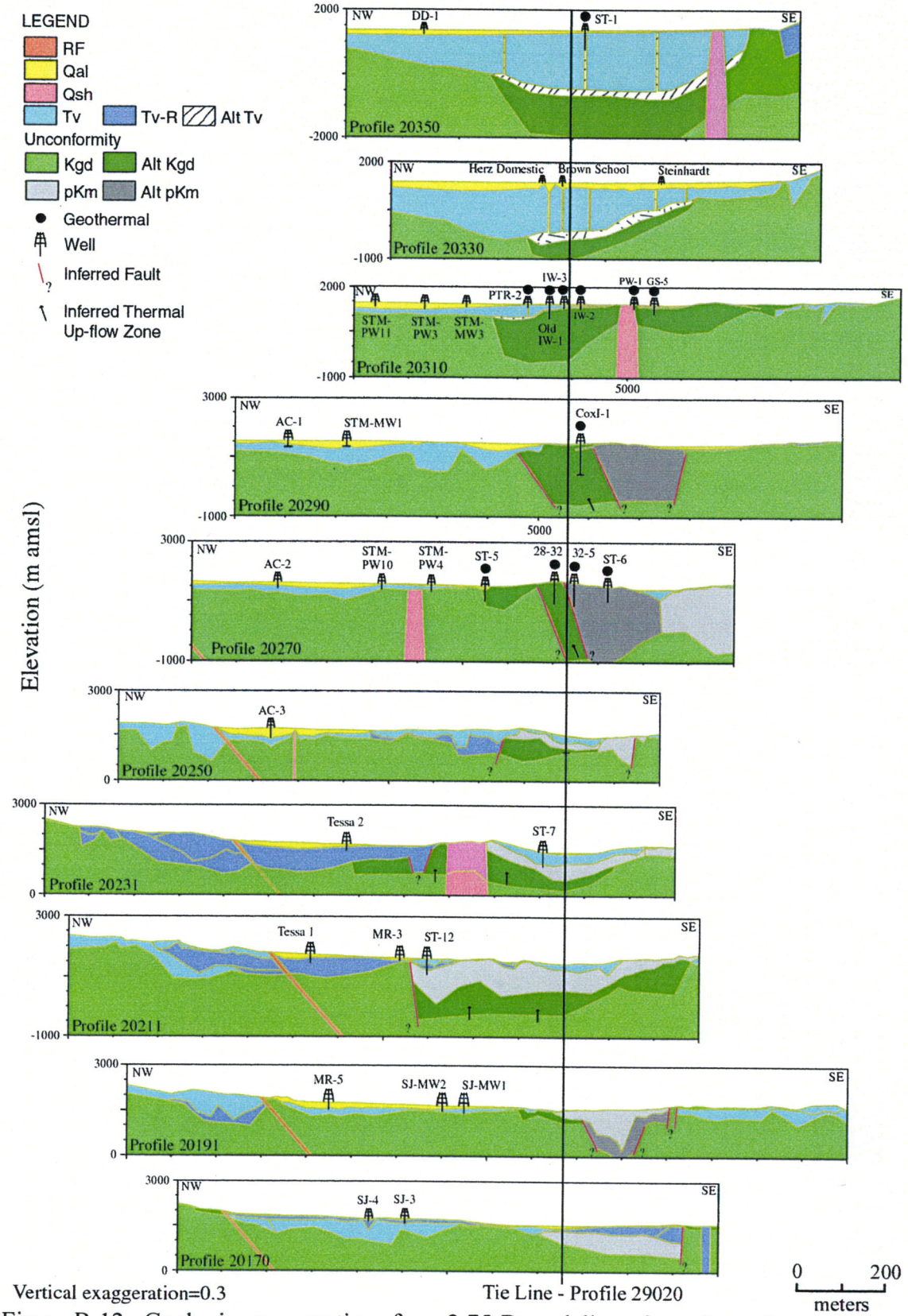

Figure B-12. Geologic cross-sections from 2.75-D modeling of gravity and aeromagnetic data.

The *pKm* is generally located in the southeastern portion of each section with locally variable lateral extent and thickness, which appears to be structurally controlled. The thickest *pKm* occurs in Profiles 20270 and 20290, which is coincident with the CPI geothermal production area. Profiles 20310, 20330, and 20350 located in the northeastern extent of the study area do not contain *pKm*. The *Alt Kgd* appears in each Profile, with exception of Profile 20170 at the southwestern extent of the study area, and has locally variable thickness and lateral dimension, which also appear structurally controlled. A small thin zone of *Alt Kgd* appears in Profile 20191 while the unit thickens toward the northeast with the thickest area occurring in Profile 20270 (CPI production area) and Profile 20350 (geothermal discharge area). The thickness of Tv varies within each profile and from profile to profile illustrating that this unit was not formed by simple layer cake geology but rather may have conformed to existing topography. The magnetic normal polarity layers are thickest in Profile 20350 toward the northeast whereas the magnetic reverse polarity layers are thickest in Profile 20321 in the central portion of the study area. The *Tv* rocks in Profiles 20211 and 20321 (Galena Fan) and in Profiles 20250, 20270, 20290, and 20310 (Mt. Rose Fan) are an important water source Washoe County and the *Tv* thickness is estimated for the first time from this study. *Alt Tv* is found in Profiles 20310, 20330, and 20350 overlying *Alt Kgd* to represent cap rock for the geothermal system. This cap rock does not occur in Profiles to the southwest where the geothermal system is close to the surface. Vertical zones in the *Alt Tv* are modeled in Profiles 20330 and 20350 to represent north-trending faults that conduct thermal water from the geothermal system to the alluvial aquifer. Little continuity is observed in Qsh dome distribution, which is consistent with mapped geology (Tabor and Ellen, 1975; Bonham and Rogers, 1983; and Bonham and Bell, 1993). The aerial extent of *Alt Kgd* is not correlated with *Qsh* suggesting that these 1.2 My domes (Silberman et al., 1979) are not directly the heat source for the geothermal area as suggested by DeRocher (1996) and Finger et al. (1994). Upflow zones of thermal are postulate to occur in Profiles 20211 and 20270 associated with the *Alt Kgd*. The discharge area of the geothermal system is represented in Profiles 20330 and 20350 as *Alt Kgd* and *Alt Tv*. A detailed discussion of the conceptual model of the geothermal system is presented in Chapter 3.

REFERENCES

Bonham, H.F., Jr., and Rogers, D.K., 1983, Geologic map, Mt. Rose NE quadrangle: Nevada Bureau of Mines and Geol., Map 4Bg.

Bonham, H.F., Jr., and Bell, J. W., 1993, Geologic map, Steamboat quadrangle: Nevada Bureau of Mines and Geol., Map 4Fg.

DeRocher, T., 1996, Historical summary of Caithness Power, Inc., Hydrologic monitoring of the Steamboat Hills region, 1987-Present, draft unpublished report for Yankee/Caithness, 46 p.

Finger, J.T., Jacobson, R.D., Hickox, C.E., and Eaton, R.R., 1994, Steamboat Hills exploratory slimhole: Drilling and testing: Sandia Nat. Lab. Report SAND94-0551, October 1994, 59 p.

Silberman, M.L., White, D.E., Keith, T.E.C., Dockter, R.D., 1979, Duration of hydrothermal activity at Steamboat Springs, Nevada, from ages of spatially associated volcanic rocks, U.S. Geol. Surv. Prof. Paper 458-D, 14 p.

Skalbeck, J.D., Shevenell, L., and Widmer, M.C., 2001, Mixing of Thermal and Non-Thermal Waters the Steamboat Hills Area, Nevada: Geothermics, 30, *in press*.

Tabor, R.W., and Ellen, S., 1975, Geologic Map, Washoe City Folio: Nevada Bur. of Mines and Geol. Environmental Series.

Table B-1. Physical properties for 2.75-D forward models.

		Magnetics (cgs)					Magnetics (SI)					Density
Line 20350												
Tv	S =	0.002	Mi =	103	Q =	3.7	S =	0.025	Mi =	1293	Q = 2.9	D = 2.47
(29020)	M =	0.003	Mr =	377			M =	3.000	Mr =	3770		
Tv-R	S =	0.002	Mi =	103	Q =	1.2	S =	0.025	Mi =	1293	Q = 1.0	D = 2.47
	M =	0.001	Mr =	126			M =	1.000	Mr =	1257		
Kgd	S =	0.0018	Mi =	93	Q =	0.1	S =	0.023	Mi =	1164	Q = 0.1	D = 2.67
	M =	0.000074	Mr =	9.3			M =	0.074	Mr =	93		
Kgd	S =	0.0018	Mi =	93	Q =	3.0	S =	0.023	Mi =	1164	Q = 2.4	D = 2.67
	M =	0.0022	Mr =	276			M =	2.200	Mr =	2765		
Alt Tv	S =	0.000002	Mi =	0.10	Q =	4.9	S =	0.00003	Mi =	1.3	Q = 3.9	D = 2.52
	M =	0.000004	Mr =	0.50			M =	0.004	Mr =	5.0		
Alt Kgd	S =	0.00047	Mi =	24	Q =	0.1	S =	0.006	Mi =	304	Q = 0.1	D = 2.52
	M =	0.00002	Mr =	2.5			M =	0.020	Mr =	25		
Qsh	S =	0.002	Mi =	103	Q =	3.7	S =	0.025	Mi =	1293	Q = 2.9	D = 2.60
	M =	0.003	Mr =	377			M =	3.000	Mr =	3770		
Line 20330												
Tv	S =	0.002	Mi =	103	Q =	3.7	S =	0.025	Mi =	1293	Q = 2.9	D = 2.47
(29020)	M =	0.003	Mr =	377			M =	3.000	Mr =	3770		
Kgd	S =	0.0018	Mi =	93	Q =	0.1	S =	0.023	Mi =	1164	Q = 0.1	D = 2.67
	M =	0.000074	Mr =	9.3			M =	0.074	Mr =	93		
Alt Tv	S =	0.000002	Mi =	0.10	Q =	4.9	S =	0.00003	Mi =	1.3	Q = 3.9	D = 2.52
	M =	0.000004	Mr =	0.50			M =	0.004	Mr =	5.0		
Alt Kgd	S =	0.00047	Mi =	24	Q =	0.1	S =	0.006	Mi =	304	Q = 0.1	D = 2.52
	M =	0.00002	Mr =	2.5			M =	0.020	Mr =	25		
Line 20310												
Tv	S =	0.002	Mi =	103	Q =	3.7	S =	0.025	Mi =	1293	Q = 2.9	D = 2.47
(29020)	M =	0.003	Mr =	377			M =	3.000	Mr =	3770		
Tv-R	S =	0.002	Mi =	103	Q =	3.7	S =	0.025	Mi =	1293	Q = 2.9	D = 2.47
	M =	0.003	Mr =	377			M =	3.000	Mr =	3770		
Tv-R	S =	0.002	Mi =	103	Q =	4.9	S =	0.025	Mi =	1293	Q = 3.9	D = 2.47
	M =	0.004	Mr =	503			M =	4.000	Mr =	5027		
Kgd	S =	0.0018	Mi =	93	Q =	0.1	S =	0.023	Mi =	1164	Q = 0.1	D = 2.67
	M =	0.000074	Mr =	9.3			M =	0.074	Mr =	93		
Alt Kgd	S =	0.00047	Mi =	24	Q =	0.1	S =	0.006	Mi =	304	Q = 0.1	D = 2.52
	M =	0.00002	Mr =	2.5			M =	0.020	Mr =	25		
Qsh	S =	0.0002	Mi =	10	Q =	0.1	S =	0.003	Mi =	129	Q = 0.1	D = 2.62
	M =	0.00001	Mr =	1.3			M =	0.010	Mr =	13		
Line 20290												
Tv	S =	0.002	Mi =	103	Q =	4.9	S =	0.025	Mi =	1293	Q = 3.9	D = 2.47
(29020)	M =	0.004	Mr =	503			M =	4.000	Mr =	5027		
Tv-R	S =	0.002	Mi =	103	Q =	4.9	S =	0.025	Mi =	1293	Q = 3.9	D = 2.57
	M =	0.004	Mr =	503			M =	4.000	Mr =	5027		
Kgd	S =	0.0018	Mi =	93	Q =	0.1	S =	0.023	Mi =	1164	Q = 0.1	D = 2.67
	M =	0.000074	Mr =	9.3			M =	0.074	Mr =	93		
Alt Kgd	S =	0.00047	Mi =	24	Q =	0.1	S =	0.006	Mi =	304	Q = 0.1	D = 2.52
	M =	0.00002	Mr =	2.5			M =	0.020	Mr =	25		
pKm	S =	0.001	Mi =	51	Q =	0.2	S =	0.013	Mi =	647	Q = 0.2	D = 2.57
	M =	0.0001	Mr =	12.6			M =	0.100	Mr =	126		
Tkp	S =	0.002	Mi =	103	Q =	4.9	S =	0.025	Mi =	1293	Q = 3.9	D = 2.47
	M =	0.004	Mr =	503			M =	4.000	Mr =	5027		

Table B-1. Physical properties for 2.75-D forward models.

		Magnetics (cgs)					Magnetics (SI)					Density
Line 20270												
Tv	S =	0.002	Mi =	103	Q =	1.2	S =	0.025	Mi =	1293	Q = 1.0	D = 2.47
(29020)	M =	0.001	Mr =	126			M =	1.000	Mr =	1257		
pKm	S =	0.0001	Mi =	5.1	Q =	0.2	S =	0.001	Mi =	65	Q = 0.2	D = 2.62
(29020)	M =	0.00001	Mr =	1.3			M =	0.010	Mr =	13		
Tv	S =	0.001	Mi =	51	Q =	2.4	S =	0.013	Mi =	647	Q = 1.9	D = 2.47
	M =	0.001	Mr =	126			M =	1.000	Mr =	1257		
Kgd	S =	0.0018	Mi =	93	Q =	0.1	S =	0.023	Mi =	1164	Q = 0.1	D = 2.67
	M =	0.000074	Mr =	9.3			M =	0.074	Mr =	93		
Alt Kgd	S =	0.00047	Mi =	24	Q =	0.1	S =	0.006	Mi =	304	Q = 0.1	D = 2.52
	M =	0.00002	Mr =	2.5			M =	0.020	Mr =	25		
RF Fault	S =	0.0018	Mi =	93	Q =	0.1	S =	0.023	Mi =	1164	Q = 0.1	D = 2.27
	M =	0.000074	Mr =	9.3			M =	0.074	Mr =	93		
pKm	S =	0.0002	Mi =	10	Q =	0.1	S =	0.003	Mi =	129	Q = 0.1	D = 2.77
	M =	0.00001	Mr =	1.3			M =	0.010	Mr =	13		
Vol Intrusive	S =	0.003	Mi =	154	Q =	0.2	S =	0.038	Mi =	1940	Q = 0.2	D = 2.75
	M =	0.0003	Mr =	38			M =	0.300	Mr =	377		
Tv	S =	0.002	Mi =	103	Q =	2.4	S =	0.025	Mi =	1293	Q = 1.9	D = 2.47
	M =	0.002	Mr =	251			M =	2.000	Mr =	2513		
Line 20250												
Tkp	S =	0.001	Mi =	51	Q =	4.9	S =	0.013	Mi =	647	Q = 3.9	D = 2.47
(29020)	M =	0.002	Mr =	251			M =	2.000	Mr =	2513		
pKm	S =	0.0001	Mi =	5.1	Q =	2.4	S =	0.001	Mi =	65	Q = 1.9	D = 2.67
(29020)	M =	0.0001	Mr =	13			M =	0.100	Mr =	126		
Tv	S =	0.001	Mi =	51	Q =	2.4	S =	0.013	Mi =	647	Q = 1.9	D = 2.47
	M =	0.001	Mr =	126			M =	1.000	Mr =	1257		
Tv-R	S =	0.001	Mi =	51	Q =	2.4	S =	0.013	Mi =	647	Q = 1.9	D = 2.47
	M =	0.001	Mr =	126			M =	1.000	Mr =	1257		
Dike-R	S =	0.003	Mi =	154	Q =	7.3	S =	0.038	Mi =	1940	Q = 5.8	D = 2.67
	M =	0.009	Mr =	1131			M =	9.000	Mr =	11310		
Kgd	S =	0.0018	Mi =	93	Q =	0.1	S =	0.023	Mi =	1164	Q = 0.1	D = 2.67
	M =	0.000074	Mr =	9.3			M =	0.074	Mr =	93		
Alt Kgd	S =	0.00047	Mi =	24	Q =	0.1	S =	0.006	Mi =	304	Q = 0.1	D = 2.52
	M =	0.00002	Mr =	2.5			M =	0.020	Mr =	25		
pKm	S =	0.0007	Mi =	36	Q =	5.9	S =	0.009	Mi =	453	Q = 4.7	D = 2.67
	M =	0.0017	Mr =	214			M =	1.700	Mr =	2136		
RF Fault	S =	0.0018	Mi =	93	Q =	0.1	S =	0.023	Mi =	1164	Q = 0.1	D = 2.27
	M =	0.000074	Mr =	9.3			M =	0.074	Mr =	93		
Tv	S =	0.002	Mi =	103	Q =	3.7	S =	0.025	Mi =	1293	Q = 2.9	D = 2.47
	M =	0.003	Mr =	377			M =	3.000	Mr =	3770		
Line 20231												
Tv	S =	0.001	Mi =	51	Q =	4.9	S =	0.013	Mi =	647	Q = 3.9	D = 2.47
(29020)	M =	0.002	Mr =	251			M =	2.000	Mr =	2513		
pKm	S =	0.0001	Mi =	5.1	Q =	2.4	S =	0.001	Mi =	65	Q = 1.9	D = 2.72
(29020)	M =	0.0001	Mr =	13			M =	0.100	Mr =	126		
pKm	S =	0.002	Mi =	103	Q =	0.5	S =	0.025	Mi =	1293	Q = 0.4	D = 2.77
	M =	0.0004	Mr =	50			M =	0.400	Mr =	503		
Kgd	S =	0.0018	Mi =	93	Q =	0.1	S =	0.023	Mi =	1164	Q = 0.1	D = 2.67
	M =	0.000074	Mr =	9.3			M =	0.074	Mr =	93		
Alt Kgd	S =	0.00047	Mi =	24	Q =	0.1	S =	0.006	Mi =	304	Q = 0.1	D = 2.52
	M =	0.00002	Mr =	2.5			M =	0.020	Mr =	25		
RF Fault	S =	0.0018	Mi =	93	Q =	0.1	S =	0.023	Mi =	1164	Q = 0.1	D = 2.27
	M =	0.000074	Mr =	9.3			M =	0.074	Mr =	93		

Table B-1. Physical properties for 2.75-D forward models.

		Magnetics (cgs)					Magnetics (SI)					Density
Line 20231 (cont.)												
Qsh	S =	0.0005	Mi =	26	Q =	2.4	S =	0.006	Mi =	323	Q =	1.9	D =	2.67
	M =	0.0005	Mr =	63			M =	0.500	Mr =	628				
Alt Qsh	S =	0.00001	Mi =	0.5	Q =	2.4	S =	0.0001	Mi =	6.5	Q =	1.9	D =	2.52
	M =	0.00001	Mr =	1.3			M =	0.010	Mr =	13				
Tv-R	S =	0.002	Mi =	103	Q =	5.1	S =	0.025	Mi =	1293	Q =	4.1	D =	2.27
(29010)	M =	0.0042	Mr =	528			M =	4.200	Mr =	5278				
Line 20211														
Tv	S =	0.001	Mi =	51	Q =	4.9	S =	0.013	Mi =	647	Q =	3.9	D =	2.47
(29020)	M =	0.002	Mr =	251			M =	2.000	Mr =	2513				
pKm	S =	0.001	Mi =	51	Q =	0.2	S =	0.013	Mi =	647	Q =	0.2	D =	2.67
(29020)	M =	0.0001	Mr =	13			M =	0.100	Mr =	126				
Kgd	S =	0.0018	Mi =	93	Q =	0.1	S =	0.023	Mi =	1164	Q =	0.1	D =	2.67
	M =	0.000074	Mr =	9.3			M =	0.074	Mr =	93				
Alt Kgd	S =	0.00047	Mi =	24	Q =	0.1	S =	0.006	Mi =	304	Q =	0.1	D =	2.52
	M =	0.00002	Mr =	2.5			M =	0.020	Mr =	25				
RF Fault	S =	0.0018	Mi =	93	Q =	0.1	S =	0.023	Mi =	1164	Q =	0.1	D =	2.27
	M =	0.000074	Mr =	9.3			M =	0.074	Mr =	93				
Tv-R	S =	0.002	Mi =	103	Q =	7.3	S =	0.025	Mi =	1293	Q =	5.8	D =	2.47
	M =	0.006	Mr =	754			M =	6.000	Mr =	7540				
Tv	S =	0.003	Mi =	154	Q =	3.3	S =	0.038	Mi =	1940	Q =	2.6	D =	2.47
	M =	0.004	Mr =	503			M =	4.000	Mr =	5027				
Tv-R	S =	0.001	Mi =	51	Q =	4.9	S =	0.013	Mi =	647	Q =	3.9	D =	2.27
	M =	0.002	Mr =	251			M =	2.000	Mr =	2513				
Tv-R	S =	0.002	Mi =	103	Q =	7.3	S =	0.025	Mi =	1293	Q =	5.8	D =	2.27
	M =	0.006	Mr =	754			M =	6.000	Mr =	7540				
Tv	S =	0.001	Mi =	51	Q =	2.4	S =	0.013	Mi =	647	Q =	1.9	D =	2.27
	M =	0.001	Mr =	126			M =	1.000	Mr =	1257				
Tv	S =	0.001	Mi =	51	Q =	4.9	S =	0.013	Mi =	647	Q =	3.9	D =	2.27
	M =	0.002	Mr =	251			M =	2.000	Mr =	2513				
Tv-R	S =	0.003	Mi =	154	Q =	0.8	S =	0.038	Mi =	1940	Q =	0.6	D =	2.37
(29010)	M =	0.001	Mr =	126			M =	1.000	Mr =	1257				
Line 20191														
Tv	S =	0.001	Mi =	51	Q =	4.9	S =	0.013	Mi =	647	Q =	3.9	D =	2.47
(29020)	M =	0.002	Mr =	251			M =	2.000	Mr =	2513				
pKm	S =	0.0001	Mi =	5.1	Q =	2.4	S =	0.001	Mi =	65	Q =	1.9	D =	2.67
(29020)	M =	0.0001	Mr =	13			M =	0.100	Mr =	126				
Tv	S =	0.002	Mi =	103	Q =	3.7	S =	0.025	Mi =	1293	Q =	2.9	D =	2.47
	M =	0.003	Mr =	377			M =	3.000	Mr =	3770				
Tv	S =	0.001	Mi =	51	Q =	2.4	S =	0.013	Mi =	647	Q =	1.9	D =	2.47
	M =	0.001	Mr =	126			M =	1.000	Mr =	1257				
Tv-R	S =	0.003	Mi =	154	Q =	7.3	S =	0.038	Mi =	1940	Q =	5.8	D =	2.47
	M =	0.009	Mr =	1131			M =	9.000	Mr =	11310				
pKm	S =	0.001	Mi =	51	Q =	2.4	S =	0.013	Mi =	647	Q =	1.9	D =	2.57
	M =	0.001	Mr =	126			M =	1.000	Mr =	1257				
Kgd	S =	0.0018	Mi =	93	Q =	0.1	S =	0.023	Mi =	1164	Q =	0.1	D =	2.67
	M =	0.000074	Mr =	9.3			M =	0.074	Mr =	93				
Alt Kgd	S =	0.00047	Mi =	24	Q =	0.1	S =	0.006	Mi =	304	Q =	0.1	D =	2.52
	M =	0.00002	Mr =	2.5			M =	0.020	Mr =	25				
RF Fault	S =	0.0018	Mi =	93	Q =	0.1	S =	0.023	Mi =	1164	Q =	0.1	D =	2.27
	M =	0.000074	Mr =	9.3			M =	0.074	Mr =	93				
Tv-R	S =	0.002	Mi =	103	Q =	7.3	S =	0.025	Mi =	1293	Q =	5.8	D =	2.47
	M =	0.006	Mr =	754			M =	6.000	Mr =	7540				

Table B-1. Physical properties for 2.75-D forward models.

		Magnetics (cgs)						Magnetics (SI)					Density
Line 20170													
Tv	S =	0.001	Mi =	51	Q =	4.9	S =	0.013	Mi =	647	Q =	3.9	D = 2.47
(29020)	M =	0.002	Mr =	251			M =	2.000	Mr =	2513			
Tv-R	S =	0.002	Mi =	103	Q =	7.3	S =	0.025	Mi =	1293	Q =	5.8	D = 2.47
(29020)	M =	0.006	Mr =	754			M =	6.000	Mr =	7540			
pKm	S =	0.0001	Mi =	5.1	Q =	2.4	S =	0.001	Mi =	65	Q =	1.9	D = 2.77
(29020)	M =	0.0001	Mr =	13			M =	0.100	Mr =	126			
Kgd	S =	0.0018	Mi =	93	Q =	0.1	S =	0.023	Mi =	1164	Q =	0.1	D = 2.67
	M =	0.000074	Mr =	9.3			M =	0.074	Mr =	93			
Alt Kgd	S =	0.00047	Mi =	24	Q =	0.1	S =	0.006	Mi =	304	Q =	0.1	D = 2.52
	M =	0.00002	Mr =	2.5			M =	0.020	Mr =	25			
Kgd	S =	0.0018	Mi =	93	Q =	0.1	S =	0.023	Mi =	1164	Q =	0.1	D = 2.47
	M =	0.000074	Mr =	9.3			M =	0.074	Mr =	93			
RF Fault	S =	0.0018	Mi =	93	Q =	0.1	S =	0.023	Mi =	1164	Q =	0.1	D = 2.27
	M =	0.000074	Mr =	9.3			M =	0.074	Mr =	93			
Tv	S =	0.001	Mi =	51	Q =	2.4	S =	0.013	Mi =	647	Q =	1.9	D = 2.47
	M =	0.001	Mr =	126			M =	1.000	Mr =	1257			
Tv	S =	0.002	Mi =	103	Q =	1.2	S =	0.025	Mi =	1293	Q =	1.0	D = 2.47
	M =	0.001	Mr =	126			M =	1.000	Mr =	1257			
Tv-R	S =	0.002	Mi =	103	Q =	7.3	S =	0.025	Mi =	1293	Q =	5.8	D = 2.47
	M =	0.006	Mr =	754			M =	6.000	Mr =	7540			
Tv	S =	0.002	Mi =	103	Q =	3.7	S =	0.025	Mi =	1293	Q =	2.9	D = 2.57
	M =	0.003	Mr =	377			M =	3.000	Mr =	3770			
Alt Kgd	S =	0.00047	Mi =	24	Q =	0.1	S =	0.006	Mi =	304	Q =	0.1	D = 2.27
	M =	0.00002	Mr =	2.5			M =	0.020	Mr =	25			
Line 29020													
Tv	S =	0.002	Mi =	103	Q =	3.7 30,	S =	0.025	Mi =	1293	Q =	2.9	D = 2.47
	M =	0.003	Mr =	377	0330, 20310		M =	3.000	Mr =	3770			
Tv	S =	0.001	Mi =	51	Q =	4.9 31	S =	0.013	Mi =	647	Q =	3.9	D = 2.47
	M =	0.002	Mr =	251			M =	2.000	Mr =	2513			
Tv	S =	0.002	Mi =	103	Q =	7.3 90	S =	0.025	Mi =	1293	Q =	5.8	D = 2.47
	M =	0.006	Mr =	754			M =	6.000	Mr =	7540			
Tv	S =	0.002	Mi =	103	Q =	1.2 70	S =	0.025	Mi =	1293	Q =	1.0	D = 2.47
	M =	0.001	Mr =	126			M =	1.000	Mr =	1257			
pKm	S =	0.0001	Mi =	5	Q =	0.2 70	S =	0.001	Mi =	65	Q =	0.2	D = 2.62
	M =	0.00001	Mr =	1.3			M =	0.010	Mr =	13			
Tv	S =	0.002	Mi =	103	Q =	2.4 50	S =	0.025	Mi =	1293	Q =	1.9	D = 2.47
	M =	0.002	Mr =	251			M =	2.000	Mr =	2513			
pKm	S =	0.0001	Mi =	5.1	Q =	2.4 50	S =	0.001	Mi =	65	Q =	1.9	D = 2.67
	M =	0.0001	Mr =	13			M =	0.100	Mr =	126			
Tv	S =	0.001	Mi =	51	Q =	4.9 31	S =	0.013	Mi =	647	Q =	3.9	D = 2.47
	M =	0.002	Mr =	251			M =	2.000	Mr =	2513			
pKm	S =	0.0001	Mi =	5.1	Q =	2.4 31	S =	0.001	Mi =	65	Q =	1.9	D = 2.72
	M =	0.0001	Mr =	13			M =	0.100	Mr =	126			
Tv	S =	0.001	Mi =	51	Q =	4.9 11	S =	0.013	Mi =	647	Q =	3.9	D = 2.47
	M =	0.002	Mr =	251			M =	2.000	Mr =	2513			
pKm	S =	0.001	Mi =	51	Q =	0.2 11	S =	0.013	Mi =	647	Q =	0.2	D = 2.67
	M =	0.0001	Mr =	13			M =	0.100	Mr =	126			
Tv	S =	0.001	Mi =	51	Q =	4.9 91	S =	0.013	Mi =	647	Q =	3.9	D = 2.47
	M =	0.002	Mr =	251			M =	2.000	Mr =	2513			
pKm	S =	0.0001	Mi =	5.1	Q =	2.4 91	S =	0.001	Mi =	65	Q =	1.9	D = 2.67
	M =	0.0001	Mr =	13			M =	0.100	Mr =	126			
Tv	S =	0.002	Mi =	103	Q =	3.7 70	S =	0.025	Mi =	1293	Q =	2.9	D = 2.47
	M =	0.003	Mr =	377			M =	3.000	Mr =	3770			

Table B-1. Physical properties for 2.75-D forward models.

		Magnetics (cgs)					Magnetics (SI)					Density
Line 29020 (cont.)												
Tv-R	S =	0.003	Mi =	154	Q =	4.9 70	S =	0.038	Mi =	1940	Q = 3.9	D = 2.47
	M =	0.006	Mr =	754			M =	6.000	Mr =	7540		
Kgd	S =	0.0018	Mi =	93	Q =	0.1	S =	0.023	Mi =	1164	Q = 0.1	D = 2.67
	M =	0.000074	Mr =	9.3			M =	0.074	Mr =	93		
Alt Kgd	S =	0.00047	Mi =	24	Q =	0.1	S =	0.006	Mi =	304	Q = 0.1	D = 2.52
	M =	0.00002	Mr =	2.5			M =	0.020	Mr =	25		
Tv-R	S =	0.003	Mi =	154	Q =	4.9	S =	0.038	Mi =	1940	Q = 3.9	D = 2.47
	M =	0.006	Mr =	754			M =	6.000	Mr =	7540		
Alt Kgd	S =	0.00047	Mi =	24	Q =	0.1	S =	0.006	Mi =	304	Q = 0.1	D = 2.52
	M =	0.00002	Mr =	2.5			M =	0.020	Mr =	25		
Kgd	S =	0.0018	Mi =	93	Q =	0.1	S =	0.023	Mi =	1164	Q = 0.1	D = 2.67
	M =	0.000074	Mr =	9.3			M =	0.074	Mr =	93		
RF Fault	S =	0.0018	Mi =	93	Q =	0.1	S =	0.023	Mi =	1164	Q = 0.1	D = 2.27
	M =	0.000074	Mr =	9.3			M =	0.074	Mr =	93		

Notes:

Tv= Tertiary volcanics (R=Reverse magnetization)
Kgd= Cretaceous granodiorite
pKm= pre-Cretaceous metamorphics
(29020)= Consistant with Tie Line
Alt= Altered
RF Fault= Range front fault
Qsh= Quaternary rhyolite dome

S = Magnetic susceptibility
M = Remanent magnetic intensity
Mi = Induced magnetization
Mr = Remanent magnetization
Q = Mr / Mi
D = Density

Table B-2. Best fit statistics for 2.75-D forward models.

Flightline	Complete Bouguer Residual Gravity Range (mGal)		Anomaly (mGal)	RMSE (mGal)	% RMSE	Reduced to Pole Residual Magnetics Range (nT)		Anomaly (nT)	RMSE (nT)	% RMSE
20170	-22.7	-28.2	5.5	0.227	4.1	-634	1305	1939	106.987	5.5
20191	-20.5	-28.0	7.5	0.279	3.7	-450	850	1300	89.213	6.9
20211	-19.3	-28.9	9.6	0.359	3.7	-415	758	1173	113.339	9.7
20231	-16.9	-28.0	11.1	0.405	3.6	-598	514	1112	97.738	8.8
20250	-17.9	-28.7	10.8	0.396	3.7	-186	439	625	62.303	10.0
20270	-14.4	-25.1	10.7	0.503	4.7	-343	407	750	57.828	7.7
20290	-14.1	-24.6	10.5	0.485	4.6	-206	1603	1809	116.832	6.5
20310	-16.2	-23.0	6.8	0.215	3.2	-588	579	1167	67.847	5.8
20330	-17.9	-26.6	8.7	0.349	4.0	-258	663	921	23.991	2.6
20350	-19.1	-27.0	7.9	0.168	2.1	-211	488	699	15.341	2.2
29020	-15.1	-39.0	23.9	1.795	7.5	-1241	870	2111	161.569	7.7
Target Value for % RMSE					5.0					10.0

RMSE: Root mean square error % RMSE: RMSE/Anomaly mGal: milliGal nT: nanoTesla

Table B-3. Data for 3-D model in Chapter 3.

UTM E (m)	UTM N (m)	Qal Thickness (m)	Tv Thickness (m)	AltKgdpKm Thickness (m)	Kgd Depth (m)
253114	4362089	0	27	0	27
253319	4361869	0	30	0	30
253932	4361210	11	192	0	203
254137	4360991	24	270	0	294
254341	4360771	34	332	0	366
254545	4360551	28	524	0	552
254750	4360332	14	486	0	500
254954	4360112	13	403	0	416
255159	4359893	8	366	0	374
255363	4359673	5	479	0	484
255567	4359454	7	624	0	631
255772	4359234	1	692	0	693
255976	4359014	32	686	0	718
256181	4358795	0	812	0	812
256385	4358575	27	731	0	758
256590	4358356	40	385	0	425
256794	4358136	0	559	0	559
256998	4357917	0	496	0	496
257203	4357697	0	306	0	306
257407	4357477	0	162	0	162
257612	4357258	19	124	0	143
257816	4357038	35	52	0	87
258021	4356819	43	51	0	94
258225	4356599	48	88	0	136
258429	4356380	33	245	0	278
258634	4356160	65	143	0	329
258838	4355940	91	96	0	507
259043	4355721	68	135	0	641
259247	4355501	45	179	0	736
259451	4355282	24	210	0	842
259656	4355062	14	283	0	938
259860	4354843	16	307	0	957
260065	4354623	29	292	0	974
260269	4354403	39	325	0	997
260474	4354184	35	460	0	1045
254623	4360501	24	588	0	612
255396	4359654	0	501	0	501
255542	4359540	0	594	0	594
255796	4359272	0	694	0	694
255929	4359134	0	691	0	691
256116	4358892	0	785	0	785
256026	4359007	90	645	0	735
256242	4358803	0	825	0	825
256483	4358485	42	317	0	359
256698	4358250	0	498	0	498

Table B-3. Data for 3-D model in Chapter 3.

UTM E (m)	UTM N (m)	Qal Thickness (m)	Tv Thickness (m)	AltKgdpKm Thickness (m)	Kgd Depth (m)
256858	4358078	0	607	0	607
257504	4357391	0	176	0	176
258554	4356255	52	226	0	278
258643	4356172	71	109	0	347
260716	4353898	27	575	0	0
263309	4352905	0	409	0	409
263106	4353125	0	323	0	323
262902	4353346	0	406	0	406
262699	4353566	0	544	0	544
262496	4353787	0	427	0	427
262292	4354007	0	239	0	239
259241	4357315	0	6	438	312
259038	4357535	0	31	378	191
258834	4357756	0	62	235	62
258631	4357976	0	96	143	96
258427	4358197	0	63	209	63
258224	4358417	49	70	0	119
258021	4358638	60	115	0	175
257817	4358858	64	119	0	183
257614	4359079	61	115	0	176
257410	4359299	92	138	0	230
257207	4359520	109	88	0	197
257003	4359740	133	55	0	188
256800	4359961	124	71	0	195
256597	4360181	129	129	0	258
256393	4360402	139	208	0	347
256190	4360622	156	256	0	412
255986	4360843	180	190	0	370
255783	4361063	191	244	0	435
255580	4361284	190	219	0	409
255376	4361504	215	230	0	445
255173	4361725	205	188	0	393
254969	4361945	153	146	0	299
254766	4362166	94	25	0	119
254563	4362386	24	390	0	414
254359	4362607	0	987	0	987
254156	4362827	0	982	0	982
253952	4363048	0	961	0	961
253749	4363268	0	991	0	991
253545	4363489	0	832	0	832
254542	4362372	0	448	0	448
258376	4358215	0	69	0	69
258368	4358223	12	55	0	67
258916	4357642	0	60	272	60
262125	4354184	0	311	0	311

Table B-3. Data for 3-D model in Chapter 3.

UTM E (m)	UTM N (m)	Qal Thickness (m)	Tv Thickness (m)	AltKgdpKm Thickness (m)	Kgd Depth (m)
260896	4357307	0	107	867	645
260693	4357527	0	311	785	710
260490	4357748	0	190	1105	775
260286	4357968	0	287	1239	862
260083	4358189	0	189	1535	912
259880	4358409	0	155	1522	1078
259676	4358630	0	99	1561	1267
259473	4358851	0	52	1620	1301
259270	4359071	0	193	1454	1209
259066	4359292	0	63	1706	1124
258863	4359512	0	32	1824	742
258660	4359733	0	15	1876	601
258456	4359954	0	83	1870	652
258253	4360174	12	233	1792	903
258050	4360395	6	366	1685	950
257846	4360615	66	154	1824	833
257643	4360836	76	111	0	187
257440	4361057	89	237	0	326
257236	4361277	44	418	0	462
257033	4361498	41	562	0	603
256830	4361718	90	654	0	744
256627	4361939	99	759	0	858
256423	4362160	128	784	0	912
256220	4362380	107	782	0	889
256017	4362601	175	578	0	753
255813	4362821	99	643	0	742
255610	4363042	0	773	0	773
255407	4363262	0	773	0	773
255203	4363483	0	808	0	808
255000	4363704	0	787	0	787
254797	4363924	0	879	0	879
254593	4364145	0	1000	0	1000
254390	4364365	0	1119	0	1119
254187	4364586	0	1171	0	1171
253983	4364807	0	644	0	644
253780	4365027	0	300	0	300
253577	4365248	0	195	0	195
257152	4361364	0	527	0	527
257754	4360694	0	162	0	162
257777	4360666	0	181	0	181
257830	4360606	0	212	613	2043
258339	4360072	0	198	620	2014
262161	4357708	0	27	0	287
261958	4357929	0	47	0	267
261755	4358149	0	176	0	339

Table B-3. Data for 3-D model in Chapter 3.

UTM E (m)	UTM N (m)	Qal Thickness (m)	Tv Thickness (m)	AltKgdpKm Thickness (m)	Kgd Depth (m)
261551	4358370	0	190	0	412
261348	4358590	0	206	468	458
261145	4358811	0	281	609	562
260942	4359032	27	323	744	714
260738	4359252	47	317	859	868
260535	4359473	43	322	897	916
260332	4359693	17	382	836	811
260128	4359914	0	363	922	717
259925	4360135	0	218	1129	597
259722	4360355	0	137	1270	516
259518	4360576	0	22	1385	387
258705	4361458	0	81	0	81
258502	4361679	7	886	0	893
258298	4361899	21	482	0	503
258095	4362120	17	443	0	460
257892	4362341	14	488	0	502
257689	4362561	36	520	0	556
257485	4362782	70	565	0	635
257282	4363002	107	667	0	774
257079	4363223	148	755	0	903
256875	4363444	189	816	0	1005
256672	4363664	193	752	0	945
256469	4363885	158	761	0	919
256265	4364105	172	775	0	947
256062	4364326	169	709	0	878
255859	4364547	101	753	0	854
255655	4364767	0	1080	0	1080
255452	4364988	0	1151	0	1151
255249	4365208	0	1099	0	1099
255046	4365429	0	1080	0	1080
254842	4365650	0	1031	0	1031
254639	4365870	0	994	0	994
254436	4366091	0	842	0	842
254232	4366311	0	587	0	587
254029	4366532	0	326	0	326
253826	4366753	0	386	0	386
255681	4364733	0	1063	0	1063
257433	4362837	74	525	0	599
258275	4361902	28	356	0	384
258625	4361538	0	173	0	173
258522	4361644	0	804	0	804
258873	4361284	0	95	0	95
259461	4360659	0	23	1302	0
259483	4360634	0	13	1350	324
260242	4359794	0	407	830	659

Table B-3. Data for 3-D model in Chapter 3.

UTM E (m)	UTM N (m)	Qal Thickness (m)	Tv Thickness (m)	AltKgdpKm Thickness (m)	Kgd Depth (m)
261095	4358882	0	320	651	683
261405	4358547	0	175	243	418
256206	4365971	201	191	0	392
256408	4365749	225	165	0	390
256610	4365528	273	160	0	433
256812	4365306	362	259	0	621
257014	4365084	256	143	0	399
257216	4364862	224	114	0	338
257418	4364641	225	106	0	331
257620	4364419	126	70	0	196
257822	4364197	128	120	0	248
258024	4363975	128	145	0	273
258226	4363754	82	178	0	260
258429	4363532	0	402	0	402
258631	4363310	0	425	0	425
258833	4363088	0	474	0	474
259035	4362867	0	366	0	366
259237	4362645	0	408	0	408
259439	4362423	0	527	0	527
259641	4362201	0	846	0	846
259843	4361980	0	859	0	859
260045	4361758	0	803	0	803
260247	4361536	0	483	303	409
260449	4361314	0	217	784	317
260651	4361092	0	107	940	326
260853	4360871	0	78	824	337
261055	4360649	35	215	444	363
261257	4360427	40	218	291	427
261459	4360205	16	193	261	400
261661	4359984	9	239	183	347
258309	4363728	0	280	0	280
260248	4361610	0	245	812	653
256850	4367044	52	225	0	277
257053	4366822	74	179	0	253
257256	4366601	102	245	0	347
257458	4366380	110	231	0	341
257661	4366159	147	263	0	410
257864	4365938	166	264	0	430
258066	4365716	172	239	0	411
258269	4365495	185	270	0	455
258472	4365274	193	370	0	563
258674	4365053	138	293	0	431
258877	4364832	85	205	0	290
259080	4364610	26	149	0	175
259282	4364389	32	165	0	197

Table B-3. Data for 3-D model in Chapter 3.

UTM E (m)	UTM N (m)	Qal Thickness (m)	Tv Thickness (m)	AltKgdpKm Thickness (m)	Kgd Depth (m)
259485	4364168	43	147	0	190
259688	4363947	52	127	0	179
259890	4363726	46	98	0	144
260093	4363505	52	65	0	117
261512	4361956	0	17	1008	17
261917	4361514	0	50	1186	1236
262931	4360408	9	90	1613	1712
263133	4360187	13	305	0	1508
263336	4359966	12	82	0	1435
263539	4359744	0	31	0	1469
263741	4359523	0	41	0	1822
263934	4359339	0	10	0	2279
263495	4359870	0	53	1390	1443
258560	4366992	119	297	0	416
258764	4366772	168	313	0	481
258968	4366552	220	365	0	585
259172	4366332	260	466	0	726
259376	4366112	165	648	0	813
259580	4365892	227	541	0	768
259784	4365672	178	475	0	653
259988	4365452	117	363	0	480
260192	4365232	78	309	0	387
260396	4365012	47	860	0	907
260600	4364792	6	972	0	978
260803	4364572	29	728	0	757
261007	4364352	99	308	0	407
261211	4364132	219	604	0	823
261415	4363912	263	455	0	718
261619	4363691	195	206	0	398
261823	4363471	92	125	591	217
262027	4363251	0	14	1552	14
262231	4363031	0	42	1994	42
262435	4362811	0	42	2038	42
262639	4362591	0	29	2027	29
262843	4362371	0	19	1093	895
263047	4362151	0	9	1934	1943
264066	4361051	90	44	0	134
264270	4360831	88	48	0	136
264474	4360611	79	38	0	117
264678	4360391	52	36	0	88
264882	4360171	0	40	0	40
265086	4359951	0	45	0	45
265290	4359731	0	64	0	64
265494	4359511	0	106	0	106
260281	4365201	72	366	0	438

Table B-3. Data for 3-D model in Chapter 3.

UTM E (m)	UTM N (m)	Qal Thickness (m)	Tv Thickness (m)	AltKgdpKm Thickness (m)	Kgd Depth (m)
260312	4365161	129	584	0	713
260925	4364475	58	192	0	250
261661	4363659	179	130	0	309
262021	4363290	0	38	0	38
262143	4363158	0	24	0	24
263931	4361254	87	45	45	132
264783	4360298	0	50	0	50
262114	4364986	72	422	960	494
262318	4364766	39	476	1311	515
262521	4364546	28	398	1492	426
262725	4364326	31	176	1672	207
262929	4364106	0	139	1731	139
263133	4363886	0	104	1311	104
263337	4363666	0	76	928	76
263949	4363006	31	57	653	88
264153	4362786	47	58	750	105
264357	4362566	33	56	857	89
264561	4362346	0	6	975	6
264765	4362126	0	5	858	5
264969	4361906	0	26	486	26
265173	4361686	0	0	253	0
265377	4361466	0	0	307	0
265581	4361246	0	0	284	0
265785	4361026	0	0	219	0
261987	4365139	91	334	0	425
263484	4363505	0	27	693	27
263595	4363391	0	0	596	0
263723	4363246	0	0	618	0
263790	4363171	0	90	684	0
264064	4362882	0	97	706	97
264387	4362526	0	42	912	42
265035	4361835	0	0	307	0
261955	4366929	255	1336	0	1591
262159	4366708	269	1160	0	1429
262363	4366488	273	1337	0	1610
262567	4366268	258	1477	0	1735
262771	4366048	234	1544	0	1778
262975	4365828	197	1513	0	1710
263179	4365608	101	1851	0	1780
263383	4365388	113	1742	237	2204
263587	4365168	146	1639	541	1818
263791	4364948	182	1576	506	1729
263994	4364728	171	1488	400	1646
264198	4364508	181	1258	917	933
264402	4364288	198	1024	874	777

Table B-3. Data for 3-D model in Chapter 3.

UTM E (m)	UTM N (m)	Qal Thickness (m)	Tv Thickness (m)	AltKgdpKm Thickness (m)	Kgd Depth (m)
264606	4364068	195	861	640	759
264810	4363848	159	714	501	654
265014	4363628	170	528	0	884
265218	4363408	177	303	0	480
265422	4363188	170	342	0	512
265626	4362968	152	347	0	499
265830	4362748	155	304	0	459
266034	4362528	90	312	0	402
263992	4365837	196	1516	0	1712
265180	4363439	187	281	0	468
266174	4362342	0	108	0	2842
262992	4365837	188	1554	0	2281
263210	4365578	36	1774	0	1810
263246	4365540	386	1453	0	2367
262148	4368661	155	784	0	939
262348	4368437	165	879	0	1044
262548	4368213	160	951	0	1111
262748	4367990	154	992	0	1146
262948	4367766	158	1081	0	1239
263148	4367542	150	1187	0	1337
263348	4367319	128	1394	0	2134
263548	4367095	121	1667	257	2635
263748	4366871	110	1848	1441	1807
263948	4366648	97	1914	1566	1726
264148	4366424	80	1951	1400	1930
264348	4366200	62	1971	1290	2082
264547	4365977	67	1967	1215	2204
264747	4365753	63	2020	1257	2205
264947	4365529	63	2074	1313	2195
265147	4365306	35	2122	1343	2209
265347	4365082	33	2073	1351	2141
265547	4364859	38	1841	1190	1911
265747	4364635	27	1147	0	2710
265947	4364411	9	1227	0	1236
266147	4364188	13	642	0	655
265690	4364684	26	1653	0	1708
265912	4364448	3	1261	0	1264
265937	4364424	4	1194	0	1198

Notes:

Qal: Quarternary alluvial deposits.
Tv: Tertiary volcanic rocks.
AltKgdpKm: Altered granodiorite and metamorphic rocks.
Kgd: Cretaceous granodiorite.

APPENDIX C

GROUND MAGNETIC DATA

Table C-1. Ground magnetic data for Figure 5 in Chapter 4.

Adjusted Distance (m)	Transect 1 TMI (nT)	Transect 3 TMI (nT)	Transect 4 TMI (nT)	Transect 5 TMI (nT)	Adjusted Distance (m)	Transect 2 TMI (nT)
-313		51269				
-305		51365				
-297		51398				
-290		51396				
-282		51391				
-274		51412				
-267		51422				
-259		51453		51251		
-252		51492		51254		
-244		51543		51246		
-236		51583		51233		
-229		51631		51238		
-221		51674		51247		
-214		51684		51269		
-206		51653		51267		
-198	51574	51639		51258		
-191	51581	51603		51240		
-183	51588	51605		51225		
-175	51588	51654		51218		
-168	51577	51676		51212		
-160	51574	51686		51204		
-153	51572	51702		51191		
-145	51581	51668		51180		
-137	51592	51651		51175		
-130	51607	51660	51443	51177	-52	51636
-122	51626	51663	51431	51182	-49	51654
-114	51642	51677	51428	51181	-45	51681
-107	51650	51693	51413	51175	-42	51703
-99	51658	51651	51407	51175	-39	51713
-92	51666	51625	51392	51178	-36	51717
-84	51659	51608	51386	51178	-33	51715
-76	51658	51606	51396	51173	-30	51709
-69	51676	51609	51407	51170	-27	51697
-61	51707	51610	51406	51184	-24	51671
-53	51698	51619	51366	51197	-21	51639
-46	51647	51609	51316	51184	-18	51610
-38	51601	51577	51285	51150	-15	51595
-31	51587	51539	51294	51115	-12	51590
-23	51628	51526	51311	51100	-9	51593
-15	51618	51467	51319	51067	-6	51596
-8	51576	51415	51225	51043	-3	51584
0	51535	51396	51154	51027	0	51565
7	51586	51403	51127	51057	3	51572
15	51673	51395	51175	51077	6	51604
23	51724	51447	51212	51079	9	51673
30	51732	51460	51218	51064	12	51715

Table C-1. Ground magnetic data for Figure 5 in Chapter 4.

Adjusted Distance (m)	Transect 1 TMI (nT)	Transect 3 TMI (nT)	Transect 4 TMI (nT)	Transect 5 TMI (nT)	Adjusted Distance (m)	Transect 2 TMI (nT)
38	51708	51466	51250	51046	15	51742
46	51697	51485	51286	51047	19	51727
54		51503	51307	51046	22	51733
61		51542	51294	51048	25	51735
69		51624	51286	51045	28	51724
76		51690	51288	51048	31	51687
84		51720	51307	51052	34	51667
92		51762	51306	51054	37	51672
99		51778	51310	51056	40	51679
107		51764	51313	51063	43	51678
115		51735	51317	51056		
122		51726	51310	51052		
130		51714	51304	51046		
137		51693	51303	51052		
145		51690	51306	51052		
152		51662	51311	51053		
160		51650	51317	51056		
168		51639	51323	51054		
175		51559	51331	51051		
183		51533	51336	51048		
190		51584	51345	51051		
198		51609	51346	51051		
206		51625	51347	51053		
213		51702	51347	51055		
221		51727	51352	51062		
228		51698	51357	51068		
236		51657	51359	51076		
244		51599	51360	51081		
251		51561	51365	51085		
259		51534	51366	51091		
267		51532	51370	51092		
274		51547	51368	51098		
282		51593	51375	51101		
289		51629	51386	51108		
297		51655	51397	51109		
305		51653	51413	51114		
312		51646	51427	51120		
320		51620	51443	51126		
328		51602	51447	51130		
335		51601	51457	51136		
343		51615	51467	51144		
350		51624	51485	51150		
358		51613	51514	51153		
366		51623	51546	51155		
373		51627	51566	51155		
381		51628	51580	51154		

Table C-1. Ground magnetic data for Figure 5 in Chapter 4.

Adjusted Distance (m)	Transect 1 TMI (nT)	Transect 3 TMI (nT)	Transect 4 TMI (nT)	Transect 5 TMI (nT)	Adjusted Distance (m)	Transect 2 TMI (nT)
388		51628	51590	51155		
396		51664	51594	51154		
404		51637	51586	51153		
411		51530	51575	51153		
419		51562	51577	51155		
427		51547	51579	51154		
434		51533	51577	51155		
442		51544	51574	51159		
449		51668	51602	51168		
457		51648	51629	51175		
465		51679	51641	51178		
472		51701	51603	51178		
480		51724	51566	51178		
488		51718	51555	51178		
495		51710	51557	51179		
503		51704		51180		
510		51698		51177		
518		51698		51181		
526		51692		51183		
533		51672		51186		
541		51647		51183		
549		51623		51182		
556		51588		51184		
564		51566		51189		
571		51577		51210		
579		51601		51227		
587		51630		51241		
594		51673		51240		
602		51733		51225		
609		51769		51186		
617		51780		51180		
625		51789		51177		
632		51786				
640		51770				
648		51744				
655		51727				
663		51712				
670		51700				
678		51678				
686		51678				
693		51681				
701		51679				
709		51683				
716		51672				
724		51646				
731		51635				

Table C-1. Ground magnetic data for Figure 5 in Chapter 4.

Adjusted Distance (m)	Transect 1 TMI (nT)	Transect 3 TMI (nT)	Transect 4 TMI (nT)	Transect 5 TMI (nT)	Adjusted Distance (m)	Transect 2 TMI (nT)
739		51626				
747		51615				
754		51608				
762		51607				
769		51596				
777		51585				
785		51574				
792		51567				
800		51571				
808		51581				
815		51591				
823		51603				
830		51613				
838		51620				
846		51621				
853		51632				
861		51637				

Notes:
TMI: Total magnetic intensity.
Adjusted distance: Mud Volcano Basin Fault set at zero distance, based on lowest magnetic intensity measurement.

Table C-2. Magnetic data for Figure 6 in Chapter 4.

Field Distance (m)	Adjusted Distance (m)	Ground Mag (GM) (nT)	GM Up 50 m (nT)	GM Up 1250 m (nT)	Draped Aeromag (nT)
0	-130	-28	-79	128.5	0.0
8	-122	-31	-82	128.4	-2.0
15	-115	-46	-85	128.3	-4.0
23	-107	-52	-89	128.1	-6.1
30	-100	-67	-93	128.0	-8.2
38	-92	-73	-97	127.9	-10.4
46	-84	-63	-102	127.8	-11.2
53	-77	-52	-108	127.7	-12.6
61	-69	-53	-113	127.6	-14.0
69	-61	-93	-120	127.4	-16.3
76	-54	-143	-126	127.2	-17.7
84	-46	-174	-133	127.1	-19.0
91	-39	-165	-139	127.0	-20.3
99	-31	-148	-146	126.9	-21.6
107	-23	-140	-151	126.7	-22.8
114	-16	-234	-157	126.6	-24.0
122	-8	-305	-161	126.6	-24.6
130	0	-332	-163	126.4	-25.2
137	7	-284	-164	126.3	-22.8
145	15	-247	-164	126.2	-20.3
152	22	-241	-163	126.1	-17.9
160	30	-209	-160	125.9	-15.6
168	38	-173	-157	125.8	-13.3
175	45	-152	-154	125.7	-11.0
183	53	-165	-151	125.6	-8.8
191	61	-173	-147	125.4	-7.6
198	68	-171	-144	125.3	-5.3
206	76	-152	-141	125.2	-3.2
213	83	-153	-138	125.1	-1.2
221	91	-149	-135	125.0	0.8
229	99	-146	-132	124.9	2.8
236	106	-142	-129	124.7	4.7
244	114	-149	-127	124.6	6.6
251	121	-155	-124	124.5	8.4
259	129	-156	-121	124.4	10.2
267	137	-153	-118	124.3	12.0
274	144	-148	-114	124.2	13.8
282	152	-142	-111	124.1	15.4
290	160	-136	-107	124.0	17.1
297	167	-128	-104	123.9	18.8
305	175	-123	-100	123.8	20.8
312	182	-114	-96	123.6	21.9
320	190	-113	-92	123.5	23.8
328	198	-112	-88	123.4	25.6
335	205	-112	-84	123.3	27.5
343	213	-107	-79	123.2	29.3

Table C-2. Magnetic data for Figure 6 in Chapter 4.

Field Distance (m)	Adjusted Distance (m)	Ground Mag (GM) (nT)	GM Up 50 m (nT)	GM Up 1250 m (nT)	Draped Aeromag (nT)
351	221	-102	-75	123.1	31.2
358	228	-100	-70	123.0	33.0
366	236	-99	-66	122.9	34.8
373	243	-94	-61	122.8	36.5
381	251	-93	-55	122.7	38.2
389	259	-89	-50	122.6	39.9
396	266	-91	-44	122.5	41.6
404	274	-84	-37	122.4	43.2
411	281	-73	-30	122.3	44.8
419	289	-62	-23	122.2	46.4
427	297	-46	-15	122.2	48.1
434	304	-32	-7	122.0	48.9
442	312	-16	2	121.9	50.4
450	320	-12	11	121.8	52.0
457	327	-2	20	121.7	53.6
465	335	8	29	121.6	54.5
472	342	26	38	121.6	55.3
480	350	55	47	121.5	56.0
488	358	87	56	121.4	56.8
495	365	107	64	121.3	57.5
503	373	121	72	121.3	58.5
511	381	131	79	121.2	59.3
518	388	135	86	121.1	60.1
526	396	127	92	121.0	60.9
533	403	116	97	120.9	61.8
541	411	118	102	120.9	62.6
549	419	120	107	120.8	63.5
556	426	118	111	120.6	63.6
564	434	115	115	120.5	64.4
572	442	143	119	120.4	65.3
579	449	170	122	120.4	66.4
587	457	182	125	120.3	67.3
594	464	144	128	120.2	68.3
602	472	107	130	120.1	69.2
610	480	96	133	120.0	70.2

Notes:
Adjusted distance: Mud Volcano Basin Fault set at zero distance, based on lowest magnetic intensity measurement.
Up: Upward continued.